Molecular and Cellular Mechanisms of Peroxisomal Fusion and Aging in Yeast

Tatiana Boukh-Viner

A Thesis

in

The Department

of

Biology

Presented in Partial Fulfillment of the Requirements

for the Degree of Doctor of Philosophy at

Concordia University

Montreal, Quebec, Canada

June 2009

CONCORDIA UNIVERSITY

Your file Votre référence
ISBN: 978-0-494-63362-5
Our file Notre référence
ISBN: 978-0-494-63362-5

ABSTRACT

Molecular and Cellular Mechanisms of Peroxisomal Fusion and Aging in Yeast

Tatiana Boukh-Viner, Ph.D.

Concordia University, 2009

Peroxisomes are organelles best known for their essential roles in lipid metabolism and hydrogen peroxide detoxification. Peroxisomal biogenesis in the yeast *Yarrowia lipolytica* is a multi-step process of temporally ordered sequential conversion of five distinct peroxisomal subforms, termed P1 to P5, into a mature peroxisomal subform P6 carrying the complete set of matrix and membrane proteins.

In the first part of my thesis, I investigate the effect of lateral heterogeneity of the peroxisomal membrane bilayer on the efficiency of the fusion between P1 and P2 in the yeast *Y. lipolytica*. My findings provide a unique view of the multistep remodeling of the protein repertoire of ergosterol- and ceramide-rich (ECR) domains found in the peroxisomal membrane during fusion of P1 and P2, and define the hierarchy of individual steps during the spatial and temporal reorganization of the peroxisome fusion machinery that only transiently associates with ECR domains.

In the second part of my thesis, I described the use of mass spectrometry-based proteomics for examining the contribution of peroxisomal proteins to longevity regulation in the yeast *Saccharomyces cerevisiae* grown under calorie restriction (CR) conditions. My proteomic analysis and experimental results from Dr. Titorenko's laboratory show that CR yeast are able to meet their metabolic requirements by remodeling their carbohydrate and lipid metabolism, which relies on functional lipid

metabolic pathways in the peroxisome. These findings suggest that peroxisomal β-oxidation of fatty acids significantly affects the rate of chronological aging in CR yeast by defining the rate of ATP production in their mitochondria but not by making ROS. I also present my research findings on longevity regulation in *S. cerevisiae* by a novel anti-aging molecule "LA" identified recently in Dr. Titorenko's laboratory. Comprehensive analysis of the proteome remodeling in yeast placed on a CR diet and exposed to LA, along with experimental data obtained through various metabolomic and functional studies in Dr. Titorenko's laboratory, demonstrate that LA extends yeast chronological lifespan by maintaining the mitochondrial production of ROS at an optimal level that does not excessively damage cellular macromolecules but triggers a potent cellular stress response.

Acknowledgements

I am grateful to my supervisor, Dr. Vladimir Titorenko, for the incredible amount of help, support and guidance I have received while being a graduate student in his laboratory.

I would like to thank the members of my committee, Dr. Storms and Dr. Zerges, for their support and valuable suggestions during the course of my graduate research and studies.

Finally, I would like to thank all the current and former members of Dr. Titorenko's laboratory including Simon Bourque, Alex Goldberg, Christopher Gregg, Tong Guo, Tatiana Iouk, Pavlo Kyryakov, Oleh Petriv, Zeinab Aziz, David Cyr, Aloysius Oluoha, Farhana Banu, Adrian Buensuceso, Andre Cerracchio, Eileen Colella, Colin Goldfinch, Svetlana Milijevic, Janine Morcos, Mehdi Noei, Reza Noei, Jonathan Solomon, and Vivianne Wong for their friendship and support.

I dedicate this thesis to my dog Slash, my family and all my friends, whose love and support made me what I am today.

Table of Contents

List of Figures

List of Abbreviations

BAPTA	1,2-Bis(2-aminophenoxy)ethane-*N,N,N',N'*-tetra_acetic acid
CaM	Calmodulin
CCCP	Carbonyl cyanide *m*-chlorophenylhydrazone
COPI	Coat protein complex I
COPII	Coat protein complex II
CR	Calorie-restricted
D	Diauxic growth phase
DAG	Diacylglycerol

DSM	Detergent-soluble membrane domains
ECR	Ergosterol- and ceramide-rich
ECP	Ergosterol- and ceramide-poor
EE	Ergosterol esters
ER	Endoplasmic reticulum
F_i	Fluorescence for intact peroxisomes
F_{ol}	Fluorescence for osmotically lysed peroxisomes
FA-CoA	CoA esters of fatty acids
FFA	Free fatty acids
GPI	Glycosylphosphatidylinositol
GTP-bp	GTP-binding and hydrolyzing proteins
L	Logarithmic growth phase
LB	Lipid bodies
LPA	Lysophosphosphatidic acid
OG	n-octyl-β-D-glucopyranoside
P1 to P5	Immature peroxisomal vesicles P1 to P5
P6	Mature peroxisomes P6
PBDs	Peroxisome biogenesis disorders
PC	Phosphatidylcholine
PD	Post-diauxic growth phase
pER	Peroxisomal ER
PI(4)P-bp	Phosphatidylinositol-4-phosphate-binding proteins
$PI(4,5)P_2$-bp	Phosphatidylinositol-4,5-bisphosphate-binding proteins

PMPs	Peroxisomal membrane proteins
PNS	Postnuclear supernatant
PPV1	Pre-peroxisomal vesicles 1
PPV2	Pre-peroxisomal vesicles 2
PS	Phosphatidylserine
PTS1	Peroxisomal targeting signal type 1
PTS2	Peroxisomal targeting signal type 2
ROS	Reactive oxygen species
SNAREs	Soluble NSF attachment protein receptors
TAG	Triacylglycerol
tER	Transitional ER
THI	Thiolase
S	Stationary phase
20KgP	20,000 x *g* pellet
20KgS	20,000 x *g* supernatant
200KgP	200,000 x *g* pellet
200KgS	200,000 x *g* supernatant.

1 Introduction

1.1 Peroxisome function and pathology

Found in almost all eukaryotic cells, peroxisomes are single membrane-bound organelles known for their essential roles in lipid metabolism and detoxification of hydrogen peroxide [1-3]. Peroxisomes constitute a highly dynamic organelle population; their number, size, morphology, protein composition and biochemical functions change in response to altered cellular demands and environmental cues [4-6]. Peroxisomes compartmentalize a number of metabolic pathways such as α- and β-oxidation of fatty acids, catabolism of purines and amino acids, and the degradation of polyamines and prostaglandins [4-6]. Catalase housed in the peroxisome detoxifies hydrogen peroxide, a reactive oxygen species (ROS) generated in several metabolic processes confined to the peroxisome, by converting it to water and oxygen [7, 8]. The molecular oxygen generated in the catalase reaction is then used by several peroxisomal oxidases to oxidize various compounds such as ethanol, methanol, formic acid, fatty acids, L- and D-amino acids, quinines and polyamines [7-10]. Peroxisomes generate a number of important structural and signaling lipids such as plasmalogens, polyunsaturated fatty acids, bile acids and cholesterol [4-6]. Recent evidence suggests that, by modulating intracellular levels of the signaling lipids retinoic acid, phytanic acid and long-chain fatty acids, peroxisomes regulate a number of developmental processes [11-17].

Peroxisomes lack DNA and thus rely on selective post-translational import of proteins required for peroxisome assembly, division and inheritance [1-3, 18-21]. All known peroxisomal proteins are encoded by nuclear genes. Many of these proteins are initially synthesized on free polysomes in the cytosol and then imported into pre-existing

peroxisomal vesicles, which recently have been shown to originate from the endoplasmic reticulum (ER) [21-28]. Some of the peroxisomal membrane proteins are initially targeted, co- or post-translationally, to the ER template for peroxisome formation [21-28]. At least 32 proteins known as peroxins drive the ATP-driven import of many proteins bearing the PTS1 or PTS2 peroxisomal targeting signals to the matrix of the peroxisome [21-28].

Mutations in the peroxin-encoding *PEX* genes result in peroxisomal biogenesis disorders (PBDs), which affect multiple peroxisomal metabolic pathways and lead to progressive neurological and physiological deficits [29-35]. The most severe form of PBDs is known as the Zellweger syndrome (ZS). Patients suffering of this PBD exhibit global developmental delay due to incomplete migration and differentiation of neuroblasts during psychomotor development as well as defects in white matter development and increased apoptosis of neurons [29-35]. ZS patients die in infancy, illustrating how indispensable peroxisomes are for normal human development and physiology, and how vital the research of peroxisomal biogenesis is for designing effective methods of PBDs treatment and prevention. To gain greater insight into the mechanisms responsible for the pathology of PBDs, current research strategies focus on defining peroxisomal contribution to the development and differentiation pathways in evolutionarily distant organisms [16, 18, 30, 36].

1.2 Peroxisome biogenesis

Until recently, peroxisomes were thought of as a static and homogeneous organelle population, where structurally and functionally identical peroxisomes increase in size by the bulk import of peroxisomal proteins and then divided to form new ones [1-3, 32-34].

According to this classical "growth and division" model, peroxisome biogenesis does not involve inter-compartmental vesicular trafficking or membrane fusion. In this model, the contribution of the ER was viewed solely as that of source of lipids for the peroxisomal membrane [1-3, 37-39]. However, a body of evidence accumulated over the last decade from studies in evolutionarily diverse organisms strongly suggests that peroxisomal population in a cell constitutes a dynamic, multi-compartmental endomembrane system, which originates from the ER and involves inter-compartmental vesicular trafficking and fusion events similar to those seen in the secretory system [26, 28, 40-53]. Furthermore, studies in the yeast *Yarrowia lipolytica* and mouse dendritic cells provided evidence that peroxisomes exist as a dynamic organelle population that consists of structurally distinct compartments having different import capacities for various proteins and lipids [18, 54-56]. In fact, individual compartments of *Y. lipolytica* peroxisomal endomembrane system appear to undergo a multi-step remodeling process of peroxisome maturation (Figure 1.1). This process is initiated by the fusion of the ER-derived pre-peroxisomal vesicles and then progresses through several consecutive steps, each involving the import of a distinct set of peroxisomal matrix proteins and transfer of certain lipid species to the peroxisomal membrane [26, 28, 40-47]. In the peroxisome biogenesis model for *Y. lipolytica*, early peroxisomal intermediates P1 and P2 are converted into a mature peroxisome P6 through multiple rounds of import of specific peroxisomal proteins and lipids (Figure 1.1) [18, 36, 40-42, 47, 61, 62]. All six peroxisomal subforms (termed P1 to P6) assembled through the multistep pathway depicted in Figure 1.1 have been purified and characterized biochemically and morphologically [18, 41, 62]. The P6 subform is a

mature, fully functional peroxisome that contains a complete set of matrix and membrane proteins [18, 41, 62].

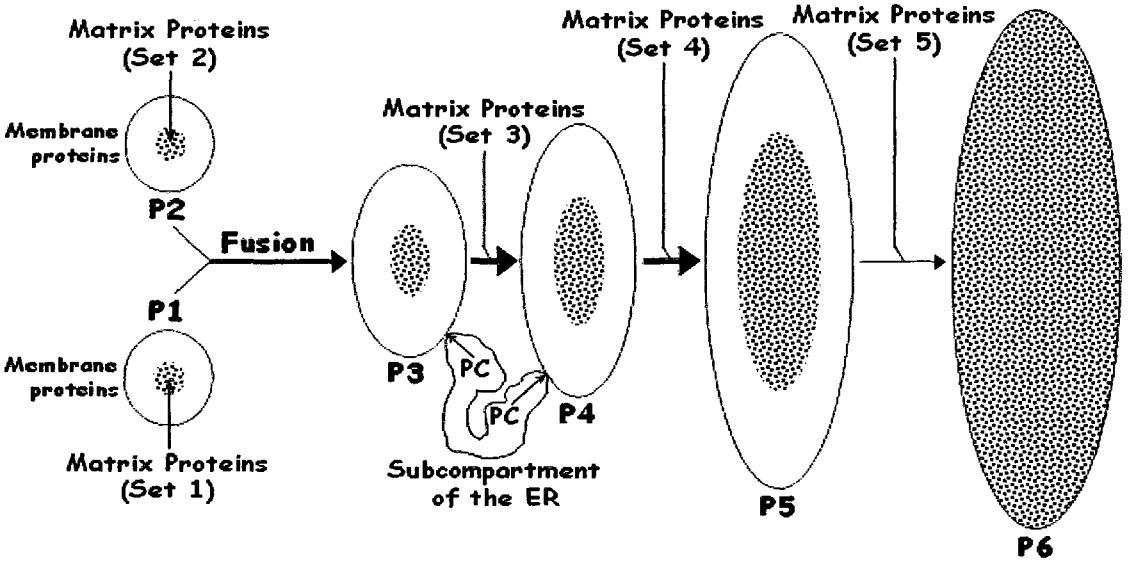

Figure 1.1. A model for peroxisome biogenesis in the yeast *Yarrowia lipolytica*.

In contrast, the earliest intermediates in the pathway, P1 and P2, contain mostly peroxisomal membrane proteins and lack the majority of matrix proteins [18, 42, 62]. Different intermediates in the peroxisome assembly pathway operating in *Y. lipolytica* differ in their import capacity for various matrix proteins [18, 28, 36, 47]. For instance, only the early peroxisomal intermediates P1 and P2 can import malate synthase, a peroxisomal matrix protein that is targeted to P1 and P2 by a PTS1 peroxisomal targeting signal [47]. Furthermore, only P2 can import the PTS3-containing acyl-CoA oxidase and the PTS2-targeted thiolase directly from the cytosol to the peroxisome matrix [47]. Moreover, the PTS1-containing 62-kDa protein can only be imported into P3, whereas the PTS1-bearing isocitrate lyase can only be imported into P4 [47]. Taken together, these findings convincingly demonstrated that the assembly of the import machines specific for different peroxisomal matrix proteins occurs in distinct intermediates of the

peroxisome assembly pathway in a time-ordered fashion [18, 28, 36, 47]. The peroxisome biogenesis model based on studies in *Y. lipolytica* has been supported by growing evidence from other model systems such as the yeast *Pichia pastoris*, mouse dendritic cells and human fibroblasts, all of which have been shown to carry out a similar multi-step peroxisome assembly pathway [21, 23, 30, 49, 54, 64-68].

In mouse dendritic cells, pre-peroxisomal vesicles are formed by protrusions of the lamellar ER extensions that detach from the ER as tubular or sac-shaped carriers of various sizes [54]. After budding off from the ER, these pre-peroxisomal carriers recruit a transporter protein PMP70, possibly along with the membrane components of the import machinery for peroxisomal matrix proteins, to form the so-called "peroxisomal reticulum". Only this peroxisomal reticulum is capable of importing post-translationally the essential peroxisomal matrix proteins thiolase and catalase [49, 54]. During the final step of the peroxisome maturation pathway operating in mouse dendritic cells, the peroxisomal reticulum serves as a template for the formation of mature globular peroxisomes [49, 54]. It is presently unknown if peroxisomal matrix proteins other than thiolase and catalase are imported to the peroxisomal reticulum or to the mature peroxisome [28]. Also, in contrast to yeast cells, no evidence exists so far in mammalian cells to suggest that their early intermediates of the peroxisome assembly pathway undergo fusion [18, 36]. Future research will show if, similar to their stepwise assembly during multi-step peroxisome maturation in yeast, the import machineries specific for different peroxisomal matrix proteins in mammalian cells also assemble in a multi-step fashion in different intermediates of the peroxisome assembly pathway [18, 28, 36]. Taken together, these findings suggest that yeast and higher eukaryotes evolved different

strategies for the formation and maintenance of their ER-derived peroxisomal endomembrane systems [28].

1.3 The ER plays an essential role in peroxisomal biogenesis

Until recently, the contribution of the ER to peroxisome biogenesis was a highly debated and controversial issue due to the conflicting evidence based on studies in different model organisms. It has been initially postulated that all peroxisomal proteins are first synthesized in the ER and only then sorted to the peroxisomal vesicles exiting their ER template [57]. This view was then challenged by the discovery that many peroxisomal proteins are, in fact, synthesized on free polysomes in the cytosol. As a result, the so-called "growth and division" model of peroxisomal biogenesis became widely accepted [1-3, 38]. However, emerging evidence from studies in evolutionarily distant organisms strongly suggests that a distinct subset of peroxisomal membrane proteins, known as group I PMPs, indeed undergoes initial sorting in the ER prior to its targeting to the peroxisome [36]. Specifically, studies in the yeast *Y. lipolytica* and mouse dendritic cells revealed that the targeting of specific PMPs to the membranes of ER-derived peroxisomal precursors is an event that precedes and is necessary for the subsequent import of various peroxisomal proteins into different intermediates of the multi-step peroxisome assembly pathway [18, 28, 36, 49, 54]. In *Y. lipolytica*, the formation of pre-peroxisomal vesicles from the ER is initiated by the post-translational import of group I PMPs into the ER, their *N*-glycosylation in the ER lumen, and their subsequent sorting to a distinct domain of the ER called the pre-peroxisomal template [36, 40-42]. Pre-peroxisomal vesicles PPV1 and PPV2 that carry the group I PMPs Pex2p and Pex16p then exit ER by budding off from the pre-peroxisomal template, which is different from the ER domain that serves

as a template for the formation of secretory vesicles [32, 40-42]. The subsequent post-translational targeting of two partially overlapping sets of group II PMPs to the ER-derived pre-peroxisomal vesicles PPV1 and PPV2 leads to the formation of immature peroxisomal vesicles P1 and P2 [18, 36, 47, 61]. The co- or post-translational import of group I PMPs to the ER and their subsequent exit from the ER via PPV1 and PPV2 are regulated by two independent mechanisms [47, 58-60]. Presently, it is unknown what structural features of group I PMPs are responsible for their targeting to, sorting within and exit from the ER.

In the yeast *Y. lipolytica*, the transfer of lipids to the peroxisomal membrane is initiated in the ER, when a subset of lipids synthesized in the ER membrane is segregated into the pre-peroxisomal template that also carries group I PMPs [26, 41, 42, 45, 46]. Distinct lipid domains of the ER membrane that are enriched in ergosterol and ceramide (ECR domains) have been implicated in the segregation of group I PMPs from the resident ER, secretory and plasma membrane proteins [28]. The availability of an in vitro assay for the ER-dependent formation of distinct proteolipid carriers would greatly facilitate the elucidation of the molecular mechanisms underlying protein and lipid sorting into either pre-peroxisomal or secretory vesicles [70-73]. Such assay would provide a valuable experimental approach for establishing the mechanisms through which ECR domains in the ER membrane govern this process [70-73].

1.4 Interplay between peroxisome assembly and division

A growing body of evidence strongly suggests that, in addition to the ER-dependent formation of pre-peroxisomal vesicles and their stepwise maturation into individual

compartments of the peroxisomal endomembrane system, the process of peroxisome biogenesis involves the division of at least some of these compartments [28]. Although the exact mechanism responsible for coordinating peroxisome assembly and division remains to be established, two models have been proposed to explain the interplay between the processes of peroxisome assembly and division [18, 28, 36, 47, 74]. According to the first model, only mature peroxisomes can undergo division, suggesting that the complete assembly of mature peroxisomes is mandatory for their subsequent proliferation by fission [18, 28, 36]. The second model predicts that the proliferation of ER-derived immature pre-peroxisomal vesicles precedes their maturation leading to the assembly of mature, fully functional peroxisomes [18, 28, 36, 47, 74]. Recent advances in live-cell imaging, including the development of novel fluorescent probes, provide powerful tools for testing the validity of these two models in evolutionarily distant organisms [28, 47].

Similar to the division of mitochondria and chloroplasts, peroxisome division is uncoupled from the cell division and requires dynamin-related GTPases [76-83]. Numerous data suggest that in yeast and human cells peroxisomes do not simultaneously grow and divide [28, 30, 74, 84, 85]. In the yeast *Y. lipolytica*, only mature, fully formed peroxisomes can undergo division, which is regulated by a mechanism that controls membrane scission in response to a signal transmitted from the matrix of the peroxisome [84]. In fact, once the total mass of proteins within the peroxisome exceeds a certain critical level, the first enzyme of fatty acid oxidation acyl-CoA oxidase (Aox) relocates from the peroxisomal matrix to the membrane [84]. Such redistribution of Aox occurs only in the mature peroxisome, where the mass of matrix proteins is at its highest.

Following its relocation from the matrix to the membrane, Aox binds to and sequesters Pex16p, a membrane-associated peroxin that prevents the proliferation of immature peroxisomes by inhibiting the scission of their membrane [84, 86]. Aox-mediated sequestering of Pex16p at the peroxisomal membrane abolishes the ability of this peroxin to inhibit membrane scission, thereby promoting division of mature peroxisomes [71]. Similar to other membrane scission events, peroxisomal membrane scission occurs after membrane bending, which is achieved through the destabilization of the membrane bilayer [88, 89, 90-101]. As energetically unfavorable processes, both scission and bending of mitochondrial, chloroplast and Golgi membranes in yeast, plant and mammalian cells are mediated by an evolutionarily conserved proteolipid machine, which includes such membrane lipids as phosphatidic acid (PA), diacylglycerol (DAG) and certain phosphoinositides [88, 89, 90-106]. The cone-shaped structure of both PA and DAG strongly induces negative membrane curvature and thus promotes membrane bending [88, 90, 102-104, 107-110]. The molecular mechanism underlying the ability of the Pex16p/Aox-dependent intraperoxisomal signaling pathway to induce the membrane scission event needed for peroxisome division in *Y. lipolytica* remains to be defined. The establishment of the contributions of various membrane lipid species and lipid domains to the processes of membrane destabilization, bending, scission and fission during peroxisome division could provide valuable information for understanding such mechanism.

Peroxisome division is also regulated by the metabolic activity of the peroxisome [111-114]. Growing evidence suggests that defects in intraperoxisomal β-oxidation pathways significantly affect peroxisomal abundance and size. For instance, the loss of

enzymatic activities of Aox, fatty acyl-CoA synthetase, multifunctional enzyme type 2 and/or 2-enoyl-CoA hydratase has been shown to alter both peroxisome size and number [111, 112, 115]. Although the mechanisms underlying this so-called metabolic control on peroxisomal division are yet to be established, the observed change in peroxisomal size and number in response to inactivation of Aox and 2-enoyl-CoA hydratase could be due to the resulting overproduction of other enzymes involved in peroxisomal β-oxidation of fatty acids [111, 112, 115].

1.5 Peroxisomes play an essential role in longevity regulation in yeast

Programmed cell death, also known as apoptosis, controls the pace of aging in eukaryotic organisms [189-192]. Recent unpublished data from Dr. Titorenko's laboratory imply that the mitochondria-dependent apoptotic death in the yeast *Saccharomyces cerevisiae* is regulated, in part, by the ß-oxidation of free fatty acids in peroxisomes. Specifically, it appears that, in addition to playing an essential role in peroxisomal biogenesis, the cytosolic shuttling receptor Pex5p for PTS1-containing peroxisomal matrix proteins links the intrinsic, mitochondria-dependent apoptotic cell death to longevity regulation in chronologically aging yeast. Lack of Pex5p shortens the chronological life span of yeast by impairing peroxisomal fatty acid oxidation, thereby causing the accumulation of excessive, cytotoxic quantities of free fatty acids. Furthermore, under calorie-restriction (CR) conditions, various mutational blocks of peroxisomal fatty acid oxidation and the resulting decrease in peroxisomal production of acetyl-CoA impair essential oxidation-reduction processes in mitochondria, promote fragmentation of the mitochondrial tubular network and trigger activation of mitochondrial pro-apoptotic signaling pathways, thereby shortening chronological life span [unpublished data from Dr. Titorenko's lab].

Moreover, recent findings from Dr. Titorenko's laboratory provide evidence that the peroxins Pex1p and Pex6p, two AAA ATPases required for peroxisome biogenesis and peroxisomal protein import, also modulate the ability of mitochondria to generate reactive oxygen species (ROS) known to accelerate organismal aging through oxidative damage of DNA, proteins and lipids [183-186].

Taken together, findings from Dr. Titorenko's laboratory suggest that fatty acid oxidation in yeast peroxisomes plays an essential role in regulating the age-related, mitochondria-controlled apoptotic cell death, thereby indirectly controlling the rate of chronological aging. The mechanisms underlying such essential role of peroxisomes in longevity regulation are addressed in chapters 10-14 of this thesis.

1.6 Molecular mechanisms underlying aging

The circle of life has been a mystery for the human kind for as long as it existed, and generations have been plagued by thirst for eternal life potions and fountains of youth. Not much have changed over the centuries, albeit the aging research field had evolved from the feared wizardry and witchcraft domain to the slightly less mystifying one of a laboratory bench top. Aging is defined as the progressive decline in the ability of an organism to resist stress, repair damage and battle disease [172-175]. In light of these detrimental effects, the purpose of aging as a biological process remains rather elusive. Currently, there are two contradictory models for aging as a biological process. One of them defines aging as a final stage of a developmental program, which is regulated by a distinct set of evolutionarily conserved signaling networks [176-179]. The other, more widely accepted model of aging proposes that this irreversible process is caused by the random accumulation of unrepaired cellular and molecular damage, which is primarily

due to harmful effects of ROS generated as by-products of the metabolic reactions taking place consistently throughout life [172, 180-182]. In fact, evidence from various model systems implicates ROS as negative regulators of life span based on the observed aging-related increase of oxidative damage to nucleic acids, proteins and lipids [183-186]. Studies in chronologically aging yeast and *Drosophila* flies further support this model of aging by showing that decreasing the amount of ROS through the over-expression of ROS-scavenging enzyme superoxide dismutase (SOD) can dramatically extend life span [187, 188].

Multiple cellular compartments generate ROS as side-products of various enzymatic reactions routinely taking place throughout life span. The contribution of mitochondria to the production of ROS is the most significant, with ATP synthesis by mitochondrial respiration accounting for as much as 90% of the overall ROS generated within a cell [189-193]. However, to a lesser extent, ROS are also made in the plasma membrane by NADPH oxidases, in the cytosol by cyclooxygenases catalyzing several oxidative reactions, and in the peroxisome during fatty acid β-oxidation [14, 31, 189-193]. Major targets of the ROS-induced oxidative damage are mitochondrial proteins, including 1) aconitase (Aco1p), an [4Fe-4S] cluster enzyme of the TCA cycle with another essential function in the maintenance of the mitochondrial genome; 2) homoaconitase (Lys4p), another [4Fe-4S] cluster enzyme involved in lysine biosynthesis in the mitochondrion; 3) succinate dehydrogenase, a dual function enzyme involved not only in the TCA cycle but also in the mitochondrial electron transfer chain (ETC) as respiratory complex II; 4) cytochrome c, a heme-containing mobile component of the mitochondrial ETC; and 5) cytochrome c oxidase, a heme-containing complex IV of the

mitochondrial ETC [189-192]. In addition, the mitochondrial DNA (mtDNA) nucleoid and the saturated fatty acids of membrane lipids are also highly susceptible to oxidative damage by ROS [189-192].

Several antioxidant scavenging pathways protect cellular components against oxidative damage by ROS. Two subforms of superoxide dismutase, one found in the cytosol (Sod1p) and another in the mitochondria (Sod2p), convert superoxide radicals to more stable and less toxic hydrogen peroxide [189-192]. Hydrogen peroxide is then further detoxified through various enzymatic reactions catalyzed by glutathione peroxidases, catalases and peroxiredoxins present in the cytosol, mitochondria and peroxisomes.

At any given time, the steady-state level of ROS is defined by the relative rates of ROS formation and detoxification in various cellular locations. While high levels of ROS have been linked to increased oxidative damage to various cellular and organellar constituents, low levels of these reactive compounds, in fact, protect cellular macromolecules against oxidative damage by activating several stress-response and damage-repair pathways [189-192]. Low intracellular and intraorganellar concentrations of ROS have been shown to prevent cells from undergoing apoptosis, a process of programmed cell suicide [189-192, 194]. Apoptotic cell death is known to occur in numerous multicellular organisms and mammals, including humans, where it plays a pivotal role in normal development and physiology [194, 195]. Recent studies show that even unicellular eukaryotic organisms, such as aging yeast cells, also die exhibiting characteristic markers of apoptosis such as DNA cleavage, chromatin condensation, externalization of phosphatidylserine in the plasma membrane, and release of cytochrome

c from mitochondria [196-198]. This emerging evidence strongly suggests that apoptotic cell death plays a major role in the aging process of yeast cells. In addition, several mammalian regulators of apoptosis have orthologues in yeast, providing further evidence that the apoptotic cell death of yeast and metazoan is an evolutionarily conserved mechanism. In yeast, these key regulators of apoptosis include metacaspase Yca1p, an HtrA2/Omi-like apoptotic serine protease Nma111p, the apoptosis inducing factor Aif1p, the histone chaperone Asf1p, and the mitochondrial fission protein Drp1p [201-204]. Moreover, similar to the metazoan organisms, apoptotic pathways in yeast are also regulated primarily by ROS [200].

Several ROS-sensing protein machines exist in the mitochondrion (protein kinases PKD1, PKCδ, Src, Abl, PI3 and Akt), plasma membrane (Ras), and cytosol (PNC1) [189-192]. There is strong evidence that low levels of ROS stimulate the interaction of the ROS-sensing proteins with some of the cytosol-to-nucleus and mitochondrion-to-nucleus shuttling proteins, such as p32 and Hsp27p, promoting their import into the nucleus, where they activate transcriptional factors and co-factors (SIRT1, FOXO3, p53, NF-κB, DET1 and COP1) responsible for the expression of genes encoding stress-response and anti-apoptotic proteins [189-192]. In addition, the inactivation of the mitochondrial pro-apoptotic factors Bad and JNK by some of the ROS sensors in the cytosol and mitochondrion in response to low ROS levels have been shown to delay apoptotic pathways that are activated intrinsically through mitochondria [189-192]. In fact, numerous findings suggest that aging of evolutionarily distant organisms is regulated, in part, through an intrinsic, mitochondria-dependent apoptotic cell death mechanism [190, 191, 205-208]. According to unpublished data from Dr. Titorenko's laboratory, the age-

related, mitochondria-controlled apoptotic death in yeast is regulated, in part, by the oxidation of free fatty acids in peroxisomes. In particular, recent evidence from Dr. Titorenko's laboratory implicates peroxisomal proteins Pex1p, Pex5p and Pex6p as the key factors controlling the rate of chronological aging in yeast by modulating the intrinsic, mitochondria-dependent apoptotic cell death.

1.7 Calorie-restricted yeast as a model system for aging research

A growing body of evidence suggests that fundamental mechanisms of aging are conserved across phyla [209-212, 238]. Our laboratory uses the yeast *S. cerevisiae*, a unicellular eukaryotic organism, to study the molecular and cellular mechanisms governing the aging process. The availability of a completely sequenced genome as well as easy genetic and biochemical manipulations make yeast a valuable model for unveiling the mechanisms of aging in multicellular eukaryotes [216, 217]. Two different methods for studying aging in *S. cerevisiae* measure either replicative or chronological life span. The replicative life span of *S. cerevisiae*, which represents the maximum replicative potential of a yeast cell, is measured by the number of daughter cells produced before senescence and can be used as a model for aging of the dividing (*i.e.*, mitotically active) mammalian cells [218]. The chronological life span of the yeast *S. cerevisiae* reflects the viability of yeast cells in a non-dividing state and has been extensively used as model for studying the aging of non-dividing (*i.e.*, post-mitotic) mammalian cells [219]. Both the replicative and the chronological life spans of yeast can be extended by a diet known as calorie-restriction (CR). This diet decreases the intake of calories derived from carbohydrates, proteins and fat by 25% - 60% without compromising the supply of essential nutrients [208, 220, 222-224]. The CR diet significantly extends life span of a

wide variety of organisms, ranging from yeast to non-human primates and does not cause irreversible reproductive and/or developmental defects that are often observed in genetically-modified long-lived mutants of yeast, flies and mice [208, 220, 222-227]. Furthermore, the CR diet delays the onset of several age-related diseases, such as atherosclerosis, cancer, and type II diabetes [228]. The CR dietary regimen has been also shown to decelerate neuronal degeneration in mouse models of age-related disorders like Parkinson's or Alzheimer's diseases [229, 230]. In fact, the aging-associated decline of spatial and psychomotor memory functions, as well as deterioration of learning capabilities due to dendritic loss, can be delayed by CR [231, 232]. In addition, the CR diet has been linked to the improved plasticity and self-repair of the brain [233].

Despite the available extensive knowledge of the beneficial effects of CR, the mechanisms underlying the CR-dependent life span extension have not been defined yet. The challenge lays in the overall complexity of the multiple effects of the CR diet on the organism's metabolic, apoptotic, and neuroendocrine functions, among possible others. Furthermore, functional changes induced by the CR diet are organ-specific and exhibit various intensities in different organ systems [233].

As a model system to study the mechanisms of aging under CR conditions, Dr. Titorenko's laboratory uses the strain BY4742 of *S. cerevisiae*. This particular strain was chosen based on its relatively short life span, which facilitates the research of its chronological aging, as well as due to the availability of a collection of its knock-out mutants from Open Biosystems [235]. In Dr. Titorenko's laboratory, the experimental set-up of a traditional CR dietary regimen is achieved by growing yeast cells in the YEPD medium with the glucose concentration in the medium lowered from 2% (non-CR

conditions) to 0.5% or 0.2% [236, 237]. The use of nutrient-rich YEPD medium with decreased glucose content does not compromise the supply of essential nutrients and vitamins, which maintains yeast cells viable as glucose is consumed, a requirement that cannot be achieved under other CR protocols that limit availability of amino acids or essential nutrients by using nutrient-limited media [219, 238]. In fact, evidence from Dr. Titorenko's laboratory indicates that the kinetics of growth rate and glucose consumption observed in yeast cells placed on the CR diet are similar to those seen under non-CR conditions (Figure 1.2).

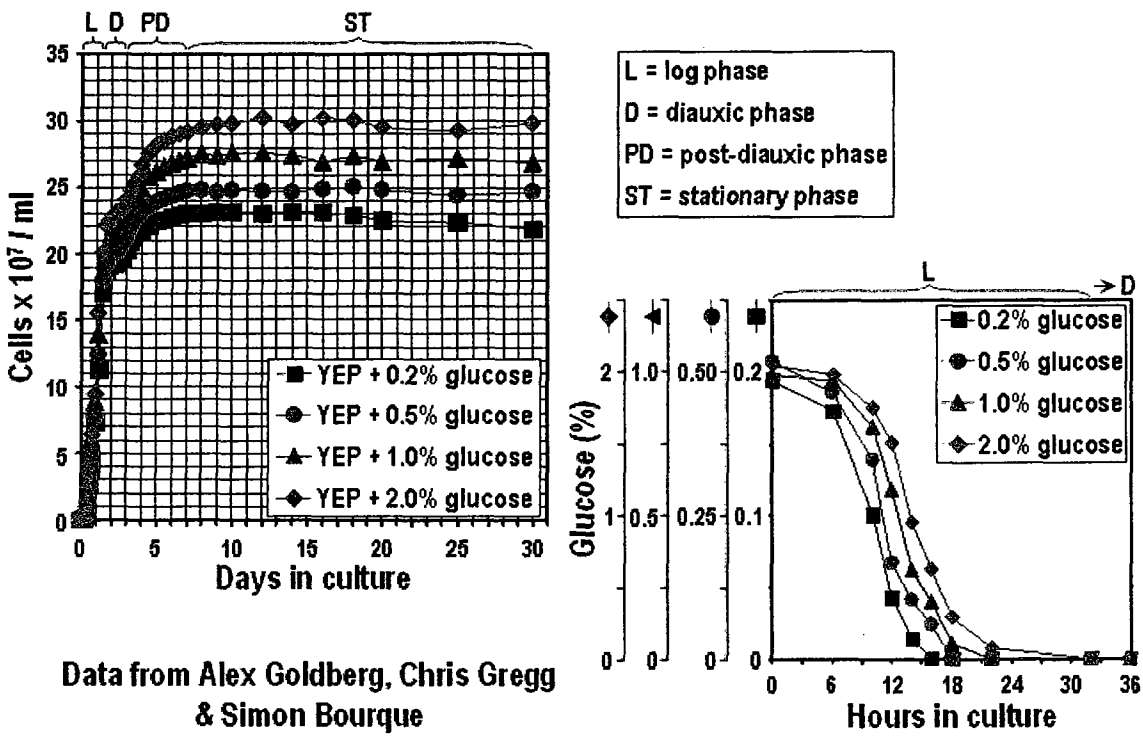

Figure 1.2. Kinetics of growth and glucose consumption for the wild-type *S. cerevisiae* strain BY4742 grown in media initially containing different concentrations of glucose.

Furthermore, the rate of aging and the degree of calorie restriction appear to be in a dose-response relationship, with the maximal life span extension of wild-type strain being achieved under CR conditions at 0.5% glucose concentration (Figure 1.3).

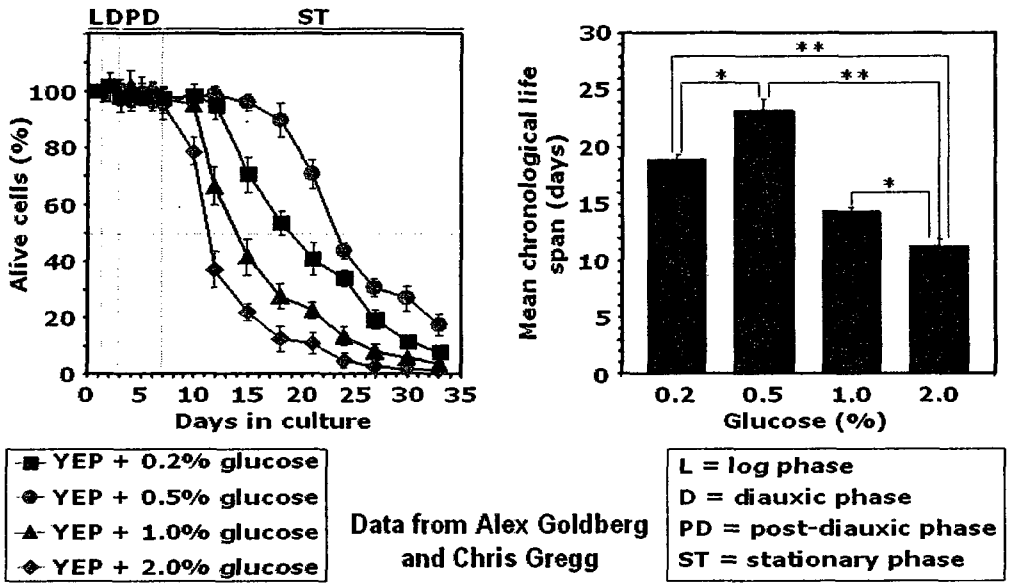

Figure 1.3. A dose-response relationship between the rate of aging and the degree of calorie restriction in the wild-type *S. cerevisiae* strain BY4742.

Moreover, the intracellular levels of ATP and the dynamics of their changes observed during chronological aging of CR yeast are very similar to those seen in the non-CR yeast, indicating that yeast growing under CR are not starving (Figure 1.4).

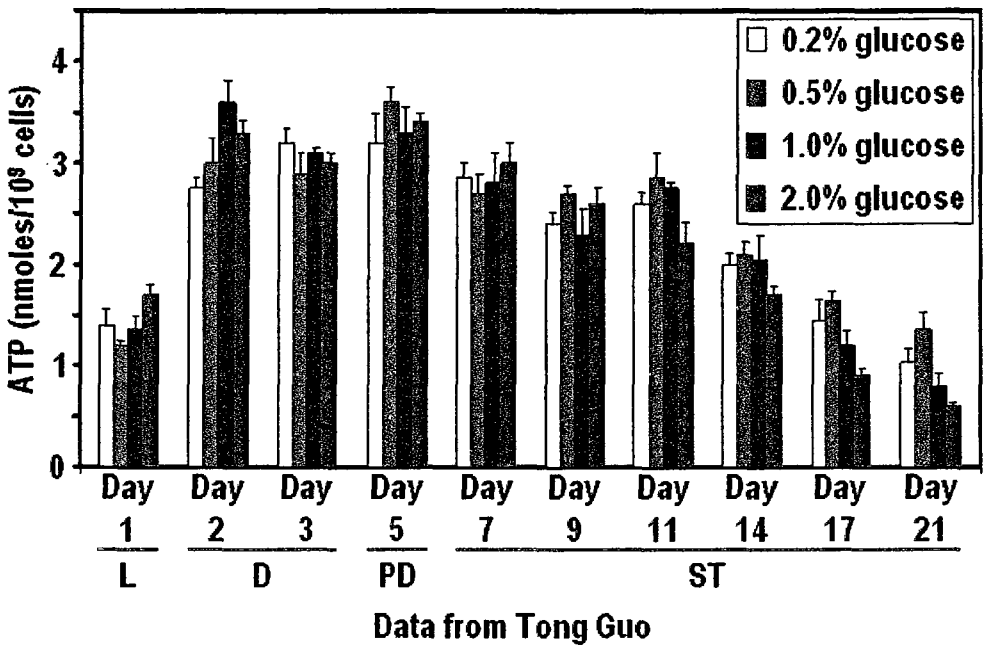

Figure 1.4. Intracellular levels of ATP and the dynamics of their change during chronological aging are very similar in CR and non-CR yeast.

Taken together, these findings imply that CR yeast must somehow remodel their metabolism to generate sufficient amounts of ATP, matching those observed in non-CR yeast, and that this CR-induced metabolic remodeling could lead to the observed life span extension.

The next section provides a detailed description on the experimental approaches used in Dr. Titorenko's laboratory to determine how yeast remodel their metabolism under CR conditions and how such remodeling modulates the age-dependent dynamics of longevity-related processes in yeast, including lipid and carbohydrate metabolism, ROS homeostasis, stability of nuclear and mitochondrial genomes, stress resistance, and apoptosis induced by stress and aging.

1.8 Using mass spectrometry-based proteomics for elucidating the mechanisms of longevity regulation in chronologically aging yeast

To define the metabolic remodeling responsible for the anti-aging effect of CR and to elucidate its regulatory mechanisms, Dr. Titorenko's laboratory employs various biochemical methods to compare CR and non-CR yeast recovered at different times of their chronological life span. in terms of their cellular and organellar proteomes, cellular and organellar lipidomes, cellular metabolomes, production of ROS, stability of nuclear and mitochondrial genomes, mitochondrial morphology, oxidation-reduction reactions in mitochondria, resistance to acute stress, age- and stress-induced apoptosis, and cell ultrastructure.

The goal of my graduate research was to use the yeast *S. cerevisiae* as a model system for identifying the key proteins controlling the rate of chronological aging. Using mass spectrometry, I compared the age-dependent dynamics of changes in cellular and organellar proteomes in CR and non-CR yeast recovered at different stages of their chronological aging. I then characterized the age-dependent dynamics of changes in cellular and organellar proteomes of the short-lived *pex5Δ* mutant strain grown under CR conditions to study the effect of peroxisomal fatty acid oxidation on age-related processes in chronologically aging yeast. I have identified numerous proteins that are enriched or depleted in total cell lysates as well as in purified mitochondria, lipid bodies and ER of *pex5Δ*, as compared to the wild-type strain of *S. cerevisiae* grown under CR conditions. In addition, I used mass spectrometry-based proteomics to monitor the effect of a novel anti-aging molecule recently identified in Dr. Titorenko's laboratory on the age-dependent dynamics of changes in cellular proteomes of chronologically aging yeast. The results of these studies, which are described and discussed in chapters 10 to 14 of the

thesis, strongly suggest that the chronological aging of yeast is a developmental program that integrates a distinct set of protein machines into what I call a modular longevity network.

1.9 Thesis outline and contributions of colleagues

I was able to define the molecular mechanisms regulating the fusion between P1 and P2 peroxisomes during the first post-ER step of the peroxisome biogenesis process in the yeast *Y. lipolytica.* A detailed description of my research findings on this topic has been published in *The Journal of Cell Biology* [116] and is presented in chapters 2 to 9 of this thesis with the Journal's permission. I contributed approximately 80% of all of the work described in this publication and prepared the first draft of the manuscript, while Dr. V. Titorenko provided intellectual leadership of this project and edited the manuscript. The numbering of figures and tables, as well as the format of abbreviations and citations presented in the paper have been changed to fit this thesis.

In chapters 10 to 14 of this thesis, I describe and discuss my findings on the molecular mechanisms regulating longevity in the yeast *S. cerevisiae.* Some of these findings are presented in two research articles that have been recently accepted for publication in *Biochemical Society Transactions* and *Experimental Gerontology*, whereas the other findings constitute an integral part of a manuscript that is currently in preparation for submission to the *PNAS USA*. I contributed approximately 50% of all of the work described in these three publications and am an equally contributed first co-author on all of them.

2 Pharmacological analysis of peroxisomal fusion

2.1 Introduction

Membrane fusion is an essential process required for the proper division of eukaryotic cells, their communication with the environment by hormones and neurotransmitters, their integration into multicellular organisms, and their invasion by enveloped viruses [125]. In addition, membrane fusion reactions are necessary for maintaining the structural integrity of organelles during mitosis and the vesicular flow between the organellar compartments of the secretory and endocytic pathways [126]. All membrane fusion reactions inside the secretory and endocytic systems are regulated by very similar mechanisms that require a common set of core proteins such as SNAREs [125]. However, the fusion of mitochondria and peroxisomes [36, 127] do not require intracellular fusion machines that function in the secretory and endocytic pathways and may therefore involve unique, yet unknown, mechanisms [125, 126].

In the yeast *Y. lipolytica*, the fusion of immature peroxisomal subforms P1 and P2 initiates the multi-step peroxisomal maturation process (Figure 1.1). It is driven by ATP hydrolysis, requires cytosolic proteins, and depends on the peroxins Pex1p and Pex6p, two AAA ATPases essential for peroxisome biogenesis [3, 18, 21, 23, 36, 40-42, 47, 61-63]. This fusion event is a multi-step process consisting of priming, docking and fusion stages (Figure 2.1) [62].

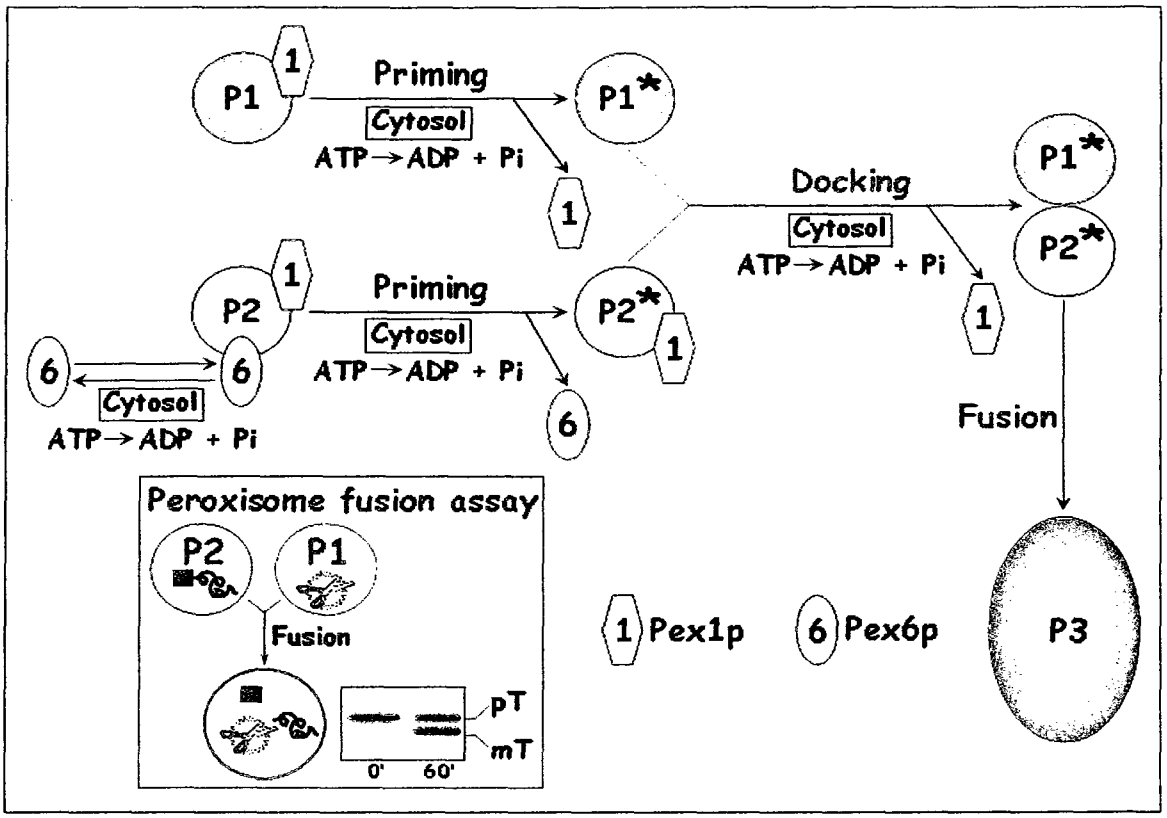

Figure 2.1. A model for the fusion of the peroxisomal subforms P1 and P2 in the yeast *Y. lipolytica*. This fusion is a multi-step process consisting of priming, docking and fusion events.

Before priming, Pex1p and Pex6p are bound to the outer face of both peroxisomal fusion partners [63]. The priming of P1 and P2 is driven by asymmetrical dissociation of these two ATPases from the surfaces of P1 and P2, which requires ATP hydrolysis and cytosolic proteins [63]. The subsequent release of Pex1p and Pex6p to the cytosol promotes the docking of primed peroxisomal fusion partners. During docking of primed P1 and P2, Pex1p is released from the surface of P2 in an ATP hydrolysis- and cytosol-dependent fashion [63]. Following the formation of a stable docking complex, P1 and P2 fuse to generate the peroxisomal subform P3. Fusion of docked P1 and P2 does not require ATP hydrolysis or cytosol [63]. P3 formed by the fusion between P1 and P2 undergoes a multi-step maturation into a fully functional peroxisome P6 through a multi-

step peroxisomal assembly pathway, as described previously (Figure 1.1) [18, 36, 40, 41, 42, 47, 61, 62].

The fusion of P1 and P2 has been reconstituted in vitro using an assay (Figure 2.1; see insert) that evaluates fusion efficiency by measuring the % conversion of thiolase, a peroxisomal matrix protein, from its precursor form (which is present only in P2) to its mature form by its proteolytic processing enzyme (which is present only in P1) [62, 63]. The availability of this rapid and quantitative in vitro fusion assay allowed me to identify several key protein and lipid compounds that are required for the fusion of P1 and P2 peroxisomes [63].

2.2 Materials and methods

Strains and growth media

The *Y. lipolytica* wild-type strain *P01d* (*MatA ura3-302 leu2-270 xpr2-302*) and mutant strain *pex5KO* (*MATA, ura3-302, leu2-270, lys8-11, pex5::LEU2*) [117] were grown in YPD media (2% glucose, 2% peptone, 1% yeast extract) to OD_{600} value of ~1.5 and then switched to YPBO media (1% oleic acid, 0.3% yeast extract, 0.5% peptone, 0.5% K_2HPO_4, 0.5% KH_2PO_4, 1% Brij-35) in order to induce peroxisome proliferation [118].

Subcellular fractionation of yeast cells

Subcellular compartments of YPBO-grown yeast cells were fractionated by differential centrifugation of lysed and homogenized cell spheroplasts at 1,000 x *g* for 8 min at 4°C using a Beckman JS13.1 rotor. The postnuclear supernatant (PNS) fraction was centrifuged further at 20,000 x *g* for 30 min at 4°C in a Beckman JS13.1 rotor, producing the pellet (20KgP) and supernatant (20KgS) fractions. The 20KgS fraction was

centrifuged at 200,000 x *g* for 1 h at 4°C using a TLA120.2 Beckman rotor yielding the pellet (200KgP) fraction, which contained immature peroxisomal subforms P1 to P5, and the supernatant (200KgS) fraction, which contained mature peroxisomal subform P6 [63].

Purification of P1 and P2 peroxisomal subforms

Immature peroxisomal subforms P1 through P5 were purified by centrifugation of the 200KgP fraction on a discontinuous sucrose gradient (18, 25, 30, 35, 40, and 53% sucrose, wt/wt) at 120,000 x *g* for 18 h at 4°C using a Beckman SW28 rotor. Thirty six fractions of 1 ml each were collected. Fractions containing different peroxisomal subforms were supplemented with 4 volumes of 0.5 M sucrose in buffer H (5 mM MES, pH 5.5; 1mM KCl; 0.5mM EDTA; 0.1% ethanol; protease inhibitors) [119]. Immature peroxisomes were pelleted onto a 150-µl layer of 2 M sucrose in buffer H by centrifugation at 200,000 x *g* for 20 min at 4°C using a Beckman TLA120.2 rotor. Pellets containing immature peroxisomal subforms P1 and P2 were resuspended in 3 ml of 50% (wt/wt) sucrose in buffer H, overlaid with 30%, 28%, 26%, 24%, 22%, and 10% (all wt/wt) sucrose in buffer H and centrifuged at 120,000 x *g* for 18 h at 4°C using a Beckman SW28 rotor. Eighteen fractions of 2 ml each were collected. Peroxisomes P1 and P2 were pelleted, resuspended and then centrifuged through the same multistep sucrose density gradient. Gradient fractions of 2 ml each were collected and peroxisomes P1 and P2 were pelleted, resuspended in T99 buffer (15 mM MES, pH 6.0; 100 mM KCl; 50 mM KOAc; 3 mM $MgCl_2$; 2 mM MgOAc) containing 250 mM sorbitol, washed twice in the same buffer and centrifuged as described above. Final suspensions of P1 and P2 in T99 buffer containing 250 mM sorbitol were used for the fusion assay [63].

In vitro peroxisome fusion assay

P1 peroxisomes were purified from unlabeled wild-type or *pex5KO Y. lipolytica* cells, whereas P2 peroxisomes were isolated from *pex5KO Y. lipolytica* cells labeled with L-[^{35}S] methionine for 30 min [118, 41]. Isolated peroxisomes P1 and P2 were individually incubated in PF buffer (T99 buffer containing 250 mM sorbitol; 1 mg cytosol/ml; 1 mM ATP; 40 mM creatine phosphate; 10 U creatine kinase/ml) for 5 min at 26°C with or without 300 μg nystatin/ml, 300 μg filipin III/ml, 300 μg amphotericin B/ml, 80 μM phosphoinositide-specific monoclonal antibodies, 1 mM ATPγS, 2 mM GTPγS or 3 mM GppNHp, in presence or absence of 1 mg/ml cytosol, which was prepared in ice-cold PF buffer [119]. Pretreated, unlabeled P1 peroxisomes were mixed with pretreated, labeled P2 peroxisomes and incubated for 90 min at 26°C [118]. Fusion reactions were stopped by incubation on ice for 3 min and then diluted 10-fold in ice-cold buffer D (15 mM MES, pH 6.0, 250 mM sorbitol, protease inhibitors). Peroxisomes P1 and P2 were re-isolated by centrifugation at 100,000 x *g* for 8 min at 4°C using a Beckman TLA120.2 rotor, resuspended in 400 μl of buffer D and re-pelleted. The precursor (pTHI) and mature (mTHI) forms of thiolase were immunoprecipitated under denaturing conditions using anti-THI antibodies covalently coupled to protein A–Sepharose [41, 63]. Immunoprecipitates were resolved by SDS-PAGE, visualized by fluorography using Amersham Biosciences ECL Western Blotting Detection Reagents and quantitated by densitometry. Digital images were acquired using the Bio-Rad VersaDoc Imaging System. Peroxisomal fusion efficiency was calculated based on percent conversion of pTHI to mTHI [118]. LiposoFast Liposome "Factory" (Avestin) system was used to construct uniformly-sized, unilamellar liposomes from PC with or without ergosterol (3:1

weight ratio), as described previously [122]. The liposomes were assembled according to manufacturer's instructions by extrusion through polycarbonate membranes with pore diameter of 100 nm.

2.3 Results

2.3.1 Presence of ergosterol in the membranes of both fusion partners is required for peroxisomal fusion in vitro

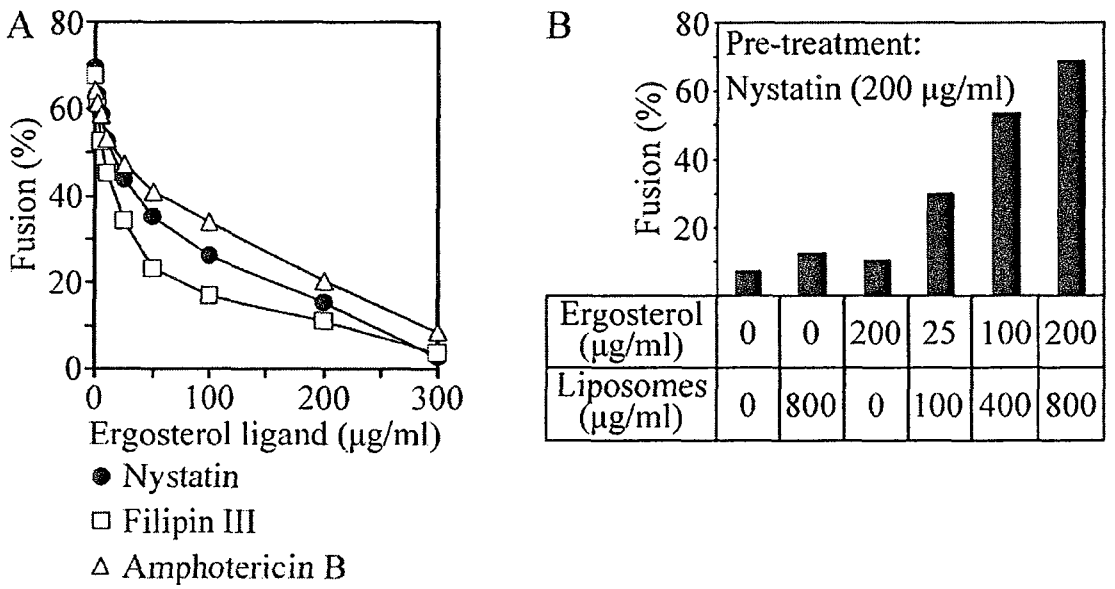

Figure 2.2. Peroxisome fusion can be reversibly inhibited by ergosterol ligands nystatin, fillipin III and amphotericin B. (A) P1 and P2 were preincubated individually for 5 min at 26°C without inhibitor or with the indicated amounts of ergosterol ligands. Pretreated P1 and P2 were then mixed and supplemented with cytosol and ATP to yield standard fusion reactions. After a 90-min incubation at 26°C, the percent conversion of the precursor form of thiolase to its mature form as a measure of fusion was calculated. (B) P1 and P2 were preincubated individually for 5 min at 26°C with nystatin (200 μg/ml). Pretreated P1 and P2 were then mixed. The samples were supplemented with cytosol and ATP to yield standard fusion reactions and incubated at 26°C in the presence or absence of liposomes without or with the indicated amounts of ergosterol. After a 90-min incubation, fusion efficiency was measured.

2.3.2 Peroxisomal fusion depends on phosphoinositides PI(4)P and PI(4,5)P_2

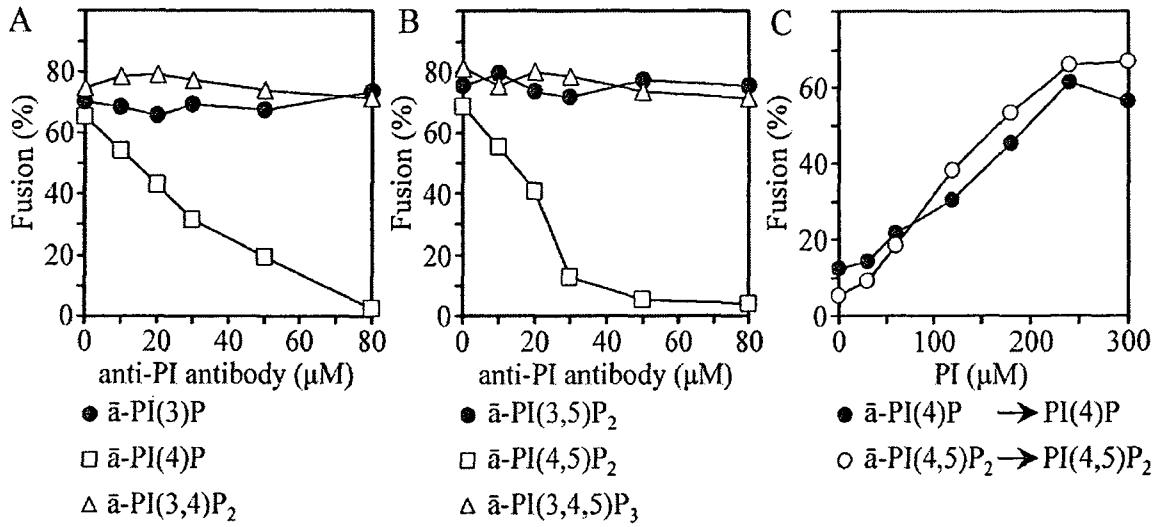

Figure 2.3. Antibodies to PI(4)P (A) and PI(4,5)P_2 (B) inhibit peroxisome fusion in a reversible manner (C). (A and B) P1 and P2 were preincubated individually for 5 min at 26°C without inhibitor or with the indicated amounts of phosphoinositide-specific antibodies (ā). Pretreated P1 and P2 were then mixed and supplemented with cytosol and ATP to yield standard fusion reactions. After a 90-min incubation at 26°C, the percent conversion of the precursor form of thiolase to its mature form as a measure of fusion was calculated. (C) P1 and P2 were preincubated individually for 5 min at 26°C antibodies to PI(4)P (60 μM) or to PI(4,5)P_2 (60 μM). Pretreated P1 and P2 were then mixed. The samples were supplemented with cytosol and ATP to yield standard fusion reactions and incubated at 26°C without or with the indicated amounts of PI(4)P or PI(4,5)P_2. After a 90-min incubation, fusion efficiency was measured.

2.3.3 Peroxisomal fusion requires the hydrolysis of GTP

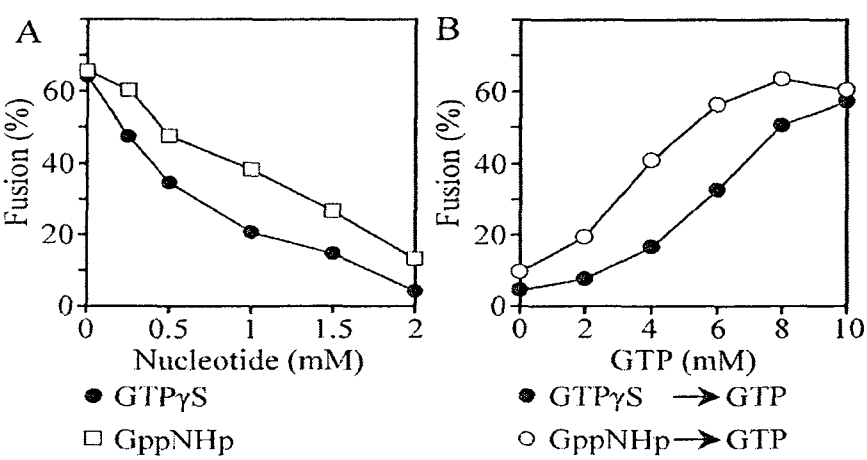

Figure 2.4. Nonhydrolyzable GTP analogues GTPγS and GppNHp inhibit peroxisome fusion (A) in a reversible manner (B). (A) P1 and P2 were preincubated individually for 5

min at 26°C without inhibitor or with the indicated amounts of nonhydrolyzable GTP analogs. Pretreated P1 and P2 were then mixed and supplemented with cytosol and ATP to yield standard fusion reactions. After a 90-min incubation at 26°C, the percent conversion of the precursor form of thiolase to its mature form as a measure of fusion was calculated. (B) P1 and P2 were preincubated individually for 5 min at 26°C with GTPγS (2 mM) or GppNHp (2 mM). Pretreated P1 and P2 were then mixed. The samples were supplemented with cytosol and ATP to yield standard fusion reactions and incubated at 26°C without or with the indicated amounts of GTP. After a 90-min incubation, fusion efficiency was measured.

2.4 Discussion

I found that peroxisomal fusion was inhibited by nystatin, filipin III, and amphotericin B (Figure 2.2A), each known for its propensity to sequester sterol lipids but not fully remove them from the membrane [123, 124]. The inhibitory effect of these ergosterol ligands on peroxisome fusion was specific as it could be reversed by phosphatidylcholine (PC)-based liposomes with ergosterol, but not by PC-based liposomes without it (Figure 2.2B). Moreover, neither of these drugs caused the dissipation of the existing Ca^{2+} gradient across the peroxisomal membrane, suggesting that the inhibitory effect of these compounds on peroxisomal fusion was not due to the impairment of overall peroxisome integrity (unpublished data from Dr. Titorenko's laboratory). Based on these findings, I concluded that ergosterol plays a specific role in the fusion of P1 and P2 peroxisomes. On note, cholesterol has been previously implicated in modulating membrane fusion during viral entry into the host organism [128]. Furthermore, studies in yeast revealed that all of the ergosterol biosynthesis enzymes are required for the proper maintenance of mitochondrial morphology, suggesting that ergosterol may also be involved in regulation of mitochondrial fusion [129, 130].

The fusion of P1 and P2 was also inhibited by monoclonal antibodies to the membrane phosphoinositides phosphatidylinositol (PI)-4-phosphate (PI(4)P) and PI-4,5-

bisphosphate ($PI(4,5)P_2$) (Figures 2.3A and 2.3B). I found that the negative effect of these antibodies on peroxisome fusion could be reversed by externally added PI(4)P and $PI(4,5)P_2$, respectively (Figure 2.3C). In contrast, monoclonal antibodies to any other phosphoinositide tested did not affect peroxisome fusion (Figures 2.3A and 2.3B), showing the specificity of its inhibition by ligands of PI(4)P and $PI(4,5)P_2$. Therefore, only these two phosphoinositides are needed for the fusion of P1 and P2. Noteworthy, a recent study of proteins interacting with $PI(4,5)P_2$ revealed 44 proteins that regulate ion transport and trafficking events, some of which also play an important role in membrane fusion and exocytosis [131]. Phosphoinositides also regulate a spatiotemporal organization of signal transduction pathways, either through direct interaction with proteins or as precursors of secondary messengers [133-136]. Furthermore, signal transduction pathways mediated by phosphoinositides are involved in key cellular processes such as vesicle and membrane trafficking, exocytosis and secretion, cell adhesion and migration, reorganization of actin skeleton, cellular proliferation, metabolism and apoptosis [138-142].

I also found that two nonhydrolyzable GTP analogs, GTPγS and GppNHp, are reversible inhibitors of peroxisome fusion. Importantly, their negative effect on the fusion can be overturned by reisolating pretreated P1 and P2 and resuspending them in the standard fusion reaction mixture supplemented with GTP (Figures 2.4A and 2.4B). These data suggest that GTP hydrolysis by GTPase(s) is required for peroxisome fusion. Of note, recent studies in *Xenopus laevis* demonstrated that GTP hydrolysis is also required for vesicle fusion during nuclear envelope assembly [132]. Moreover, GTP hydrolysis is

also essential for successful docking and fusion events during homotypic vacuole fusion in yeast [143].

2.5 Conclusions

My pharmacological analysis of peroxisome fusion in vitro provided the first evidence that, in addition to ATP hydrolysis and cytosolic proteins, the fusion of P1 and P2 peroxisomes requires ergosterol, the membrane phosphoinositides PI(4)P and PI(4,5)P_2 and GTP hydrolysis. In order to establish the roles of these compounds in peroxisome fusion, I next examined their contribution to the individual stages of the fusion process. The results of these studies are discussed below.

3 Dynamics of peroxisome priming

3.1 Introduction

Fusion of P1 and P2 is a multistep process that includes priming, docking and fusion events [62, 63]. Priming (activation) of P1 and P2 prior to their physical contact commits both fusion partners to subsequent docking. Priming requires two AAA ATPases, Pex1p and Pex6p [62, 63]. Before priming, Pex1p is associated with the cytosolic surface of P1, while Pex1p and Pex6p are bound to the outer face of P2 [63]. During priming, ATP hydrolysis triggers cytosol-dependent release of Pex1p from P1 and of Pex6p from P2, whereas P2-associated Pex1p remains bound to the organelle [63]. Using an in vitro peroxisome fusion assay, I evaluated the requirements for the release of AAA ATPases during peroxisome priming. The extent of release of Pex1p from P1 and of Pex6p from P2 is known to be a measure of priming efficiency [62].

3.2 Materials and methods

In vitro assay for the release of Pex1p and Pex6p from P1 and P2

L-[^{35}S] methionine-labeled P1 and P2 were individually incubated for 5 min at 26°C in PF buffer with or without 300 μg nystatin/ml, 300 μg filipin III/ml, 300 μg amphotericin B/ml, 80 μM phosphoinositide-specific monoclonal antibodies, 1 mM ATPγS, 2 mM GTPγS or 3 mM GppNHp, in presence or absence of 1 mg/ml cytosol. Pretreated peroxisomes P1 and P2 were supplemented with 1 mM ATP, 40 mM creatine phosphate and 10 U creatine kinase/ml, and incubated individually for 10 min at 26°C with or without 1 μg unlabeled cytosol/ml. P1 and P2 were re-isolated by centrifugation at 100,000 x *g* for 5 min at 4°C using a Beckman TLA120.2 rotor. Proteins from pellet and supernatant fractions were immunoprecipitated under denaturing conditions with protein A-Sepharose-linked anti-Pex1p and/or anti-Pex6p antibodies, resuspended in 400 μl of buffer D and re-pelleted.

Immunoaffinity chromatography

Peroxisomal proteins recovered from pellet and supernatant fractions in the in vitro assay for the release of Pex1p and Pex6p from P1 and P2 were subjected to immunoaffinity chromatography under denaturing conditions. Anti-Pex1p and anti-Pex6p antibodies were covalently linked to protein A-Sepharose [121]. Protein samples in PF buffer were diluted in equal volumes of 4% SDS, heated for 10 min at 65°C, cooled to room temperature and treated with four volumes of 62.5 mM Tris-HCl (pH 7.5) buffer containing 190 mM NaCl, 1.25% (vol/vol) Triton X-100 and 6 mM EDTA. Non-specific binding of proteins was eliminated by incubating samples for 20 min at 4°C with protein A-Sepharose that was washed five times with 10 mM Tris-HCl (pH 7.5) buffer. Proteins

specifically bound by protein A-Sepharose were washed five times with 50 mM Tris-HCl (pH 7.5) buffer containing 150 mM NaCl and 1% (vol/vol) Triton X-100. Washed proteins were eluted with 2% SDS solution for 5 min at 95°C, resolved by SDS-PAGE and visualized by fluorography [118].

Protein-lipid overlay assay

P1 and P2 were purified from L-[^{35}S] methionine-labeled cells and osmotically lysed. Peroxisomal membranes were pelleted by centrifugation and subjected to a protein-lipid overlay assay to estimate the phospholipids-binding specificity of peroxisomal membrane proteins. Peroxisomal membrane pellets were resuspended in TBSO buffer (10 mM Tris-HCl (pH 8.0), 150 mM NaCl and 0.5% n-OG), incubated on ice for 30 min and centrifuged at 100,000 x *g* for 30 min at 4°C. Supernatants of n-OG-solubilized membrane proteins were incubated at 5 μg/ml with the PIP-Strip (Echelon Biosciences) at 4°C overnight. The PIP-Strips were then washed five times with TBSO buffer, and binding of phospholipids to peroxisomal membrane proteins was visualized by autoradiography.

Detergent solubility of PI(4)P- and PI(4,5)P_2-binding proteins was evaluated by spotting 100 pmol of PI(4)P- and PI(4,5)P_2 on nitrocellulose membrane arrays and using the cut-out spots containing single phosphoinositides in the protein-lipid overlay assay. Membrane pellets recovered after centrifugation of osmotically lysed P1 and P2 were resuspended in ice-cold MBS buffer with or without the detergent of interest. Samples were incubated on ice for 30 min and centrifuged at 100,000 x *g* for 30 min at 4°C.

Supernatants of n-OG-solubilized membrane proteins were then used to perform the protein-lipid overlay assay as described previously.

The levels of PI(4)P- and PI(4,5)P_2-binding proteins in fractions of flotation gradients used for the fractionation of Brij 35-treated membranes of P1 and P2 were evaluated by spotting 100 pmol of PI(4)P- and PI(4,5)P_2 on nitrocellulose membrane arrays and using the cut-out spots containing single phosphoinositides in the protein-lipid overlay assay. Equal volumes of flotation gradient fractions were diluted with nine volumes of TBSO buffer and then processed for the protein-lipid overlay assay as described previously.

3.3 Results

3.3.1 The release of Pex1p from P1 and Pex6p from P2 requires ergosterol, PI(4)P, PI(4,5)P_2, cytosolic proteins and ATP hydrolysis but does not depend on GTP hydrolysis

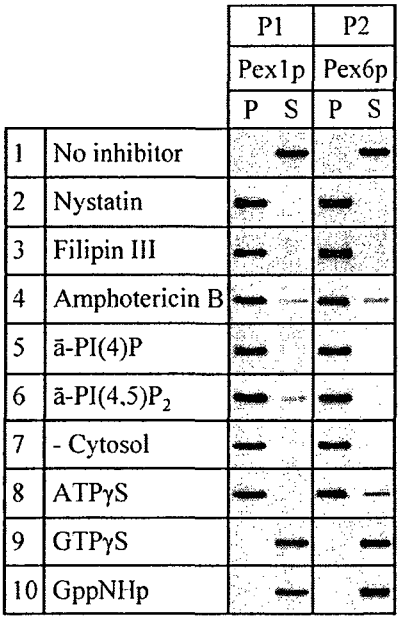

Figure 3.1. Effect of various inhibitors of peroxisome fusion on the release of Pex1p from P1 and Pex6p from P2 during priming of both fusion partners. *L*-[^{35}S]methionine-

labeled P1 and *L*-[^{35}S]methionine-labeled P2 were preincubated individually for 5 min at 26°C with or without nystatin (an ergosterol ligand), phosphoinositide-specific antibodies, ATPγS, or nonhydrolyzable GTP analogs. Pretreated P1 and P2 were then supplemented with ATP and incubated individually in the presence or absence of unlabeled cytosol, as indicated. After a 10-min incubation at 26°C, peroxisomal vesicles were pelleted. Pex1p and Pex6p were immunoprecipitated under denaturing conditions from the pellet (P) and supernatant (S) fractions. Immunoprecipitates were resolved by SDS-PAGE and visualized by fluorography.

3.3.2 During peroxisome priming, membrane proteins of P1 and P2 bind specifically to PI(4)P and PI(4,5)P_2 and remain attached to the cytosolic surfaces of P1 and P2 through electrostatic interactions

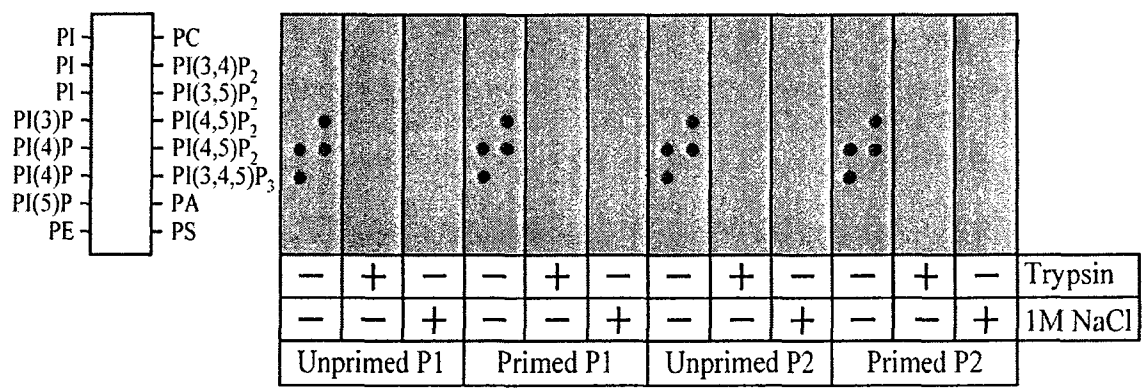

Figure 3.2. Testing the ability of P1- and P2-associated proteins to bind to various phosphoinositides and phospholipids and assessing the topology of the association of PI(4)P- and PI(4,5)P_2 –binding proteins with both fusion partners during their priming. Intact P1 and P2 labeled with *L*-[^{35}S]methionine were primed individually by incubation with unlabeled cytosol and ATP or remained unprimed. Equal aliquots of primed and unprimed peroxisomes (30 μg of protein per aliquot) were treated with 30 μg of trypsin or 1 M NaCl for 30 min on ice. Peroxisomes were then osmotically lysed and subjected to centrifugation. The pellet of membranes recovered after such centrifugation was solubilized with a detergent, n-octyl-β-D-glucopyranoside. Detergent-soluble membrane proteins were analyzed by protein-lipid overlay assay using commercial PIP-Strips. Lipid-binding proteins were visualized by autoradiography.

3.3.3 During peroxisome priming, GTP-binding proteins are permanently attached, through non-electrostatic interactions, only to the cytosolic surface of P1, but do not associate with P2

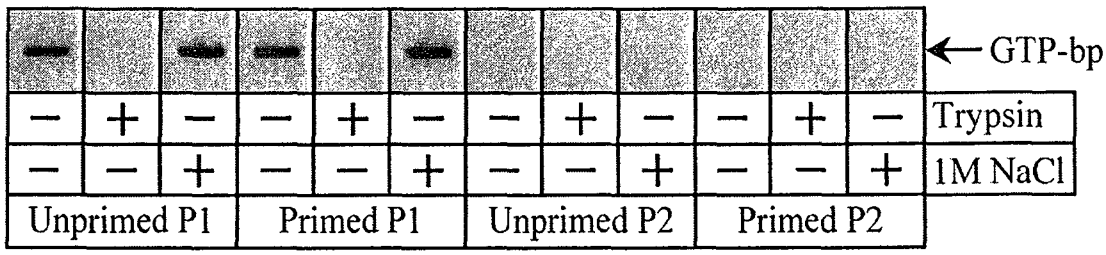

Figure 3.3. Testing the ability of P1- and P2-associated proteins to bind to GTP and assessing the topology of the association of GTP-binding proteins (GTP-bp) with P1 during its priming. Unlabeled intact P1 and P2 were primed individually by incubation with unlabeled cytosol and ATP or remained unprimed. Equal aliquots of primed and unprimed peroxisomes (30 μg of protein per aliquot) were treated with 30 μg of trypsin or 1 M NaCl for 30 min on ice. Peroxisomes were then osmotically lysed and subjected to centrifugation. The pellet of membranes recovered after such centrifugation was solubilized with a detergent, n-octyl-β-D-glucopyranoside. Detergent-soluble membrane proteins were analyzed by GTP slot-blot with guanosine 5'-[α-^{32}P]triphosphate. GTP-bp were visualized by autoradiography.

3.4 Discussion

My data provide evidence that priming of both fusion partners requires 1) cytosolic proteins; 2) ATP hydrolysis; 3) a particular type of AAA ATPase (Pex1p for P1 and Pex6p for P2); 4) ergosterol; and 5) PI(4)P and PI(4,5)P_2 (Figure 3.1). However, priming of P1 and P2 does not depend on GTP hydrolysis (Figure 3.1).

The observed susceptibility of peroxisome fusion to anti-PI(4)P and anti-PI(4,5)P_2 antibodies suggests that PI(4)P- and PI(4,5)P_2-binding proteins (bp) associate with P1 and/or P2. Using PIP-Strips spotted with various phosphoinositides and phospholipids, I demonstrated that membrane proteins of P1 and P2 solubilized with a detergent, n-octyl-β-D-glucopyranoside (n-OG), bind only to PI(4)P and PI(4,5)P_2 but not to any other phosphoinositide or phospholipid tested (Figure 3.2). PI(4)P- and PI(4,5)P_2-bp of intact

peroxisomes were sensitive to digestion by external protease and were completely solubilized by 1 M NaCl (Figure 3.2). Thus, these proteins are attached to the cytosolic surfaces of P1 and P2 through electrostatic interactions. Importantly, I found that neither PI(4)P- nor PI(4,5)P_2-bp release from the outer faces of P1 and P2 during their priming (Figure 3.2).

Peroxisome fusion was sensitive to nonhydrolyzable GTP analogs, suggesting the involvement of P1- and/or P2-attached GTP-binding and hydrolyzing proteins in this process. The association of GTP-bp with P1 was confirmed by GTP slot-blot (Figure 3.3). The observed susceptibility of the P1-attached GTP-bp to digestion by trypsin added to intact P1 and the inability of 1 M NaCl to solubilize the GTP-bp (Figure 3.3) imply that the association of GTP-bp with the outer face of P1 is not due to electrostatic interactions. Importantly, I found that GTP-bp does not release from the outer face of P1 vesicles during its priming (Figure 3.3).

3.5 Conclusions

Altogether, my findings provide evidence that the release of AAA ATPases Pex1p and Pex6p from the cytosolic surfaces of P1 and P2 peroxisomes, a hallmark event of peroxisome priming for docking, requires ergosterol, PI(4)P, PI(4,5)P_2, cytosolic proteins and ATP hydrolysis but does not depend on GTP hydrolysis. Furthermore, both fusion partners have PI(4)P and PI(4,5)P_2-bp attached to their outer faces. Moreover, the cytosolic surface of P1 (but not of P2) carries GTP-bp. It should be stressed that neither PI(4)P-, PI(4,5)P_2- nor GTP-bp dissociate from the cytosolic surfaces of P1 and P2 during their priming for docking, suggesting that they might be required on the

subsequent membrane docking and/or merging steps of the peroxisome fusion process. The importance of PI(4)P-, PI(4,5)P_2- nor GTP-bp in membrane docking and merging is addressed in the following chapters of the thesis.

4 Dynamics of peroxisome docking

4.1 Introduction

Following their priming, peroxisomes P1 and P2 form a stable docking complex, called P1/P2, in the presence of ATP and cytosolic proteins [62, 63]. The docking of P1 and P2 is characterized by the release of Pex1p from the surface of P2, which is driven by ATP hydrolysis and requires cytosolic proteins [62]. The formation of the docking complex P1/P2 can be reconstituted in vitro by first individually priming P1 and P2 with ATP and cytosol and then incubating the pre-primed fusion partners together in the presence of ATP and cytosol [62, 63]. The P1/P2 docking complex can then be separated from undocked P1 and P2 peroxisomes, as well as from the fusion product P3, by flotation on a multistep sucrose gradient [62, 63]. The requirements for docking of P1 and P2 can therefore be evaluated using a previously described in vitro assay, in which the efficiency of peroxisome docking for fusion is assessed by monitoring the extent of the recovery of P1/P2 in the flotation gradient [62, 63]. In addition, by evaluating the effect of various compounds on the release of Pex1p from individually pre-primed P2 following their addition to separately pre-primed P1, the requirements for this hallmark event of peroxisome docking for fusion can be established.

4.2 Materials and methods

In vitro assay for peroxisome docking

P1 and P2 vesicles were individually preprimed by incubation in PF buffer (15 mM MES, pH 6.0, 100 mM KCl, 50 mM KOAc, 3 mM $MgCl_2$, 2 mM MgOAc) containing 250 mM sorbitol, 1 mg cytosol/ml, 1 mM ATP, 40 mM creatine phosphate, and 10 U creatine kinase/ml. After incubation for 10 min at 26°C, peroxisomal vesicles were pelleted by centrifugation at 100,000 × g for 5 min at 4°C in a TLA120.2 rotor, resuspended in ice-cold PF buffer containing 250 mM sorbitol, and repelleted. Peroxisomal vesicles were then resuspended in PF buffer supplemented with 250 mM sorbitol and incubated individually with or without 300 μg nystatin/ml, 80 μM phosphoinositide-specific monoclonal antibodies, 2 mM GTPγS or 1 mM ATPγS, in the presence or absence of 1 mg cytosol/ml, as indicated. After incubation for 5 min at 26°C, P1 and P2 were mixed and supplemented with 1 mM ATP, 40 mM creatine phosphate and 10 U creatine kinase/ml. After a 10-min incubation at 26°C, a 80-μl sample of peroxisomal vesicles was transferred to the bottom of a 5-ml ultraclear centrifuge tube (Beckman) and supplemented with 4 volumes of 62.5% (w/w) sucrose in ice-cold PF buffer in order to adjust the sucrose concentration of the sample to 50% (w/w). The sample was then overlaid with 500 μl of 30% sucrose, 600 μl of 28% sucrose, 1 ml of 26% sucrose, 1 ml of 24% sucrose, 1 ml of 22% sucrose, and 500 μl of 10% sucrose (all w/w in PF buffer). After centrifugation at 200,000 × g for 18 h at 4°C in a SW50.1 rotor (Beckman), 9 fractions of 555 μl each were collected. Proteins recovered in equal volumes of gradient fractions were precipitated by adding 6 volumes of acetone, resolved by SDS-PAGE, and then visualized by immunoblotting with anti-Pex1p, anti-Pex16p and anti-thiolase

antibodies. Equal volumes of gradient fractions were also subjected to the protein-lipid overlay assay, GTP slot-blot, lipid extraction, and thin-layer chromatography.

In vitro assay of association of Pex1p with P2 during peroxisome docking

P1 and P2 were individually preprimed by incubation with cytosol and ATP for 10 min at 26°C. Peroxisomal vesicles were then reisolated by centrifugation, washed, and resuspended in buffer. Reisolated P1 and P2 were incubated individually for 5 min at 26°C with or without ergosterol ligands, phosphoinositide-specific antibodies, ATPγS, or nonhydrolyzable GTP analogs in the presence or absence of cytosol, as indicated. P1 and P2 were then mixed and supplemented with ATP. Following a 10-min incubation at 26°C, peroxisomal vesicles were subjected to centrifugation to yield supernatant and pellet fractions. Recovered proteins were resolved by SDS-PAGE and immunoblotted with antibodies to Pex1p.

In vitro assay of association of lipid- and GTP-bp with P1 and P2 during peroxisome docking

Intact P1 and P2, either labeled with *L*-[^{35}S]methionine or unlabeled, were primed individually by incubation with cytosol and ATP for 10 min at 26°C. Peroxisomal vesicles were then reisolated by centrifugation, washed, and resuspended in buffer. Preprimed P1 and P2 were mixed and supplemented with ATP. After a 10-min incubation at 26°C, peroxisomal vesicles were osmotically lysed and subjected to centrifugation to yield supernatant (matrix proteins) and pellet (membrane proteins) fractions. Pelleted membrane proteins were solubilized with a detergent, n-OG. Detergent-soluble membrane proteins were analyzed by protein-lipid overlay assay using commercial PIP-

Strips or by GTP slot-blot with guanosine 5'-[α-^{32}P]triphosphate. Lipid- and GTP-binding proteins were visualized by autoradiography.

To evaluate the requirements for the release of PI(4,5)P_2-bp from P1 and P2 during peroxisome priming, *L*-[^{35}S]methionine-labeled P1 and P2 were individually preprimed by incubation with cytosol and ATP for 10 min at 26°C. Peroxisomal vesicles were then reisolated by centrifugation, washed, and resuspended in buffer. Reisolated P1 and P2 were incubated individually for 5 min at 26°C with or without nystatin, GTPγS, ATPγS, or anti-Pex1p antibodies in the presence or absence of cytosol, as indicated. P1 and P2 were then mixed and supplemented with ATP. Following a 10-min incubation at 26°C, peroxisomal vesicles were osmotically lysed and subjected to centrifugation to yield supernatant (matrix proteins) and pellet (membrane proteins) fractions. Pelleted membrane proteins were solubilized with n-OG. Detergent-soluble membrane proteins were analyzed by protein-lipid overlay assay using commercial PIP-Strips. Lipid-binding proteins were visualized by autoradiography.

4.3 Results

4.3.1 Peroxisome docking requires ergosterol, PI(4,5)P_2, cytosolic proteins and the hydrolysis of ATP and GTP

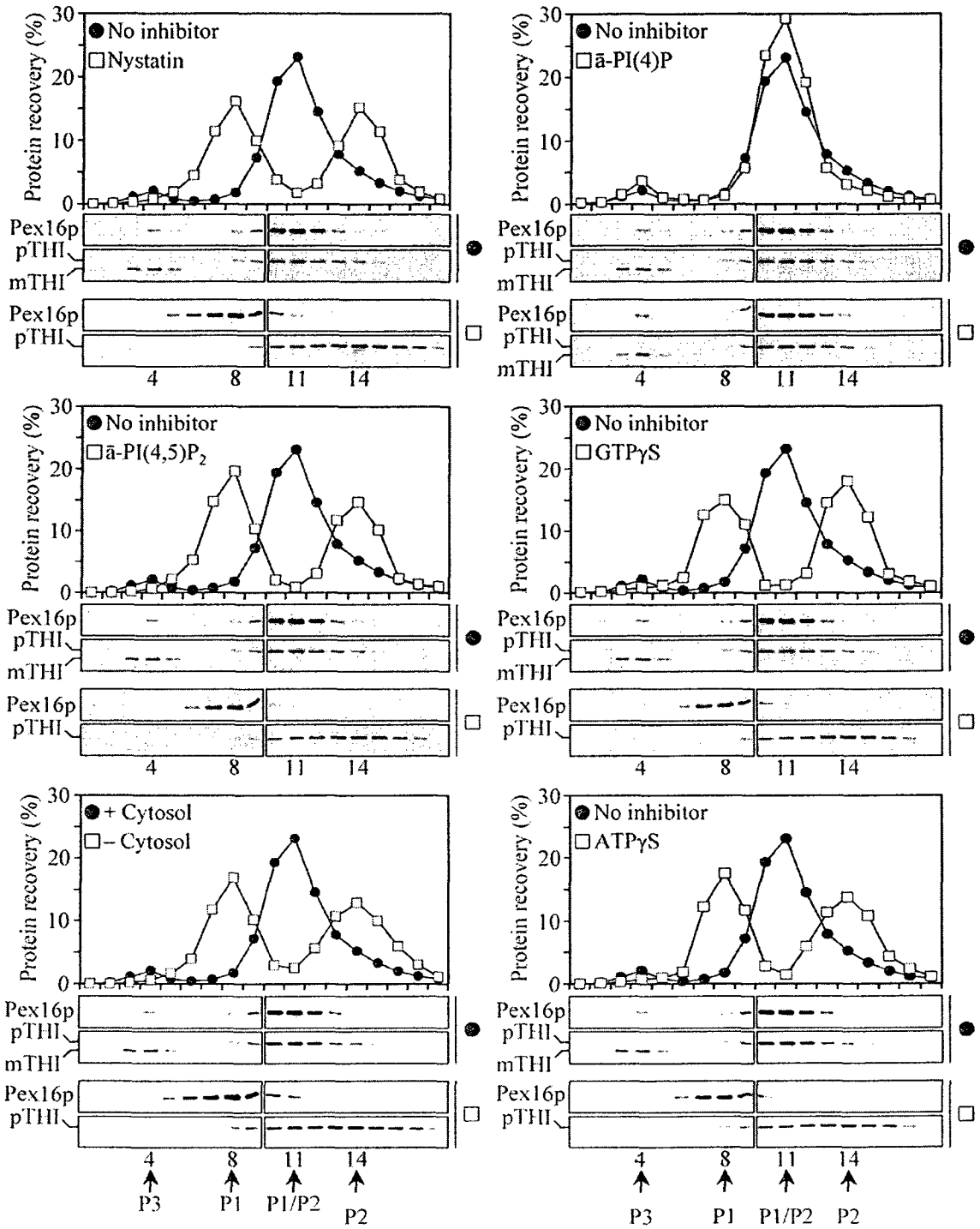

Figure 4.1. Peroxisome docking is inhibited by the ergosterol ligand nystatin, antibodies specific to PI(4,5)P_2, absence of cytosol, nonhydrolyzable GTP analogue GTPγS and

nonhydrolyzable ATP analogue ATPγS. P1 and P2 were individually preprimed by incubation with cytosol and ATP for 10 min at 26°C. Peroxisomal vesicles were then reisolated by centrifugation, washed, and resuspended in buffer. Reisolated P1 and P2 were incubated individually for 5 min at 26°C with or without nystatin, phosphoinositide-specific monoclonal antibodies, GTPγS, or ATPγS in the presence or absence of cytosol, as indicated. P1 and P2 were then mixed and supplemented with ATP. After a 10-min incubation at 26°C, peroxisomal vesicles were subjected to fractionation by flotation on a multistep sucrose gradient. The percent recovery of loaded protein is presented. Equal volumes of gradient fractions were analyzed by immunoblotting with anti-Pex16p and anti-THI antibodies. The peak fractions for P1 and P2, their docking complex (P1/P2) and the product of their fusion (P3) are indicated. The positions of pTHI, which was found in P2 and P1/P2, and of mTHI, which was associated with P3, are shown.

4.3.2 The docking-specific release of P2-associated Pex1p from the membrane to the cytosol depends on ergosterol, cytosolic proteins, and the hydrolysis of ATP and GTP, but does not require PI(4)P or PI(4,5)P_2

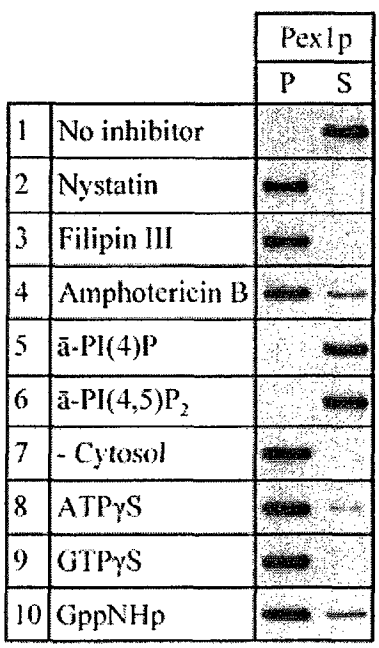

Figure 4.2. The docking-specific release of Pex1p from P2 to the cytosol is inhibited by several ergosterol ligands, the absence of cytosol, nonhydrolyzable analogues of ATP and GTP, but not by antibodies specific to PI(4)P or PI(4,5)P_2. P1 and P2 were individually preprimed by incubation with cytosol and ATP for 10 min at 26°C. Peroxisomal vesicles were then reisolated by centrifugation, washed, and resuspended in buffer. Reisolated P1 and P2 were incubated individually for 5 min at 26°C with or without ergosterol ligands, phosphoinositide-specific antibodies, ATPγS, or nonhydrolyzable GTP analogs in the presence or absence of cytosol, as indicated. P1 and P2 were then mixed and

supplemented with ATP. Following a 10-min incubation at 26°C, peroxisomal vesicles were subjected to centrifugation to yield supernatant (S) and pellet (P) fractions. Recovered proteins were resolved by SDS-PAGE and immunoblotted with antibodies to Pex1p.

4.3.3 Docking-specific dissociation of PI(4,5)P_2-bp from the membranes of both fusion partners depends on ergosterol, GTP hydrolysis, cytosolic proteins, ATP hydrolysis and Pex1p

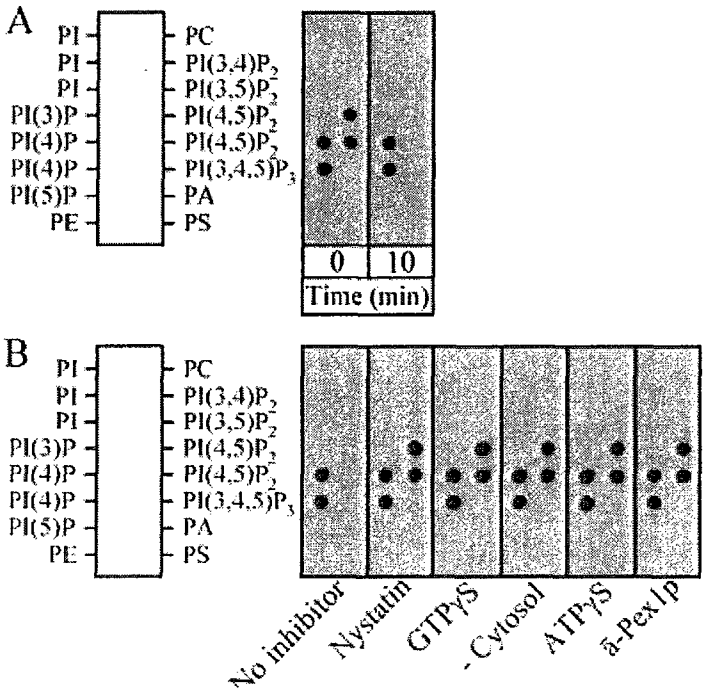

Figure 4.3. Docking-specific dissociation of PI(4,5)P_2-bp from the membranes of both fusion partners (A) is inhibited by the ergosterol ligand nystatin, the absence of cytosol, nonhydrolyzable analogues of ATP and GTP, and antibodies specific to Pex1p (B). (A) Intact P1 and P2 labeled with *L*-[^{35}S]methionine were primed individually by incubation with cytosol and ATP for 10 min at 26°C. Peroxisomal vesicles were then reisolated by centrifugation, washed, and resuspended in buffer. Preprimed P1 and P2 were mixed and supplemented with ATP. After a 10-min incubation at 26°C, peroxisomal vesicles were osmotically lysed and subjected to centrifugation to yield supernatant (matrix proteins) and pellet (membrane proteins) fractions. Pelleted membrane proteins were solubilized with a detergent, n-OG. Detergent-soluble membrane proteins were analyzed by protein-lipid overlay assay using commercial PIP-Strips. Lipid-binding proteins were visualized by autoradiography. (B) *L*-[^{35}S]methionine-labeled P1 and P2 were individually preprimed by incubation with cytosol and ATP for 10 min at 26°C. Peroxisomal vesicles were then reisolated by centrifugation, washed, and resuspended in buffer. Reisolated P1 and P2 were incubated individually for 5 min at 26°C with or without nystatin, GTPγS,

ATPγS, or anti-Pex1p antibodies in the presence or absence of cytosol, as indicated. P1 and P2 were then mixed and supplemented with ATP. Following a 10-min incubation at 26°C, peroxisomal vesicles were osmotically lysed and subjected to centrifugation to yield supernatant (matrix proteins) and pellet (membrane proteins) fractions. Pelleted membrane proteins were solubilized with n-OG. Detergent-soluble membrane proteins were analyzed by protein-lipid overlay assay using commercial PIP-Strips. Lipid-binding proteins were visualized by autoradiography.

4.3.4 GTP-bp remain associated with the membrane of P1 during peroxisome docking

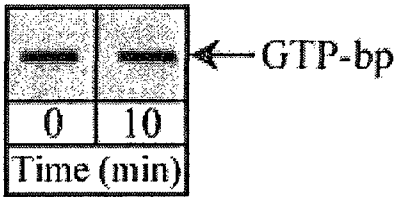

Figure 4.4. During docking of primed P1 and P2, GTP-bp do not dissociate from the surface of P1. Unlabeled intact P1 and P2 were primed individually by incubation with cytosol and ATP for 10 min at 26°C. Peroxisomal vesicles were then reisolated by centrifugation, washed, and resuspended in buffer. Preprimed P1 and P2 were mixed and supplemented with ATP. After a 10-min incubation at 26°C, peroxisomal vesicles were osmotically lysed and subjected to centrifugation to yield supernatant (matrix proteins) and pellet (membrane proteins) fractions. Pelleted membrane proteins were solubilized with a detergent, n-OG. Detergent-soluble membrane proteins were analyzed by GTP slot-blot with guanosine 5'-[α-^{32}P]triphosphate. GTP-binding proteins were visualized by autoradiography.

4.4 Discussion

I found that the formation of the P1/P2 docking complex between primed P1 and P2 was compromised when primed peroxisomes P1 and P2 were individually treated with the ergosterol ligand nystatin, monoclonal antibodies to PI(4,5)P_2, GTPγS, ATPγS, or in the absence of cytosol, prior to being mixed to initiate their docking (Figure 4.1). These findings suggest that the peroxisome docking process cannot proceed without ergosterol, PI(4,5)P_2, GTP hydrolysis, ATP hydrolysis and cytosolic proteins. Furthermore, I demonstrated that the release of Pex1p from P2 to the cytosol, a hallmark event of peroxisome docking, requires ergosterol, cytosolic proteins, ATP and GTP hydrolysis,

but does not depend on PI(4)P- or PI(4,5)P_2-bp (Figure 4.2). In addition, I found that PI(4,5)P_2-bp, but not PI(4)P-bp, dissociated from the outer faces of both fusion partners during the docking process (Figure 4.3A), and that this release depends on ergosterol, hydrolysis of ATP and GTP, cytosolic proteins, as well as Pex1p (Figure 4.3B). In contrast, GTP-bp remained associated to the outer face of P1 peroxisomes during and after the docking process (Figure 4.4), suggesting that GTP hydrolysis might be required for the fusion of docked P1 and P2. Of note, studies of vacuole fusion in yeast provided evidence that the docking step of vacuole fusion may trigger a GTPase-regulated Ca^{2+} release from the vacuole. This, in turn, promotes the recruitment of calmodulin, a calcium sensor protein, to the vacuole and its complex formation with phosphatase 1, thereby activating a downstream signaling cascade that leads to membrane fusion [144, 145].

4.5 Conclusions

Using the in vitro docking assay for evaluating the recovery of the P1/P2 docking complex following the treatment of primed P1 and P2 with various inhibitors of the overall process of peroxisome fusion, I provided evidence that peroxisome docking depends on 1) ATP hydrolysis; 2) cytosolic proteins; 3) P2-bound Pex1p; 4) ergosterol; 5) PI(4,5)P_2; and 5) GTP hydrolysis by GTPase(s). In contrast, the docking of primed P1 and P2 does not require PI(4)P. My data also demonstrated that only PI(4,5)P_2-bp dissociate from the outer faces of both fusion partners during the docking process, and that such dissociation depends on ergosterol, ATP and GTP hydrolysis, cytosolic proteins, as well as Pex1p. On the contrary, GTP-bp remain associated with the cytosolic face of P1 peroxisomes during and after their docking with primed P2, suggesting a possible involvement of these proteins in the subsequent fusion of docked P1 and P2.

5 Ergosterol- and ceramide-rich domains in the peroxisomal membrane

5.1 Introduction

Cholesterol in mammals and ergosterol in yeasts are the major constituents of lipid rafts, dynamic domains of the plasma membrane that have been implicated in membrane protein trafficking, signal transduction, organization of the cytoskeleton, and pathogen internalization [123, 147, 149, 150]. My observation that ergosterol ligands prevent the release of Pex1p and Pex6p from P1 and P2 vesicles, thereby inhibiting their priming and docking for fusion, suggests that ergosterol-rich domains, perhaps lipid raft(s), in the membranes of P1 and P2 carry both these AAA ATPases and somehow activate the peroxisome fusion machinery. Lipid rafts are defined operationally as membrane domains that are insoluble in cold nonionic detergents and are enriched in sterols, sphingolipids and glycolipids [147]. To verify the existence of such domains in the membranes of P1 and P2 and to purify them for further characterization, I solubilized the membranes of unprimed P1 and P2 with Brij35, a nonionic detergent with the highest hydrophilic-lipophilic (HLB) ratio, and then isolated the detergent-resistant membrane domains by centrifugation on a discontinuous sucrose density gradient. These purified membrane domains of P1 and P2 were rich in ergosterol and ceramide. I therefore call them the ergosterol- and ceramide-rich (ECR) membrane domains. Following their purification, ECR domains were visualized by electron microscopy and subjected to a detailed analysis of their protein and lipid composition. My mass spectrometric analysis identified Pex1p and Pex6p as abundant constituents of ECR domains in the peroxisomal membrane.

5.2 Materials and methods

Osmotic lysis of peroxisomes

P1 and P2 peroxisomes were lysed by incubation on ice for 20 min in LC buffer (20 mM HEPES-KOH (pH 8.0) and 50 mM NaCl).

Detergent treatment of peroxisomal membranes

The pellet of membranes recovered after centrifugation of osmotically lysed P1 or P2 was resuspended in ice-cold MBS buffer (25 mM MES-KOH, pH 6.5, 150 mM NaCl) to a final concentration of 2 mg/ml. Equal aliquots of the suspension of membranes were then supplemented with one of the following detergents: Brij 30, Brij 35, Brij 72, Brij 96V, CHAPS, cholic acid (sodium salt), n-octyl-ß-D-glucopyranoside (n-OG), Triton X-100, and Tween 20. 5 mg of detergent was used for the treatment of 1 mg of peroxisomal membrane protein. After incubation on ice for 30 min, samples were subjected to centrifugation at 100,000 × g for 30 min at 4°C. Equal portions of the pellet and supernatant fractions were analyzed by SDS-PAGE, followed by immunoblotting or silver staining. Equal portions of both fractions were also subjected to protein-lipid overlay assays, GTP slot-blot, lipid extraction, and thin-layer chromatography (TLC).

Isolation of ECR membrane domains

Peroxisomes P1 and P2 were osmotically lysed and centrifuged. The membrane pellets were then resuspended in ice-cold MBS buffer (25 mM MES/KOH, pH 6.5, and 150 mM NaCl) to a final concentration of 2 mg/ml, supplemented with Brij 35 detergent (5mg of detergent/mg of peroxisomal membrane protein), and incubated on ice for 30 min. A 300

µl-aliquot of Brij 35-treated membranes was transferred to the bottom of a 5 ml Ultraclear centrifuge tube (Beckman Coulter) and supplemented with four volumes of 65% (wt/wt) sucrose in ice-cold MBS buffer in order to adjust the sucrose concentration of the sample to 52% (wt/wt). The sample was overlaid with 600 µl of 30% sucrose, 600 µl of 25% sucrose, 600 µl of 20% sucrose, 600 µl of 15% sucrose, 600 µl of 10% sucrose, and 500 µl of 5% sucrose (all wt/wt in MBS buffer). The sample was then centrifuged for 18 h at 200,000 *g* at 4°C using a SW50.1 rotor (Beckman Coulter). Nine fractions of 555 µl each were collected. Peroxisomal proteins recovered in equal volumes of gradient fractions were precipitated by adding six volumes of acetone, resolved by SDS-PAGE, and visualized by immunoblotting or silver staining. Equal volumes of gradient fractions were also used for the protein-lipid overlay assay, GTP slot-blot, lipid extraction, and TLC.

Electron microscopy

Detergent-resistant ECR domains floated to low density during centrifugation in a sucrose density gradient and peaked in fraction 7 of the gradient. A 200-µl aliquot of purified ECR domains in MBS buffer (25 mM MES/KOH, pH 6.5, and 150 mM NaCl) was mixed with 400 µl of ice-cold 150 mM sodium cacodylate buffer, pH 7.2, containing 3% glutaraldehyde. Immediately after mixing the sample and glutaraldehyde solution, 600 µl of 2% OsO_4 in ice-cold CD buffer (100 mM sodium cacodylate, pH 7.2) was added. After a 2-h incubation on ice, fixed ECR domains were sedimented at 100,000 × g for 20 min at 4°C in a Beckman TLS55 rotor onto a bed (25–50 µl) of hardened, low-melting 2.5% NuSieve GTG agarose (FMC). The pellet was postfixed in a solution of 1% OsO_4 plus 2.5% $K_2Cr_2O_7$ in ice-cold CD buffer for 2 h on ice. The pellet was then rinsed

twice with ice-cold CD buffer and exposed to 0.05% tannic acid in the same buffer. After a 30-min incubation on ice, the pellet was washed once with ice-cold CD buffer and three times with water. The pellet was incubated overnight with 2% uranyl acetate in water at 4°C and then washed three times with water. After dehydration in a graded ethanol series, the fixed and stained sample was embedded in Poly/Bed 812 epoxy resin (Polysciences). Silver/gold thin sections from the embedded blocks were examined in a JEOL JEM-2000FX transmission electron microscope.

Lipid analyses

For extraction of lipids, 1.2 ml of chloroform/methanol (1:1, v/v) were added to each of the 555-µl fractions recovered in the sucrose density gradient for isolation of ergosterol- and ceramide-rich membrane domains. After incubation on ice for 15 min, samples were subjected to centrifugation at 20,000 × g for 15 min at 4°C. The chloroform phase was separated and dried under nitrogen. The lipid film was dissolved in 60 µl of chloroform (for the analysis of ergosterol and ceramide) or 60 µl of chloroform/methanol (1:1, v/v) (for the analysis of glycerophospholipids). 20 µl of each sample were spotted on 60Å silica gel plates for TLC (Whatman). The lipids were developed in the following solvent systems: chloroform/acetone (4:1, v/v) (for the analysis of ergosterol and ceramide) and chloroform/methanol/water (65:25:4, v/v) (for the analysis of glycerophospholipids). All lipids were detected using 5% phosphomolybdic acid in ethanol and visualized by heating for 30 min at 110°C. Lipids were quantitated by densitometric analysis of TLC plates as described previously [151], using lipid standards in the 0.1-0.5 µg range for calibration.

To evaluate the distribution of ceramide and PS between the two leaflets of the membrane bilayers of P1 and P2 vesicles, the suspension of purified P1 or P2 in ice-cold buffer H (10 mM MES-KOH, pH 5.5, 250 mM sorbitol, 1 mM KCl, 0.5 mM EDTA, 1 × protease inhibitor cocktail [PIC] [84]) at 1 mg protein/ml was divided into two equal aliquots. One aliquot remained untreated, whereas peroxisomal vesicles in the other aliquot were lysed by incubation on ice for 20 min in 20 mM HEPES-KOH buffer, pH 8.0, containing 50 mM NaCl and 1 × PIC. The pellet of membranes recovered after centrifugation of osmotically lysed P1 or P2 was resuspended in ice-cold buffer H at 1 mg protein/ml. Two-fold serial dilutions of intact P1 or P2 vesicles (from the first aliquot) and of the membranes recovered after osmotic lysis of these vesicles (from the second aliquot) in the range of 10-160 μg protein/ml were made in ice-cold buffer H. Anti-ceramide mouse IgG or anti-PS mouse IgM were added to concentrations 0.5 and 1 μg/ml, respectively. After incubation for 30 min on ice, samples were subjected to centrifugation at 100,000 × g for 8 min at 4°C. The pellets were resuspended in 200 μl of ice-cold buffer H and supplemented with fluorescein-conjugated goat anti-mouse IgG or fluorescein-conjugated goat anti-mouse IgM antibodies at 2.5 and 5 μg/ml, respectively. After incubation for 30 min on ice, samples were subjected to centrifugation at 100,000 × g for 8 min at 4°C. The pellets were resuspended in 200 μl of ice-cold buffer H and supplemented with Alexa Fluor 488 rabbit anti-fluorescein/Oregon Green IgG at 15 μg/ml. Following incubation for 30 min on ice, samples were subjected to centrifugation at 100,000 × g for 8 min at 4°C. The pellets were resuspended in 200 μl of ice-cold buffer H and supplemented with Alexa Fluor 488 goat anti-rabbit IgG at 20 μg/ml. After incubation for 30 min on ice, samples were subjected to centrifugation at 100,000 × g for

8 min at 4°C. The pellets were resuspended in 200 µl of ice-cold buffer H and placed into the wells of a 96-well microplate. The fluorescence of samples was measured using the Wallac Victor 2 Multi-label microplate fluorescence reader with filters set at 485 (+/- 7.5) nm (excitation) and 510 (+/- 5) nm (emission). Controls were made for each dilution of intact P1 and P2 and of peroxisomal membranes recovered after osmotic lysis of these peroxisomal vesicles. The controls included normal mouse IgG or IgM at 0.5 and 1 µg/ml, respectively, added instead of anti-ceramide mouse IgG or anti-PS mouse IgM. Background fluorescence, which was due to the nonspecific binding of mouse IgG, mouse IgM, and/or fluorescein- or Alexa Fluor 488-labeled antibodies to the peroxisomal membrane, was subtracted.

Protein identification by mass spectrometry

Proteins were precipitated by adding trichloroacetic acid to the final concentration of 10%, incubated on ice for 30 min, pelleted by centrifugation, and then washed with ice-cold 80% acetone. Dried protein pellets were then resuspended in the SDS-PAGE sample buffer and the pH was adjusted to neutral using 2 M Tris/HCl (pH 8.8). The samples were boiled for 5 min at 63°C, centrifuged for 30 sec at 16,000 x g, loaded onto a 7.5%, 10%, 12.5% or 16% gel and resolved by SDS-PAGE. Following an overnight incubation of the gels in 50% methanol, proteins were visualized by silver staining using the mass spectrometry-compatible silver staining kit (Bio-Rad Silver Staining Plus) according to the manufacturer's instructions. To optimize subsequent mass spectrometry analysis, two modifications were made to the original procedure: the fixing step was reduced to 10 min and the staining step was terminated no later then 10 min following its beginning. The

protein bands of interest were excised from the silver-stained gel using razor blades along with a piece of a gel lacking proteins to be used as a control sample. The excised bands were cut into pieces ($1mm^3$) and then placed into siliconized 0.5 ml Eppendorf tubes. The gel pieces were then washed with distilled water and destained for 30 min at room temperature. The destaining solution was then removed and the gel pieces were washed twice with distilled water. The gel pieces were subsequently dehydrated by incubation in acetonitrile for 5 min at 37°C and dried at 37°C for 10 min to remove any residual acetonitrile. The proteins were then reduced by incubation in 10 mM DTT for 30 min at 37°C and alkylated by incubation in 55 mM IAA in the dark for 20 min at 37°C. Reduced and alkylated proteins were then dehydrated twice by 5-min incubation in acetonitrile at 37°C and dried for 10 min at 37°C to remove any residual acetonitrile. The proteins were then subjected to trypsin digestion. Following a 6-hr incubation at 37°C, the supernatants containing the majority of the peptides were placed in a new set of siliconized 0.5 ml Eppendorf tubes and the remaining peptides were extracted from the gel pieces first by incubation in 50% acetonitrile and then by incubation in 5% formic acid pre-mixed with an equal volume of acetonitrile. The pooled peptide extracts for each sample were supplemented with a 10 mM DTT solution to a final concentration of 1 mM in order to reduce oxidation during the subsequent drying and storage steps. The peptide extracts were dried overnight in the SpeedVac centrifuge at room temperature ('Low' temperature setting). The peptide extracts were then resuspended in 10 µl of the 5% methanol, 0.1% TFA solution and desalted using a C18 ZipTip (Millipore), according to the manufacture's instructions. Desalted peptides were then mixed in 1:1 ratio with the matrix solution, spotted on the MALDI plate, dried and subjected to mass spectrometric

analysis of peptide masses by MALDI [154, 155]. Three standard peptides (*i.e.*, angiotensin I, glufibrinopeptide and ACTH, all from Sigma) premixed with the matrix solution in 1:1 ratio were used to calibrate the Micromass M@LDI Mass Spectrometer (Micromass) prior to sample analysis. The mass spectrometer operated in the positive ion mode with an added reflection feature. The following instrumental settings were used to optimize the reflection/positive mode operation: 1) the pulse voltage, which has been optimized for the highest resolution of peptides, was 2375 V; 2) the source voltage used for the ion acceleration was set at 15000 V; 3) the reflection voltage used to refract ions was set at 2000 V; 4) the detector voltage was set at 1900 V; and 5) the TLF Delay was 750ms. The laser energy settings were manually adjusted prior to data acquisition in order to obtain a good signal to noise ratio for analyte ions and on-scale peaks with sustained signal after multiple laser shots. The instrument calibration using the three peptide standards mentioned above provided the most accurate mass measurements in the range of 1200-2500 m/z. Once calibrated, the mass spectrometer was used to acquire 10-15 individual mass spectra for each sample spot, which were then combined into one and manually analyzed to make a list of sample-specific monoisotopic peptide masses and their respective intensities for each recovered peptide. Protein identity was established using Mascot Peptide Mass Fingerprinting method (Matrix Science). Sample-specific peptide masses were used to search an NCBI database, a non-redundant protein database maintained by the National Center for Biotechnology Information (NCBI) that feature additional search tools like BLAST (The Basic Local Alignment Search Tool) and Entrez (The Life Sciences Search Engine). The search criteria were set as follows: 1) NCBInr as the protein sequence database; 2) *Saccharomyces cerevisiae* as the search-limiting

taxonomy group; 3) trypsin as the enzyme used for protein digestion; with up to one allowed missed cleavage site; 4) monoisotopic as the peptide mass value used; 5) carbamidomethyl (cysteine as *S*-carbamidomethyl derivate) as a fixed type of the protein modification; 6) oxidation (M) (oxidized forms of methionine) as a variable type of the protein modification that may have occurred during the sample preparation/handling; 7) unrestricted protein mass; 8) peptide mass tolerance of 100 ppm or lower; 9) MH+ as the precursor peptide charge state being expected as "1+"; and 10) the experimentally generated list of peptide masses as the query, with maximum number of hits set at 50. The experimental mass spectrometry data is then compared to the calculated peptide masses for each database sequence entry by the Mascot engine using the Mowse scoring algorithm, which assigns a probability-based Mowse score for each individual set of experimental mass spectrometry data. Based on this probability score, Mascot can then provide an objective measure of the significance of a protein hit by defining the cut-off score for the calculated protein hit to be significant (*i.e.* $p < 0.05$). Only significant protein hits with $p < 0.05$ and sequence coverage > 10% were considered and selected based on their molecular weight and the probability-based Mowse score. Pex1p, a 100 kDa protein, was identified by 12 specific peptide matches (m/z ratio of 700 to 2400) covering 15.4% of its sequence with mass accuracy better then 100 ppm. Pex6p, a 116 kDa protein, was identified by 10 specific peptide matches (m/z ratio of 1000 to 2400) covering 14.1% of its sequence with mass accuracy better then 100 ppm.

5.3 Results

5.3.1 Different protein and lipid constituents of the membranes of unprimed P1 and P2 differ in their solubility in detergents with various HLB values

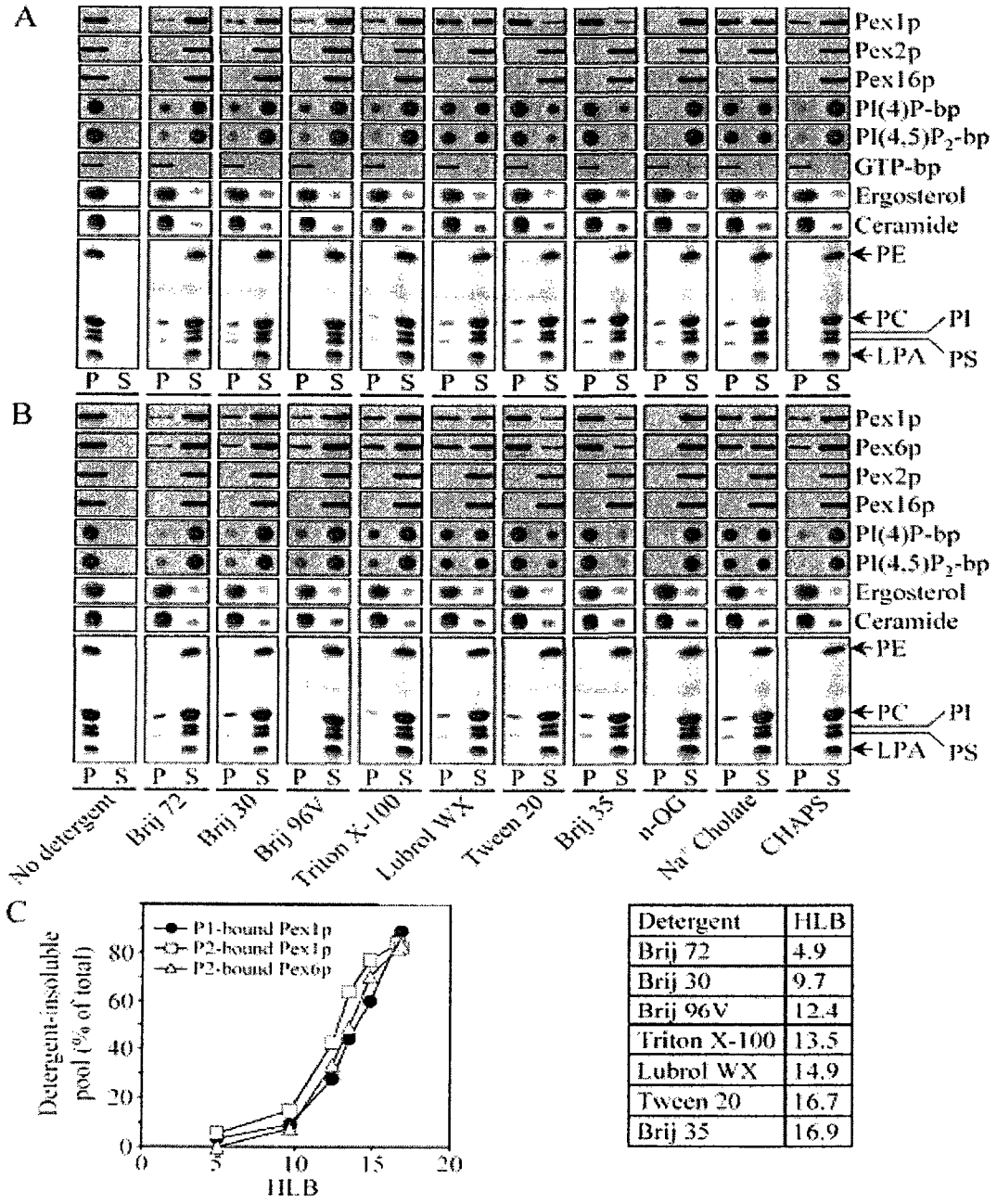

Detergent	HLB
Brij 72	4.9
Brij 30	9.7
Brij 96V	12.4
Triton X-100	13.5
Lubrol WX	14.9
Tween 20	16.7
Brij 35	16.9

Figure 5.1. Effect of various detergents on the solubility of proteins and lipids associated with the membranes of unprimed P1 and P2. (A and B) The pellet of membranes recovered after centrifugation of osmotically lysed unprimed P1 (A) or P2 (B) was resuspended in ice-cold MBS buffer. Equal aliquots of the suspension of membranes were then exposed to various detergents as described in "Materials and methods". After a 30-min incubation on ice, samples were subjected to centrifugation at 100,000 × g for 30 min at 4°C to yield pellet (*P*, detergent-insoluble) and supernatant (*S*, detergent-soluble)

fractions. Proteins from equal portions of the pellet and supernatant fractions were immunoblotted with the indicated antibodies. Equal portions of the pellet and supernatant fractions were also subjected to protein-lipid overlay assays using nitrocellulose membrane arrays spotted with PI(4)P or $PI(4,5)P_2$, GTP slot-blot, and lipid extraction, which was followed by thin-layer chromatography (TLC) and visualization of lipids. (C) The extent of insolubility of P1- and P2-bound Pex1p and Pex6p in various nonionic detergents of the polyoxyethylene group was quantitated by densitometric analysis of immunoblots presented in (A) and (B). The values of hydrophilic-lipophilic balance (HLB) for the indicated detergents are from [154].

5.3.2 Many membrane proteins of peroxisomes P1 and P2 resist solubilization by various detergents

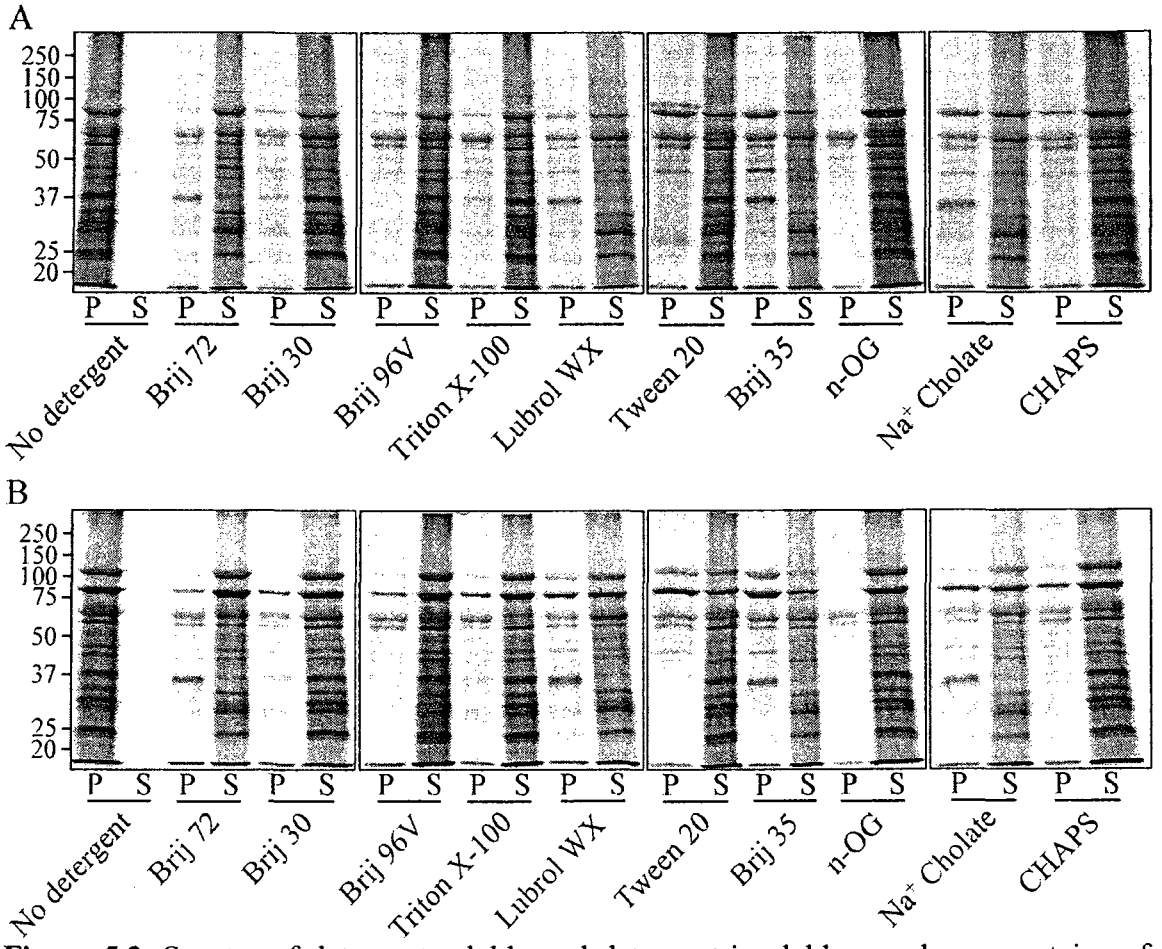

Figure 5.2. Spectra of detergent-soluble and detergent-insoluble membrane proteins of the immature peroxisomal vesicles P1 and P2. Unprimed P1 (A) or P2 (B) vesicles were osmotically lysed and subjected to centrifugation at 4°C to yield supernatant (matrix proteins) and pellet (peroxisomal membranes) fractions. Pelleted membranes were resuspended in ice-cold MBS buffer. Equal aliquots of the suspension of membranes were then exposed to various detergents as described in Supplemental Materials and Methods. The samples were subjected to centrifugation at 100,000 × g for 30 min at 4°C

to yield pellet (*P*, detergent-insoluble) and supernatant (*S*, detergent-soluble) fractions. Proteins from equal portions of the pellet and supernatant fractions were analyzed by SDS-PAGE and silver staining.

5.3.3 Membranes of unprimed P1 and P2 peroxisomes contain detergent-resistant domains that are highly enriched in ergosterol and ceramide and carry key components of the peroxisome fusogenic machinery including Pex1p, Pex6p, GTP-bp, PI(4)P-bp and PI(4,5)P_2-bp

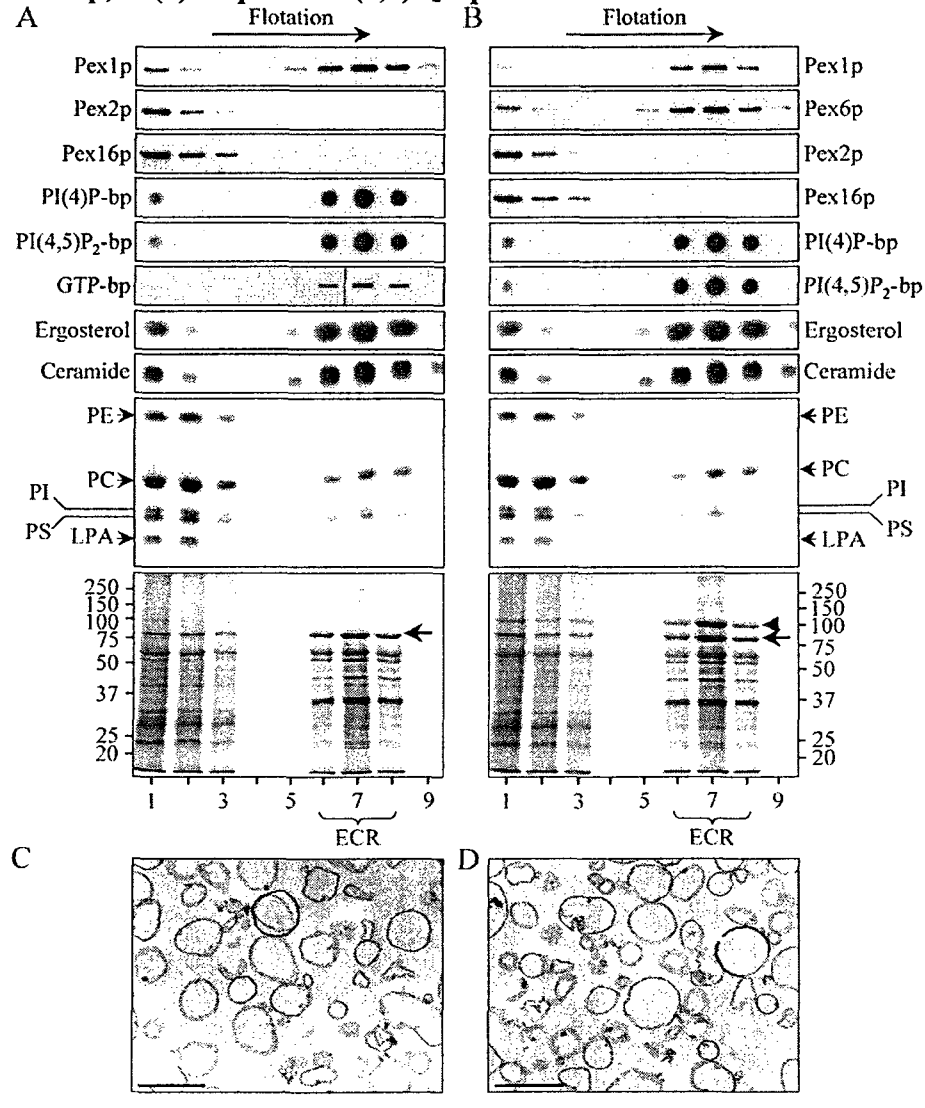

Figure 5.3. Pex1p, Pex6p, phosphoinositide- and GTP-binding proteins associate with ECR membrane domains that can float to low density during centrifugation in a sucrose density gradient. (A and B) The pellet of membranes recovered after centrifugation of osmotically lysed unprimed P1 (A) or P2 (B) was resuspended in ice-cold MBS buffer and supplemented with a nonionic detergent, Brij 35. After incubation on ice for 30 min, the Brij 35-treated membranes were subjected to centrifugation by flotation in a

discontinuous sucrose density gradient. Proteins from equal volumes of gradient fractions were immunoblotted with the indicated antibodies. Equal volumes of gradient fractions were also subjected to protein-lipid overlay assays using nitrocellulose membrane arrays spotted with PI(4)P or PI(4,5)P_2, GTP slot-blot, and lipid extraction, which was followed by thin-layer chromatography and visualization of lipids. The positions of Pex1p (arrow) and Pex6p (arrowhead), which were identified by mass spectrometric peptide mapping, are indicated. (C and D) Electron micrographs of ECR domains recovered in the low-density fraction 7 of the flotation sucrose density gradients presented in (A) and (B), respectively. Bar, 100 nm.

5.3.4 Membranes of unprimed P1 and P2 are rich in ergosterol and ceramide

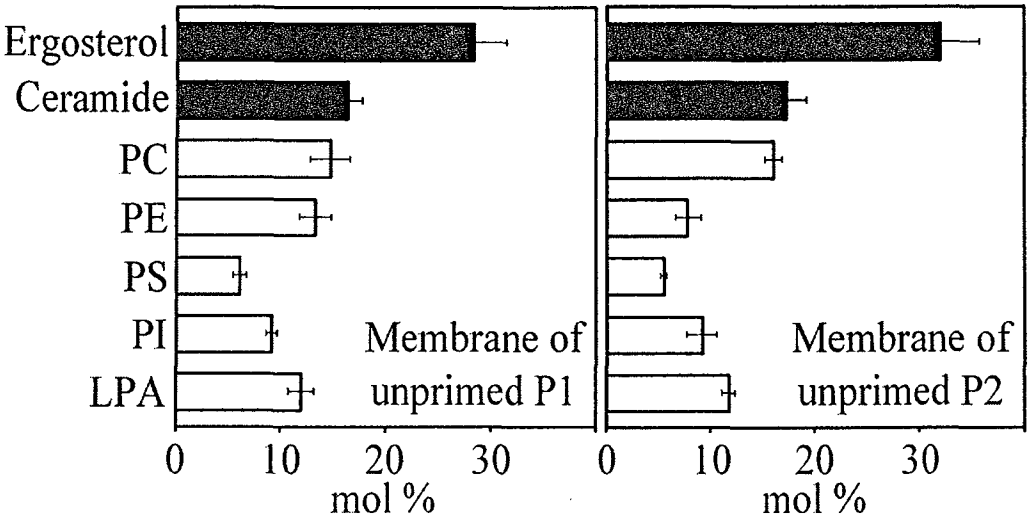

Figure 5.4. Lipid concentrations in the total membranes of P1 and P2 vesicles. Lipids extracted from membranes of unprimed P1 and P2 were analyzed by TLC and quantitated as described in "Materials and methods". Concentrations of individual lipid species are presented in mole percent (mol %).

5.3.5 ECR domains in the membranes of unprimed P1 and P2 are enriched in ergosterol and ceramide but are depleted in glycerophospholipids

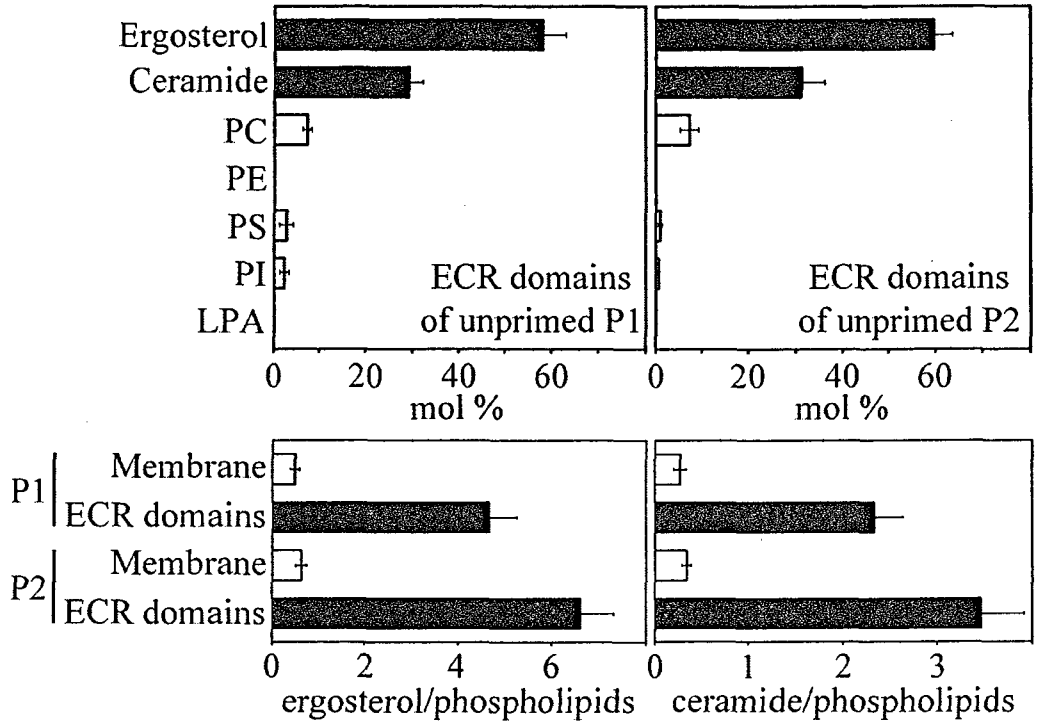

Figure 5.5. Lipid concentrations in ECR domains of membranes of P1 and P2 vesicles. ECR domains were purified as described in "Materials and methods". The mol % concentrations of individual lipid species recovered in the low-density fractions 5 to 9 of the flotation gradients are shown. Ergosterol/total glycerophospholipids and ceramide/total glycerophospholipids ratios for ECR domains were calculated.

5.3.6 ECR domains represent a substantial fraction of the membranes of unprimed P1 and P2

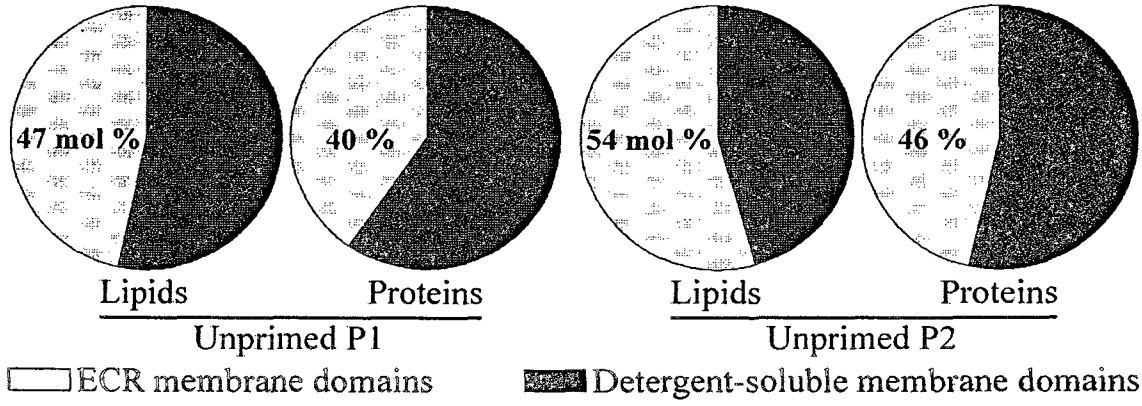

Figure 5.6. Lipids and proteins in fractions of the flotation gradients shown in Figure 5.3 were quantitated. Percent recoveries of lipids and proteins in ECR domains and in detergent-soluble portions of the membranes of P1 and P2 are presented.

5.3.7 Ceramide, a sphingolipid component of ECR domains, is distributed symmetrically between the two leaflets of the membrane in unprimed P1 and P2

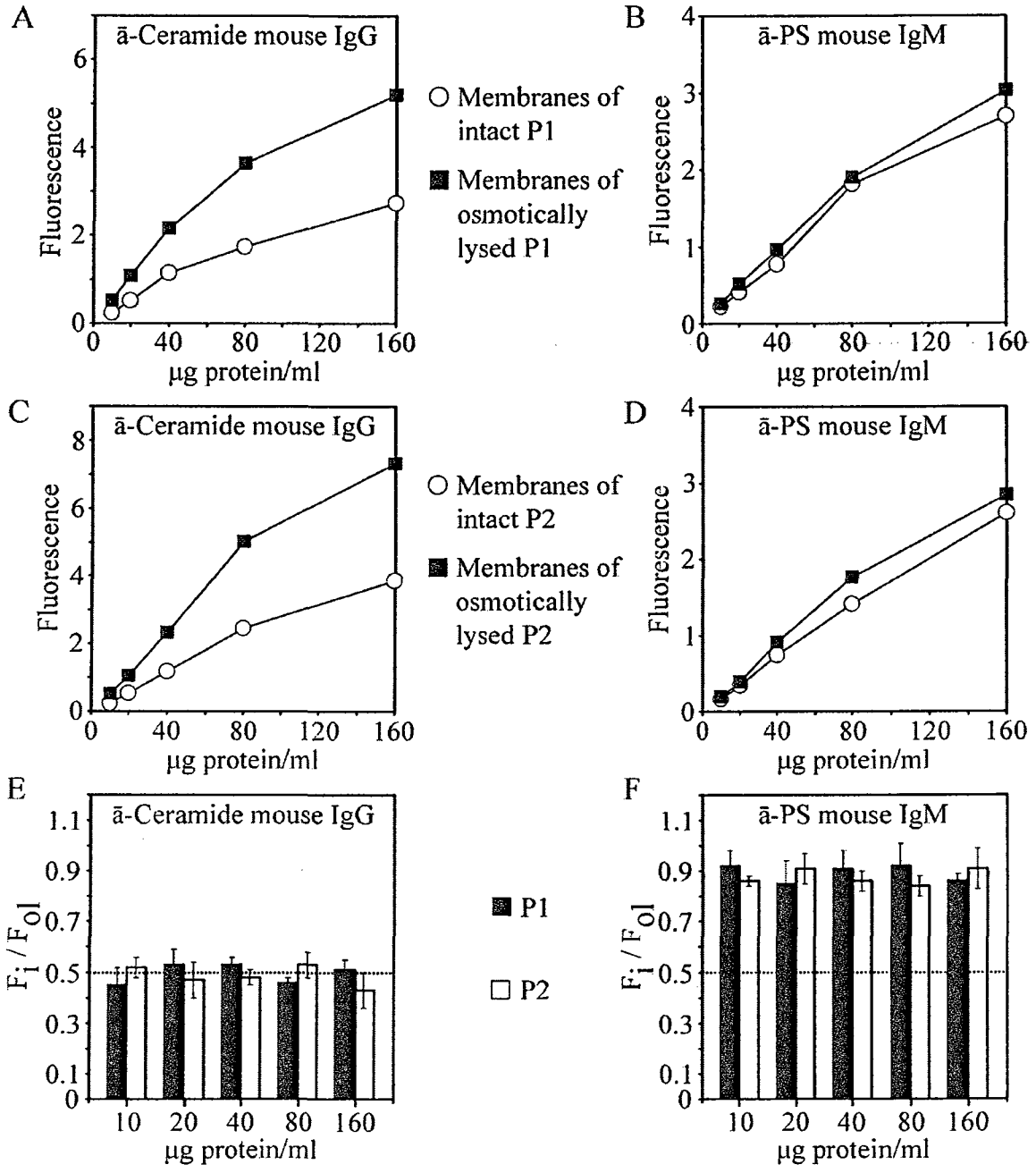

Figure 5.7. Ceramide is distributed symmetrically between the two leaflets of the peroxisomal membrane, while phosphatidylserine (PS) associates mostly with the cytosolic leaflet. (A-D) A suspension of purified P1 or P2 was divided into two equal aliquots. One aliquot remained untreated, while peroxisomal vesicles in the other aliquot

were osmotically lysed. Two-fold serial dilutions of intact P1 or P2 (from the first aliquot) and of the membranes recovered after centrifugation of osmotically lysed P1 or P2 (from the second aliquot) in the range of 10-160 μg protein/ml were exposed to anti-ceramide mouse IgG or anti-PS mouse IgM. All samples were then treated with fluorescein-conjugated goat anti-mouse IgG or fluorescein-conjugated goat anti-mouse IgM antibodies. To amplify the signals from fluorescein-labeled secondary antibodies, the samples were first labeled with Alexa Fluor 488 rabbit anti-fluorescein/Oregon Green IgG and then treated with Alexa Fluor 488 goat anti-rabbit IgG. The Alexa Fluor 488 fluorescence at 510 nm was monitored in individual samples. Controls were made for the nonspecific binding of mouse IgG, mouse IgM, and/or fluorescein- or Alexa Fluor 488-labeled antibodies to the membrane, and background fluorescence was subtracted. (E and F) The ratio "fluorescence for intact vesicles (F_i)/fluorescence for osmotically lysed vesicles (F_{ol})" was calculated for each dilution of intact P1 and P2 and of the membranes recovered after osmotic lysis of these peroxisomal vesicles. This ratio is equal to the fraction of the total pool of a monitored lipid that is located in the outer (cytosolic) leaflet of the membrane.

5.4 Discussion

Treatment with the cold nonionic detergent Brij 35 followed by sucrose density gradient centrifugation by flotation allowed me to separate the detergent-insoluble protein and lipid constituents of the membranes of unprimed P1 and P2 from their detergent-soluble counterparts. My analysis of the protein compositions of gradient fractions revealed that the P1-bound membrane proteins Pex1p, PI(4)P-bp, PI(4,5)P_2-bp and GTP-bp (Figure 5.3A) as well as the P2-bound membrane proteins Pex1p, Pex6p, PI(4)P-bp and PI(4,5)P_2-bp (Figure 5.3B) were recovered in the low density fractions (fractions 5-9), demonstrating that they resist solubilization by Brij 35 and, thus, reside in distinct detergent-resistant membrane domains. In contrast, the peroxisomal membrane proteins Pex2p and Pex16p were recovered in the high density fractions of the gradient (fractions 1-3), indicating that they were completely solubilized by Brij35 (Figures 5.3A and 5.3B). Moreover, I found that the ability of various nonionic detergents of the polyoxyethylene group to solubilize Pex1p and Pex6p is inversely proportional to their HLB values (Figure 5.1C). Taken together, these findings suggest that the observed propensity of

Pex1p, Pex6p, phosphoinositide- and GTP-bp to resist solubilization by Brij 35 was not due to an overall lower efficiency of Brij 35 as a detergent, but reflected a specific phenomenon. Of note, a nonionic detergent of the nonpolyoxyethylene group, n-octyl-ß-D-glucopyranoside (n-OG), solubilized most of the membrane proteins, including Pex1p and Pex6p, that resisted solubilization by Brij 35 and other detergents (Figures 5.1A, 5.1B and 5.2). Considering the demonstrated ability of n-OG to preserve the membrane-bound complexes of cytoskeletal proteins and their interacting protein partners [150], it is unlikely that the P1- and P2-bound membrane proteins associate with the cytoskeleton. Thus, it seems that the observed insolubility of a distinct set of membrane proteins in Brij 35 was not due to their interactions with components of the cytoskeleton.

My TLC analysis of the lipid composition of the Brij 35-treated membranes of P1 and P2 revealed that the fractions of the flotation gradient that contained detergent-insoluble proteins were significantly enriched in ergosterol and ceramide but contained only minor amounts of glycerophospholipids (Figure 5.3). In contrast, the major portion of each of the five glycerophospholipids associated with the membranes of P1 and P2 was soluble in the detergent and was found in the high-density bottom fractions 1 to 3 (Figure 5.3). Only minor amounts of the glycerophospholipids phosphatidylcholine (PC) and phosphatidylserine (PS) and traces of phosphatidylinositol (PI) were seen in the low-density fractions 6 to 8 enriched in the components of ECR domains, whereas phosphatidylethanolamine (PE) and lysophosphatidic acid (LPA) were not found in these fractions (Figure 5.3). The Brij 35-insoluble structures purified from the membranes of P1 and P2 and recovered in the low-density fractions of the gradient appeared as 25- to 80-nm unilamellar vesicles of varied shape (Figure 5.3C).

My detailed analysis of the lipid makeup of the membranes of both fusion partners revealed that both ergosterol and ceramide were at high levels in the membranes of unprimed P1 and P2 (Figure 5.4). Ergosterol constituted 28-32 mol % of lipids in these membranes, whereas ceramide was present at 15-17 mol % (Figure 5.4). ECR domains were substantially enriched in both these lipids as compared to the total membranes of P1 and P2 (Figure 5.5). These detergent-resistant membrane domains contained 58-60 mol % of ergosterol and 29-31 mol % of ceramide (Figure 5.5). In contrast, ECR domains were highly depleted in all five glycerophospholipids (Figure 5.5). Accordingly, ergosterol/total glycerophospholipids and ceramide/total glycerophospholipids ratios for ECR domains greatly exceeded the ratios for the total membranes of P1 and P2 (Figure 5.5). My data also imply that ECR domains represent a substantial fraction of the membranes of unprimed P1 and P2 vesicles, as 47-54 mol % of membrane lipids and 40-46 % of membrane proteins were recovered in these domains (Figure 5.6).

In eukaryotic cells, lipids are asymmetrically arranged between the two leaflets of the plasma membrane bilayer [123]. Glycolipids and sphingomyelin, the two major sphingolipid components of lipid rafts in mammals, and the glycerophospholipid PC reside predominantly in the outer (exoplasmic) leaflet of the plasma membrane [123]. In contrast, the glycerophospholipids PE, PI and PS are restricted to the inner (cytosolic) leaflet of the plasma membrane [123]. Cholesterol, a major sterol constituent of lipid rafts in mammals, is equally distributed across the bilayer [142]. Using monoclonal antibodies to ceramide and PS, I evaluated the transbilayer distribution of these two lipids in the membranes of unprimed P1 and P2. In the membranes of osmotically lysed P1 and P2, both leaflets of the bilayer were accessible to anti-ceramide and anti-PS antibodies

(Figure 5.7). In contract, in the membranes of intact P1 and P2, these monoclonal antibodies could detect only ceramide and PS that resided in the cytosolic leaflet (Figure 5.7). The levels of ceramide recovered in the membranes of osmotically lysed P1 and P2 exceeded the levels of this sphingolipid detected in intact membranes of both vesicles (Figures 5.7A and 5.7C), with about half of the ceramide located in the outer (cytosolic) leaflet of the bilayer (Figure 5.7E). I therefore concluded that the sphingolipid component of ECR domains is distributed symmetrically between the two leaflets of the membrane bilayers in P1 and P2. In contrast, the glycerophospholipid PS resides predominantly in the outer (cytosolic) leaflets of the membranes of P1 and P2. In fact, the vast majority of this lipid in intact P1 and P2 was accessible to anti-PS antibodies (Figures 5.7B, 5.7D and 5.7F).

Taken together, my findings provide evidence for the existence of detergent-resistant ECR domains in the membranes of unprimed P1 and P2 vesicles. These domains: 1) contain a distinct set of membrane proteins, including Pex1p, Pex6p and several other essential components of the peroxisome fusion machinery; 2) are highly enriched, as compared to a detergent-soluble portion of the peroxisomal membrane, in ergosterol and ceramide; and 3) differ from well characterized detergent-insoluble lipid rafts in the plasma membrane with respect to the nature of their sphingolipid constituent and its unusual distribution across the membrane bilayer. Of note, studies in plants *Arabidopsis thaliana* and *Allium porrum* demonstrated the existence of distinct detergent-resistant domains in the plasma membrane and Golgi apparatus that, akin to ECR domains in the membranes of P1 and P2 peroxisomes, are also enriched in sterols,

sterylglucosides, and glucosylceramides (GluCer) and contain only minute amounts of glycerophospholipids [153].

5.5 Conclusion

In sum, my findings provide the comprehensive evidence for the existence of detergent-resistant ECR domains in the membranes of unprimed P1 and P2 peroxisomes. In contrast to a detergent-soluble portion of the peroxisomal membrane, these unique membrane domains are highly enriched in ergosterol and ceramide. ECR domains house a distinct set of peroxisomal membrane proteins, such as Pex1p and Pex6p, along with several other key components of the peroxisome fusogenic machinery, including proteins that bind to GTP, PI(4)P and $PI(4,5)P_2$. Furthermore, my data on a symmetrical distribution of the ceramide component of ECR domains between the two leaflets of the peroxisomal membrane imply that these detergent-resistant domains in the peroxisomal membrane differ from the lipid raft domains in the plasma membrane.

6 Remodeling of ECR domains during peroxisome priming and docking

6.1 Introduction

My findings described in chapter 5 of this thesis imply that many essential protein components of the peroxisome fusion machinery, including the AAA ATPases Pex1p and Pex6p, PI(4)P-bp, $PI(4,5)P_2$-bp and GTP-bp, reside in ECR domains in the membranes of unprimed P1 and P2 peroxisomes. The release of P1-bound Pex1p and of P2-associated Pex6p from the organelle surface to the cytosol is a hallmark event of the priming of P1 and P2 [64]. It was unclear if during priming these AAA ATPases are released to the

cytosol directly from ECR domains or, alternatively, if they first relocate from ECR domains to an ergosterol- and ceramide-poor portion of the membrane and only then dissociate from the peroxisome surface. I therefore sought to define the dynamics of changes (if any) in the association of Pex1p, Pex6p and other components of the peroxisome fusion machinery with ECR domains during peroxisome priming and docking.

6.2 Materials and methods

Analysis of the remodeling of protein and lipid constituents of ECR domains during peroxisome priming

P1 or P2 vesicles were incubated individually with cytosol and ATP at 26°C. Equal aliquots of peroxisomal vesicles were taken at different time points. P1 and P2 were subjected to osmotic lysis, followed by centrifugation. The pellets of membranes recovered after such centrifugation were resuspended in ice-cold MBS buffer and supplemented with a detergent, Brij 35. After incubation on ice for 30 min, the Brij 35-treated membranes were subjected to centrifugation by flotation in a discontinuous sucrose density gradient. Equal volumes of gradient fractions were subjected to immunoblotting with antibodies to peroxisomal membrane proteins, protein-lipid overlay assay using nitrocellulose membrane arrays spotted with PI(4)P or $PI(4,5)P_2$, GTP slot-blot, and lipid extraction, which was followed by TLC and visualization of lipids.

Analysis of the remodeling of protein and lipid constituents of ECR domains during peroxisome docking

P1 and P2 were incubated individually with cytosol and ATP at 26°C. After a 10-min incubation, P1 and P2 were pelleted, resuspended in a buffer, and mixed. Samples were

incubated at 26°C with or without cytosol, ATP, nystatin, GTPγS, ATPγS, antibodies to Pex1p or antibodies to PI(4)P. Equal aliquots of peroxisomal vesicles were taken at the times indicated. Samples were subjected to osmotic lysis, followed by centrifugation. The pellets of membranes recovered after such centrifugation were resuspended in ice-cold MBS buffer and supplemented with a detergent, Brij 35. After incubation on ice for 30 min, the Brij 35-treated membranes were subjected to centrifugation by flotation in a discontinuous sucrose density gradient. Equal volumes of gradient fractions were subjected to immunoblotting with antibodies to peroxisomal membrane proteins, protein-lipid overlay assay using nitrocellulose membrane arrays spotted with PI(4)P or PI(4,5)P_2, GTP slot-blot, and lipid extraction, which was followed by TLC and visualization of lipids.

6.3 Results

6.3.1 Priming-specific relocation of Pex1p in P1 and of Pex6p in P2 from ECR domains to a detergent-soluble portion of the membrane requires ergosterol, PI(4)P and PI(4,5)P_2, whereas the subsequent release of both these AAA ATPases into the cytosol depends on ATP hydrolysis and cytosolic proteins

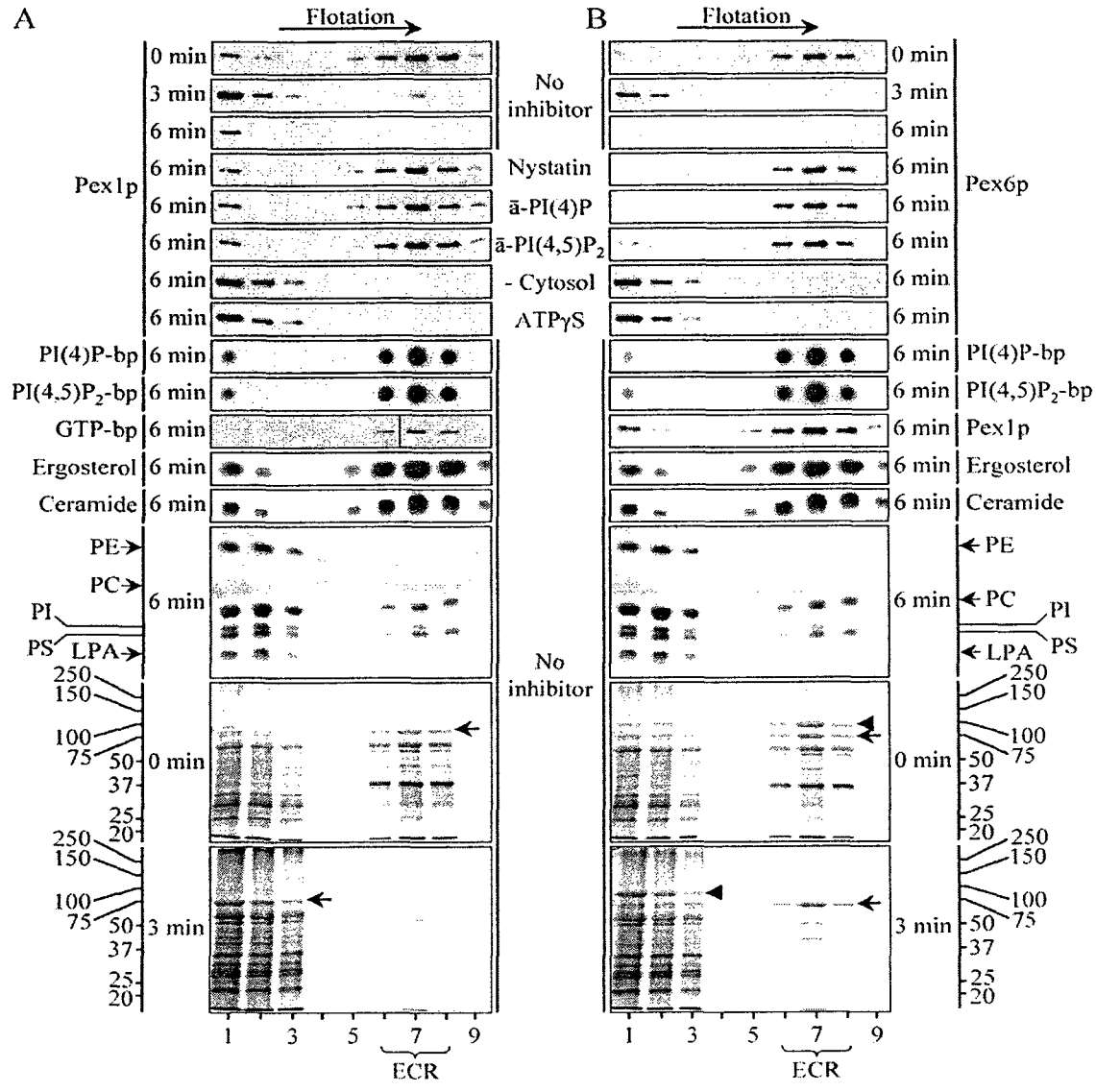

Figure 6.1. Pex1p and Pex6p move from detergent-resistant ECR domains to a detergent-soluble portion of the membrane during peroxisome priming. P1 (A) or P2 (B) vesicles were incubated individually with cytosol and ATP at 26°C. Equal aliquots of peroxisomal vesicles were taken at the times indicated. P1 and P2 were subjected to osmotic lysis, followed by centrifugation. The pellets of membranes recovered after such centrifugation were resuspended in ice-cold MBS buffer and supplemented with a detergent, Brij 35. After incubation on ice for 30 min, the Brij 35-treated membranes were subjected to centrifugation by flotation in a discontinuous sucrose density gradient. Equal volumes of gradient fractions were subjected to immunoblotting with antibodies to peroxisomal membrane proteins, protein-lipid overlay assay using nitrocellulose membrane arrays spotted with PI(4)P or $PI(4,5)P_2$, GTP slot-blot, and lipid extraction, which was followed by TLC and visualization of lipids. The positions of Pex1p (arrow) and Pex6p (arrowhead), which were identified by mass spectrometric peptide mapping, are indicated.

6.3.2 Docking-specific relocation of PI(4,5)P_2-bp from ECR domains to an ergosterol- and ceramide-poor portion of the membrane requires ergosterol, GTP hydrolysis and Pex1p, whereas similar lateral movement of Pex1p along the membrane depends on ergosterol only; the subsequent release of Pex1p and PI(4,5)P_2-bp from ergosterol- and ceramide-poor membrane domains to the cytosol requires cytosolic proteins and ATP hydrolysis

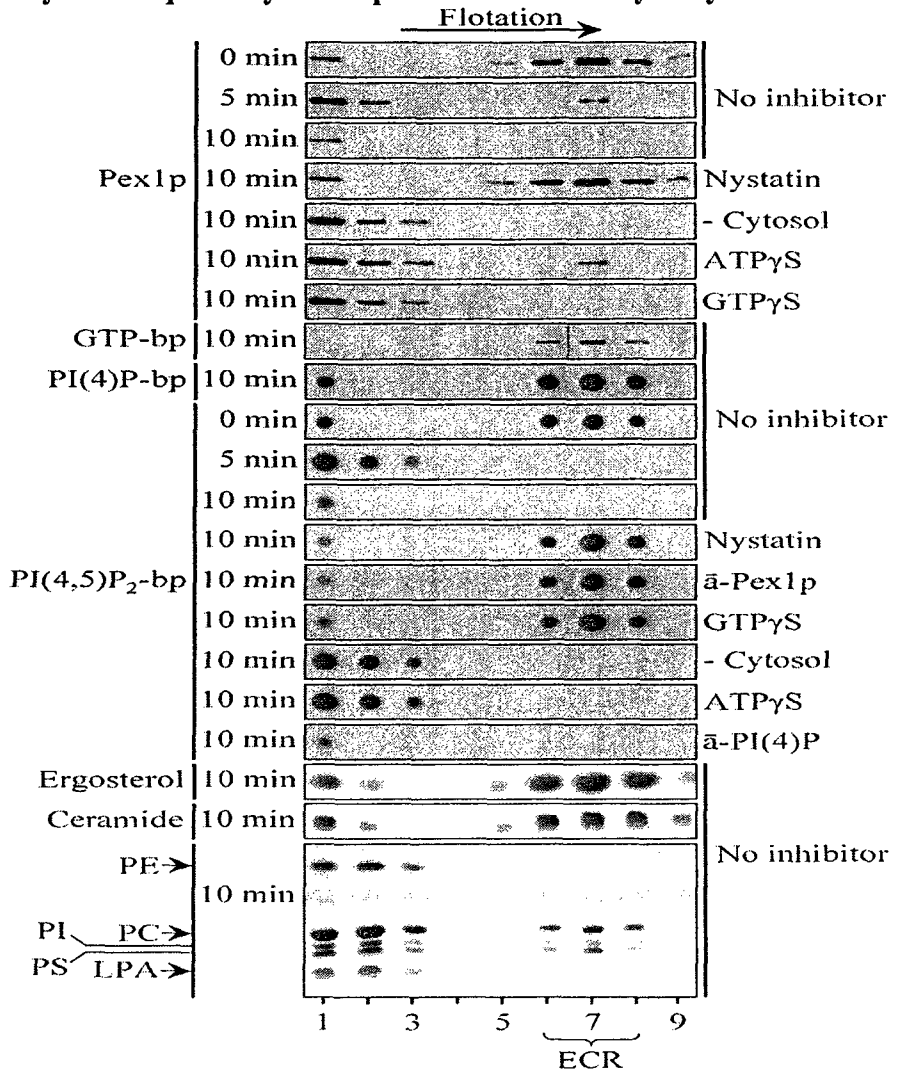

Figure 6.2. PI(4,5)P_2-binding proteins and P2-bound Pex1p segregate from ECR domains during peroxisome docking. P1 and P2 were incubated individually with cytosol and ATP at 26°C. After a 10-min incubation, P1 and P2 were pelleted, resuspended in a buffer, and mixed. Samples were incubated at 26°C with or without cytosol, ATP, nystatin, GTPγS, ATPγS, antibodies to Pex1p or antibodies to PI(4)P. Equal aliquots of peroxisomal vesicles were taken at the times indicated. Samples were subjected to osmotic lysis, followed by centrifugation. The pellets of membranes recovered after such centrifugation were resuspended in ice-cold MBS buffer and supplemented with a detergent, Brij 35. After incubation on ice for 30 min, the Brij 35-treated membranes were subjected to centrifugation by flotation in a discontinuous sucrose density gradient. Equal volumes of gradient fractions were subjected to immunoblotting with antibodies to

peroxisomal membrane proteins, protein-lipid overlay assay using nitrocellulose membrane arrays spotted with PI(4)P or PI(4,5)P_2, GTP slot-blot, and lipid extraction, which was followed by TLC and visualization of lipids.

6.4 Discussion

The release of P1-bound Pex1p and of P2-associated Pex6p from the organelle surface to the cytosol is a hallmark event of the priming of P1 and P2 [64]. My findings provide evidence that this event includes two consecutive steps. Specifically, both AAA ATPases initially relocate from ECR domains to an ergosterol- and ceramide-poor portion of the membrane, from which they are then released to the cytosol. In fact, when Brij 35 extracts of the membranes of unprimed P1 and P2 were subjected to centrifugation by flotation in a sucrose density gradient, the majority of P1-bound Pex1p and of P2-associated Pex6p was recovered in detergent-resistant ECR domains (Figures 6.1A and 6.1B). However, already by 3 min of priming, both proteins were seen only in detergent-soluble, ergosterol- and ceramide-poor membrane domains that were recovered in the high-density bottom fractions 1 to 3 of the gradient (Figures 6.1A and 6.1B). By 6 min of priming, both AAA ATPases were released from these detergent-soluble domains to the cytosol (Figures 6.1A and 6.1B). The two consecutive steps in the priming-specific release of Pex1p and Pex6p from the organelle surface to the cytosol have different requirements. Whereas the relocation of both proteins from ECR domains to an ergosterol- and ceramide-poor portion of the membrane depends on ergosterol, PI(4)P, and PI(4,5)P_2, their subsequent release to the cytosol requires cytosolic proteins and ATP hydrolysis (Figures 6.1A and 6.1B).

I also found that priming of P1 and P2 led to dramatic changes in protein composition of ECR domains, with the majority of proteins being relocated from these

domains to ergosterol- and ceramide-poor domains already by 3 min of priming (Figures 6.1A and 6.1B). Only a few proteins, including P1-bound GTP-bp, P2-associated Pex1p and proteins that bind PI(4)P or PI(4,5)P_2 on the cytosolic faces of both fusion partners, remained associated with ECR domains (Figures 6.1A and 6.1B). On the other hand, the lipid repertoire of ECR domains did not undergo any noticeable remodeling during priming of P1 and P2 (compare Figures 5.3 and 6.1).

My findings also imply that the docking of preprimed P1 and P2 results in further remodeling of the protein repertoire of their ECR domains (Figure 6.2). As I found, by 5 min of docking, P2-associated Pex1p and proteins that bind PI(4,5)P_2 on the cytosolic faces of both fusion partners moved from these floating membrane domains to detergent-soluble, ergosterol- and ceramide-poor domains recovered in the high-density bottom fractions of the flotation gradient (Figure 6.2). The movement of Pex1p and PI(4,5)P_2-bp to a detergent-soluble portion of the membranes was followed by the release of these proteins to the cytosol, which was evident after 10 min of docking (Figure 6.2). Not all proteins moved away from ECR domains during peroxisome docking. The group of ECR resident proteins included P1-associated GTP-bp and proteins that bind PI(4)P on the cytosolic faces of both fusion partners (Figure 6.2). Furthermore, no dramatic changes in lipid composition of ECR domains were observed during docking of separately primed P1 and P2 (compare Figs. 6.1 and 6.2).

6.5 Conclusions

My analysis of the dynamics of changes in the association of several essential components of the peroxisome fusion machinery with ECR domains and an ergosterol- and ceramide-poor portion of the membrane during peroxisome priming and docking for fusion suggest the following order of events. The priming-specific release of Pex1p from P1 and of Pex6p from P2 to the cytosol occurs in two consecutive steps. The priming of P1 is initiated by the relocation of Pex1p from its ECR domains to its ergosterol- and ceramide-poor membrane domains, which depends on ergosterol, PI(4)P and $PI(4,5)P_2$. The subsequent release of Pex1p from the ergosterol- and ceramide-poor membrane domains of P1 to the cytosol requires cytosolic proteins and ATP hydrolysis. Similarly, the priming of P2 commences with the relocation of Pex6p from its ECR domains to its ergosterol- and ceramide-poor membrane domains and depends on ergosterol, PI(4)P and $PI(4,5)P_2$. The subsequent release of Pex6p from P2 to the cytosol requires cytosolic proteins and ATP hydrolysis. Furthermore, peroxisome docking is initiated by the relocation of $PI(4,5)P_2$-binding proteins from ECR domains to ergosterol- and ceramide-poor membrane domains of both fusion partners, and needs ergosterol, GTP hydrolysis and Pex1p. The next step of peroxisome docking is characterized by the relocation of Pex1p from ECR domains to ergosterol- and ceramide-poor membrane domains of P2, which depends on ergosterol. The formation of the P1/P2 docking complex is completed by the release of Pex1p and $PI(4,5)P_2$–bp into the cytosol from an ergosterol- and ceramide-poor portion of the peroxisomal membrane, which takes place in an ATP hydrolysis- and cytosol-dependent fashion.

7 Hierarchy of the multi-step remodeling of ECR domains during peroxisome priming and docking

7.1 Introduction

In order to explore the hierarchy of ergosterol-, PI(4)P-, PI(4,5)P_2-, GTP hydrolysis-, cytosol-, and ATP hydrolysis-dependent steps during the priming- and docking-specific remodeling of the membrane-associated peroxisome fusion machinery, I developed and then used a two-stage inhibition assay. This assay examines whether the step affected by one inhibitor precedes, occurs in parallel, or follows the step sensitive to another inhibitor. For example, in the two-stage assay for the priming-specific movement of P1-bound Pex1p and of P2-associated Pex6p from detergent-resistant ECR domains to detergent-soluble, ergosterol- and ceramide-poor membrane domains, the fusion partners P1 and P2 are initially (the first stage) incubated individually with inhibitor 1. Separately pretreated P1 and P2 vesicles are then reisolated by centrifugation and washed in buffer. During the second stage, pretreated and washed peroxisomal vesicles are supplemented with inhibitor 2 and the compound that overcomes the block imposed by inhibitor 1. After incubation, the effect of the sequential treatment with inhibitors on the monitored event, *i.e.* the relocation of P1-bound Pex1p and of P2-associated Pex6p from ECR domains to an ergosterol- and ceramide-poor portion of the peroxisomal membrane, is assessed. To evaluate the efficiency of the monitored event, Brij 35-treated membranes of P1 and P2 are subjected to centrifugation by flotation in a discontinuous sucrose density gradient as described in "Materials and methods" in chapter 5 of this thesis, and the recovery of Pex1p or Pex6p in gradient fractions is examined by immunoblotting. If the step affected by inhibitor 2 precedes the step sensitive to inhibitor 1, or if these steps occur in parallel to each other, the requirement for the inhibitor 2-sensitive step must be

fulfilled while the inhibitor 1-susceptible step is affected. In this case, the monitored event will proceed during the second stage. In contrast, if the step affected by inhibitor 2 occurs after the step sensitive to inhibitor 1, the monitored event will not proceed during the second stage, even in the presence of the compound that overcomes the block imposed by inhibitor 1. The same logic can be applied when the two inhibitors are added in the reverse order, namely when the exposure to inhibitor 2 precedes the treatment with inhibitor 1, which is supplemented together with the compound that overcomes the block imposed by inhibitor 2. Based on the results of the sequential treatment with two inhibitors added in two different orders, the decisive conclusion about the order of any pair of steps, which are sensitive to these inhibitors, can be made. In fact, if step 1 precedes step 2, the monitored event will be affected only when the exposure to inhibitor 1 precedes the treatment with inhibitor 2. In contrast, if step 1 follows step 2, the monitored hallmark event will be affected only when the exposure to inhibitor 1 follows the treatment with inhibitor 2.

7.2 Materials and methods

Two-stage assay for establishing the order of individual steps during peroxisome priming

P1 or P2 were preincubated individually for 5 min at 26°C with or without nystatin (an ergosterol ligand), phosphoinositide-specific monoclonal antibodies, or ATPγS in the presence or absence of cytosol. Pretreated peroxisomal vesicles were then reisolated by centrifugation, washed, and resuspended in buffer containing liposomes with ergosterol, nystatin, phosphoinositides, phosphoinositide-specific antibodies, cytosol, ATPγS, or ATP. After a 5-min incubation at 26°C, samples were supplemented with cytosol and

ATP to yield standard fusion reactions and incubated at 26°C. Equal aliquots of peroxisomal vesicles were taken at different time points. P1 and P2 were then pelleted by centrifugation. Samples were subjected to osmotic lysis, followed by centrifugation. The pellets of membranes recovered after such centrifugation were resuspended in ice-cold MBS buffer and supplemented with a detergent, Brij 35. After incubation on ice for 30 min, the Brij 35-treated membranes were subjected to centrifugation by flotation in a discontinuous sucrose density gradient. Proteins recovered in equal volumes of gradient fractions were resolved by SDS-PAGE and immunoblotted with antibodies to Pex1p or Pex6p.

Two-stage assay for defining the hierarchy of individual steps during peroxisome docking

P1 and P2 were individually preprimed by incubation with cytosol and ATP for 10 min at 26°C. Peroxisomal vesicles were then reisolated by centrifugation, washed, and resuspended in a buffer. Reisolated P1 and P2 were incubated individually for 5 min at 26°C with or without GTPγS, ATPγS or nystatin in the presence or absence of cytosol. P1 and P2 were then reisolated by centrifugation, washed, and resuspended in buffer containing GTP, GTPγS, ATPγS, ATP, liposomes with ergosterol, antibodies to Pex1p, or nystatin in the presence or absence of cytosol. After a 5-min incubation at 26°C, P1 and P2 were mixed and supplemented with cytosol and ATP to yield standard fusion reactions. Samples were incubated at 26°C. Equal aliquots of peroxisomal vesicles were taken at different time points. P1 and P2 were then pelleted by centrifugation. Samples were subjected to osmotic lysis, followed by centrifugation. The pellets of membranes recovered after such centrifugation were resuspended in ice-cold MBS buffer and

supplemented with a detergent, Brij 35. After incubation on ice for 30 min, the Brij 35-treated membranes were subjected to centrifugation by flotation in a discontinuous sucrose density gradient. Proteins recovered in equal volumes of gradient fractions were resolved by SDS-PAGE and immunoblotted with antibodies to Pex1p. Equal volumes of gradient fractions were also subjected to protein-lipid overlay assays using nitrocellulose membrane arrays spotted with $PI(4,5)P_2$.

7.3 Results

7.3.1 Priming-specific relocation of Pex1p and Pex6p from ECR domains to ergosterol- and ceramide-poor membrane domains of P1 and P2 is a multi-step process in which the ergosterol-dependent step occurs first and is followed by the steps requiring PI(4)P and $PI(4,5)P_2$, respectively; the subsequent dissociation of both AAA ATPases is initiated by a cytosol-dependent step, which enables the following step requiring ATP hydrolysis

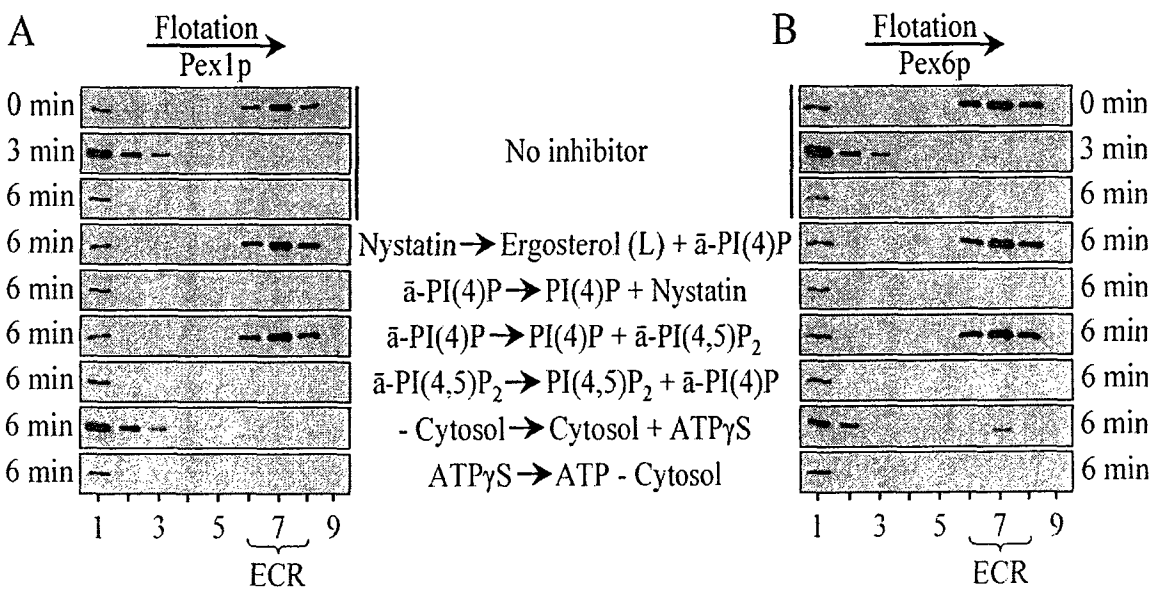

Figure 7.1. The hierarchy of peroxisome priming-specific events that result in the relocation of Pex1p, Pex6p and $PI(4,5)P_2$-binding proteins from ECR domains to a detergent-soluble portion of the membrane, followed by their release to the cytosol. P1 (A) or P2 (B) vesicles were preincubated individually for 5 min at 26°C with or without nystatin (an ergosterol ligand), phosphoinositide-specific monoclonal antibodies, or ATPγS in the presence or absence of cytosol, as indicated. Pretreated peroxisomal vesicles were then reisolated by centrifugation, washed, and resuspended in buffer containing liposomes with ergosterol, nystatin, phosphoinositides, phosphoinositide-

specific antibodies, cytosol, ATPγS, or ATP, as indicated. After a 5-min incubation at 26°C, samples were supplemented with cytosol and ATP to yield standard fusion reactions and incubated at 26°C. Equal aliquots of peroxisomal vesicles were taken at the times indicated. P1 and P2 were then pelleted by centrifugation. Samples were subjected to osmotic lysis, followed by centrifugation. The pellets of membranes recovered after such centrifugation were resuspended in ice-cold MBS buffer and supplemented with a detergent, Brij 35. After incubation on ice for 30 min, the Brij 35-treated membranes were subjected to centrifugation by flotation in a discontinuous sucrose density gradient. Proteins recovered in equal volumes of gradient fractions were resolved by SDS-PAGE and immunoblotted with antibodies to Pex1p (A) or Pex6p (B).

7.3.2 Docking-specific relocation of PI(4,5)P_2-bp from ECR domains to ergosterol- and ceramide-poor membrane domains is a multi-step process in which the ergosterol-dependent step occurs first and is followed by the step requiring both GTP hydrolysis and Pex1p; the subsequent relocation of Pex1p from ECR domains to ergosterol- and ceramide-poor membrane domains of P2 progresses in an ergosterol-dependent fashion; the following dissociation of Pex1p and PI(4,5)P_2-bp from the membrane is initiated by a cytosol-dependent step, which enables the following step requiring ATP hydrolysis

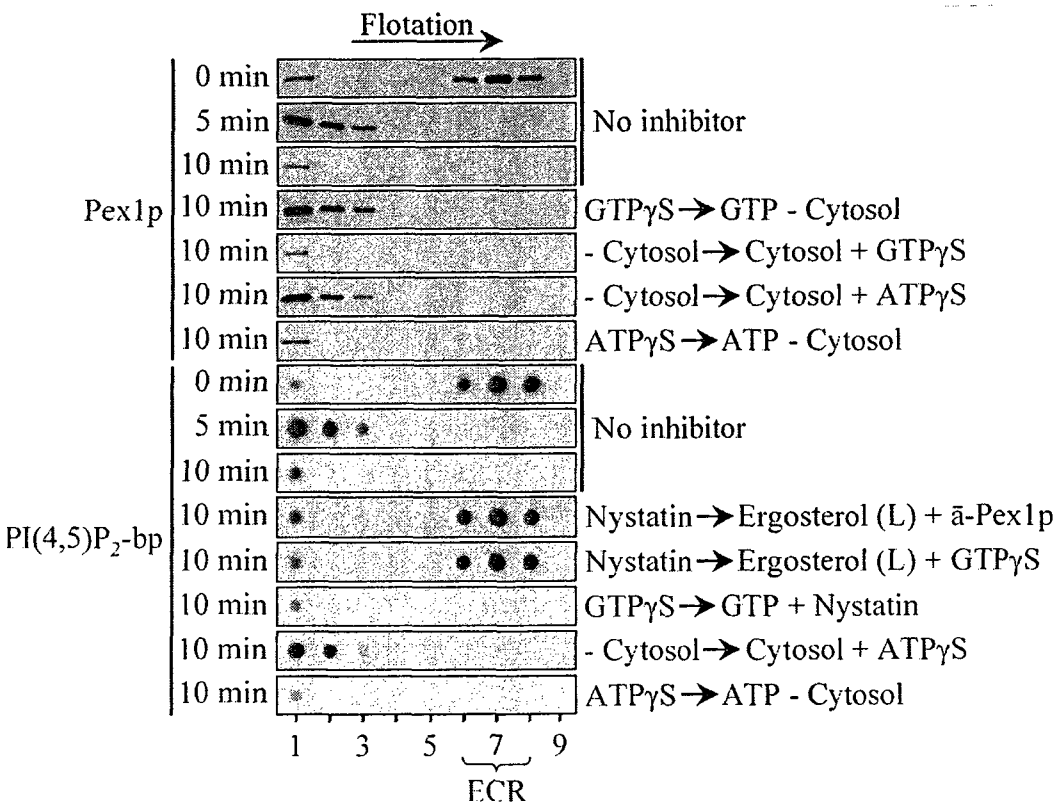

Figure 7.2. The hierarchy of peroxisome docking-specific events that result in the relocation of Pex1p and PI(4,5)P_2-binding proteins from ECR domains to a detergent-soluble portion of the membrane, followed by their release to the cytosol. P1 and P2 were

individually preprimed by incubation with cytosol and ATP for 10 min at 26°C. Peroxisomal vesicles were then reisolated by centrifugation, washed, and resuspended in a buffer. Reisolated P1 and P2 were incubated individually for 5 min at 26°C with or without GTPγS, ATPγS or nystatin in the presence or absence of cytosol, as indicated. P1 and P2 were then reisolated by centrifugation, washed, and resuspended in buffer containing GTP, GTPγS, ATPγS, ATP, liposomes with ergosterol, antibodies to Pex1p, or nystatin in the presence or absence of cytosol, as indicated. After a 5-min incubation at 26°C, P1 and P2 were mixed and supplemented with cytosol and ATP to yield standard fusion reactions. Samples were incubated at 26°C. Equal aliquots of peroxisomal vesicles were taken at the times indicated. P1 and P2 were then pelleted by centrifugation. Samples were subjected to osmotic lysis, followed by centrifugation. The pellets of membranes recovered after such centrifugation were resuspended in ice-cold MBS buffer and supplemented with a detergent, Brij 35. After incubation on ice for 30 min, the Brij 35-treated membranes were subjected to centrifugation by flotation in a discontinuous sucrose density gradient. Proteins recovered in equal volumes of gradient fractions were resolved by SDS-PAGE and immunoblotted with antibodies to Pex1p. Equal volumes of gradient fractions were also subjected to protein-lipid overlay assays using nitrocellulose membrane arrays spotted with $PI(4,5)P_2$.

7.4 Discussion

Using the two-stage assay for the priming-specific lateral movement of Pex1p and Pex6p in the membrane, I found that the ergosterol-dependent step precedes the PI(4)P-requiring step. In fact, no such movement was seen when unprimed peroxisomes were initially exposed to nystatin, then reisolated, washed and exposed to anti-PI(4)P antibody in the presence of ergosterol-containing liposomes that overcome the block imposed by nystatin treatment (Figure 7.1). In contrast, when nystatin and anti-PI(4)P antibody were added in the reverse order and PI(4)P was used during the second stage to overcome the block imposed by anti-PI(4)P antibody, the priming-specific lateral movement of Pex1p and Pex6p was not impaired, and both AAA ATPases were successfully released to the cytosol (Figure 7.1). Using the two-stage assay, I also established that the PI(4)P-dependent step during the priming-specific relocation of Pex1p and Pex6p to ergosterol-

and ceramide-poor domains is followed by the PI(4,5)P_2-requiring step (Figure 7.1). Moreover, my findings imply that the lateral movement of Pex1p and Pex6p to ergosterol- and ceramide-poor membrane domains during peroxisome priming is followed by their cytosol- and ATP hydrolysis-dependent release from these domains to the cytosol (Figure 7.1). In the two-stage assay, such release of both AAA ATPases was impaired when unprimed peroxisomes were initially incubated in the presence of ATP, but in the absence of cytosol, then reisolated and exposed to cytosol and the nonhydrolyzable analogue ATPγS (Figure 7.1). In contrast, both AAA ATPases were successfully released to the cytosol when cytosolic proteins and ATPγS were added in the reverse order (Figure 7.1). Thus, the cytosol-dependent step during this priming-specific event is a prerequisite for a step that needs ATP hydrolysis.

Using the two-stage assay for the docking-specific release of Pex1p to the cytosol, I also established that the GTP hydrolysis-dependent step precedes a step that requires cytosolic proteins. In fact, Pex1p was not released to the cytosol when separately primed P1 and P2 were mixed, treated with the nonhydrolyzable analogue GTPγS in the presence of cytosol, then reisolated and exposed to GTP, which overcomes the block imposed by GTPγS treatment (Figure 7.2). In contrast, the release of Pex1p to the cytosol was not compromised when separately primed P1 and P2 were mixed, incubated in the absence of cytosol, then reisolated and exposed to cytosol and GTPγS (Figure 7.2). Using the two-stage assay, I also showed that the cytosol-dependent step during the docking-specific release of Pex1p to the cytosol is followed by a step that requires ATP hydrolysis (Figure 7.2).

Moreover, I found that, another docking-specific event, the lateral segregation of PI(4,5)P_2-bp from ECR domains, requires ergosterol, Pex1p and GTP hydrolysis (Figure 7.2). In the two-stage assay, both the Pex1p- and the GTP hydrolysis-dependent steps follow a step that requires ergosterol. Indeed, the PI(4,5)P_2-bp did not move to a detergent-soluble portion of the membrane when the exposure of separately primed and mixed P1 and P2 to nystatin preceded the treatment with monospecific antibodies to Pex1p or with GTPγS, added together with ergosterol-containing liposomes to overcome the block imposed by nystatin exposure (Figure 7.2). Noteworthy, in the beginning of peroxisome docking, PI(4,5)P_2-bp are attached to both fusion partners, Pex1p can only be found on the cytosolic face of P2, and the only GTP-bp that can be detected is the one(s) that reside(s) on the outer surface of P1. Together, these findings suggest that the docking-specific segregation of P1-bound PI(4,5)P_2-bp from ECR domains requires GTP-bp, whereas such segregation of P2-associated PI(4,5)P_2-bp depends on Pex1p.

The last stage in the process of spatial rearrangement of PI(4,5)P_2-bp on the cytosolic surfaces of both fusion partners involves their cytosol- and ATP hydrolysis-dependent release from a detergent-soluble portion of the membrane to the cytosol. Using the two-stage assay, I found that the cytosol-dependent step during such release of PI(4,5)P_2-bp is followed by a step that requires ATP hydrolysis (Figure 7.2).

7.5 Conclusions

Altogether, my findings suggest the following model for the multistep remodeling of the peroxisome fusion machinery in the membranes of P1 and P2 (Figure 7.3). In unprimed P1 and P2, all identified essential components of this machinery, including Pex1p, Pex6p,

PI(4)P-bp, PI(4,5)P_2-bp and GTP-bp, are attached to the cytosolic surface of ECR domains. Priming of fusion partners is initiated by the lateral movement of P1-associated Pex1p and P2-bound Pex6p from ECR domains to an ergosterol- and ceramide-poor portion of the membrane. This essential event in the process of activating fusion partners for subsequent docking includes at least three consecutive steps. The initial ergosterol-dependent step is followed by a PI(4)P-dependent step, which precedes a step that requires PI(4,5)P_2. After their segregation from ECR domains, both P1-associated Pex1p and P2-bound Pex6p are released to the cytosol. Such release of both AAA ATPases from an ergosterol- and ceramide-poor portion of the membrane is mandatory for the priming of both fusion partners and includes two steps. The first step requires cytosolic proteins, whereas the next step is driven by ATP hydrolysis. Priming of P1 and P2 is followed by their docking.

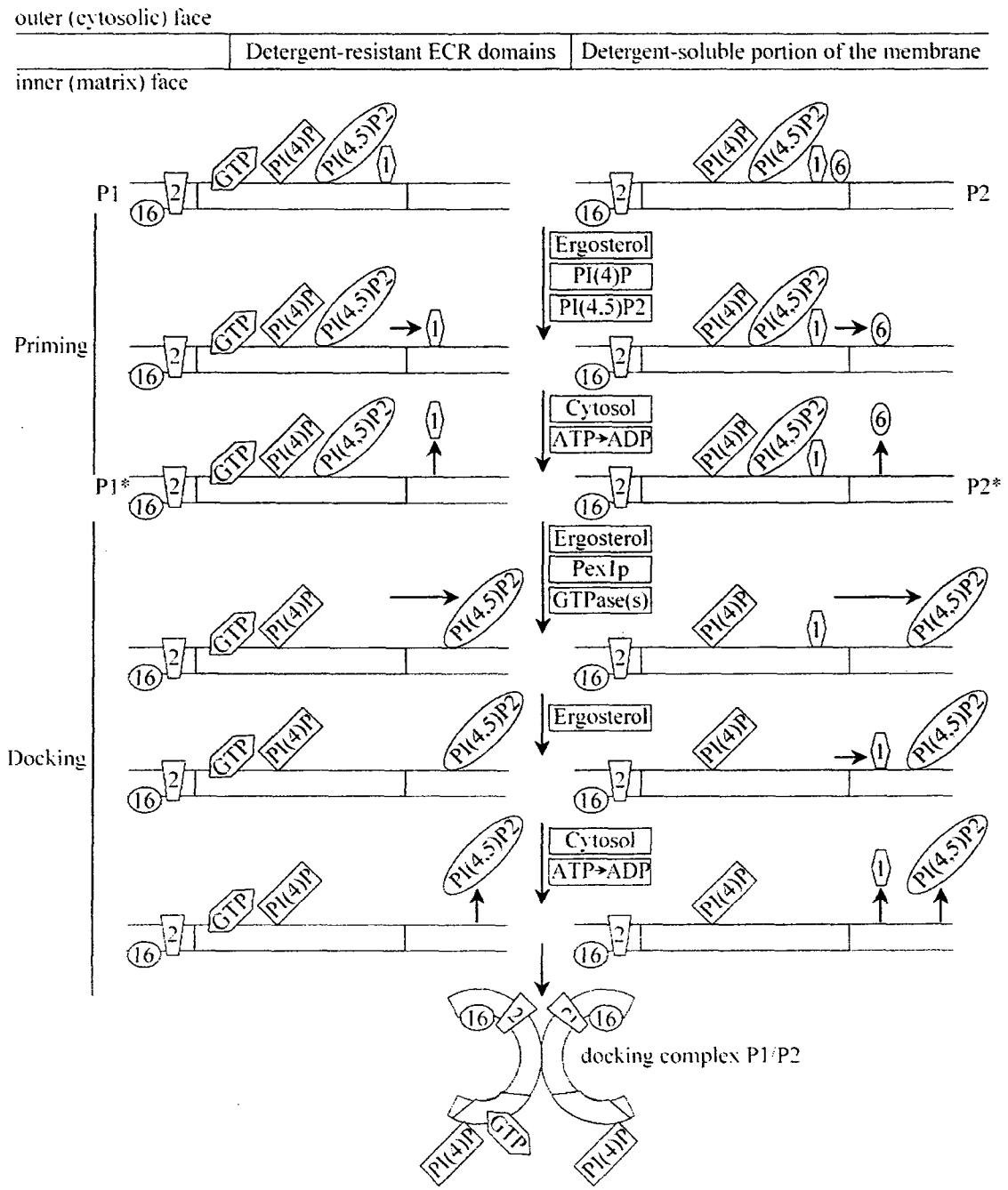

Figure 7.3. A model for the multistep remodeling of the peroxisome fusion machinery. The multicomponent peroxisome fusion machinery, which only transiently resides in ECR membrane domains of P1 and P2 vesicles, undergoes multiple rounds of temporal and spatial reorganization during priming and docking of both fusion partners.

Docking of primed peroxisomal vesicles is a multistep process, which begins with the lateral movement of PI(4,5)P_2-bp in the membranes of P1 and P2 from ECR domains to

ergosterol- and ceramide-poor domains. This lateral movement of $PI(4,5)P_2$-bp occurs in three consecutive steps. The first step needs ergosterol in the membranes of both fusion partners. The second step depends on Pex1p that resides in ECR domains of P2 vesicles. The third step requires GTP hydrolysis by GTPase(s), perhaps by GTP-bp in ECR domains of P1 vesicles. The docking-specific lateral movement of $PI(4,5)P_2$-bp in the membranes of P1 and P2 is followed by the ergosterol-dependent relocation of P2-bound Pex1p from ECR domains to ergosterol- and ceramide-poor domains. After their lateral movement to ergosterol- and ceramide-poor portions of the membranes of both fusion partners, P1-associated $PI(4,5)P_2$-bp and P2-bound $PI(4,5)P_2$-bp and Pex1p are released to the cytosol. Such release of $PI(4,5)P_2$-bp and Pex1p begins with a cytosol-dependent step, which is followed by a step that requires ATP hydrolysis. By the end of the docking process, PI(4)P-bp and GTP-bp remain in ECR domains of P1 and P2.

8 Dynamics of peroxisomal fusion

8.1 Introduction

In order to establish the requirements for the fusion of docked P1 and P2, I isolated the P1/P2 peroxisome docking complex by flotation on a multistep sucrose gradient and used the in vitro fusion assay to assess how various compounds known to inhibit fusion of other organellar membranes influence the merge of lipid bilayers of docked P1 and P2 peroxisomes. For instance, I used the proton ionophore carbonyl cyanide *m*-chlorophenylhydrazone (CCCP), which is known to impair vacuole fusion and the fusion of the mitochondrial inner membranes, to define the role of proton gradient across the peroxisomal membrane in the fusion between docked P1 and P2 [156-159]. Furthermore,

to test if the fusion of docked P1 and P2 requires Ca^{2+} gradient across the peroxisomal membrane along with Ca^{2+}-ATPases, I used the Ca^{2+}-sequestering compounds ionomycin, thapsigargin and cyclopiazonic acid, all of which have been shown to prevent the homotypic fusion of vacuoles [159, 160]. Moreover, to evaluate if peroxisome fusion depends on extracellular Ca^{2+} and its intracellular sensor protein calmodulin (CaM), I used the membrane non-permeable Ca^{2+} chelator 1,2-bis(o-aminophenoxy)ethane N,N,N',N'-tetraacetic acid (BAPTA) and the CaM antagonist W7, which have been shown to inhibit endosome and homotypic vacuole fusion [144, 159, 161-163]. Noteworthy, calmodulin is a highly conserved intracellular Ca^{2+}-binding protein, which is expressed in all cell types [164, 165]. The binding of CaM to Ca^{2+} leads to the conformational change in its structure by exposing the two hydrophobic domains of CaM, which in turn activate the receptor proteins that it targets [165]. W7 is a CaM antagonist that binds to CaM in a Ca^{2+}-dependent manner through hydrophobic and electrostatic interactions, thereby preventing other proteins from interacting with CaM [161]. Therefore, in order to test if the peroxisome fusion process also requires Ca^{2+}/CaM-activated proteins, I used anti-CaM antibodies, calmodulin binding domain (CBD) and calmodulin inhibitory peptide (CIP) in order to impair the CaM-dependent activation of these proteins.

Following the identification of a set of components inhibiting the peroxisome fusion process, I used the two-stage assay described in chapter 7 of this thesis in order to establish the hierarchy of fusion-specific steps that involve these components and to define a mechanism by which each of these components drives the merge of lipid bilayers surrounding docked P1 and P2 peroxisomes.

8.2 Materials and methods

In vitro assay for evaluating the importance of the proton and calcium gradients for peroxisome fusion

Unprimed peroxisomes P1 and P2 were resuspended in a buffer containing cytosol, ATP and ATP regenerative system, mixed, and incubated on ice for 15 min in the presence or absence of CCCP, ionomycin, cyclopiazonic acid or thapsigargin at various concentrations. The samples were then transferred to 26°C. After a 90-min incubation of the standard fusion reactions at 26°C, the fusion efficiency was evaluated as described previously in the section "Materials and methods' of chapter 2.

In vitro assay for assessing the role of peroxisomal Ca^{2+} in the peroxisome fusion process

Unprimed peroxisomes P1 and P2 were resuspended in a buffer containing cytosol, mixed, and incubated on ice for 15 min in the presence or absence of BAPTA at various concentrations. The standard fusion reactions were then set up by adding ATP and ATP regenerative system. The samples were then transferred to 26°C. After incubation for 90 min at 26°C, the efficiency of peroxisome fusion was evaluated as described in the section "Materials and methods' of chapter 2.

In vitro assay for evaluating the role of CaM in peroxisome fusion

Unprimed peroxisomes P1 and P2 were resuspended in a buffer, mixed, and incubated on ice for 15 min in the presence of either intact or heat-inactivated anti-CaM antibodies at various concentrations. The peroxisomes were then reisolated by centrifugation at 4°C and supplemented with cytosol, ATP and ATP regenerative system. The samples were

then transferred to 26°C. The standard fusion reactions were incubated for 90 min at 26°C. The efficiency of peroxisome fusion was then evaluated as described in the section "Materials and methods' of chapter 2.

In vitro assay for evaluating the importance of CaM-activated proteins for peroxisome fusion

Unprimed peroxisomes P1 and P2 were resuspended in a buffer, mixed, and incubated on ice for 15 min in the presence or absence of CaM antagonists W7, CaM Binding Domain (CBD), or CaM Inhibitory Peptide (CIP) at various concentrations. The peroxisomes were then reisolated by centrifugation at 4°C and supplemented with cytosol, ATP and ATP regenerative system. The samples were then transferred to 26°C. The standard fusion reactions were allowed to proceed for 90 min at 26°C. The efficiency of peroxisome fusion was then evaluated as described in the section "Materials and methods' of chapter 2. To determine if the effects of various CaM-binding compounds and CaM antagonists on peroxisome fusion were reversible (and, therefore, specific), unprimed peroxisomes P1 and P2 were resuspended in a buffer, mixed, and incubated on ice for 15 min in the presence or absence of anti-CaM antibodies, W7, CBD or CIP at various concentrations. The peroxisomes were then reisolated by centrifugation at 4°C and resuspended in a buffer with or without purified CaM added to a final concentration of 10 μM or 50 μM. The standard fusion reactions were then set up by adding cytosol, ATP and ATP regenerative system. After a 90-min incubation at 26°C, the efficiency of peroxisome fusion was evaluated as described in the section "Materials and methods' of chapter 2.

In vitro assay for evaluating the requirements for the fusion of docked P1 and P2

P1 and P2 were primed individually with cytosol and ATP at 26°C, mixed, and incubated with cytosol and ATP at 26°C. The resulting P1/P2 docking complex was purified by flotation centrifugation on a multi-step sucrose gradient and resuspended in a buffer containing cytosol. This complex was incubated for 15 min on ice with or without nystatin, fillipin III, amphotericin B, anti-PI(4)P, anti-PI(4,5)P_2, ATPγS, anti-Pex1p, anti-Pex6p, GTPγS, GppNHp, CCCP, ionomycin, cyclopiazonic acid, thapsigargin, BAPTA, anti-CaM antibodies, W7, CBD or CIP in the presence or absence of cytosol. The peroxisomes were then reisolated by centrifugation at 4°C and resuspended in a buffer containing cytosol, ATP and ATP regenerative system. The samples were then transferred to 26°C. After a 90-min incubation at 26°C, the efficiency of peroxisome fusion was evaluated as described in the section "Materials and methods" of chapter 2.

Two-stage assay for defining the order of individual steps during peroxisome fusion

P1 and P2 were primed individually with cytosol and ATP at 26°C, mixed, and incubated with cytosol and ATP at 26°C. The resulting P1/P2 docking complex was purified by flotation centrifugation on a multi-step sucrose gradient and then incubated on ice for 15 min in presence of CCCP. The peroxisomes were then reisolated by centrifugation at 4°C, washed, and resuspended in a buffer containing ionomycin. The samples were then transferred to 26°C. After a 90-min incubation at 26°C, the efficiency of peroxisome fusion was evaluated as described in the section "Materials and methods" of chapter 2. The order of inhibitor addition was then reversed and the docking complex was first incubated on ice for 15 min in the presence of ionomycin, reisolated by centrifugation,

washed and incubated in the presence of CCCP on ice for 15 min. The samples were then transferred to 26°C. After a 90-min incubation at 26°C, the efficiency of peroxisome fusion was evaluated as described in the section "Materials and methods" of chapter 2. The two-stage inhibition assay was also performed using the following inhibitors tested in a pair-wise manner: nystatin, anti-PI(4)P, anti-PI(4,5)P_2, cytosol, ATPγS, anti-Pex1p, anti-Pex6p, GTPγS, GppNHp, CCCP, ionomycin, cyclopiazonic acid, thapsigargin, BAPTA, anti-CaM, W7, CBD, or CIP.

In vitro assay for evaluating the dynamics of CaM association with the peroxisomal membrane and of changes in Ca^{2+} concentration during peroxisome fusion

P1 and P2 were primed individually with cytosol and ATP at 26°C, mixed, and incubated with cytosol and ATP at 26°C. The resulting P1/P2 docking complex was purified by flotation centrifugation on a multi-step sucrose gradient and then incubated for 90 min at 26°C in the presence or absence of CCCP or nonhydrolyzable GTP analogues, with aliquots taken at different time points. The samples were then centrifuged to obtain the peroxisomal (pellet) and extraperoxisomal (supernatant) fractions. The level of peroxisome-bound CaM was assessed by immunoblotting with anti-CaM antibodies. The concentration of extracellular Ca^{2+} was monitored by spectrophotometry.

8.3 Results

8.3.1 Proton gradient across the peroxisomal membrane is essential for peroxisome fusion

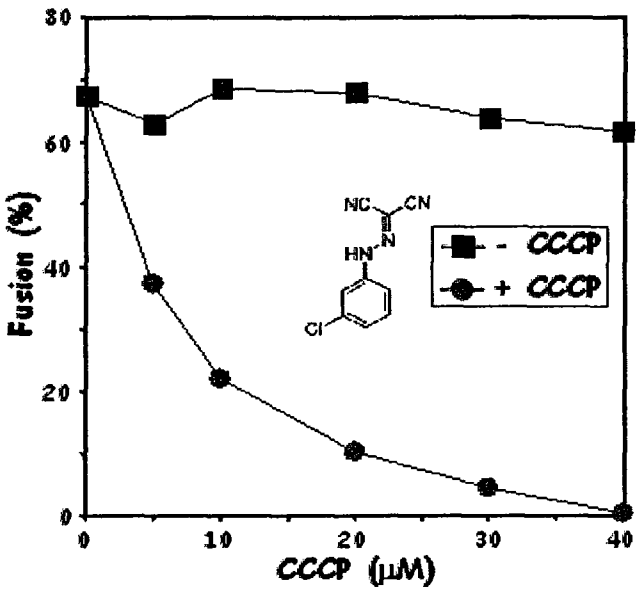

Figure 8.1. Peroxisome fusion is inhibited by the H^+ ionophore CCCP. Unprimed peroxisomes P1 and P2 were resuspended in a buffer containing cytosol, ATP and ATP regenerative system, mixed, and incubated on ice for 15 min in the presence or absence of CCCP at various concentrations. The samples were then transferred to 26°C. After a 90-min incubation of the standard fusion reactions at 26°C, the fusion efficiency was evaluated as described previously in the section "Materials and methods' of chapter 2.

8.3.2 Peroxisome fusion requires active maintenance of the Ca^{2+} gradient across the peroxisomal membrane

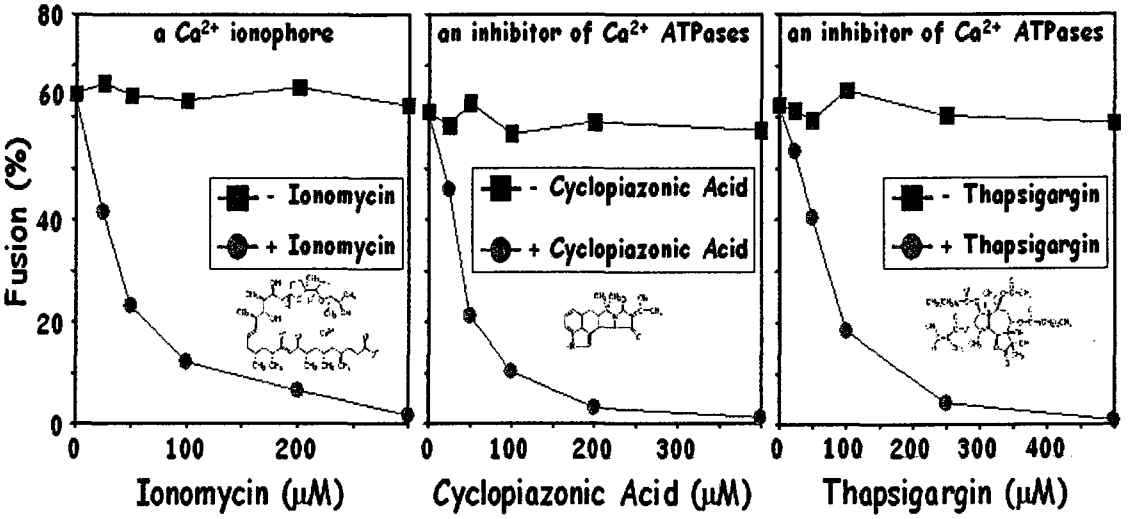

Figure 8.2. Peroxisome fusion is inhibited by the Ca^{2+} ionophore ionomycin and two inhibitors of Ca^{2+}-dependent ATPases, cyclopiazonic acid and thapsigargin. Unprimed peroxisomes P1 and P2 were resuspended in a buffer containing cytosol, ATP and ATP regenerative system, mixed, and incubated on ice for 15 min in the presence or absence of ionomycin, cyclopiazonic acid or thapsigargin at various concentrations. The samples were then transferred to 26°C. After a 90-min incubation of the standard fusion reactions at 26°C, the fusion efficiency was evaluated as described previously in the section "Materials and methods' of chapter 2.

8.3.3 Peroxisome fusion depends on the presence of Ca^{2+} on the peroxisome surface

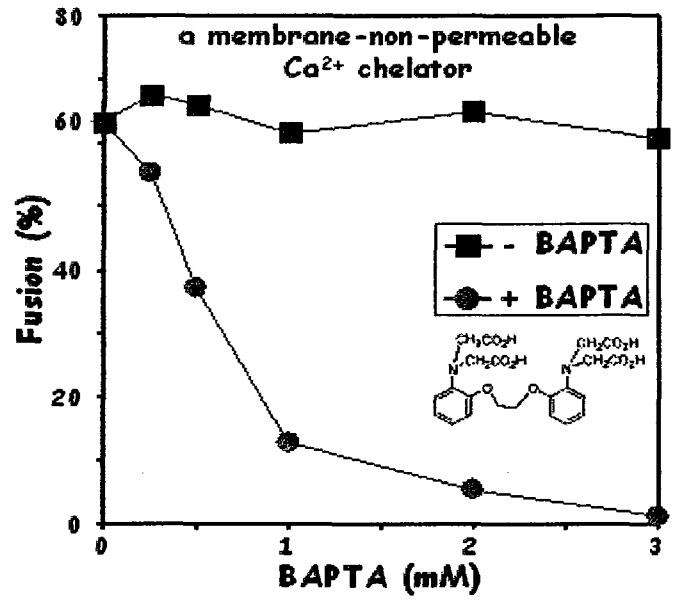

Figure 8.3. Peroxisome fusion is inhibited by the membrane-non-permeable Ca^{2+} chelator BAPTA (1,2-Bis(2-aminophenoxy)ethane-*N,N,N',N'*-tetraacetic acid). Unprimed peroxisomes P1 and P2 were resuspended in a buffer containing cytosol, mixed, and incubated on ice for 15 min in the presence or absence of BAPTA at various concentrations. The standard fusion reactions were then set up by adding ATP and ATP regenerative system. The samples were then transferred to 26°C. After incubation for 90 min at 26°C, the efficiency of peroxisome fusion was evaluated as described in the section "Materials and methods' of chapter 2.

8.3.4 Peroxisome fusion requires CaM, a cytosolic Ca^{2+}-binding protein

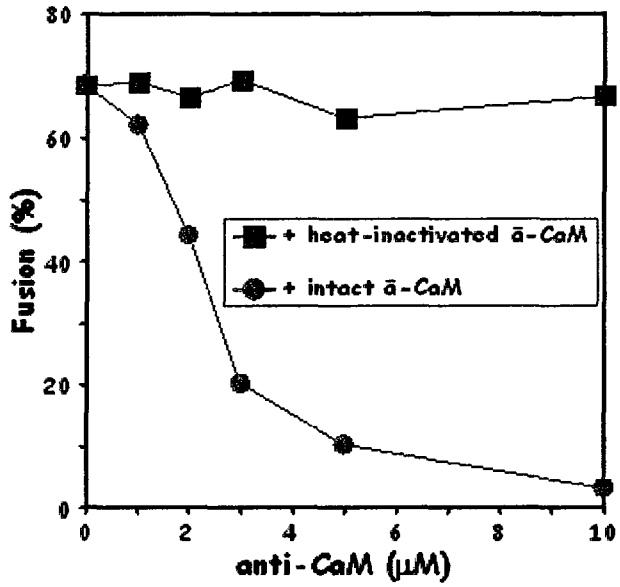

Figure 8.4. Peroxisome fusion is inhibited by monoclonal antibodies to CaM. Unprimed peroxisomes P1 and P2 were resuspended in a buffer, mixed, and incubated on ice for 15 min in the presence of either intact or heat-inactivated anti-CaM antibodies at various concentrations. The peroxisomes were then reisolated by centrifugation at 4°C and supplemented with cytosol, ATP and ATP regenerative system. The samples were then transferred to 26°C. The standard fusion reactions were incubated for 90 min at 26°C. The efficiency of peroxisome fusion was then evaluated as described in the section "Materials and methods' of chapter 2.

8.3.5 Peroxisome fusion depends on Ca^{2+}/CaM-dependent protein kinases and phosphodiesterases

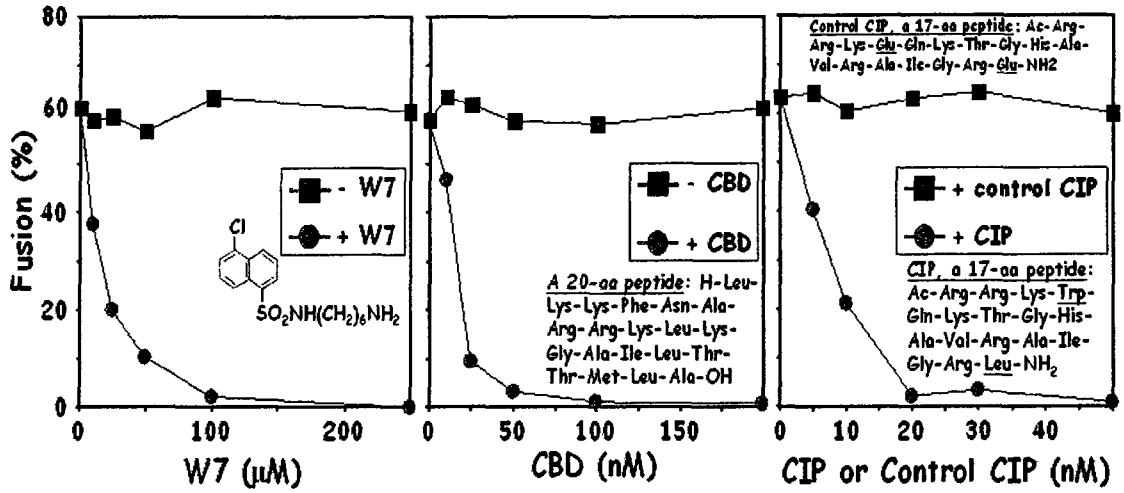

Figure 8.5. Peroxisome fusion is inhibited by the CaM antagonists W7, Calmodulin Binding Domain (CBD) and Calmodulin Inhibitory Peptide (CIP), all of which impair the activation of Ca^{2+}/CaM-dependent protein kinases and phosphodiesterases. Unprimed peroxisomes P1 and P2 were resuspended in a buffer, mixed, and incubated on ice for 15 min in the presence or absence of W7, CBD or CIP at various concentrations. The peroxisomes were then reisolated by centrifugation at 4°C and supplemented with cytosol, ATP and ATP regenerative system. The samples were then transferred to 26°C. The standard fusion reactions were allowed to proceed for 90 min at 26°C. The efficiency of peroxisome fusion was then evaluated as described in the section "Materials and methods' of chapter 2.

8.3.6 Inhibitory effects of anti-CaM antibodies and CaM antagonists on peroxisome fusion can be reversed by CaM in a concentration-dependent fashion and is, therefore, specific

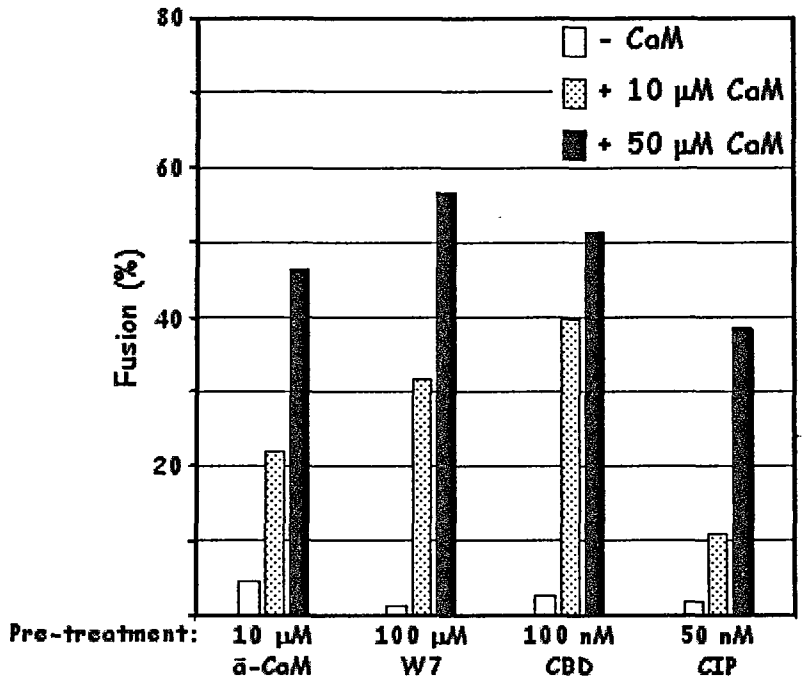

Figure 8.6. The negative effect of anti-CaM antibodies and CaM antagonists is specific because it can be reversed by CaM in a concentration-dependent manner. Unprimed peroxisomes P1 and P2 were resuspended in a buffer, mixed, and incubated on ice for 15 min in the presence or absence of anti-CaM antibodies, W7, CBD or CIP at various concentrations. The peroxisomes were then reisolated by centrifugation at 4°C and resuspended in a buffer with or without purified CaM added to a final concentration of 10 μM or 50 μM. The standard fusion reactions were then set up by adding cytosol, ATP and ATP regenerative system. After a 90-min incubation at 26°C, the efficiency of peroxisome fusion was evaluated as described in the section "Materials and methods' of chapter 2.

8.3.7 Fusion of the docked peroxisomes requires GTP hydrolysis, the gradients of H^+ and Ca^{2+} across the peroxisomal membrane, presence of Ca^{2+} on the peroxisomal surface, CaM, and Ca^{2+}/CaM-dependent protein kinases and phosphodiesterases

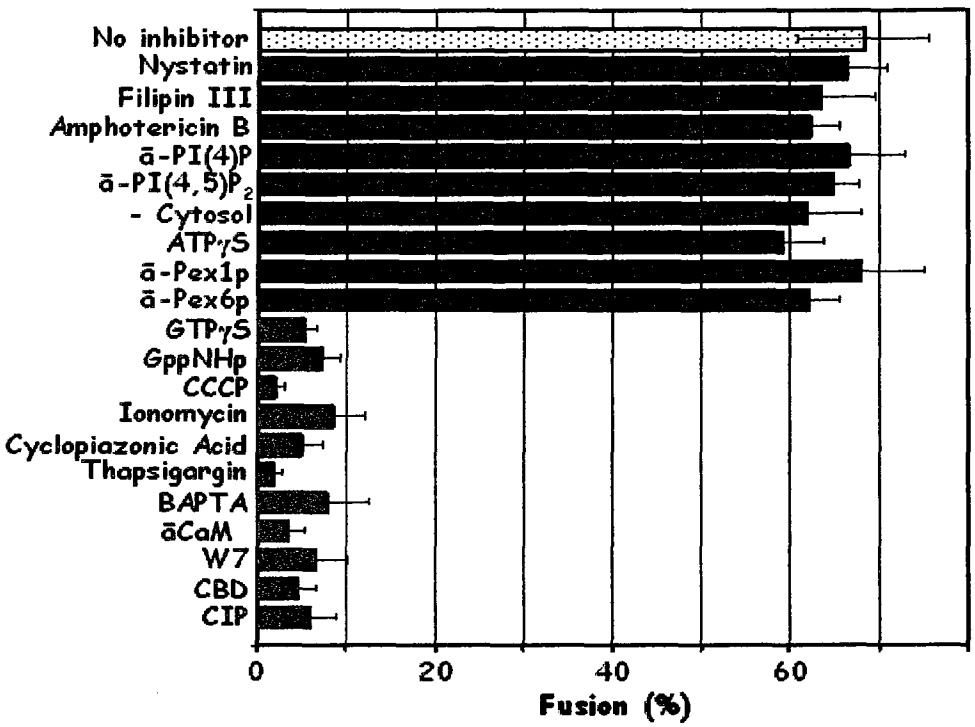

Figure 8.7. The requirements for the fusion of docked peroxisomes P1 and P2. P1 and P2 were primed individually with cytosol and ATP at 26°C, mixed, and incubated with cytosol and ATP at 26°C. The resulting P1/P2 docking complex was purified by flotation centrifugation on a multi-step sucrose gradient and resuspended in a buffer containing cytosol. This complex was incubated for 15 min on ice with or without nystatin, fillipin III, amphotericin B, anti-PI(4)P, anti-PI(4,5)P_2, ATPγS, anti-Pex1p, anti-Pex6p, GTPγS, GppNHp, CCCP, ionomycin, cyclopiazonic acid, thapsigargin, BAPTA, anti-CaM antibodies, W7, CBD or CIP in the presence or absence of cytosol. The peroxisomes were then reisolated by centrifugation at 4°C and resuspended in a buffer containing cytosol, ATP and ATP regenerative system. The samples were then transferred to 26°C. After a 90-min incubation at 26°C, the efficiency of peroxisome fusion was evaluated as described in the section "Materials and methods" of chapter 2.

8.3.8 The H^+ gradient-dependent step during fusion of docked P1 and P2 precedes the steps that require the $Ca2^+$ gradient across the peroxisomal membrane and Ca^{2+} on the outer peroxisome surface

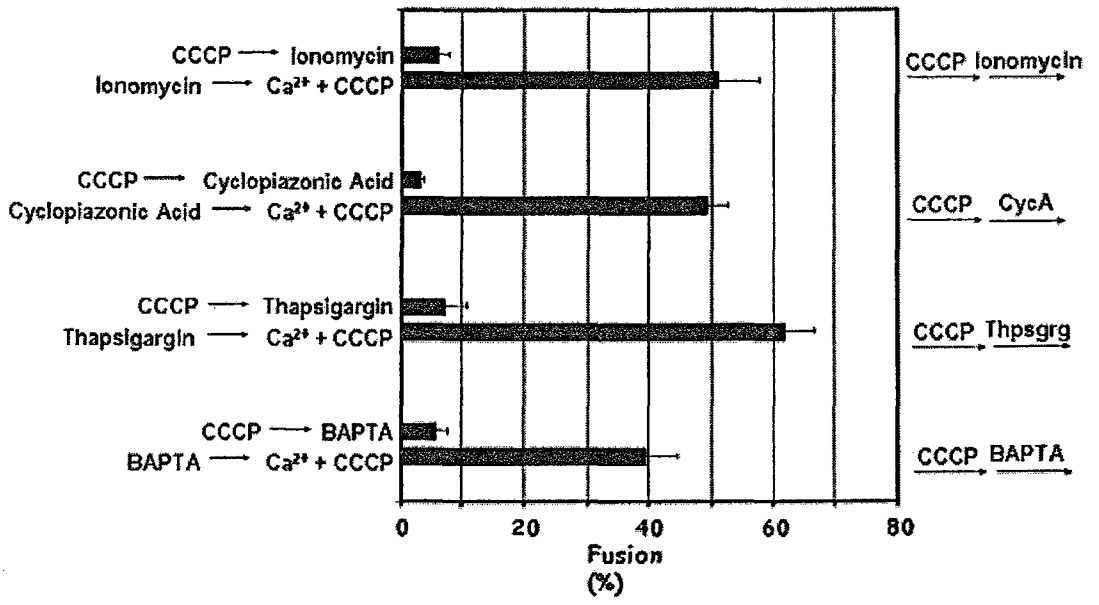

Figure 8.8. The fusion of docked P1 and P2 is initiated by the H^+ gradient-dependent step that precedes the steps requiring the Ca^{2+} gradient across the peroxisomal membrane and presence of Ca^{2+} on the outer face of the peroxisome. P1 and P2 were primed individually with cytosol and ATP at 26°C, mixed, and incubated with cytosol and ATP at 26°C. The resulting P1/P2 docking complex was purified by flotation centrifugation on a multi-step sucrose gradient and then incubated on ice for 15 min in presence of CCCP. The peroxisomes were then reisolated by centrifugation at 4°C, washed, and resuspended in a buffer containing ionomycin. The samples were then transferred to 26°C. After a 90-min incubation at 26°C, the efficiency of peroxisome fusion was evaluated as described in the section "Materials and methods" of chapter 2. The order of inhibitor addition was then reversed and the docking complex was first incubated on ice for 15 min in the presence of ionomycin, reisolated by centrifugation, washed and incubated in the presence of CCCP on ice for 15 min. The samples were then transferred to 26°C. After a 90-min incubation at 26°C, the efficiency of peroxisome fusion was evaluated as described in the section "Materials and methods" of chapter 2. This two-stage inhibition assay was also performed using other inhibitors of peroxisome fusion that were tested in a pair-wise manner as indicated.

8.3.8 The H^+ gradient-dependent step during fusion of docked P1 and P2 precedes the step that requires CaM

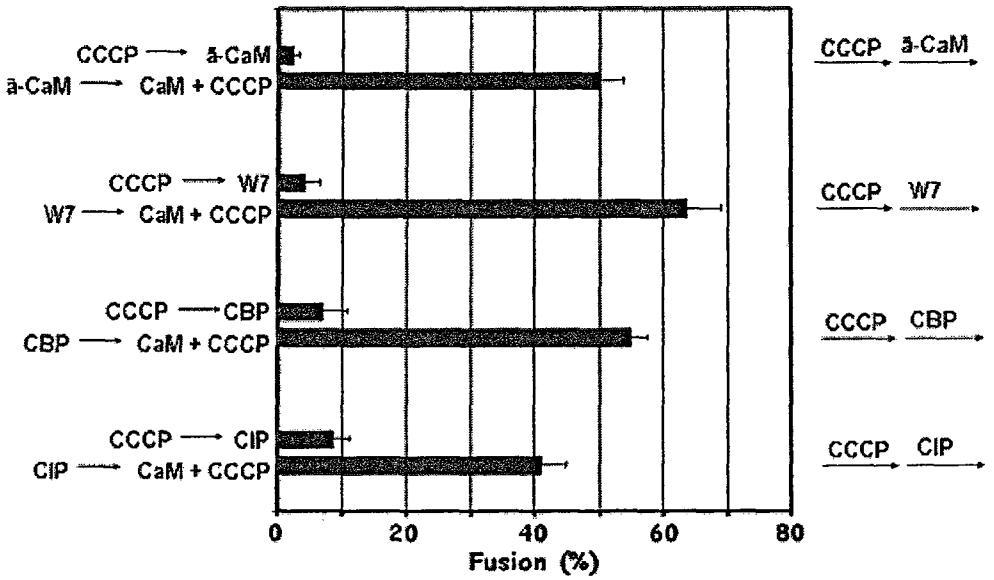

Figure 8.9. The H^+ gradient-dependent step of the peroxisome fusion process precedes the step that requires CaM. P1 and P2 were primed individually with cytosol and ATP at 26°C, mixed, and incubated with cytosol and ATP at 26°C. The resulting P1/P2 docking complex was purified by flotation centrifugation on a multi-step sucrose gradient and then incubated on ice for 15 min in presence of CCCP. The peroxisomes were then reisolated by centrifugation at 4°C, washed, and resuspended in a buffer containing anti-CaM antibodies. Following a 15-min incubation on ice, the samples were transferred to 26°C. After a 90-min incubation at 26°C, the efficiency of peroxisome fusion was evaluated as described in the section "Materials and methods" of chapter 2. The order of inhibitor addition was then reversed and the docking complex was first incubated on ice for 15 min in the presence of anti-CaM antibodies, reisolated by centrifugation, washed and incubated in the presence of CCCP on ice for 15 min. The samples were then transferred to 26°C. After a 90-min incubation at 26°C, the efficiency of peroxisome fusion was evaluated as described in the section "Materials and methods" of chapter 2. This two-stage inhibition assay was also performed using other inhibitors of peroxisome fusion that were tested in a pair-wise manner as indicated.

8.3.10 The Ca^{2+} gradient-dependent step during fusion of docked P1 and P2 occurs before CaM-dependent step

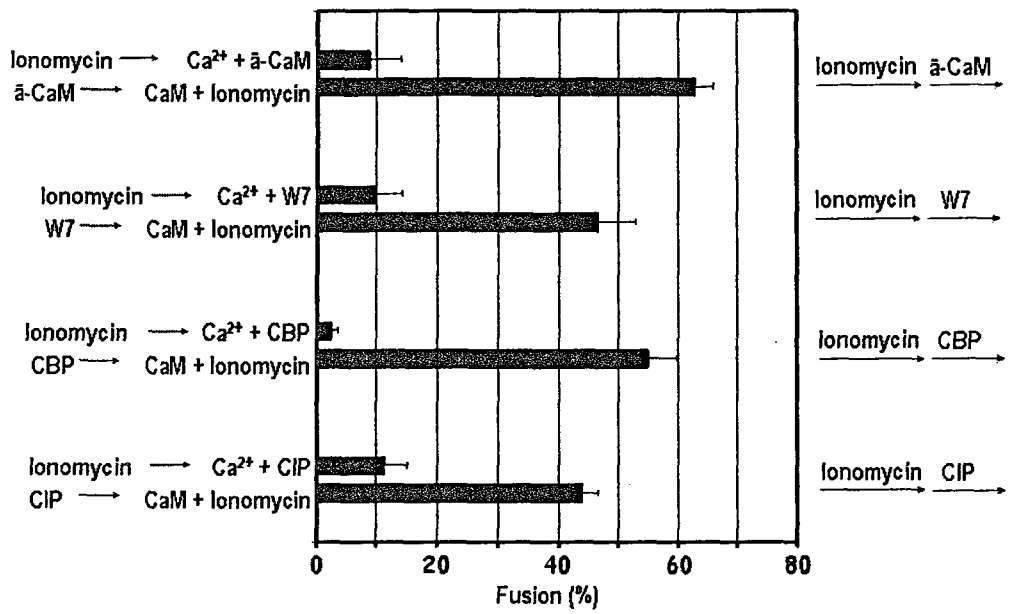

Figure 8.10. During fusion of docked P1 and P2, the Ca^{2+} gradient-dependent step precedes the step requiring CaM. P1 and P2 were primed individually with cytosol and ATP at 26°C, mixed, and incubated with cytosol and ATP at 26°C. The resulting P1/P2 docking complex was purified by flotation centrifugation on a multi-step sucrose gradient and then incubated on ice for 15 min in presence of ionomycin. The peroxisomes were then reisolated by centrifugation at 4°C, washed, and resuspended in a buffer containing Ca^{2+} and anti-CaM antibodies. Following a 15-min incubation on ice, the samples were transferred to 26°C. After a 90-min incubation at 26°C, the efficiency of peroxisome fusion was evaluated as described in the section "Materials and methods" of chapter 2. The order of inhibitor addition was then reversed and the docking complex was first incubated on ice for 15 min in the presence of anti-CaM antibodies, reisolated by centrifugation, washed and incubated in the presence of CaM and ionomycin on ice for 15 min. The samples were then transferred to 26°C. After a 90-min incubation at 26°C, the efficiency of peroxisome fusion was evaluated as described in the section "Materials and methods" of chapter 2. This two-stage inhibition assay was also performed using other inhibitors of peroxisome fusion that were tested in a pair-wise manner as indicated.

8.3.11 The CaM-dependent step during fusion of docked P1 and P2 precedes the step that requires GTP hydrolysis by GTPase(s)

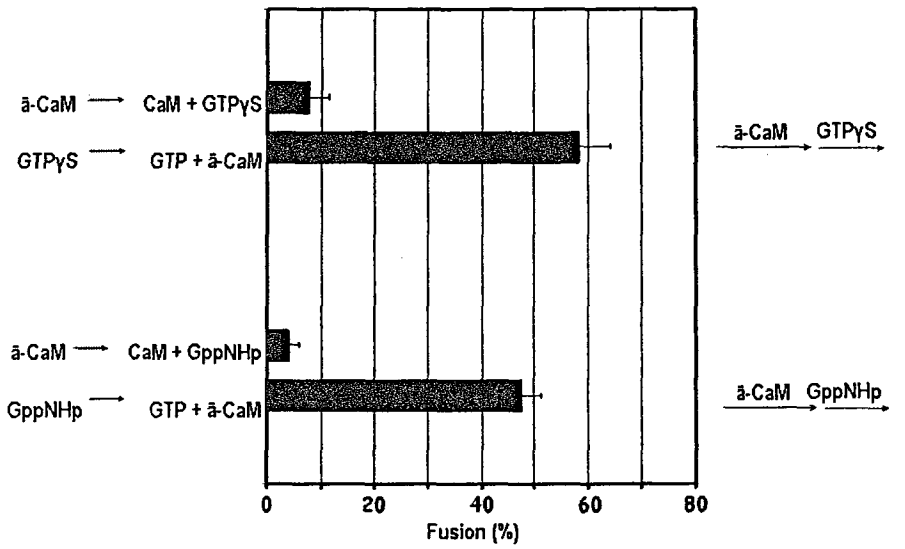

Figure 8.11. During fusion of docked P1 and P2, the CaM-dependent step occurs before the step that requires GTP hydrolysis. P1 and P2 were primed individually with cytosol and ATP at 26°C, mixed, and incubated with cytosol and ATP at 26°C. The resulting P1/P2 docking complex was purified by flotation centrifugation on a multi-step sucrose gradient and then incubated on ice for 15 min in presence of anti-CaM antibodies. The peroxisomes were then reisolated by centrifugation at 4°C, washed, and resuspended in a buffer containing CaM and the nonhydrolyzable GTP analogue GTPγS. Following a 15-min incubation on ice, the samples were transferred to 26°C. After a 90-min incubation at 26°C, the efficiency of peroxisome fusion was evaluated as described in the section "Materials and methods" of chapter 2. The order of inhibitor addition was then reversed and the docking complex was first incubated on ice for 15 min in the presence of GTPγS, reisolated by centrifugation, washed and incubated in the presence of GTP and GTPγS on ice for 15 min. The samples were then transferred to 26°C. After a 90-min incubation at 26°C, the efficiency of peroxisome fusion was evaluated as described in the section "Materials and methods" of chapter 2. This two-stage inhibition assay was also performed using other inhibitors of peroxisome fusion that were tested in a pair-wise manner as indicated.

8.3.12 During fusion of P1 and P2, the CCCP-sensitive release of Ca^{2+} from the organelle lumen and subsequent recruitment of cytosolic CaM to the organelle surface are followed by the uptake of Ca^{2+} into the lumen and release of CaM from the surface to the cytosol

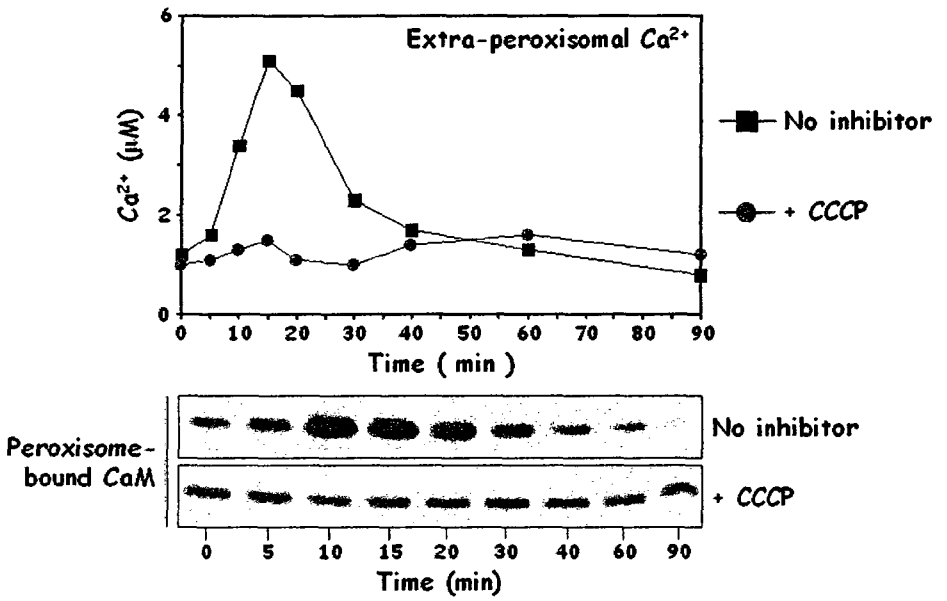

Figure 8.12. Fusion of docked P1 and P2 is initiated by the release of Ca^{2+} from the organelle lumen, which is followed by the recruitment of cytosolic CaM to the organelle surface, influx of Ca^{2+} into the peroxisomal lumen and release of CaM from the peroxisomal surface back to the cytosol. P1 and P2 were primed individually with cytosol and ATP at 26°C, mixed, and incubated with cytosol and ATP at 26°C. The resulting P1/P2 docking complex was purified by flotation centrifugation on a multi-step sucrose gradient and then incubated for 90 min at 26°C in the presence or absence of CCCP, with aliquots taken at different time points. The samples were then centrifuged to obtain the peroxisomal (pellet) and extraperoxisomal (supernatant) fractions. The level of peroxisome-bound CaM was assessed by immunoblotting with anti-CaM antibodies. The concentration of extracellular Ca^{2+} was monitored by spectrophotometry.

8.3.13 During fusion of P1 and P2, both the uptake of $Ca2^+$ into the lumen and release of CaM from the surface to the cytosol require GTP hydrolysis

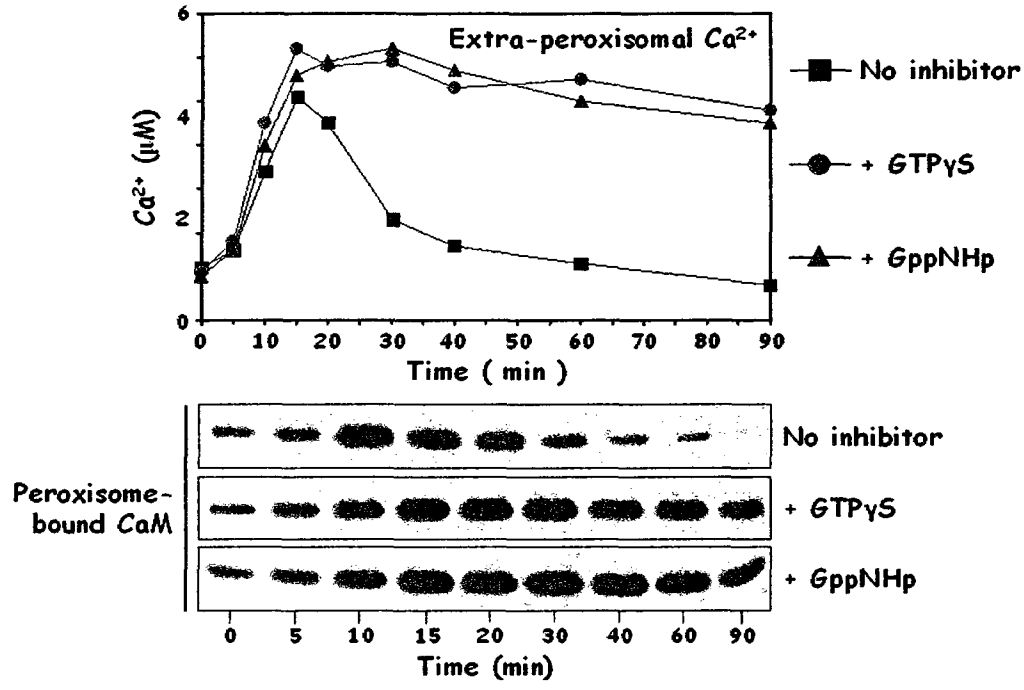

Figure 8.13. Inhibition of GTP hydrolysis prevents the influx of Ca^{2+} back into the peroxisomal lumen and impairs the release of CaM from the peroxisomal surface back to the cytosol. P1 and P2 were primed individually with cytosol and ATP at 26°C, mixed, and incubated with cytosol and ATP at 26°C. The resulting P1/P2 docking complex was purified by flotation centrifugation on a multi-step sucrose gradient and then incubated for 90 min at 26°C in the presence or absence of the nonhydrolyzable GTP analogues GTPγS or GppNHp, with aliquots taken at different time points. The samples were then centrifuged to obtain the peroxisomal (pellet) and extraperoxisomal (supernatant) fractions. The level of peroxisome-bound CaM was assessed by immunoblotting with anti-CaM antibodies. The concentration of extracellular Ca^{2+} was monitored by spectrophotometry.

8.4 Discussion

I found that fusion of docked P1 and P2 is inhibited by CCCP, an H^+ ionophore that disrupts the proton gradient across the peroxisomal membrane, thus demonstrating the importance of establishing such gradient for the fusion process (Figure 8.1). Peroxisome fusion was also inhibited by the Ca^{2+} ionophore ionomycin and by two inhibitors of Ca^{2+}-dependent ATPases, namely cyclopiazonic acid and thapsigargin, suggesting that the

maintenance of Ca^{2+} gradient across the peroxisomal membrane is also essential for the fusion process (Figure 8.2). Furthermore, fusion of docked P1 and P2 depends on the presence of Ca^{2+} and CaM on the outer peroxisomal face, as can be concluded from the inhibitory effect of both the membrane non-permeable Ca^{2+} chelator BAPTA and anti-CaM monoclonal antibodies on the fusion process (Figures 8.3 and 8.4). Moreover, certain CaM- and Ca^{2+}-activated proteins are also required for peroxisome fusion since the fusion of docked P1 and P2 was impaired in the presence of compounds that inhibit Ca^{2+}/CaM-dependent protein kinases and phosphodiesterases (Figure 8.5). Importantly, the negative effect of anti-CaM antibodies and CaM antagonists (W7, CBD or CIP) on the fusion of docked P1 and P2 is specific because it can be reversed by CaM in a concentration-dependent manner (Figure 8.6).

Of note, my findings imply that, in contrast to peroxisome priming and docking for fusion, the fusion of docked peroxisomes does not depend on ergosterol, PI(4)P, $PI(4,5)P_2$, cytosolic proteins, ATP hydrolysis, Pex1p or Pex6p (Figure 8.7). However, akin to the docking of primed P1 and P2, their subsequent fusion requires GTP hydrolysis since the nonhydrolyzable GTP analogues GTPγS and GppNHp inhibit peroxisome fusion in vitro (Figure 8.7). Interestingly, the P1-associated GTP-bp remains bound to the organelle surface throughout the entire fusion process, suggesting that these membrane-attached GTP-binding and hydrolyzing proteins may constitute an important part of the machinery driving the fusion of docked peroxisomes.

My data on the two-stage inhibition assay enabled to establish the hierarchy of individual steps taking place during fusion of docked P1 and P2. Specifically, using this assay I revealed that fusion of docked P1 and P2 is initiated by the H^+ gradient-dependent

step, which precedes the steps that require the Ca^{2+} gradient across the peroxisomal membrane, Ca^{2+} on the outer peroxisome surface, and CaM (Figures 8.8 and 8.9). Importantly, the Ca^{2+} gradient-dependent step during fusion of docked P1 and P2 occurs before CaM-dependent step (Figure 8.10). Moreover, my data imply that the CaM-dependent step during fusion of docked P1 and P2 precedes the step that requires GTP hydrolysis by GTPase(s) (Figure 8.11).

By monitoring the dynamics of changes in the association of CaM with the outer peroxisome face and in the concentration of Ca^{2+} in the extra-peroxisomal medium, I provided evidence that, during fusion of P1 and P2, the CCCP-sensitive (i.e., the H^+ membrane gradient-dependent) release of Ca^{2+} from the organelle lumen and subsequent recruitment of cytosolic CaM to the organelle surface are followed by the uptake of Ca^{2+} into the lumen and release of CaM from the surface to the cytosol (Figure 8.12). Moreover, my data imply that, during fusion of P1 and P2, both the uptake of Ca^{2+} into the lumen and release of CaM from the surface to the cytosol require GTP hydrolysis (Figure 8.13).

Taken together, my findings suggest the following model for fusion of docked P1 and P2 peroxisomes (Figure 8.14). The fusion of P1 and P2 is a multistep process that is initiated by the proton gradient-dependent release of the Ca^{2+} ions from the peroxisomal lumen to the cytosol and their tight association with the peroxisomal surface (Figure 8.14).

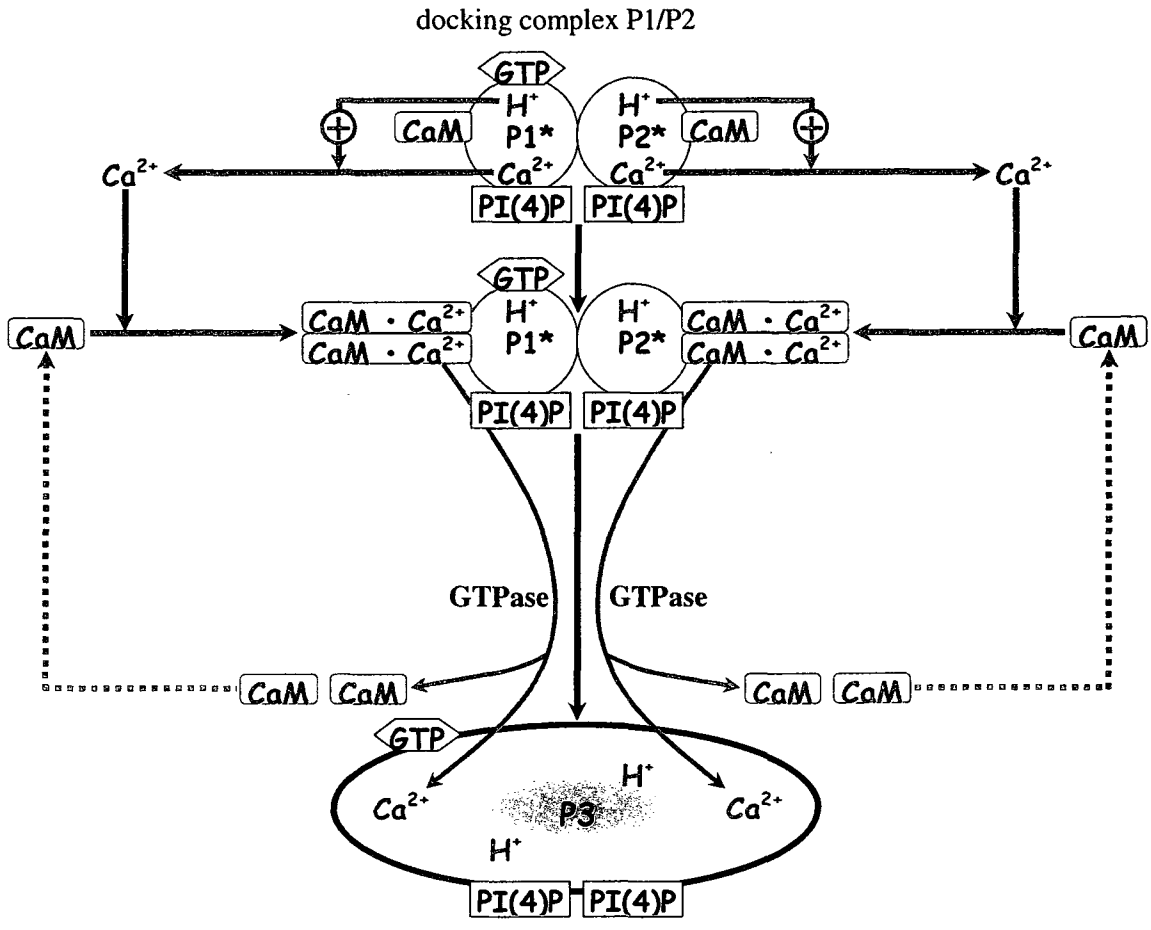

Figure 8.14. My model for fusion of docked peroxisomes P1 and P2. See text for details.

The Ca^{2+} ions that tightly associate with the peroxisome surface then recruit cytosolic CaM, which in turn activates the Ca^{2+}/CaM-dependent protein kinases and/or phosphodiesterases. The signal transduction pathways initiated by these Ca^{2+}/CaM-dependent protein kinases and/or phosphodiesterases promote the hydrolysis of GTP by the peroxisome-bound GTPase(s), which drive the fusion of docked P1 and P2 peroxisomes. During the resulting merge of lipid bilayers surrounding P1 and P2, CaM is released from the peroxisomal surface to the cytosol, perhaps due to the influx of the Ca^{2+}

ions into the peroxisomal lumen (Figure 8.14). Importantly, all the merge of lipid bilayers, release of CaM and influx of Ca^{2+} are driven by the hydrolysis of GTP by the peroxisome-bound GTPase(s).

8.5 Conclusions

My molecular analysis of a multi-step process of the fusion of docked P1 and P2 peroxisomes revealed the fusion process is initiated by the H^+-gradient driven efflux of Ca^{2+} from the peroxisome lumen and is followed by the recruitment of CaM from the cytosol to the peroxisomal surface. CaM on the outer face of the docking complex activates the Ca^{2+}/CaM-dependent protein kinases and/or phosphodiesterases, which in turn activate the hydrolysis of GTP by the peroxisome-bound GTPase(s). GTP hydrolysis drives the merge of lipid bilayers surrounding P1 and P2, release of CaM from the peroxisomal surface to the cytosol, and influx of the Ca^{2+} ions into the peroxisomal lumen.

9 The mechanism of peroxisome fusion: Summary and suggestions for future work

9.1 Do ECR domains exist in the peroxisomal membrane or are they an artifact of the detergent insolubility assay?

The assay for insolubility of protein and lipid constituents of cellular membranes in cold detergents has been widely used for the identification of lipid rafts [124, 146]. The validity of this assay has been demonstrated by the identification of numerous detergent-resistant membrane assemblies of proteins and lipids that have been implicated in a variety of essential cellular processes [87, 149]. However, recent findings suggested potential caveats associated with the interpretation of results of the detergent insolubility

assay [149]. It was concluded that only a decrease or an increase in the detergent insolubility of a membrane protein at different consecutive steps of a cellular process could provide proof for the lateral movement of the protein of interest from one membrane domain to another [87, 149].

I used the detergent solubilization approach to study the dynamics of temporal and spatial reorganization of the multicomponent peroxisome fusion machinery in the membranes of P1 and P2. I found that a distinct set of protein components of this machinery in unprimed P1 and P2 resisted solubilization by the detergent Brij 35. Individual components of the fusion machinery became detergent-soluble, and were eventually released to the cytosol, at different steps of the peroxisome fusion process. Moreover, I defined a hierarchy in which various inhibitors of peroxisome fusion selectively affected the lateral movement of their protein targets in the peroxisomal membrane. Taken together, my findings provide evidence that detergent-resistant ECR domains in the membranes of P1 and P2 do not represent an artifact of the detergent insolubility assay. On the contrary, these membrane domains exist as dynamic assemblies of a distinct set of proteins and lipids whose remodeling during peroxisome priming and docking is mandatory for the fusion of peroxisomal membranes.

9.2 Unique properties of ECR domains in the peroxisomal membrane

My analysis of ECR domains in the peroxisomal membrane revealed that they have two important features in common with the well characterized lipid raft domains in the plasma membrane. First, ECR domains constitute a significant portion of the membranes of unprimed P1 and P2, with about half of membrane lipids and proteins being recovered

in these membrane domains. Lipid rafts in the plasma membrane also represent a substantial fraction of the membrane [116, 167]. In certain cells, the plasma membrane resembles a dense assembly of numerous types of small lipid rafts that, once cells are stimulated, form larger assemblies (or flotillas) [167]. It remains to be established if ECR domains in the peroxisomal membrane represent several distinct types of ergosterol- and ceramide-rich microdomains, which differ in their protein composition and collide in response to certain stimuli. Second, both ECR domains in the peroxisomal membrane and lipid rafts in the plasma membrane are dynamic. As I found, when P1 and P2 vesicles are stimulated for priming and docking, numerous protein constituents of ECR domains rapidly move from these domains to an ergosterol- and ceramide-poor portion of the membrane. Likewise, lipid raft proteins in the plasma membrane are extremely mobile and undergo rapid lateral diffusion even in unstimulated cell membranes [168].

My findings also imply that some properties of ECR domains in the membranes of P1 and P2 vesicles distinguish them from well characterized lipid raft domains in the plasma membrane. Sphingolipids of lipid rafts in the plasma membrane have large polar head groups that are attached to their sphingosine base [90]. In contrast, no polar head group is attached to the sphingosine base of ceramide [90], an abundant sphingolipid component of ECR domains. It should be noted that ceramide in model membranes forms detergent-insoluble lipid domains that are significantly more stable than those formed in the presence of plasma membrane sphingolipids [120]. Moreover, by stabilizing lipid raft domains in endoplasmic reticulum (ER) membranes, ceramide could enhance the association of glycosylphosphatidylinositol (GPI)-anchored proteins with lipid rafts, thereby promoting selective sorting of these proteins into vesicles distinct from those

carrying many other secretory and plasma membrane proteins [73]. It remains to be elucidated if ceramide could promote the assembly of the ECR domain-based peroxisome fusion machinery in unprimed P1 and P2.

Another distinct feature of ECR domains is the unusual distribution of their sphingolipid component, ceramide, across the membrane bilayers in P1 and P2. In the plasma membrane, sphingolipids are restricted to the outer leaflet, as they are unable to move across the bilayer [116, 149, 166]. These lipids cluster with cholesterol, which preferentially interacts with sphingolipids rather than glycerophospholipids, thereby forming distinct lipid raft domains in the outer leaflet of the plasma membrane [149]. In contrast, in the membranes of P1 and P2, the sphingolipid ceramide is distributed symmetrically between the two leaflets of the bilayers. The bulk of ceramide, which spontaneously flips across the membrane bilayer with a half-time of ~ 10 min [90, 166], is in ECR domains of the membranes of P1 and P2. It remains to be seen whether the symmetric distribution of ceramide across the peroxisomal membrane and its ability to flip between the two leaflets of the bilayer promote the coordination of events that occur in the cytosolic and lumenal leaflets of ECR domains.

9.3 ECR domains undergo remodeling during peroxisomal fusion

My findings provided evidence that that ECR domains in the membranes of P1 and P2 are dynamic assemblies of a distinct set of lipids and proteins, including Pex1p, Pex6p, GTP-binding and hydrolyzing proteins, and proteins that specifically bind to two membrane phosphoinositides, PI(4)P and PI(4,5)P_2 [116]. Moreover, I demonstrated that ECR domains act as organizing platforms during peroxisomal fusion by orchestrating the

spatiotemporal reorganization of protein teams that transiently reside in ECR domains and control peroxisome fusion [116]. Based on my findings, I proposed a model for the multistep remodeling of the peroxisomal fusion machinery in the membrane bilayers of P1 and P2 [116]. According to this model, all identified essential components of the peroxisomal fusogenic machinery, including Pex1p, Pex6p, GTP-bp, PI(4)P-bp and $PI(4,5)P_2$-bp, are associated with the cytosolic face of ECR domains in membranes of unprimed P1 and P2. Priming of both peroxisomal fusion partners is initiated by the lateral movement of P1-bound Pex1p and P2-associated Pex6p from ECR domains to an ergosterol- and ceramide-poor portion of peroxisomal membranes. The priming event consists of three consecutive steps, with the first step requiring ergosterol in the peroxisomal membrane, the second step depending on PI(4)P, and the third step relying on $PI(4,5)P_2$. The priming step is completed after both AAA ATPases, Pex1p and Pex6p, get released from the peroxisome surface to the cytosol, which occurs in two consecutive steps that require cytosolic proteins and ATP hydrolysis, respectively. The priming of P1 and P2 activates them for subsequent docking, which also proceeds through multiple steps. Peroxisome docking begins with the relocation of $PI(4,5)P_2$-bp from ECR domains to ergosterol- and ceramide-poor portions in the their membranes of both fusion partners. This lateral movement progresses through three consecutive steps, with the first step requiring ergosterol in the membrane bilayers of both fusion partners, second depending on Pex1p on the cytosolic face of ECR domains in P2, and the third step requiring GTP hydrolysis by GTPase(s), perhaps by GTP-bp in ECR domains of P1. Following the lateral movement of $PI(4,5)P_2$-bp in the membranes of P1 and P2, Pex1p also relocates from ECR domains of P2 to its ergosterol- and ceramide-poor domains in an ergosterol-

dependent fashion. The formation of a stable docking complex is completed by the release of P1-associated PI(4,5)P_2-bp as well as of P2-bound PI(4,5)P_2-bp and Pex1p into the cytosol, which occurs in two consecutive steps that depend on cytosolic proteins and ATP hydrolysis, respectively. Of note, PI(4)P-bp and GTP-bp remain associated with ECR domains of the membrane bilayers of P1 and P2 after the P1/P2 docking complex has been formed, suggesting that these proteins are required for the subsequent fusion process. The fusion of docked peroxisomes begins with the H^+-gradient-driven efflux of Ca^{2+} from the peroxisomal lumen, which recruits CaM from the cytosol to the peroxisomal surface where CaM activates Ca^{2+}/CaM-dependent protein kinases and/or phosphodiesterases. The signal transduction pathway(s) activated by these proteins, including the hydrolysis of GTP, drives the fusion reaction leading to the formation of larger peroxisome P3. The fusion of docked P1 and P2 is culminated by the influx of Ca^{2+} back into the peroxisomal lumen and by the concomitant release of CaM from the peroxisomal surface back to the cytosol. It would be interesting to see how this established remodeling of the peroxisome fusogenic machinery residing in the membranes of both fusion partners changes the physical properties and topology of lipid bilayers in which this machinery operates, thereby triggering peroxisome docking and subsequent fusion of the peroxisomal membranes. Future studies could also focus on identifying the interacting partners of the currently known protein components of the peroxisome fusion machinery, such as Pex1p, Pex6p and CaM. Furthermore, it would be interesting to see if these interacting protein partners dissociate from Pex1p, Pex6p and CaM following their lateral relocation from ECR domains to an ergosterol- and ceramide-poor portion of the membrane or their release to the cytosol. Immunoaffinity

chromatography using anti-Pex1p, anti-Pex6p and anti-CaM antibodies covalently linked to Protein A Sepharose can be used to purify the corresponding bait proteins along with their interacting protein partners from the structurally and functionally distinct membrane domains isolated from both P1 and P2 peroxisomes in their unprimed, individually pre-primed, docked or fused states and at the different consecutive steps of the peroxisome fusion process. Moreover, these experiments could be carried out not only with peroxisomes purified from wild-type strain, but also with peroxisomes isolated from mutant strains that lack individual components of the peroxisome fusogenic protein machinery identified that I identified. These future studies would provide new insight into the molecular dynamics of the complex machinery governing peroxisome fusion though coordination of numerous protein and lipid constituents of the peroxisomal membrane.

10 Comparative analyses of cellular and mitochondrial proteomes of wild-type strain of the yeast *S. cerevisiae* that aged chronologically under CR or non-CR conditions

10.1 Introduction

The identification and characterization of numerous long-lived mutants resulted in the establishment of a distinct set of proteins that regulate longevity in yeast, worms, flies and mice. These regulatory proteins function in a wide range of cellular processes such as stress response and protein folding, programmed cell death (apoptosis), cell cycle and growth, autophagy and proteasomal protein degradation, actin organization, signal transduction, nuclear DNA replication, chromatin assembly and maintenance, ribosome translation and biogenesis, carbohydrate and lipid metabolism, oxidative metabolism in mitochondria, NAD^+ homeostasis, amino acid biosynthesis and degradation, and ammonium and amino acid uptake [210, 217, 218, 238, 239]. It should be stressed that the spatiotemporal organization and function of these numerous cellular processes is controlled by a limited set of evolutionarily conserved proteins referred to as the "master regulators". They include 1) the sirtuins family of NAD^+-dependent protein deacetylases and ADP ribosylases in yeast, worms, flies and mammals [211, 217, 239, 240]; 2) the proteins involved in nutrient- or insulin/IGF-1-like signaling pathways in evolutionarily distant organisms [210, 242, 243]; 3) the nutrient-responsive protein kinases TORC1, Sch9p and PKA in yeast [217]; 4) the stress-response activating transcriptional factors Msn2p, Msn4p and Rim15, which are modulated in yeast by TORC1, Sch9p and PKA [217, 217, 241]; 5) the transcriptional factors Rtg1p and Rtg3p that are required for the maintenance of glutamate homeostasis and are modulated in yeast by a mitochondrion-to-nucleus signal transduction pathway [244]; 6) the transcription factor DAF-16 in worms

regulated by the insulin/IGF-1 signaling (IIS) pathway as well as other IIS-independent mechanisms [242, 243]; 7) the transcription factor PHA-4 specific for the diet restriction in worms [245]; and 8) some transcription factors of the FOXO forkhead family in flies and mammals [246].

To identify the cellular processes that might play a critical role in longevity regulation and, perhaps, to rank their relative contributions to aging, I used mass spectrometry to compare cellular and mitochondrial proteomes of wild-type strain of the yeast *S. cerevisiae* that aged chronologically under CR or non-CR conditions. I have identified numerous proteins that are enriched or depleted in total cell lysates and pure mitochondria of long-lived yeast grown under CR conditions on 0.2% or 0.5% glucose, as compared to those of short-lived yeast grown under non-CR conditions on 1% or 2% glucose.

10.2 Materials and methods

Strains and media

The wild-type strain BY4742 (*MATα his3Δ1 leu2Δ0 lys2Δ0 ura3Δ0*) was grown in YP medium (1% yeast extract, 2% peptone) containing 0.2%, 0.5%, 1% or 2% glucose as carbon source. Cells were cultured at 30°C with rotational shaking at 200 rpm in Erlenmeyer flasks at a "flask volume/medium volume" ratio of 5:1.

Preparation of total cell lysates

An aliquot containing 1 x 10^9 cells was centrifuged for 7 min at 3,000 rpm at room temperature. Pelleted cells were washed twice with distilled water and further centrifuged

for 3 min at 16,000 x g at room temperature. The recovered cell pellet was then resuspended in 500 µl of 4% CHAPS in 25 mM Tris/HCl buffer (pH 8.5) and centrifuged for 15 sec at 16,000 x g at room temperature. The cells were then washed again, first by resuspending them in 500 µl of 4% CHAPS in 25 mM Tris/HCl buffer (pH 8.5) and then by centrifuging for 15 sec at 16,000 x g at room temperature. The pellet of washed cells was then resuspended in 1 ml of ice-cold 4% CHAPS in 25 mM Tris/HCl buffer (pH 8.5), divided into 5 equal aliquots of 200 µl each and placed in Eppendorf tubes kept on ice. Each 200 µl aliquot was supplemented with ~100 µl of glass beads and vortexed three times for 1 minute. Apart from the vortexing steps, the samples were kept on ice at all times. Glass beads and cell debris were then pelleted by 5 min centrifugation at 16,000 x g at 4°C. The resulting supernatant of the glass bead lysate was immediately transferred into a pre-chilled Eppendorf tube and stored at -20°C for further analysis.

Isolation of the crude mitochondrial fraction

Yeast cells were pelleted at 3,000 x g for 5 min at room temperature, washed twice with distilled water, resuspended in DTT buffer (100 mM Tris-H_2SO_4, pH 9.4, 10 mM dithiothreitol [DTT]), and incubated for 20 min at 30°C to weaken the cell wall. The cells were then washed with Zymolyase buffer (1.2 M sorbitol, 20 mM potassium phosphate, pH 7.4), centrifuged at 3,000 x g for 5 min at room temperature, and incubated with 3 mg/g (wet wt) of Zymolyase-100T in 7 ml/g (wet wt) Zymolyase buffer for 45 min at 30°C. Following an 8-min centrifugation at 2,200 x g at 4°C, the isolated spheroplasts were washed in ice-cold homogenization buffer (5 ml/g) (0.6 M sorbitol, 10 mM Tris-HCl, pH7.4, 1 mM EDTA, 0.2% (w/v) BSA) and then centrifuged at 2,200 x g for 8 min

at 4°C. Washed spheroplasts were homogenized in ice-cold homogenization buffer using 15 strokes. The cell debris was removed by centrifuging the resulting homogenates at 1,500 x g for 5 min at 4°C. The supernatant was further centrifuged at 3,000 x g for 5 min at 4°C to remove residual cell debris. The resulting supernatant was then centrifuged at 12,000 x g for 15 min at 4°C to pellet mitochondria. The remnant cell debris was removed by centrifuging the mitochondrial fraction at 3,000 x g for 5 min at 4°C. The resulting supernatant was then centrifuged at 12,000 x g for 15 min at 4°C to obtain the crude mitochondrial pellet, which was then resuspended in 3 ml of SEM Buffer (250 mM sucrose, 1 mM EDTA, 10 mM MOPS, pH 7.2) and used for the purification of mitochondria as described below.

Purification of mitochondria devoid of microsomal and cytosolic contaminations

A sucrose gradient was made by carefully overlaying 1.5 ml of 60% sucrose with 4 ml of 32% sucrose, 1.5 ml of 23% sucrose, and then 1.5 ml of 15% sucrose (all in EM buffer; 1 mM EDTA, 10 mM MOPS, pH 7.2). Finally, a 3-ml aliquot of the crude mitochondrial fraction in SEM buffer was applied to the gradient and centrifuged at 134,000 x g (33,000 rpm) overnight at 2°C in vacuum (Rotor SW50Ti, Beckman). The purified mitochondria found at the 60%/32% sucrose interface were carefully removed and stored at - 80°C.

Protein precipitation, SDS-PAGE and silver staining of gels

Protein concentration was determined using the RC DC protein assay kit (Bio-Rad) according to the manufacturer's instructions. Proteins were then precipitated using TCA as described previously (section "Materials and methods" in chapter 5.2) and resuspended

in the SDS-PAGE sample buffer to a final concentration of 1 mg/ml. Proteins were then resolved on 7.5%, 10%, 12.5% or 16% SDS-PAGE gels as described previously (section "Materials and methods" in chapter 5.2). The Bio-Rad unstained molecular marker and a 0.1 mg/ml solution of BSA in the SDS-PAGE sample buffer were also subjected to SDS-PAGE. The proteins were then visualized by silver staining as described previously (section "Materials and methods" in chapter 5.2).

Protein identification by mass spectrometry

Selected protein bands were excised from a silver-stained gel and prepared for the mass-spectrometric peptide mapping as described previously (section "Materials and methods" in chapter 5.2). My modifications to the standard procedure included supplementing the excised protein bands with a band containing 2 μg of bovine serum albumin (BSA) protein, which was resolved in a different well of the same SDS-PAGE gel. Therefore, the samples were supplemented with double volumes (as compared to the standard volumes) of all reagents, including the trypsin buffer (100 μl/tube). Mass accuracy was further improved by performing the internal calibration of peptide mass spectra for each sample using two intense peptide masses from BSA (1479.8 and 1639.9) and one intense peptide mass from trypsin (1045.5). The proteins were identified by the Mascot peptide mass fingerprinting method as described previously (see section "Materials and methods" in chapter 5.2).

Calculating the relative level of a protein of interest using BSA

For calculating the relative level of a protein of interest, the intensity of the monoisotopic peak of each peptide recovered from the band containing this protein was divided by the intensity of the monoisotopic peak of a BSA peptide with the monoisotopic mass closest to the mass of the peptide of interest. For evaluating relative levels of the protein of interest found in the samples to be compared, a ratio "the intensity of the monoisotopic peak of a peptide originated from the protein of interest/the intensity of the monoisotopic peak of a BSA peptide with the monoisotopic mass closest to the mass of the peptide of interest" was calculated for each peptide originated from the protein of interest. Based on these data, the average value for relative levels of the protein of interest found in the two compared samples was calculated. The method for evaluating relative levels of the protein of interest recovered in different samples was validated by calculating relative levels of several standard proteins in the samples supplemented with different quantities of each of these proteins.

Validation of the BSA-based relative quantitation method

Several control experiments have been performed in order to validate the mass spectrometric approach for protein identification and quantitation described above. The amount of BSA required for the simultaneous trypsin digestion along with the protein band of interest has been optimized as outlined below. Four protein bands stained with silver and containing different amounts of BSA (*i.e.*, 2 μg, 5 μg, 10 μg or 20 μg) were excised from the SDS-PAGE gel, cut into 1-mm^3 pieces and combined in an Eppendorf

tube with a similarly stained and excised band of an unknown protein (Figures 10.1 and 10.2).

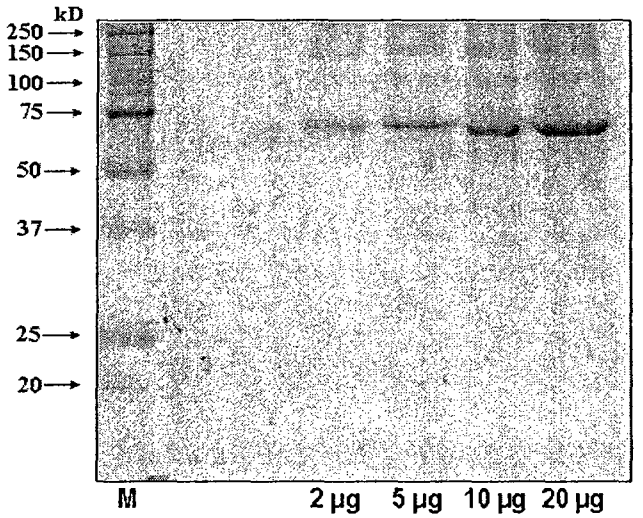

Figure 10.1. Different quantities of BSA were subjected to SDS-PAGE in a 12.5%-gel and then stained with silver.

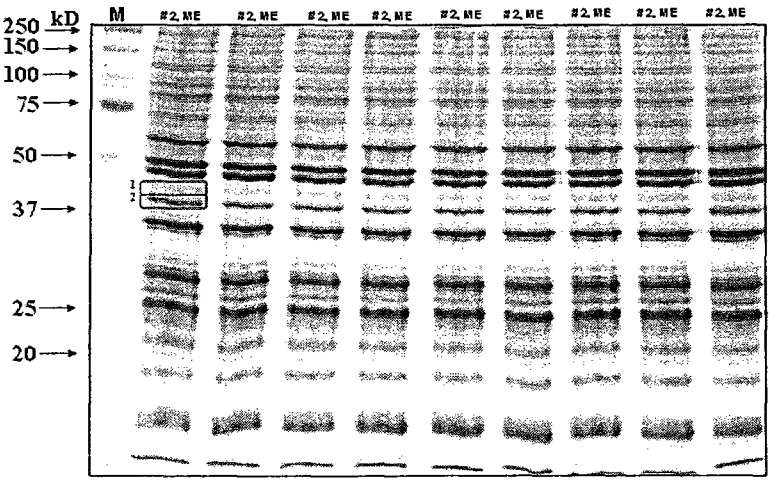

Figure 10.2. The protein bands of interest (labeled 1 and 2) were randomly selected among the proteins that were recovered in total cell lysates of *S. cerevisiae* following SDS-PAGE in a 12.5%-gel and silver staining. 10 µg of protein were loaded per a well.

Two unknown proteins with different abundance observed on the silver-stained gel were used in the experiment. Both proteins were recovered from the total cell lysate of *S.*

cerevisiae that has been subjected to SDS-PAGE followed by silver staining (Figure 10.2). The same amount of each protein was added as a protein band excised from the gel to each of the tubes containing 2 μg, 5 μg, 10 μg or 20 μg of BSA. The resulting unknown protein/BSA mixtures were then subjected to the mass spectrometric analysis as described previously. The monoisotopic peptide masses of BSA and unknown protein, along with their respective intensities, were grouped separately for each sample. The identities of unknown proteins were established (using the Mascot Peptide Mass Fingerprinting engine) as Act1p for the major component of the protein band 1 and Adh1p for the major component of the protein band 2 (Figure 10.2). The identification of Act1p, a 42 kD yeast actin protein, was based on the mass spectrometric peptide mapping analysis of 7 peptides that covered 24% of the Act1p sequence with mass accuracy 50 ppm over the mass to charge (m/z) ratio range of 763 to 2705. The identification of Adh1p, a 37 kD yeast alcohol dehydrogenase I protein, was based on the mass spectrometric peptide mapping analysis of 8 peptides that covered 28% of the Adh1p sequence with mass accuracy 50 ppm over the range of 709 to 2312 m/z. The intensity of the monoisotopic peak for each of the recovered BSA, Act1p and Adh1p peptides was then used to calculate: 1) the relative to each other levels of Act1p and Adh1p, with each of these two proteins being initially added in the same amount to each of the four samples that were supplemented with different amounts of BSA; and 2) the relative to Act1p and Adh1p levels of BSA in each of the four samples initially supplemented with different amounts of BSA. To calculate the relative to each other levels of Act1p and Adh1p, the intensity of the monoisotopic peak of each peptide originated from Act1p or Adh1p was divided by the intensity of the monoisotopic peak of a BSA peptide with the

monoisotopic mass closest to the mass of the analyzed peptide. Based on this ratio, the average value for the levels of Act1p and Adh1p relative to BSA was calculated in each of the four samples supplemented with different amounts of BSA (Figure 10.3A).

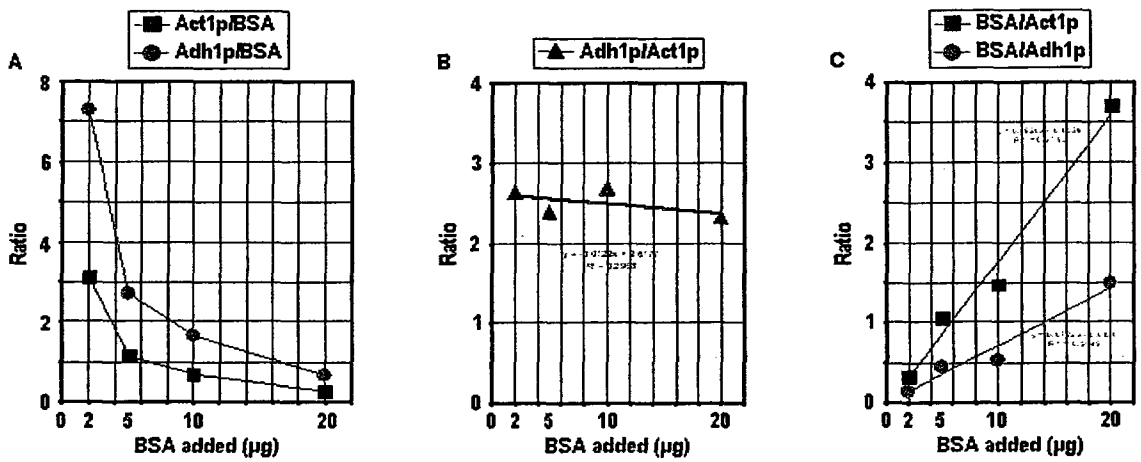

Figure 10.3. (A) The average value for the levels of Act1p and Adh1p relative to BSA in each of the four samples containing 2 µg, 5 µg, 10 µg and 20 µg of BSA. (B) The relative to each other levels of Act1p and Adh1p in each of the four samples supplemented with 2 µg, 5 µg, 10 µg and 20 µg of BSA. (C) The average value for the levels of BSA relative to Act1p or Adh1p in each of the four samples supplemented with 2 µg, 5 µg, 10 µg and 20 µg of BSA.

The ratio of the Act1p and Adh1p levels to each other was then calculated in each of the four samples supplemented with different amounts of BSA. Of note, the calculated ratio of the Act1p levels relative to the Adh1p levels did not show significant deviation for each of the four samples, regardless of the amount of BSA added to them (Figure 10.3B).

The relative levels of BSA to the levels of Act1p and Adh1p were then calculated in each of the four samples initially supplemented with different amounts of BSA. The intensity of the monoisotopic peak of each BSA peptide was then divided by the intensity of the monoisotopic peak of an Act1p or Adh1p peptide, with the monoisotopic mass of the BSA peptide being closest to the mass of the analyzed peptide. Based on this ratio,

the average value for the levels of BSA relative to Act1p or Adh1p was calculated in each of the four samples initially supplemented with different amounts of BSA (Figure 10.3C). Importantly, the calculated ratio of the BSA levels versus the levels of either Act1p or Adh1p in the four samples containing different amounts of BSA correlated with the amount of BSA added to each of them (Figure 10.3C). Taken together, the results of the control experiments have validated the developed mass spectrometric approach for relative quantitation of the proteins of interest.

10.3 Results

10.3.1 CR diet alters the proteome of yeast beginning of the post-diauxic (PD) phase of growth

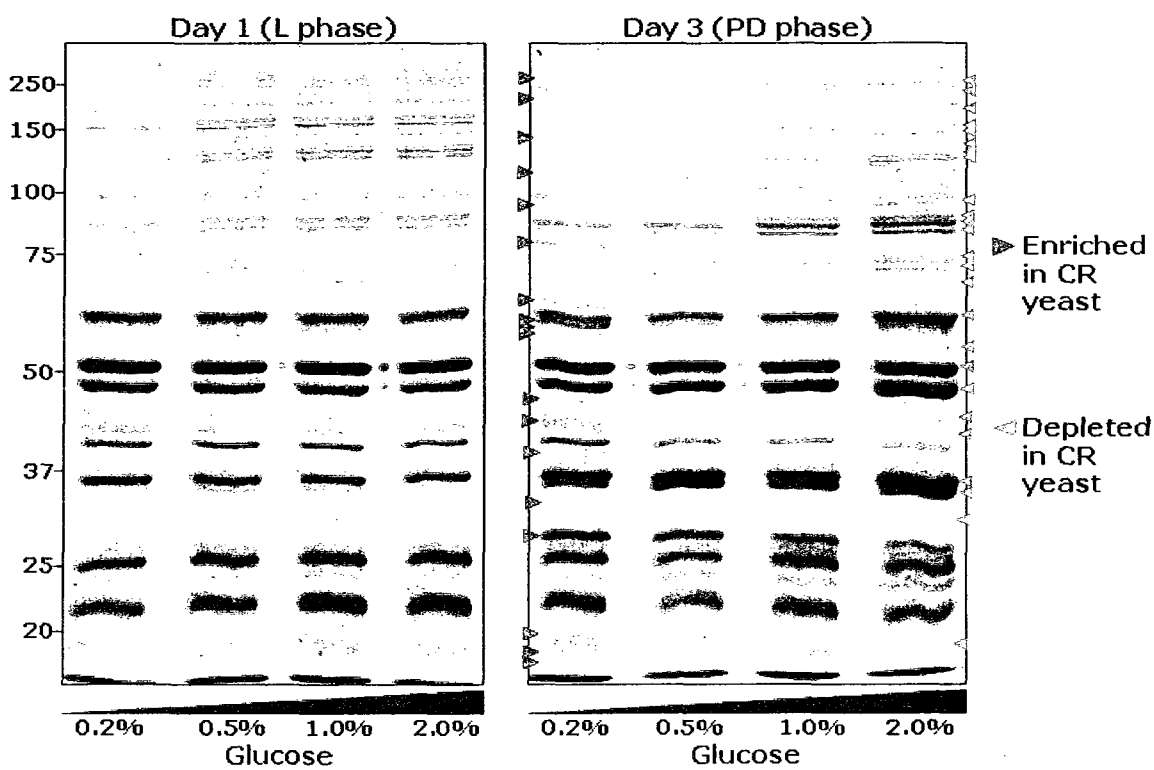

Figure 10.4. Silver-stained 12.5% SDS-PAGE gels of proteins recovered from total lysates of wild-type *S. cerevisiae* cells grown under CR (0.2% or 0.5% glucose) or non-CR (1% or 2% glucose) conditions.

10.3.2 CR alter the age-dependent dynamics of changes in the levels of numerous proteins that function in carbohydrate and lipid metabolism

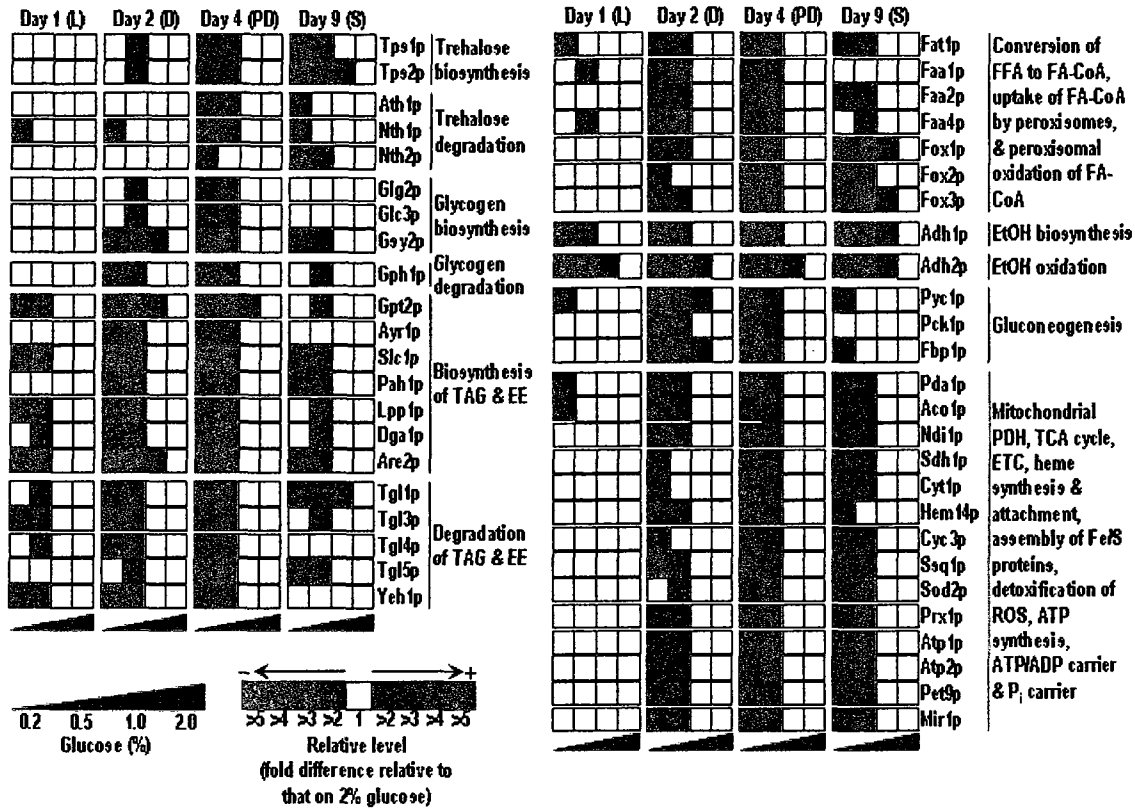

Figure 10.5. Relative levels of proteins recovered in total lysates of wild-type *S. cerevisiae* cells grown under CR conditions, as compared to those under non-CR conditions.

10.3.3 CR increases the levels of components of the pyruvate dehydrogenase (PDH) multienzyme complex and TCA cycle recovered in pure mitochondria

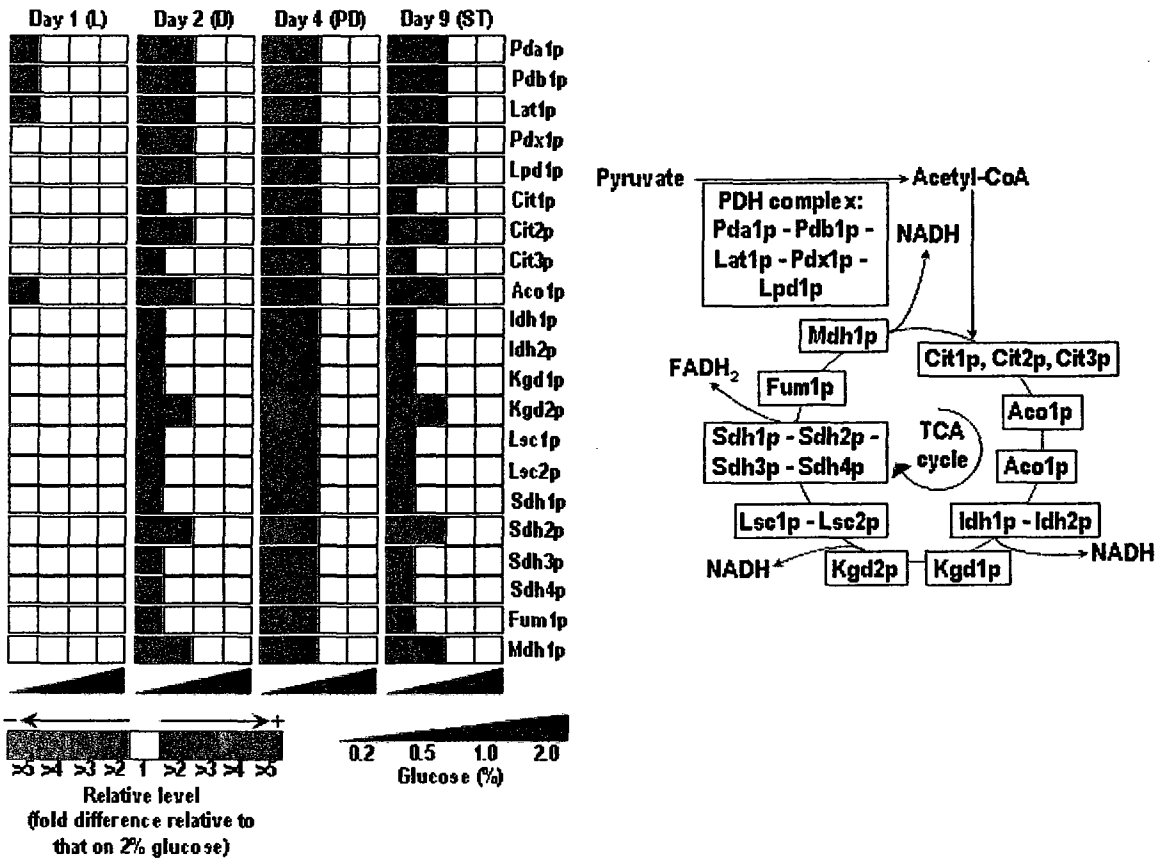

Figure 10.6. Relative levels of protein components of the mitochondrial PDH complex and TCA cycle recovered in purified mitochondria of wild-type *S. cerevisiae* cells grown under CR conditions, as compared to those under non-CR conditions.

10.3.4 CR remodels the mitochondrial electron transfer chain (ETC), heme synthesis and attachment, ATP synthesis, and carriers for ATP/ADP and P_i

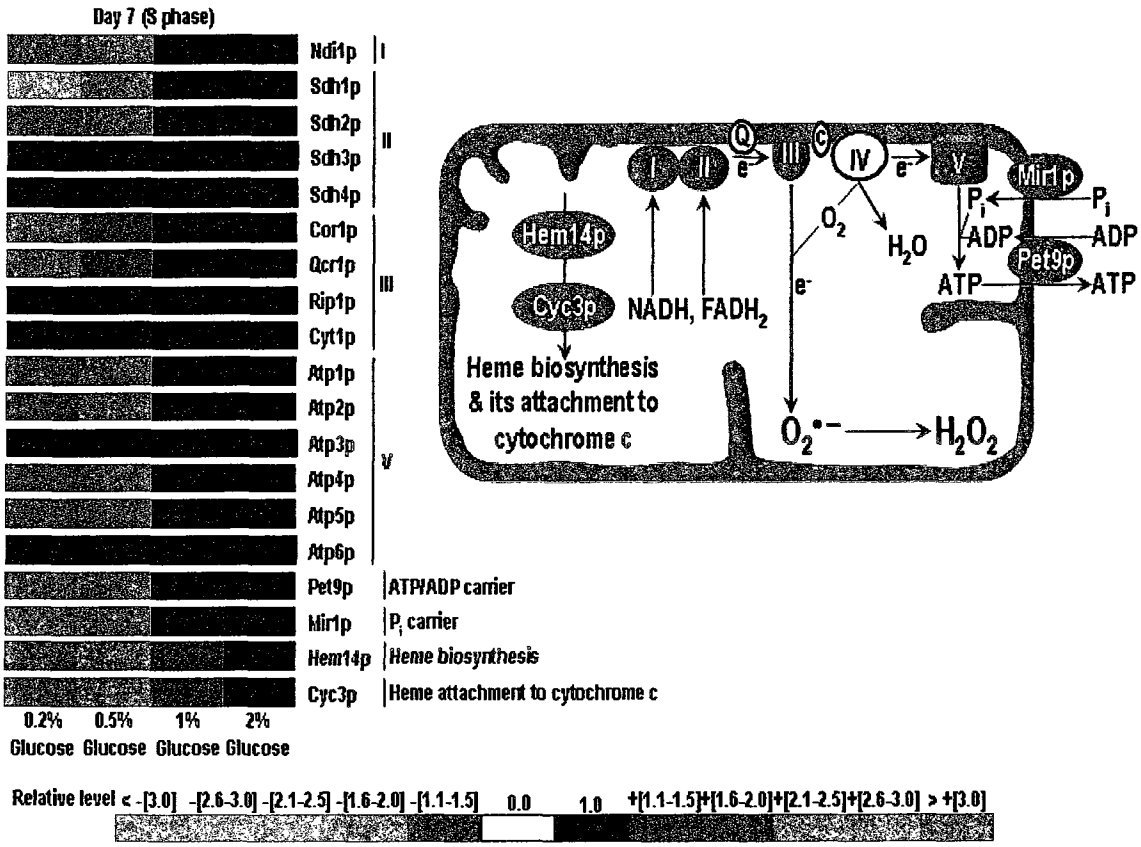

Figure 10.7. Relative levels of proteins involved in the mitochondrial ETC, heme synthesis and attachment, ATP synthesis, and ATP/ADP and P_i carriers recovered in purified mitochondria of wild-type *S. cerevisiae* cells grown under CR conditions, as compared to those under non-CR conditions.

10.3.5 CR alters the levels of proteins that bind to mitochondrial DNA (mtDNA) and modulates the age-dependent dynamics of such binding for mitochondrial aconitase

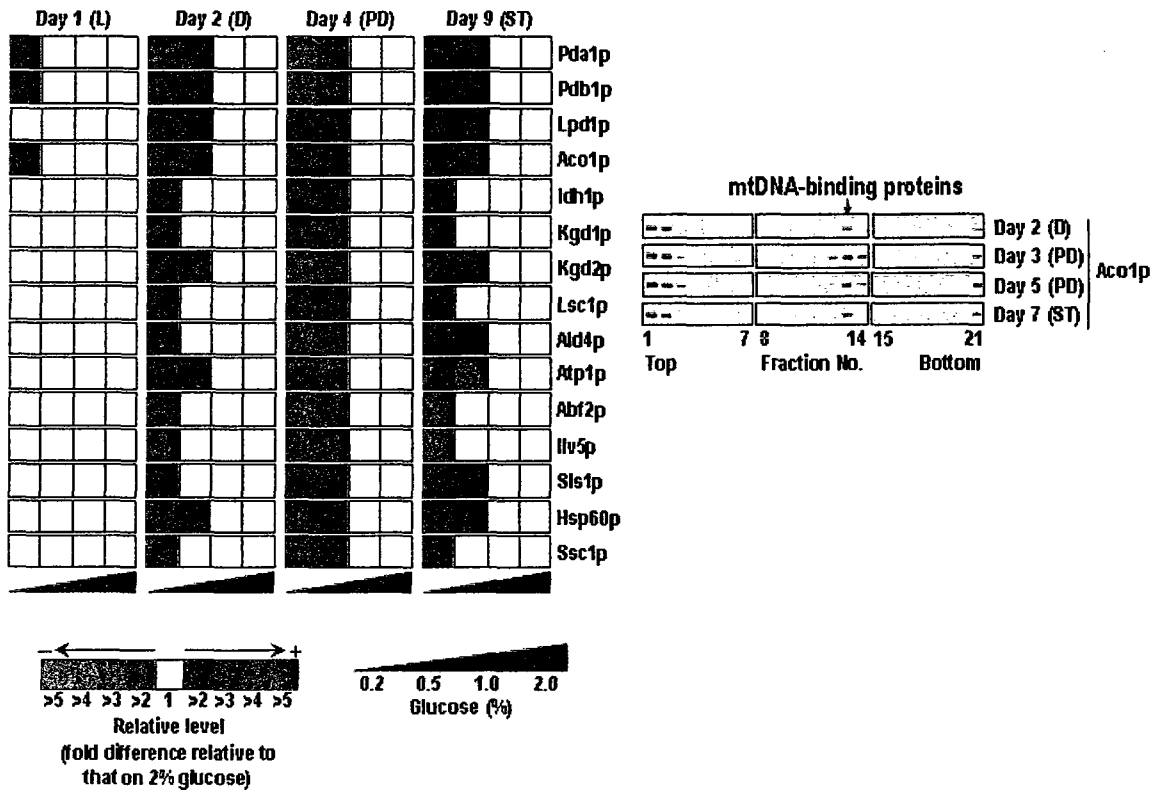

Figure 10.8. Relative levels of proteins that bind to mtDNA and the age-dependent dynamics of such binding for one of them (*i.e.*, aconitase Aco1p) in mitochondria of wild-type yeast cells grown under CR conditions, as compared to those under non-CR conditions.

10.4 Discussion

My mass spectrometric analysis of the age-dependent dynamics of changes in proteomes of chronologically aging yeast revealed that the CR diet remodels several key cellular processes, including carbohydrate and lipid metabolism, ethanol biosynthesis and degradation, the synthesis and transport of ATP, the production of ROS and stress response. Importantly, my conclusion that chronologically aging yeast placed on the CR diet undergo specific remodeling of a distinct set of metabolic processes are in agreement

with the results of metabolomic and lipidomic analyses carried out in Dr. Titorenko's laboratory.

10.4.1 During chronological aging of yeast, CR specifically remodels carbohydrate and lipid metabolism

Data from Dr. Titorenko's laboratory imply that CR promotes the age-dependent accumulation of glycogen and trehalose, the two major glucose storage compounds in yeast [247].

The intracellular levels of glycogen increased sharply in logarithmic (L) phase, regardless of initial glucose concentration in the medium (Figure 10.9A). During the subsequent diauxic (D) and post-diauxic (PD) phases, CR yeast continued to accumulate glycogen, whereas non-CR yeast rapidly consumed it (Figure 10.9A). In contrast to non-CR yeast, yeast under CR began to degrade their reserved glycogen only when they entered stationary (ST) phase (Figure 10.9A). Of note, the degree of CR influenced both glycogen storage and its consumption. In fact, CR yeast grown on 0.5% glucose reserved more glycogen by the end of PD phase and then consumed it in ST phase somewhat faster, as compared to CR yeast grown on 0.2% glucose (Figure 10.9A).

The non-reducing disaccharide trehalose accumulates in yeast undergoing nutrient starvation or entering ST growth phase [247-250]. Therefore, it has been considered as a reserve carbohydrate [247-250]. Recent studies, however, revealed that the major function of trehalose in yeast consists in enabling the survival of cells exposed to elevated temperature or ROS [250, 251]. By maintaining the optimal steady-state level of trehalose, yeast preserve native conformation of their proteins during and immediately after being exposed to these stresses [250, 251]. As recent findings from Dr. Titorenko's

laboratory revealed, yeast began to accumulate trehalose when they entered PD phase (Figure 10.9B). Trehalose levels increased during PD and ST phases. The rise of trehalose was considerably greater in slowly aging CR yeast than in rapidly aging non-CR yeast (Figure 10.9B). Thus, CR promotes the age-dependent accumulation of this non-reducing disaccharide. Noteworthy, trehalose in CR yeast grown on 0.5% glucose, a diet that provides the maximal benefit of CR for longevity, increased mainly in PD phase and reached a plateau soon after cells have entered ST phase (Figure 10.9B). Conversely, trehalose in CR yeast grown on 0.2% glucose, a diet providing only a modest CR-dependent life-span extension, increased predominantly throughout ST phase and eventually reached the steady-state level exceeding that in CR yeast grown on 0.5% glucose (Figure 10.9B).

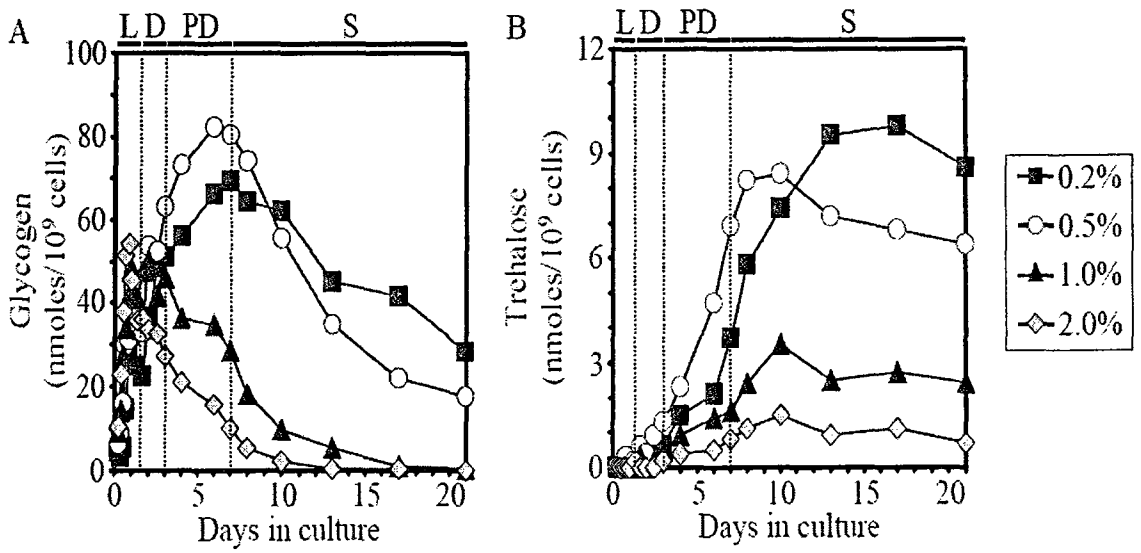

Figure 10.9. The dynamics of age-dependent changes in the intracellular levels of glycogen (A) and trehalose (B) during chronological aging of wild-type of the yeast *S. cerevisiae* (data from Dr. Titorenko's laboratory).

These findings from Dr. Titorenko's laboratory on the effect of CR on the age-dependent accumulation of glycogen and trehalose are in agreement with the data of my

proteomic analysis. In fact, I found that CR not only elevates the levels of proteins involved in glycogen biosynthesis, such as Glg2p, Glc3p and Gsy2p, but also decreases the level of Gph1p, which function in glycogen degradation (Figure 10.5). Furthermore, my proteomic analysis revealed that the levels of proteins involved in trehalose biosynthesis, such as Tps1p and Tps2p, are increased in CR yeast, as compared to those observed in non-CR yeast, with the most significant increase in the protein levels seen during ST phase (Figure 10.5). In addition, Ath1p, Nth1p and Nth2p, all of which are involved in trehalose degradation, are present at lower levels in CR yeast as compared to non-CR yeast (Figure 10.5).

My conclusion that CR causes a specific remodeling of lipid metabolism by altering the age-related dynamics of changes in the levels of proteins that function in lipid biosynthesis and degradation is supported by recent findings from Dr. Titorenko's laboratory. Proper control of fat deposition and mobilization is essential for maintaining energy homeostasis, thereby playing a role in longevity regulation [252-255]. In yeast, triacylglycerols (TAG) and ergosteryl esters (EE) are two major species of neutral lipids that are deposited in so-called lipid bodies (LB; [256]). TAG and EE serve as the main storage molecules for free fatty acids (FFA), diacylglycerols (DAG) and ergosterol (ERG). Therefore, the ability of yeast to modulate the biosynthesis and degradation of neutral lipids is crucial for regulating 1) energy homeostasis; 2) phospholipid and cardiolipin biosynthesis; 3) neutralization of excessive amounts of membrane-perturbing species of FFA and ERG; 4) FFA- and DAG-induced lipoapoptosis; and 5) DAG-dependent signal transduction networks [29, 30]. All these processes are currently viewed as vital for modulating the pace of aging [211, 239, 252-260]. Using thin-layer

chromatography (TLC) for measuring TAG and EE extracted from whole yeast cells, Dr. Titorenko's laboratory found that the concentrations of TAG and EE in wild-type cells increased gradually in L and D phases, reaching substantially higher levels in non-CR yeast than in CR yeast (Figures 10.10 and 10.12). During the subsequent PD phase, CR yeast rapidly consumed TAG and EE until their complete exhaustion in early ST phase, whereas non-CR yeast continued to accumulate both these lipids (Figures 10.10 and 10.12).

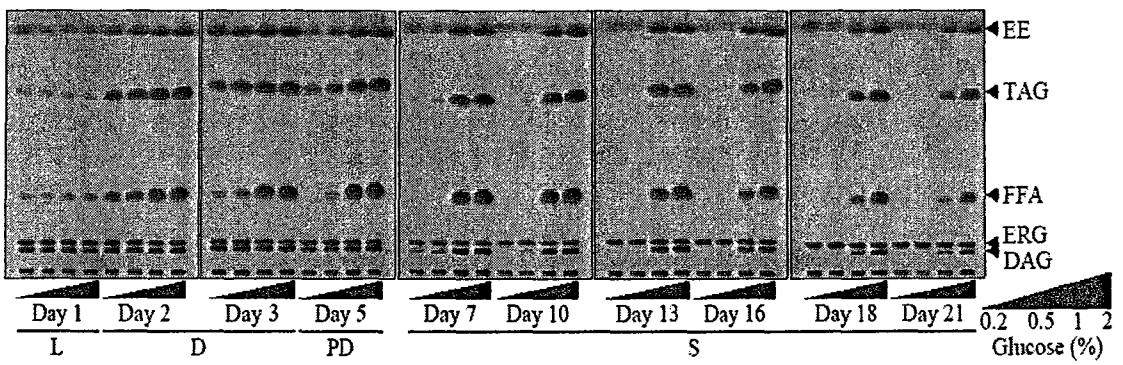

Figure 10.10. CR promotes the consumption of neutral lipids deposited in lipid bodies. Spectra of lipids extracted from equal numbers of yeast cells and analyzed by TLC. Cells were cultured in YP medium containing 0.2%, 0.5%, 1% or 2% glucose. Abbreviations: DAG, diacylglycerols; EE, ergosteryl esters; ERG, ergosterol; ER, endoplasmic reticulum; FA-CoA, CoA esters of fatty acids; FFA, free fatty acids; TAG, triacylglycerols (data from Dr. Titorenko's laboratory).

In contrast to yeast under CR, non-CR yeast began to degrade their deposited neutral lipids only after they have entered ST phase (Figures 10.10 and 10.12). The use of fluorescence microscopy for visualizing TAG and EE in living cells supported the notion that CR diet considerably accelerates the mobilization of LB-deposited neutral lipids (Figures 10.11 and 10.12A).

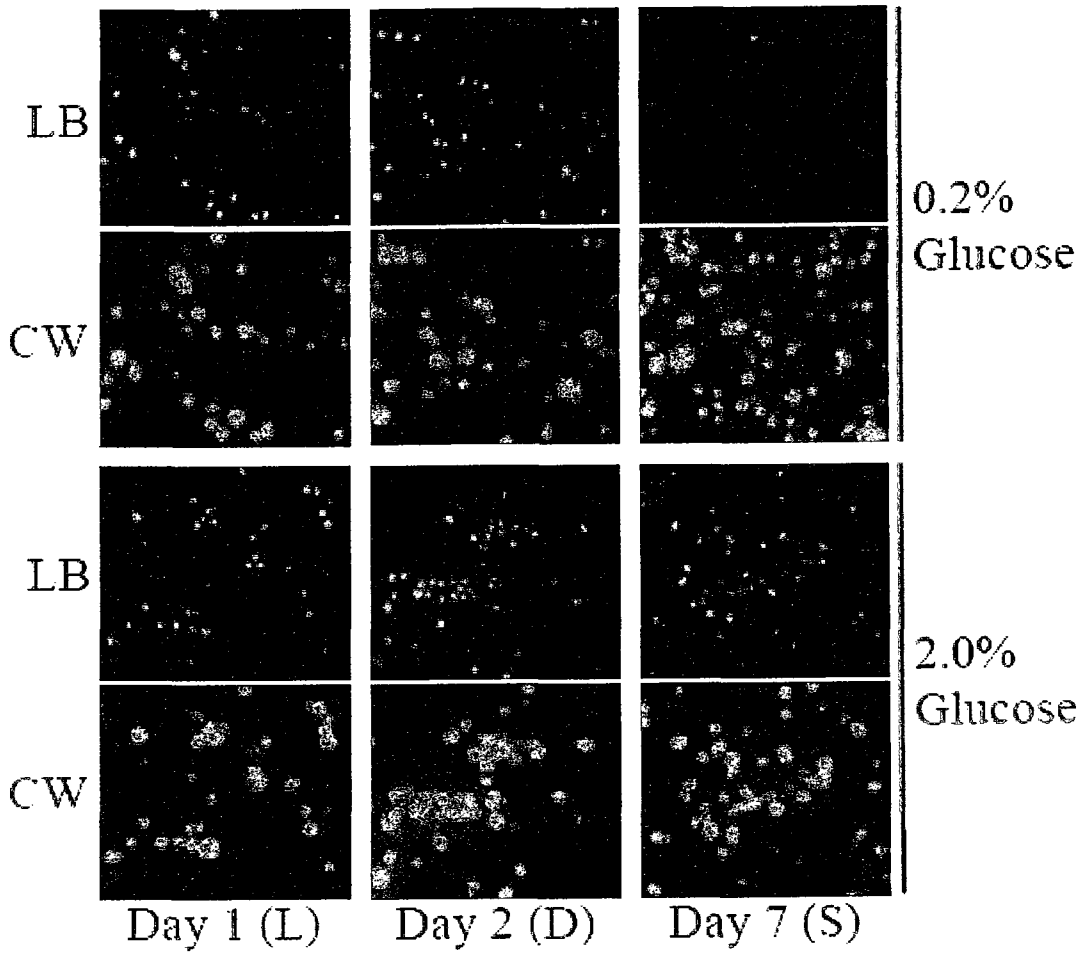

Figure 10.11. CR promotes the consumption of neutral lipids deposited in lipid bodies. Yeast cells were visualized using Calcofluor White M2R (CW; 25 μM) and stained with BODIPY 493/503 to detect neutral lipids of lipid bodies (LB). Cells were cultured in YP medium containing 0.2% or 2% glucose (data from Dr. Titorenko's laboratory).

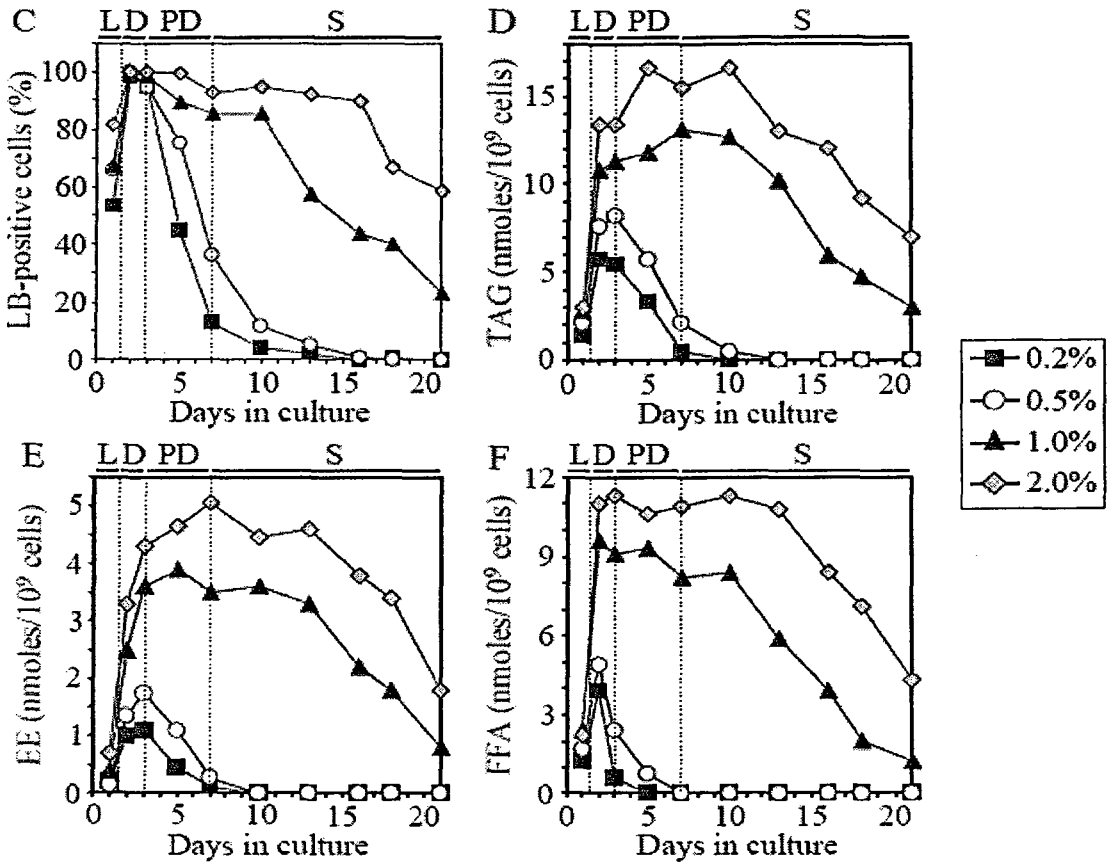

Figure 10.12 CR promotes the consumption of neutral lipids deposited in lipid bodies. (C) Percent of cells that contain lipid bodies. Images similar to the representative images shown in Figure 10.11 were quantitated. (D-F) Lipid species shown in Figure 10.10 were quantitated by densitometric analysis of TLC plates. Cells were cultured in YP medium containing 0.2%, 0.5%, 1% or 2% glucose. Abbreviations: EE, ergosteryl esters; FFA, free fatty acids; TAG, triacylglycerols (data from Dr. Titorenko's laboratory).

As Dr. Titorenko's laboratory found, consistent with the ER origin of LB, both TAG and EE were initially synthesized in the ER of CR and non-CR cells during L and D phases, prior to being relocated to LB (Figure 10.13). CR yeast rapidly consumed these LB-confined lipids during PD phase, completely exhausting their fat depot by the end of it (Figure 10.13). In contrast, non-CR yeast continued to accumulate both TAG and EE within their LB during PD phase. The age-dependent buildup of neutral lipids in LB of

non-CR yeast coincided with the deceleration of their exit from the ER *en route* to LB (Figure 10.13), perhaps due to a negative feedback loop regulating this process.

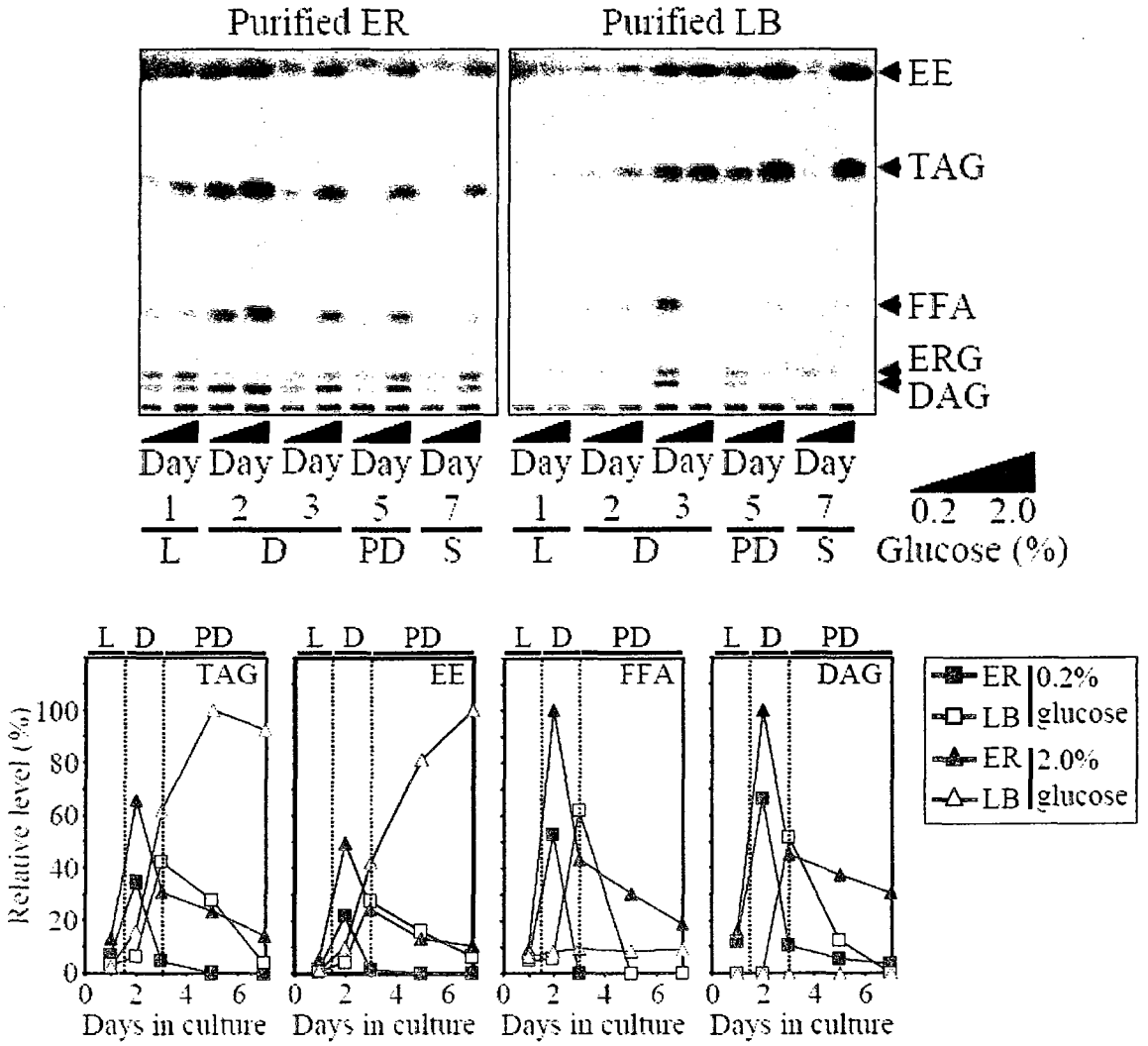

Figure 10.13. CR promotes the consumption of neutral lipids deposited in lipid bodies. Spectra of lipids that were extracted from purified endoplasmic reticulum (ER) and lipid bodies (LB) of yeast. The equivalent of 200 μg of ER proteins and 20 μg of lipid body proteins was used for lipid extraction at each time point. Lipids were analyzed by TLC and quantitated by densitometric analysis of TLC plates. Each plot shows a representative experiment repeated 3 times with similar results. Cells were cultured in YP medium containing 0.2% or 2% glucose. Abbreviations: DAG, diacylglycerols; EE, ergosteryl esters; ERG, ergosterol; ER, endoplasmic reticulum; FA-CoA, CoA esters of fatty acids; FFA, free fatty acids; TAG, triacylglycerols (data from Dr. Titorenko's laboratory).

As Dr. Titorenko's laboratory found, the biosynthesis of FFA and DAG during early D phase was followed by their ER-confined incorporation into TAG during late D phase (Figure 10.13). Soon after their relocation from the ER to LB, TAG in CR yeast were subjected to lipolysis resulting in the formation of FFA and DAG, both of which were rapidly degraded by the end of PD phase (Figure 10.13). Alternatively, non-CR yeast accumulated significant quantities of both FFA and DAG within the ER during PD phase (Figure 10.13).

All these data from Dr. Titorenko's laboratory on the age-dependent dynamics of lipidomes in chronologically aging CR and non-CR yeast are in agreement with the results of my quantitative proteomic analysis (Figure 10.5). As I found, during L phase, the levels of proteins involved in the biosynthesis of TAG and EE, such as Gpt2p, Ayr1p, Slc1p, Pah1p, Lpp1p, Dga1p, and Are2p, in CR yeast are lower than in non-CR yeast (Figure 10.5). During the subsequent D and PD phases, the levels of these proteins in Cr yeast decrease even further and become significantly lower than in non-CR yeast (Figure 10.5). In contrast, as my proteomic analysis revealed, the CR diet has an opposite effect on the levels of proteins involved in the degradation of TAG and EE, such as Tgl1p, Tgl3p, Tgl4, and Yeh1p. Specifically, during L phase, the levels of these proteins in CR yeast are higher than in non-CR yeast (Figure 10.5). The stimulating effect of the CR diet on the levels of proteins that function in lipid degradation becomes even more pronounced in D and PD phases (Figure 10.5). Taken together, my findings support the notion that the CR diet increases the levels of the key enzymes involved in the lipolytic consumption of neutral lipids deposited in lipid bodies, concurrently decreasing the levels of enzymes catalyzing the biosynthesis of these storage lipids.

Furthermore, according to my proteomic analysis, CR also modulates the levels of proteins that function in the formation of CoA esters of fatty acids (FA-CoA) and in their subsequent uptake and oxidation by peroxisomes. In fact, the CR diet greatly elevates the levels of Fat1p, Faa1p, Faa2p, Faa4p, Fox1p, Fox2p and Fox3p throughout yeast life span (Figure 10.5). My findings satisfactorily explain a stimulating effect of the CR diet on the consumption of fatty acids during an early stage of yeast chronological aging, which has recently bee reported by Dr. Titorenko's laboratory (Figures 10.10, 10.11 and 10.12).

10.4.2 CR alters the age-related dynamics of ethanol biosynthesis and degradation

Recent data from Dr. Titorenko's laboratory imply that CR greatly accelerates catabolism of ethanol, a product of glucose fermentation in yeast (Figure 10.14). Ethanol has been shown to modulate the rate of chronological aging in yeast by a yet-to-be characterized mechanism [261]. As Dr. Titorenko's laboratory recently found, CR greatly accelerated the catabolism of ethanol, a product of glucose fermentation (Figure 10.14). Importantly, it seems that such stimulatory effect of CR on ethanol catabolism is important for providing the benefit of CR for longevity. In fact, CR yeast completely consumed ethanol by day 2, at least 10 days before the beginning of their viability decline (Figure 10.14). Conversely, non-CR yeast were unable to consume substantial quantities of ethanol prior the age-dependent decline of their viability has begun (Figures 10.14 and 1C). Moreover, the level of ethanol accumulated in non-CR yeast correlated with the initial concentration of glucose in the medium, being inversely proportional to their chronological life span (Figure 10.14 and 1D). Therefore, it is likely that the stimulatory effect of CR on ethanol catabolism is one of the key factors required for the life span extension by the CR diet.

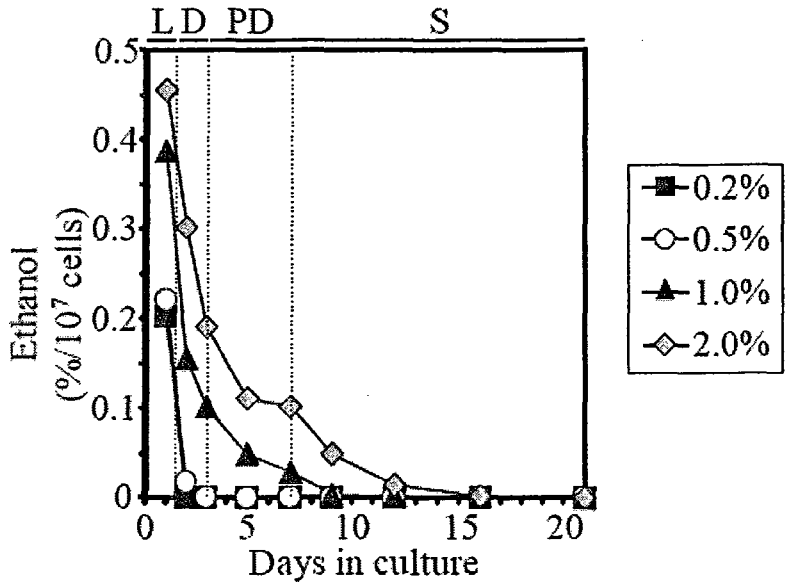

Figure 10.14. CR greatly accelerates ethanol catabolism. The dynamics of age-dependent changes in the extracellular concentrations of ethanol during chronological aging of wild-type cells. Cells were continuously cultivated in rich YP medium initially containing 0.2%, 0.5%, 1% or (data from Dr. Titorenko's laboratory).

The results of my quantitative proteomic analysis provide an explanation for the observed by Dr. Titorenko's laboratory ability of the CR diet to accelerate ethanol consumption. As I found, CR substantially increases the level of Adh1p, an enzyme catalyzing ethanol biosynthesis, and greatly increases the level of Adh2p, an enzyme involved in ethanol degradation (Figure 10.5). Thus, it is conceivable that the CR diet increases ethanol consumption (Figure 10.14) by altering the levels of enzymes involved in its biosynthesis and degradation.

10.4.3 CR remodels mitochondrial functions

My quantitative proteomic analysis also revealed that the CR diet remodel several protein teams that function in essential processes confined to mitochondria (Figure 10.5). In fact, according to my data, CR increases the levels of such mitochondrial proteins as Pda1p,

Aco1p, Ndi1p, Sdh1p, Cyt1p, Hem14p, Cyc3p, Ssq1p, Sod2p, Prx1p, Atp1p, Atp2p, Pet9p and Mir1p (Figure 10.5). These proteins play the major roles in 1) the formation of acetyl-CoA and its subsequent oxidation via the tricarboxylic acid (TCA) cycle; 2) the mitochondrial electron transport chain (ETC) and oxidative phosphorylation coupled to ATP synthesis; and 3) the detoxification of mitochondrially formed ROS. Furthermore, my quantitative proteomic analysis of mitochondria purified from *S. cerevisiae* cells grown under CR and non-CR conditions (Figure 10.6) showed that the CR diet increases the levels of all five protein components of the mitochondrial PDH complex (Pda1p, Pdb1p, Lat1p, Pdx1p, and Lpd1p), along with all of the TCA cycle enzymes (Cit1p, Cit2p, Cit3p, Aco1p, Idh1p, Idh2p, Kgd1p, Kgd2p, Lsc1p, Lsc2p, Sdh1p, Sdh2p, Sdh3p, Sdh4p, Fum1p and Mdh1p). In addition, my quantitative analysis of the mitochondrial proteomes revealed that the CR diet also increases the levels of proteins involved in the mitochondrial ETC (Ndi1p, Sdh2p, Cor1p and Qcr1p), ATP synthesis (Atp1p, Atp2p, Atp4p and Atp5p), ATP/ADP and P_i carriers (Pet9p and Mir1p), and heme biosynthesis (Hem14p) and attachment (Cyc3p) (Figure 10.7). Moreover, I demonstrated that the CR diet also increases the levels of certain proteins that bind to mitochondrial DNA (mtDNA), such as Pda1p, Pdb1p, Lpd1p, Aco1p, Idh1p, Kgd1p, Kgd2p, Lsc1p, Ald4p, Atp1p, Sis1p, Hsp60p and Ssc1p (Figure 10.8). Of note, the levels of some other mtDNA-binding proteins, such as Abf2p and Ilv5p, were decreased under CR conditions (Figure 10.8).

Altogether, the results of my quantitative proteomic analysis provide evidence that the CR diet greatly promotes the production of acetyl-CoA by the PDH complex and its subsequent oxidation in the TCA cycle. Furthermore, by specifically altering the levels of

components of the mitochondrial ETC and ROS detoxification, CR specifically modulates the age-dependent dynamics of changes in the concentration of ROS.

10.4.4 Specific remodeling of metabolism in yeast placed on the CR diet

Altogether, the results of my quantitative proteomic analysis and the data of metabolomic and functional analyses conducted in Dr. Titorenko's laboratory suggest the following model for the remodeling of carbohydrate and lipid metabolism in chronologically aging CR yeast (Figure 10.15).

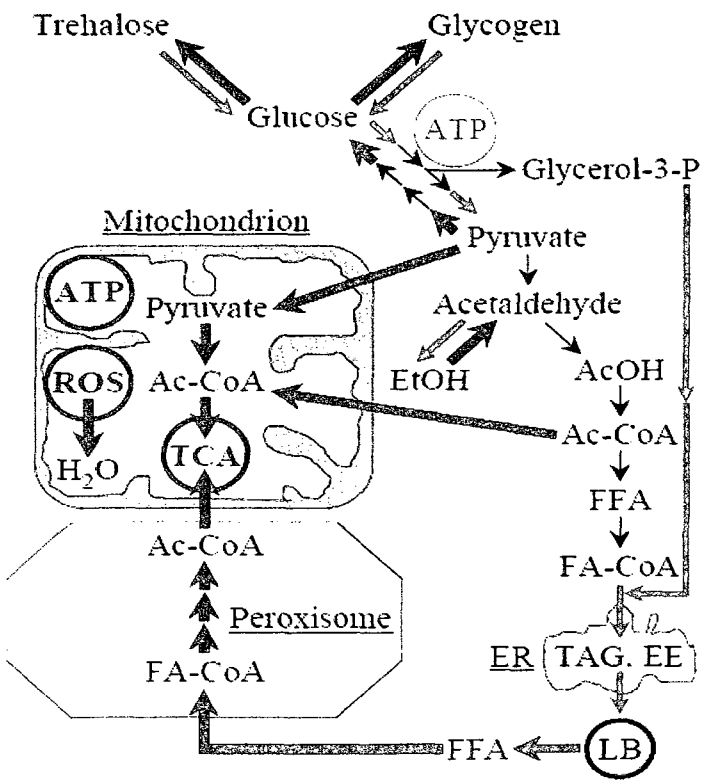

Figure 10.15. A model for the remodeling of carbohydrate and lipid metabolism in chronologically aging yeast *S. cerevisiae* grown under CR conditions (The processes that are accelerated under CR conditions are shown in red, while those processes that are decelerated under CR conditions are shown in green).

In this model, chronologically aging non-CR yeast meet their metabolic requirements primarily by carrying out glycolysis and degrading the storage carbohydrates glycogen and trehalose. The resulting production of ethanol due to fermentation affects the peroxisomal function by inhibiting the synthesis of enzymes involved in the breakdown of free fatty acids through peroxisomal β-oxidation pathway. The resulting diminished peroxisomal production of acetyl-CoA leads to a decrease in the mitochondrial function and promotes mitochondrial fragmentation, thereby triggering cytochrome c release and the resulting activation of mitochondria-controlled apoptosis. In addition, the accumulation of free fatty acids and DAG in non-CR yeast promotes the necrotic cell death. The cumulative effect of these age-related changes in cellular processes shortens the chronological life span of non-CR yeast. In contrast to non-CR yeast, chronologically aging CR yeast fulfill their metabolic requirements by establishing a distinct pattern of carbohydrate and lipid metabolism, in which the bulk of ATP is produced through gluconeogenetic pathways and the increased consumption of neutral lipids. Under CR conditions, yeast accumulate glycogen and trehalose, the two major glucose storage compounds, by elevating the levels of enzymes catalyzing their biosynthesis and decreasing the levels of enzymes required for their degradation. At the same time, CR promotes the remodeling of lipid metabolism in chronologically aging yeast by accelerating the lipolytic consumption of the LB-deposited neutral lipids TAG and EE. The considerable amounts of FFAs generated due to such lipolysis are rapidly converted to FA-CoA, which is then metabolized into acetyl-CoA through the peroxisomal β-oxidation pathway, whose function is greatly accelerated by the CR diet. The peroxisomally-produced acetyl-CoA is then used by mitochondria of CR yeast to

synthesize the bulk of ATP. As a result, increased peroxisomal activity leads to an increase in the mitochondrial function and promotes the maintenance of the mitochondrial network, thereby down-regulating the proapoptotic mitochondrial signaling. At the same time, the concentration of ROS generated in mitochondria of CR yeast during oxidative phosphorylation is maintained at a threshold, non-toxic level, thereby resulting in the activation of stress response, which in turn helps to prevent and repair the oxidative damage to cellular macromolecules. In addition, the increased lipolysis of neutral lipids under CR conditions results in significantly diminished amounts of free fatty acids and DAG in the cytosol, thus preventing cell death by necrosis. The cumulative effect of these age-related changes in cellular processes extends the chronological life span of non-CR yeast.

10.5 Conclusions

My quantitative proteomics analysis, along with the data obtained from metabolomic and functional analyses carried out in Dr. Titorenko's laboratory, provides evidence that, in contrast to non-CR yeast that produce the bulk of ATP by glycolytic oxidation of the glycogen- and trehalose-derived glucose, chronologically aging CR yeast generate the majority of their ATP in mitochondria by oxidizing the pool of acetyl-CoA generated in peroxisomes via β-oxidation of free fatty acids. In order to validate this model of life-span extension through a specific remodeling of metabolism in CR yeast, I evaluated the contribution of mitochondrial and peroxisomal processes to the beneficial effect of CR on longevity by comparing the age-related dynamics of changes in the proteomes of

mitochondria of wild-type strain and the short-lived mutant *pex5Δ*, which is impaired in peroxisomal β-oxidation of fatty acids.

11 The comparative analysis of mitochondrial proteomes of wild-type and the short-lived *pex5Δ* mutant strains placed on the CR diet

11.1 Introduction

Most eukaryotic cells contain mitochondria, the double membrane-bound organelles of the prokaryotic origin that generate cellular energy in the form of ATP via oxidative phosphorylation. As mentioned previously, mitochondrial activity is responsible for over 90% of total intracellularily produced ROS known to play a major role in the biological aging of yeasts, worms, flies, mice and mammals. Numerous studies in evolutionary distant organisms suggest that the aging is regulated, in part, by an intrinsically induced, mitochondria-controlled apoptotic cell death mechanism [192, 196, 197, 200, 203, 204]. According to the data from Dr. Titorenko's laboratory, the age-dependent, mitochondria-controlled apoptotic death in yeast is regulated by the extent of fatty acid oxidation in peroxisomes, suggesting that peroxisomal fatty acid oxidation plays a key role in longevity regulation by modulating mitochondria-controlled apoptosis. One of the crucial evidence for the link between peroxisomes and mitochondria in longevity regulation came from findings in Dr. Titorenko's laboratory showing that Pex5p, a cytosolic shuttling receptor for peroxisomal import of PTS1-containing proteins, modulates the rate of chronological aging by regulating the intrinsic, mitochondria-dependent apoptotic cell death mechanism. Dr. Titorenko's laboratory also demonstrated that the short-lived *pex5Δ* mutant is highly sensitive to the exogenously induced apoptosis and does not

survive a long-term exposure to various stresses (Figure 11.1). It should be stressed that the CR diet greatly increases the detrimental effects of the *pex5Δ* mutation on the life span of yeast (Figure 11.2).

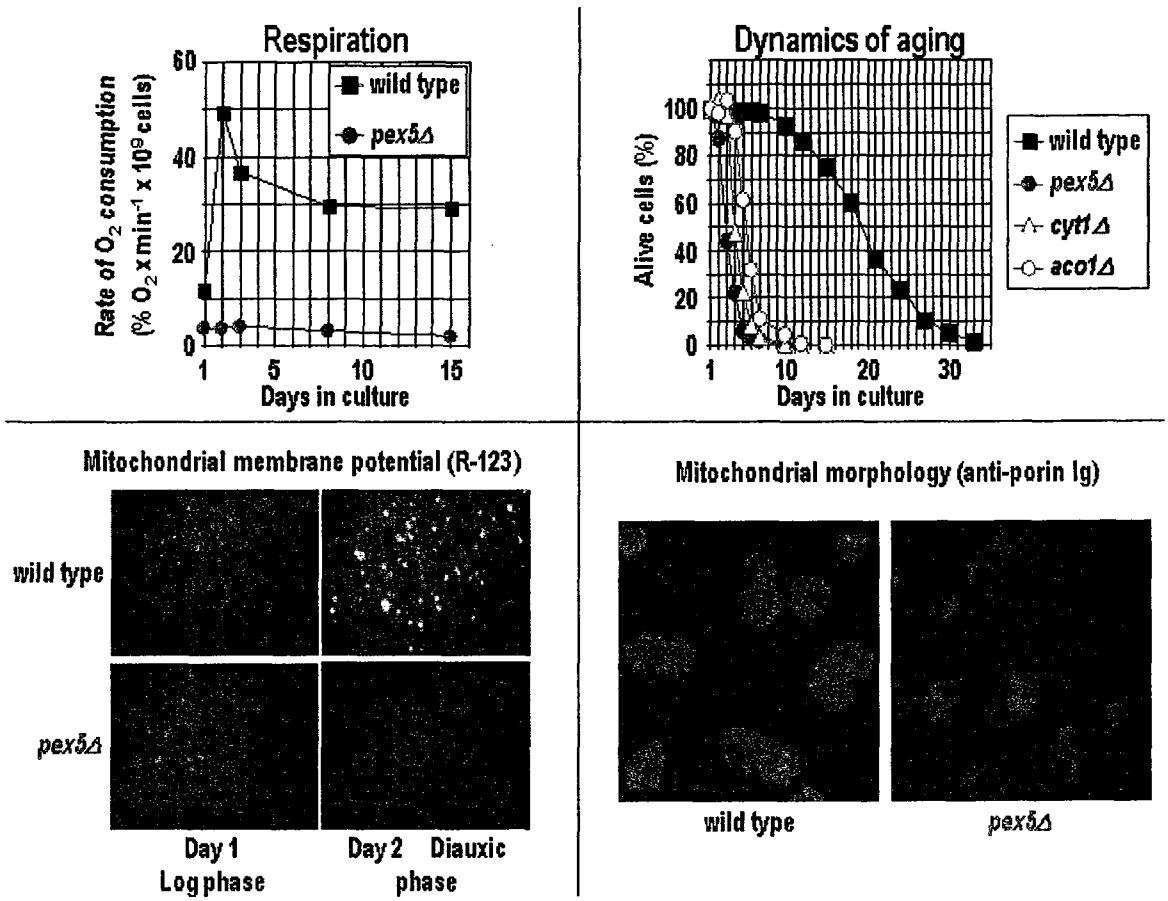

Figure 11.1. The *pex5Δ* mutation alters the morphology of mitochondria and impairs their function in *S. cerevisiae* cells grown under CR conditions.

The availability of the short-lived *pex5Δ* mutant, whose defect in peroxisomal oxidation of free fatty acids greatly affects the morphology of mitochondria and impairs their function (Figures 11.1), allowed me to identify mitochondrial proteins that, in response to signals emanating from the peroxisome, control the rate of chronological aging of CR yeast. These proteins, whose levels in highly purified mitochondria of the short-lived *pex5Δ* mutant strain were significantly altered (as compared to those of wild-

type strain), were identified and quantitated using mass spectrometry as described previously (section 10.2, "Materials and methods").

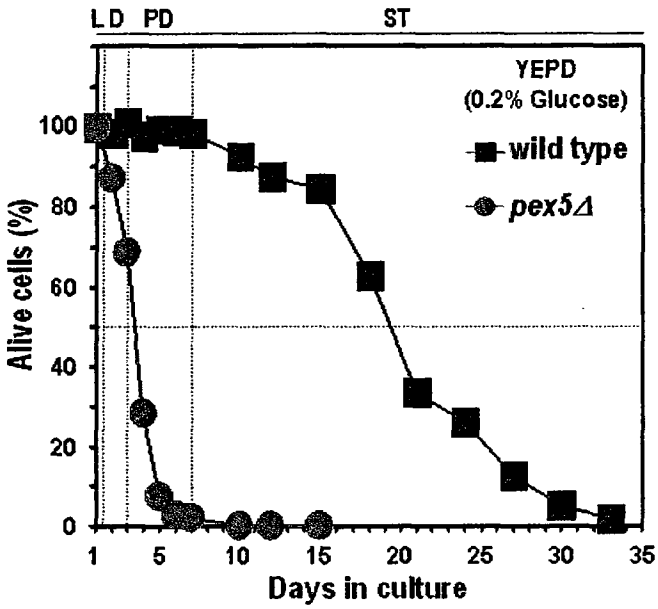

Figure 11.2. The *pex5Δ* mutation dramatically shortens chronological life span of *S. cerevisiae* under CR conditions.

11.2 Materials and methods

Strains, media, reagents and solutions

The wild-type strain *Saccharomyces cerevisiae* BY4742 (*MATα his3Δ1 leu2Δ0 lys2Δ0 ura3Δ0*) and mutant strain *pex5Δ* (*MATα his3Δ1 leu2Δ0 lys2Δ0 ura3Δ0 pex5Δ::kanMX4*) were used in this study. The components of YEPD (0.2% glucose) medium were as follows: 1% yeast extract, 2% peptone and 0.2% glucose.

Isolation of the crude mitochondrial fraction

Yeast cells were pelleted at 3,000 x g for 5 min at room temperature, washed twice with distilled water, resuspended in DTT buffer (100 mM Tris-H_2SO_4, pH 9.4, 10 mM

dithiothreitol [DTT]), and incubated for 20 min at 30°C to weaken the cell wall. The cells were then washed with Zymolyase buffer (1.2 M sorbitol, 20 mM potassium phosphate, pH 7.4), centrifuged at 3,000 x g for 5 min at room temperature, and incubated with 3 mg/g (wet wt) of Zymolyase-100T in 7 ml/g (wet wt) Zymolyase buffer for 45 min at 30°C. Following an 8-min centrifugation at 2,200 x g at 4°C, the isolated spheroplasts were washed in ice-cold homogenization buffer (5 ml/g) (0.6 M sorbitol, 10 mM Tris-HCl, pH7.4, 1 mM EDTA, 0.2% (w/v) BSA) and then centrifuged at 2,200 x g for 8 min at 4°C. Washed spheroplasts were homogenized in ice-cold homogenization buffer using 15 strokes. The cell debris was removed by centrifuging the resulting homogenates at 1,500 x g for 5 min at 4°C. The supernatant was further centrifuged at 3,000 x g for 5 min at 4°C to remove residual cell debris. The resulting supernatant was then centrifuged at 12,000 x g for 15 min at 4°C to pellet mitochondria. The remnant cell debris was removed by centrifuging the mitochondrial fraction at 3,000 x g for 5 min at 4°C. The resulting supernatant was then centrifuged at 12,000 x g for 15 min at 4°C to obtain the crude mitochondrial pellet, which was then resuspended in 3 ml of SEM Buffer (250 mM sucrose, 1 mM EDTA, 10 mM MOPS, pH 7.2) and used for the purification of mitochondria as described below.

Purification of mitochondria devoid of microsomal and cytosolic contaminations

A sucrose gradient was made by carefully overlaying 1.5 ml of 60% sucrose with 4 ml of 32% sucrose, 1.5 ml of 23% sucrose, and then 1.5 ml of 15% sucrose (all in EM buffer; 1 mM EDTA, 10 mM MOPS, pH 7.2). Finally, a 3-ml aliquot of the crude mitochondrial fraction in SEM buffer was applied to the gradient and centrifuged at 134,000 x g (33,000

rpm) overnight at 2°C in vacuum (Rotor SW50Ti, Beckman). The purified mitochondria found at the 60%/32% sucrose interface were carefully removed and stored at - 80°C.

Protein precipitation, SDS-PAGE and silver staining of gels

Protein concentration was determined using the RC DC protein assay kit (Bio-Rad) according to the manufacturer's instructions. Proteins were then precipitated using TCA as described previously (section "Materials and methods" in chapter 5.2) and resuspended in the SDS-PAGE sample buffer to a final concentration of 1 mg/ml. Proteins were then resolved on 7.5%, 10%, 12.5% or 16% SDS-PAGE gels as described previously (section "Materials and methods" in chapter 5.2). The Bio-Rad unstained molecular marker and a 0.1 mg/ml solution of BSA in the SDS-PAGE sample buffer were also subjected to SDS-PAGE. The proteins were then visualized by silver staining as described previously (section "Materials and methods" in chapter 5.2).

Protein identification by mass spectrometry

Selected protein bands were excised from a silver-stained gel and prepared for the mass-spectrometric peptide mapping as described previously (section "Materials and methods" in chapter 5.2). My modifications to the standard procedure included supplementing the excised protein bands with a band containing 2 μg of bovine serum albumin (BSA) protein, which was resolved in a different well of the same SDS-PAGE gel. Therefore, the samples were supplemented with double volumes (as compared to the standard volumes) of all reagents, including the trypsin buffer (100 μl/tube). Mass accuracy was further improved by performing the internal calibration of peptide mass spectra for each

sample using two intense peptide masses from BSA (1479.8 and 1639.9) and one intense peptide mass from trypsin (1045.5). The proteins were identified by the Mascot peptide mass fingerprinting method as described previously (see section "Materials and methods" in chapter 5.2).

Calculating the relative level of a protein of interest using BSA

For calculating the relative level of a protein of interest, the intensity of the monoisotopic peak of each peptide recovered from the band containing this protein was divided by the intensity of the monoisotopic peak of a BSA peptide with the monoisotopic mass closest to the mass of the peptide of interest. For evaluating relative levels of the protein of interest found in the samples to be compared, a ratio "the intensity of the monoisotopic peak of a peptide originated from the protein of interest/the intensity of the monoisotopic peak of a BSA peptide with the monoisotopic mass closest to the mass of the peptide of interest" was calculated for each peptide originated from the protein of interest. Based on these data, the average value for relative levels of the protein of interest found in the two compared samples was calculated. The method for evaluating relative levels of the protein of interest recovered in different samples was validated by calculating relative levels of several standard proteins in the samples supplemented with different quantities of each of these proteins.

11.3 Results

11.3.1 The *pex5Δ* mutation alters the levels of numerous mitochondrial proteins

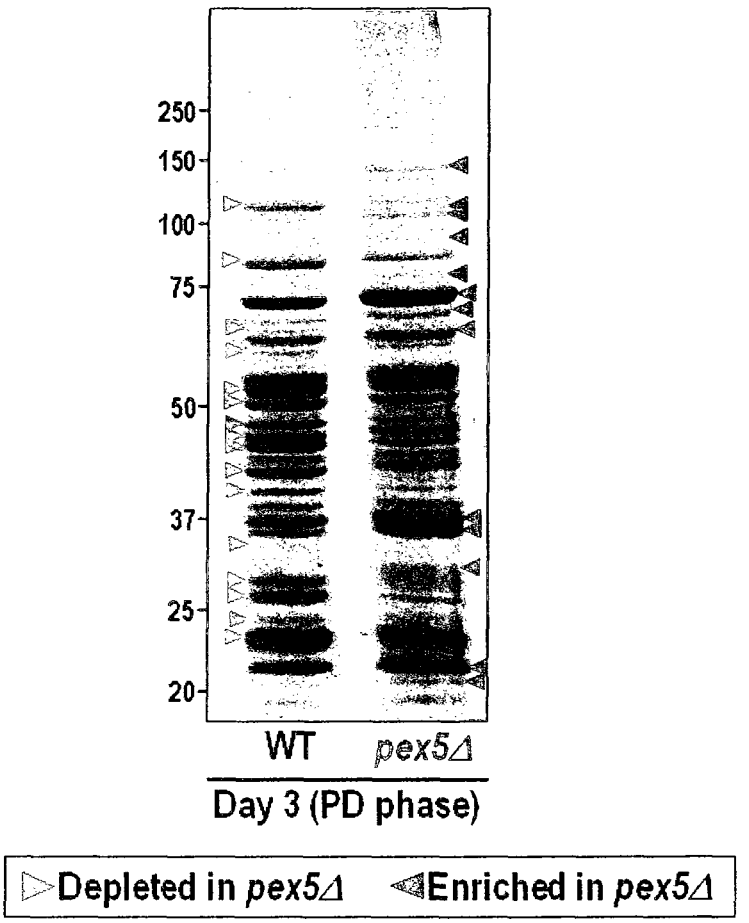

Figure 11.3. Protein spectra of purified mitochondria of wild-type and *pex5Δ* placed on CR diet.

11.3.2 The *pex5Δ* mutation decreases the levels of components of the PDH complex and TCA cycle in mitochondria

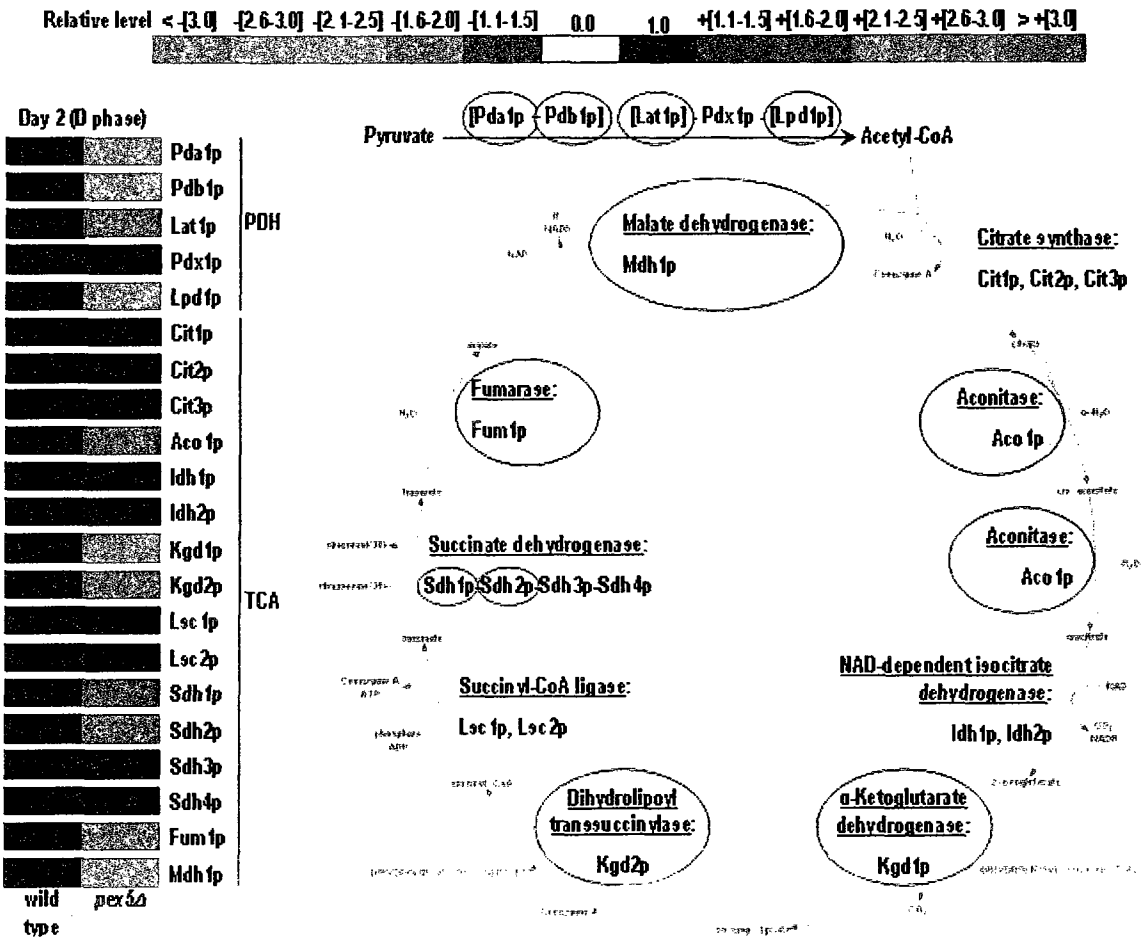

Figure 11.4. Relative levels of protein components of the mitochondrial PDH complex and TCA cycle recovered from purified mitochondria of wild-type and *pex5Δ S. cerevisiae* cells that were grown under CR conditions and recovered for analysis upon reaching D phase.

11.3.3 The *pex5Δ* mutation decreases the levels of proteins involved in the mitochondrial ETC, heme synthesis and attachment, ATP synthesis, and ATP/ADP and P_i transport across the membrane

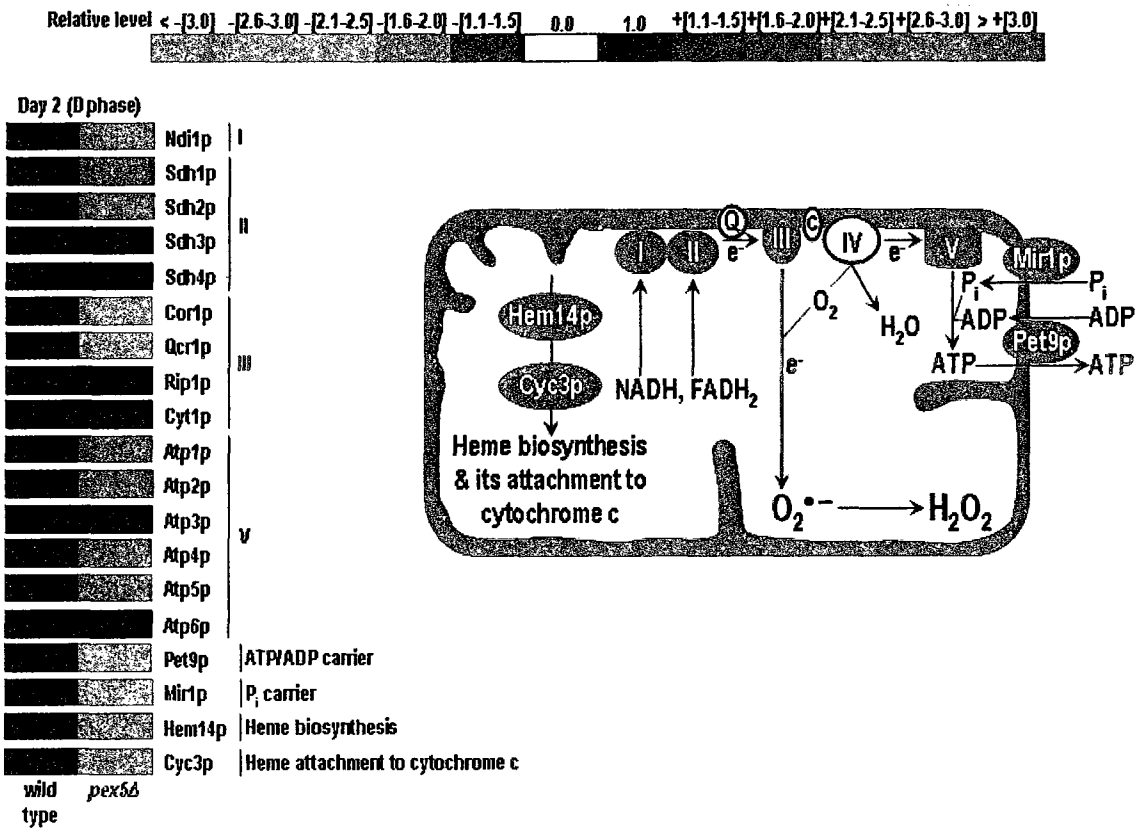

Figure 11.5. Relative levels of proteins involved in the mitochondrial ETC, heme synthesis and attachment, ATP synthesis, and of ATP/ADP and P_i carriers recovered from purified mitochondria of wild-type and *pex5Δ S. cerevisiae* cells that were grown under CR conditions and recovered for analysis upon reaching D phase.

11.3.4 The *pex5Δ* mutation significantly affects mitochondrial morphology by altering the levels of mitochondrial proteins involved in mitochondrial fission and fusion

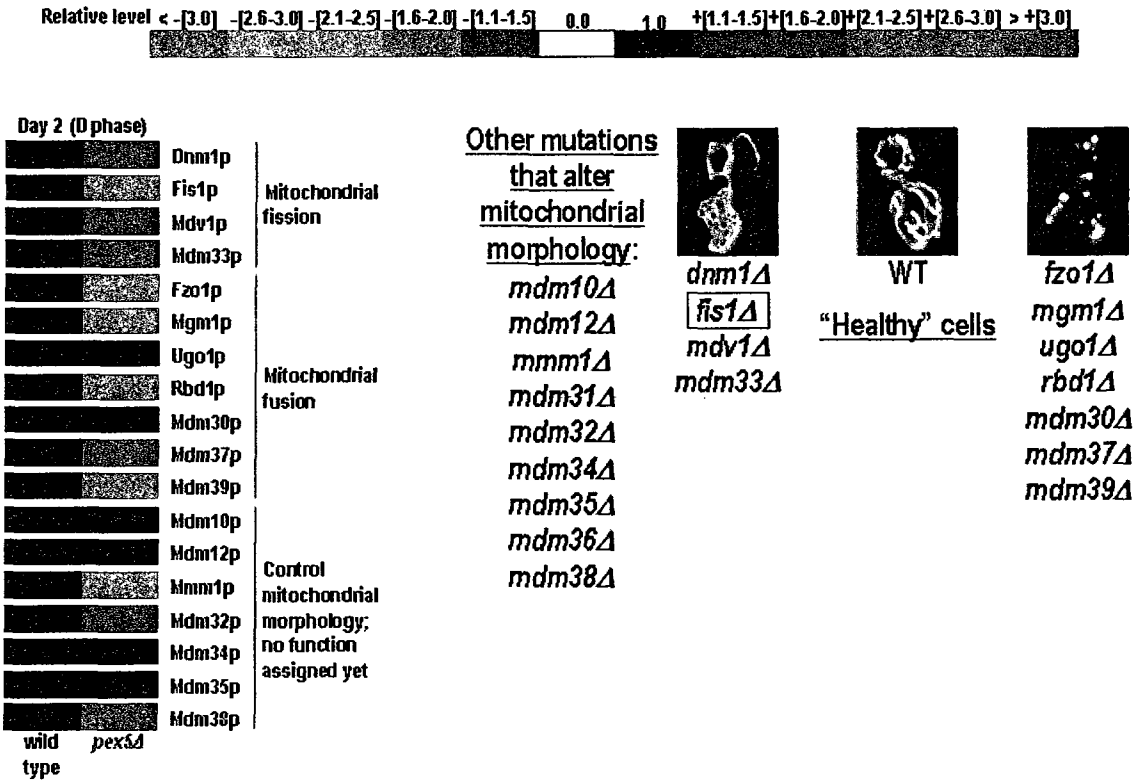

Figure 11.6. Relative levels of proteins involved in mitochondrial fission and fusion recovered from purified mitochondria of wild-type and *pex5Δ S. cerevisiae* cells that were grown under CR conditions and recovered for analysis upon reaching D phase.

11.3.5 The p*ex5Δ* mutation significantly decreases the levels of proteins that detoxify ROS to protect mitochondrial macromolecules from oxidative damage

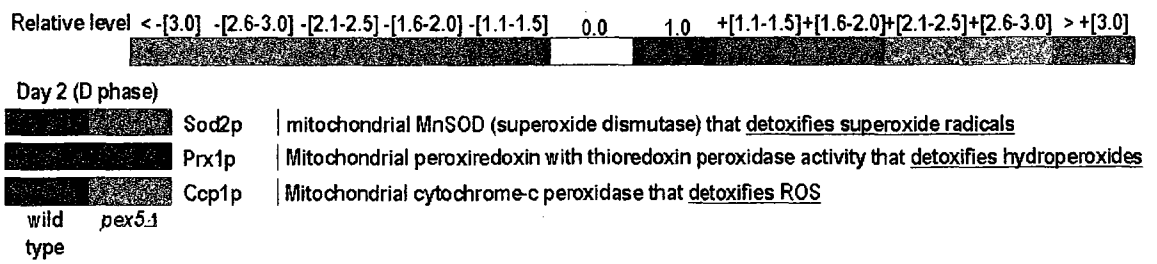

Figure 11.7. The *pex5Δ* mutation remodels protein team that protects mitochondrial macromolecules from oxidative damage.

11.3.6 The *pex5Δ* mutation increases the levels of some chaperone proteins that control the unfolding of proteins during their translocation into the mitochondrial matrix and/or protein folding/refolding in the mitochondrial matrix

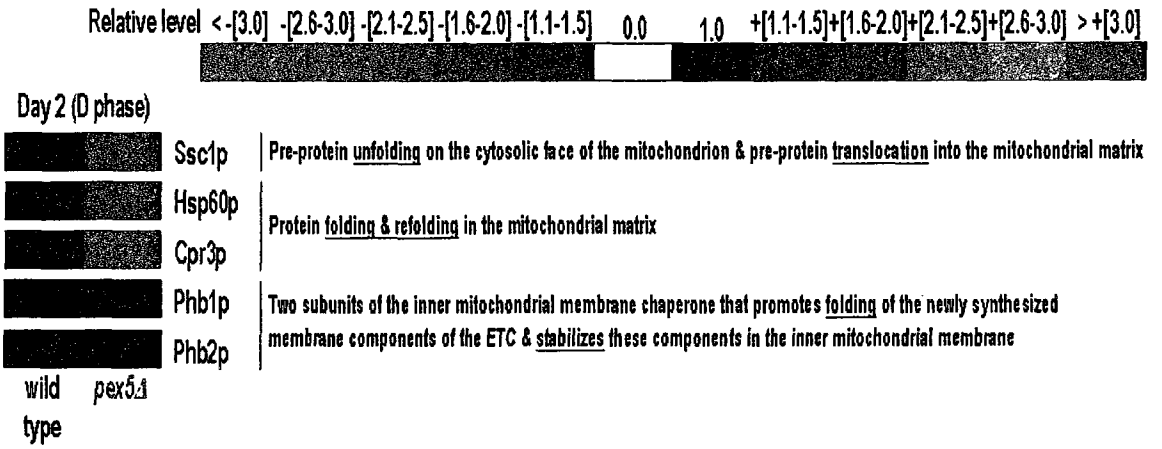

Figure 11.8. The *pex5Δ* mutation remodels protein machineries that control the unfolding of proteins during their translocation into the mitochondrial matrix and/or protein folding/refolding in the mitochondrial matrix.

11.3.7 The *pex5Δ* mutation alters the levels of mitochondrial proteins involved in the biosynthesis of various amino acids and/or stabilization of mitochondrial DNA (mtDNA)

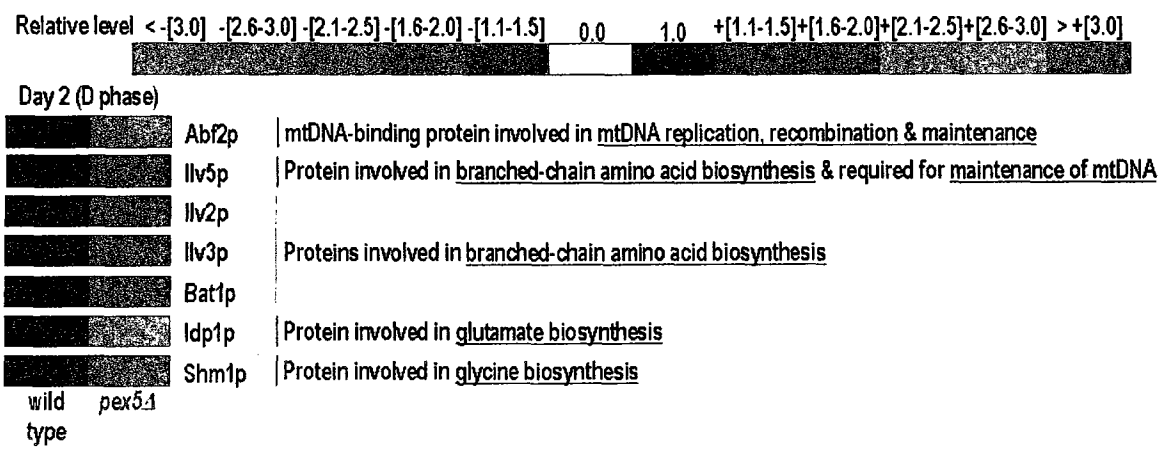

Figure 11.9. The *pex5Δ* mutation remodels protein machineries that control biosynthesis of various amino acids and/or stabilize mitochondrial DNA (mtDNA).

11.3.8 The long-lived mitochondrial mutants *idh1Δ* & *idh2Δ* have increased levels of cytosolic anti-stress chaperones and proteins that decompose ROS in the cytosol

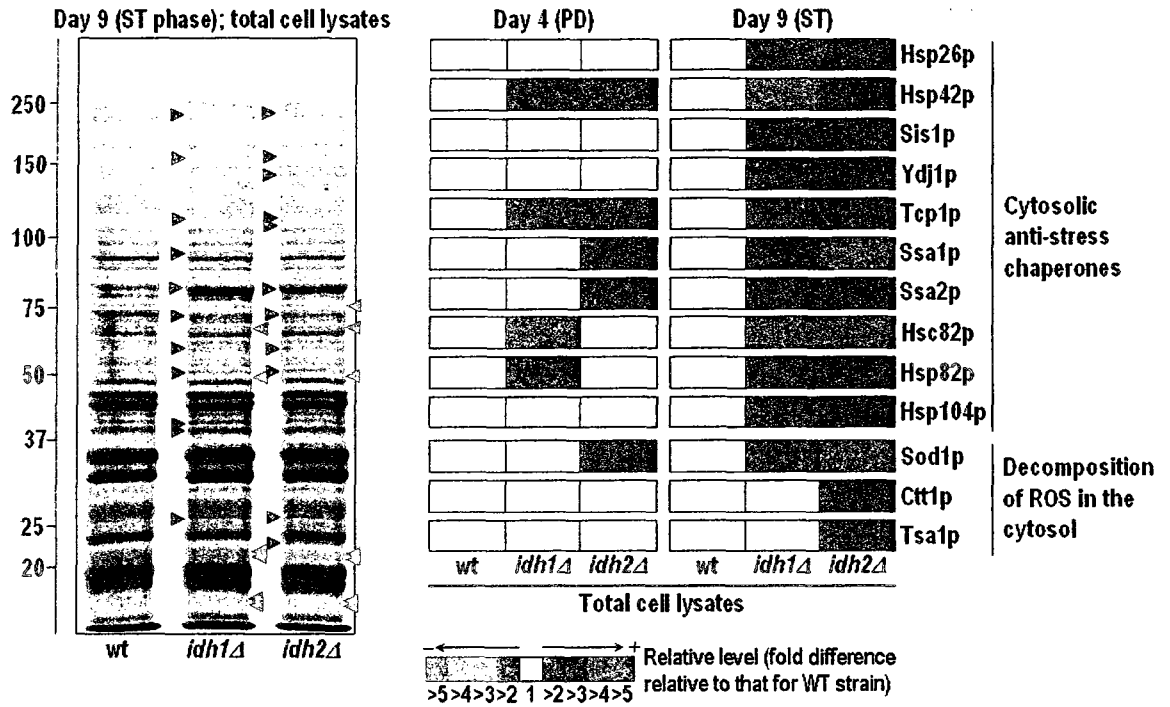

Figure 11.10. Quantitative analysis of cellular proteomes of WT, *idh1Δ* & *idh2Δ* mutants revealed that both mutations elevate the levels of cytosolic anti-stress chaperones and proteins that decompose ROS in the cytosol, thereby protecting other proteins from oxidative damage.

11.3.9 The long-lived mitochondrial mutants *idh1Δ* and *idh2Δ* have increased levels of the mitochondrial proteins involved in the import of other proteins into the mitochondrial matrix, folding and refolding of mitochondrial proteins following stress exposure, decomposition of ROS, and protection of mtDNA from oxidative damage

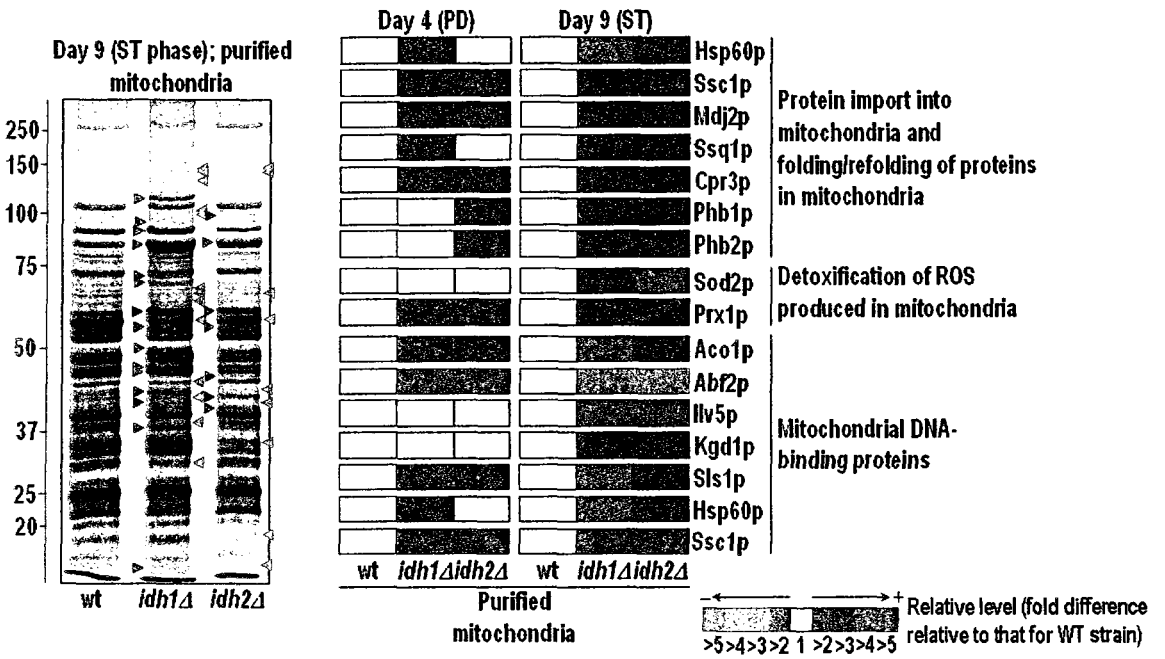

Figure 11.11. The long-lived *idh1Δ* and *idh2Δ* mutants have elevated levels of mitochondrial enzymes involved in protein import into the mitochondrial matrix, protein folding and refolding following stress exposure, degradation of ROS and protection of mtDNA from oxidative damage.

11.4 Discussion

My quantitative proteomic analysis revealed numerous mitochondrial proteins whose levels have been altered in mitochondria of the short-lived *pex5Δ* mutant strain (as compared to those of wild-type strain) grown under CR conditions. These findings imply that the Pex5p-dependent assembly of peroxisomes plays an essential role in longevity regulating by modulating a distinct set of mitochondrial processes, as described below.

11.4.1 The *pex5Δ* mutation alters the mitochondrial PDH complex and impairs the TCA cycle in mitochondria

According to my quantitative proteomic analysis, the *pex5Δ* mutation substantially decreases the levels of almost all protein subunits (except Pdx1p) of the mitochondrial PDH complex (Figure 11.4). The pyruvate dehydrogenase (PDH) multienzyme complex catalyzes the formation of acetyl-CoA and NADH in the mitochondrion (Figure 11.12).

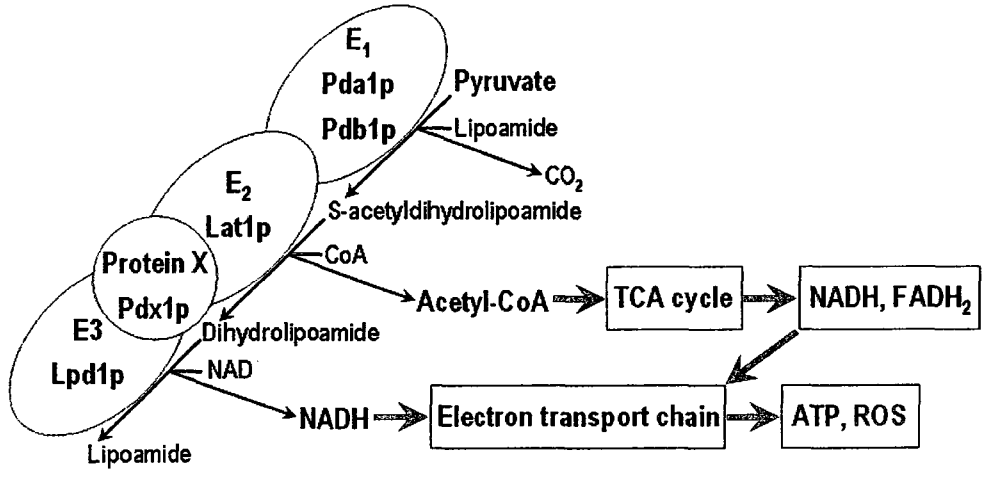

Figure 11.12. The pyruvate dehydrogenase (PDH) multienzyme complex in the yeast *S. cerevisiae.*

Acetyl-CoA formed by the PDH complex acts as a substrate for the citrate synthase-dependent reaction of the TCA cycle in mitochondria, whereas NADH provides reduced equivalents to drive the mitochondrial ETC. Thus, proper functioning of the PDH complex is crucial for the synthesis of ATP in mitochondria. The PDH complex consists of four enzyme subunits: the E1 subunit composed of Pda1p and Pdb1p, the E2 subunit Lat1p, the E3 subunit (Lpd1p), and the X subunit Pdx1p (Figure 11.12). The observed in the *pex5Δ* mutant strain decrease in levels of the Pda1p, Pdb1p and Lat1p

(the E1 and E2 subunits of the PDH complex) greatly reduces acetyl-CoA formation and ATP production in the mitochondria (Figure 11.4). Furthermore, the *pex5Δ* mutation lowers the levels of Lpd1p (E3), thus also decreasing the rate of mitochondrial NADH formation (Figure 11.4). Of note, enzymatic activities of the PDH complex subunits appear to play a crucial role in regulation of the chronological aging of *S. cerevisiae.* In fact, recent work in Dr. Titorenko's laboratory demonstrated that the mutants lacking either E1 or E2 subunits of PDH are short-lived, whereas those lacking the X or E3 subunits exhibit prolonged life span (Figure 11.13)

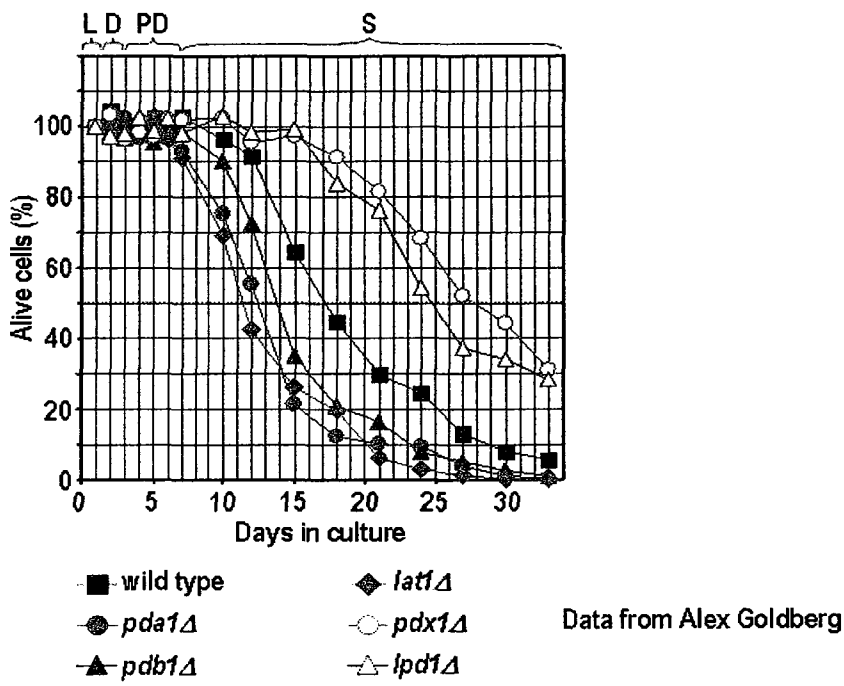

Figure 11.13. Lack of the Pda1p, Pdb1p or Lat1p components of the mitochondrial PDH complex shortens the chronological life span of *S. cerevisiae* grown under CR conditions, whereas the lack of Pdx1p and Lpd1p subunits extends its life span.

Based on my proteomic data implicating mitochondrial PDH complex as a rate-limiting factor in the aging process, and taking into account the research findings of my colleagues in Dr. Titorenko's laboratory on life span extension in *S. cerevisiae* mutants lacking either X or E3 subunits, I propose the following model for the integration of the

mitochondrial PDH complex into the cellular longevity network. Lack of either X (Pdx1p) or E3 (Lpd1p) subunits of the mitochondrial PDH complex prevents the NADH synthesis but does not impair the formation of acetyl-CoA, and thus does not compromises the TCA cycle activity in the *pdx1Δ* or *lpd1Δ* mutants (Figure 11.14).

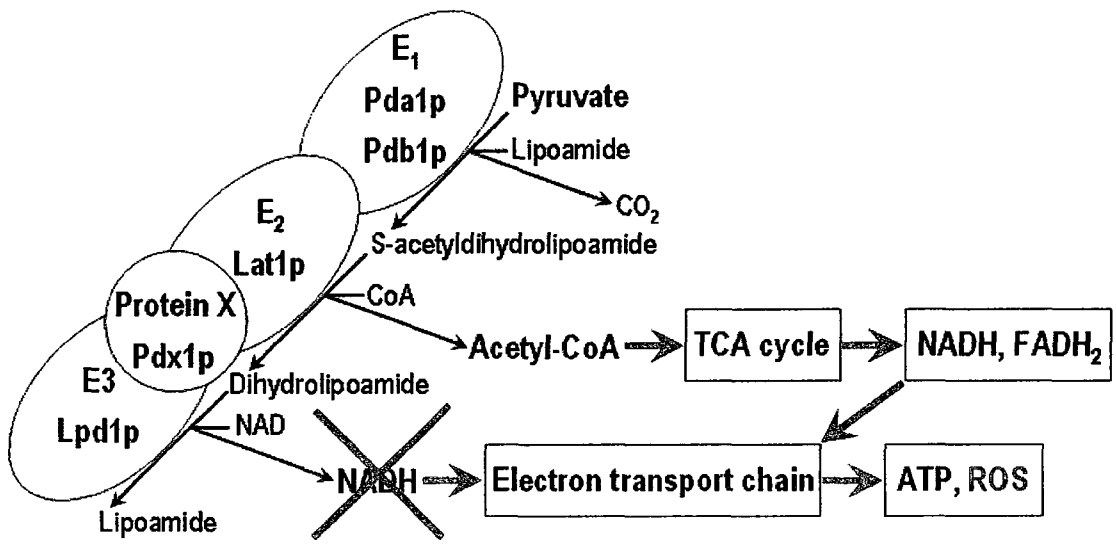

Figure 11.14. Remodeling of the PDH multienzyme complex in the long-lived *pdx1Δ* and *lpd1Δ* mutants of *S. cerevisiae* grown under CR conditions.

However, the impairment of NADH synthesis by the PDH complex in the mitochondria of the *pdx1Δ* and *lpd1Δ* mutants slows down electron flow through the ETC, thus lowering the production of ROS and reducing amount of ROS-mediated oxidative damage to mitochondrial macromolecules. The anticipated decrease in the amount of ROS produced in mitochondria of the *pdx1Δ* and *lpd1Δ* mutants has been confirmed by Dr. Titorenko's laboratory, thus supporting my hypothesis that the reduction of ROS-mediated oxidative damage to mitochondrial macromolecules is the major cause in the chronological life span extension observed in these mutants.

On the contrary, lack of Pda1p, Pdb1p or Lat1p components of the PDH complex impairs the synthesis of both acetyl-CoA and NADH, thereby decelerating the TCA cycle as well as the mitochondrial ETC and, thus, lowering the synthesis of ATP (Figure 11.15). The insufficient ATP production in mitochondria of *pda1Δ*, *pdb1Δ* and *lat1Δ* mutants could therefore explain their shorter lifespan (Figure 11.15).

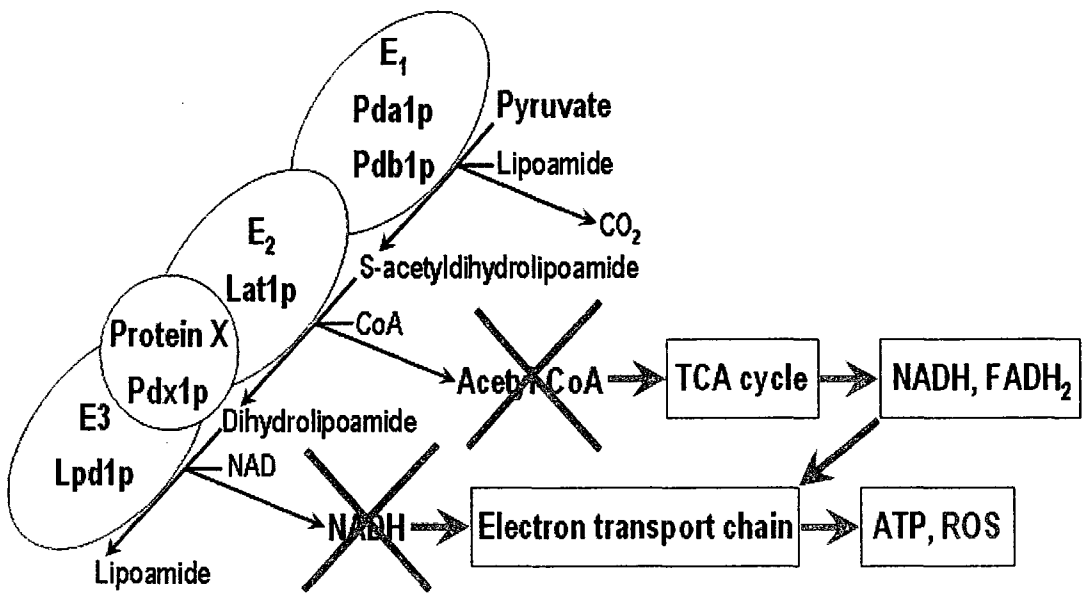

Figure 11.15. Remodeling of the PDH multienzyme complex in the short-lived *pda1Δ*, *pdb1Δ* and *lat1Δ* mutants of *S. cerevisiae* grown on CR diet.

My quantitative proteomic analysis also revealed that the *pex5Δ* mutation decreases the levels of enzymes involved in the mitochondrial TCA cycle, such as Aco1p, Kgd1p, Kgd2p, and Fum1p (Figure 11.4). In addition, the *pex5Δ* mutation lowers the levels of the Sdh2p subunit of the mitochondrial succinate dehydrogenase (SDH) complex, which also catalyzes one of the mandatory reactions in the TCA cycle (Figure 11.4). Of note, these four TCA cycle enzymes and the Sdh2p subunit of the SDH complex have no redundant protein counterparts, which do exist for several other enzymes involved in the TCA cycle. As a result, a mutant strain lacking any of these five mitochondrial proteins has a

partially impaired TCA cycle activity and generates insufficient amounts of ATP, which could account for the observed life span shortening in such mutants. Furthermore, my proteomic analysis also revealed that the *pex5Δ* mutation does not alter the levels of TCA cycle enzymes that have redundant subforms, such as Cit1p and Cit3p, Idh1p and Idh2p, as well as Lsc1p and Lsc2p (Figure 11.4). In fact, mutants lacking only one redundant subform of these TCA cycle enzymes live longer than wild-type strain and are more resistant to elevated temperature and oxidative stress, which is consistent with the elevated levels of numerous stress-protecting proteins observed in all these mutants (Figures 11.10, 11.11, 11.16 and 11.17). Moreover, consistent with my proteomic data, studies in Dr. Titorenko's laboratory also showed that the long-lived mutants *idh1Δ* or *idh2Δ* have lower frequencies of mtDNA mutations, which can explain their longer (as compared to wild-type strain) life span (Figure 11.18).

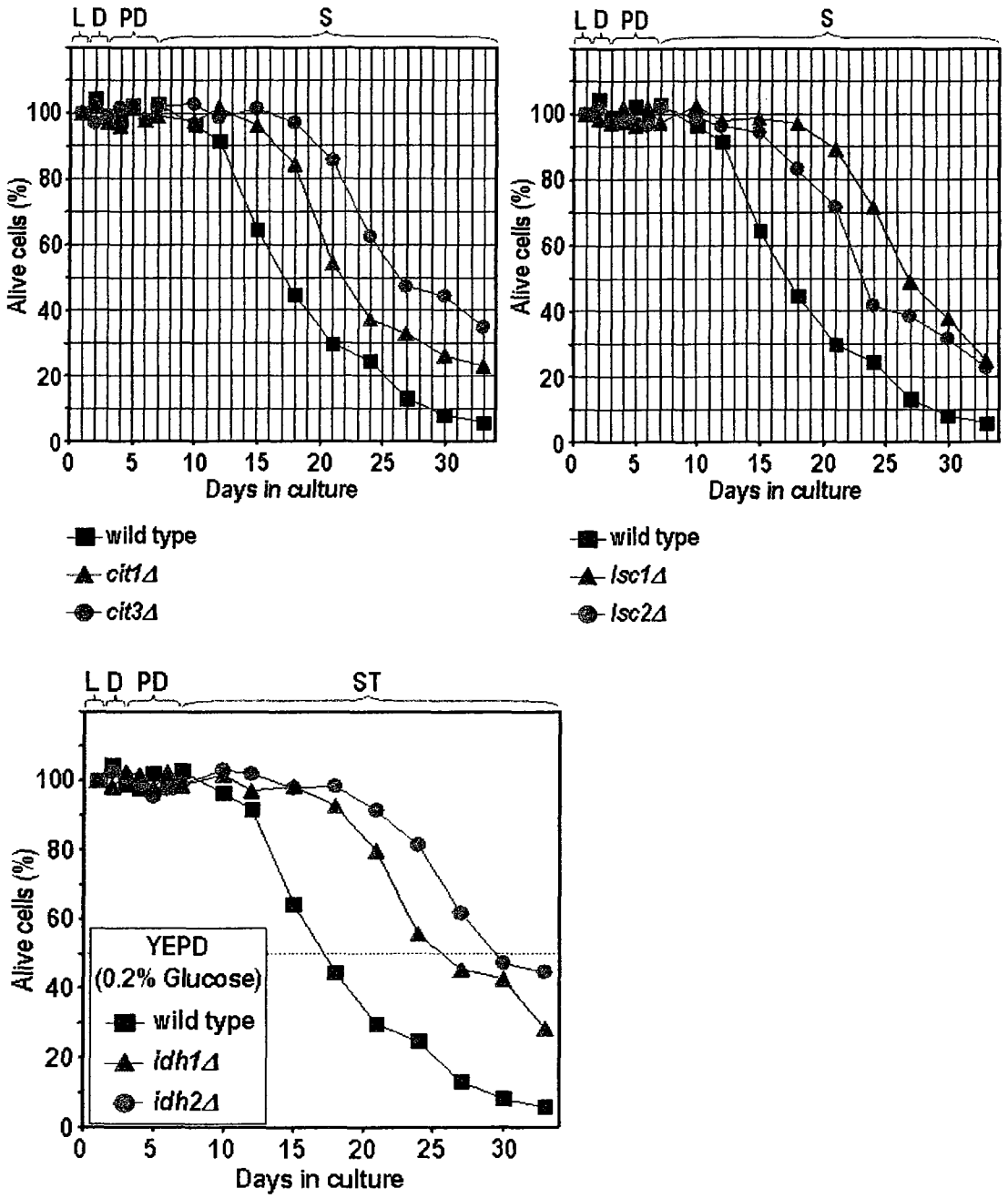

Figure 11.16. Lack of the Cit1p, Cit3p, Lsc1p, Lsc2p, Idh1p or Idh2p components of the mitochondrial TCA cycle extends the chronological life span of *S. cerevisiae* grown under CR conditions.

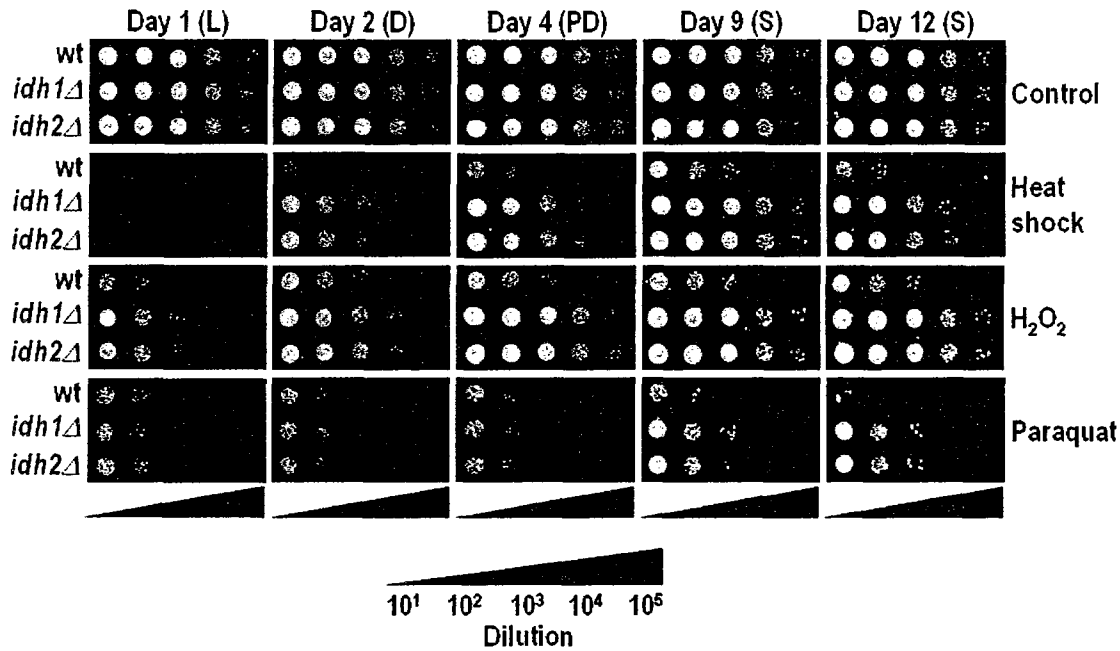

Figure 11.17. Chronologically aging CR yeast carrying the *idh1Δ* or *idh2Δ* mutation have increased resistance to elevated temperatures and oxidative stress, which is consistent with the elevated levels of numerous stress-protecting proteins observed in these mutants.

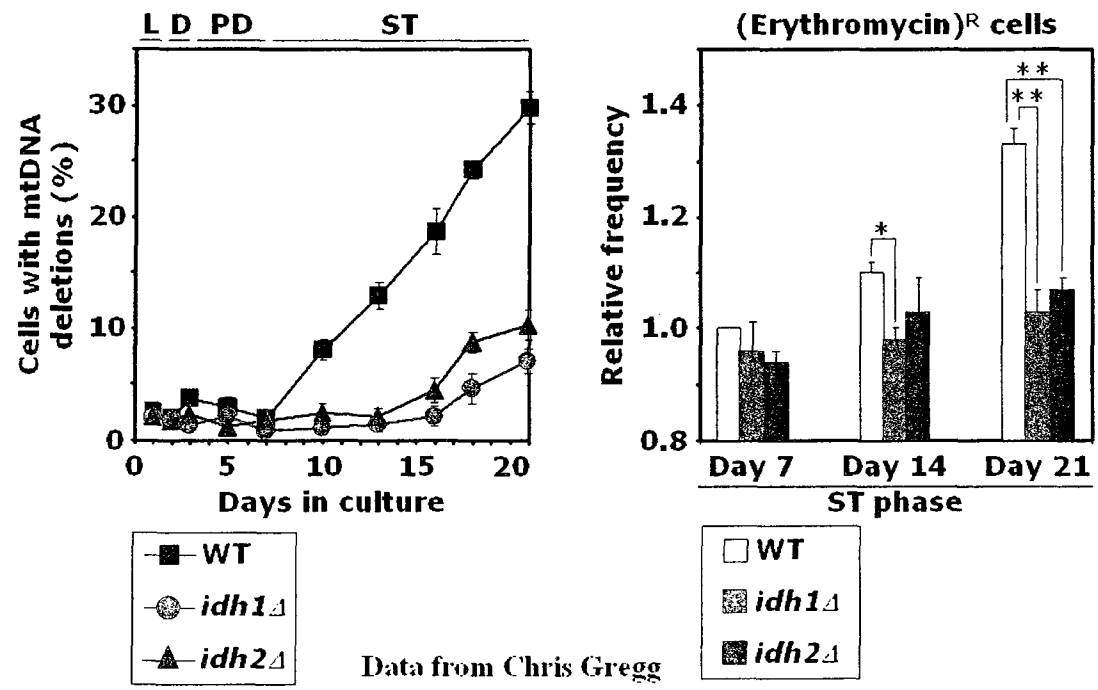

Figure 11.18. Chronologically aging CR yeast carrying the *idh1Δ* or *idh2Δ* mutation show decreased frequencies of mtDNA mutations, which is consistent with the elevated levels of numerous proteins that bind to mtDNA and protect it from oxidative damage.

Taken together, my proteomic data implicating certain components of the mitochondrial TCA cycle as the regulators of the chronological aging in *S. cerevisiae*, along with the recent findings from Dr. Titorenko's laboratory on the life span extension in mutants lacking a single redundant subform of several TCA cycle enzymes, strongly suggest the following scenario for the integration of the mitochondrial TCA cycle into the cellular longevity network. Lack of a single isoform of either the mitochondrial citrate synthase, NAD-dependent isocitrate dehydrogenase or succinyl-CoA ligase does not impair the ability of mitochondria to produce NADH and $FADH_2$ and, thus, do not impair ATP synthesis. However, lack of a single isoform of each of these enzymes also decreases the amounts of NADH and $FADH_2$ produced, thereby slowing down electron flow through the mitochondrial ETC, lowering the amount of ROS generated during this process and, consequently, reducing the extent of oxidative damage of mitochondrial macromolecules by ROS. The predicted by my hypothesis decreased ROS production in the *cit1p, cit3p, idh1p, idh2p, lsc1p* and *lsc2p* mutants has been recently confirmed in Dr. Titorenko's laboratory and could satisfactorily explain the life span extension observed in these mutants.

11.4.2 The *pex5Δ* mutation remodels the protein machineries regulating mitochondrial ETC, heme biosynthesis and attachment, ATP synthesis, and ATP/ADP exchange

I also found that the *pex5Δ* mutation decreases the levels of certain protein components of the mitochondrial ETC and ATP synthase, including the mitochondrial ETC complex I constituent Ndi1p, the mitochondrial ETC complex II constituent Sdh2p (a subunit of the succinate dehydrogenase complex), the mitochondrial ETC complex III subunits Cor1p

and Qcr1p, and the Atp1p, Atp2p, Atp4p and Atp5p subunits of the ATP synthase F1 catalytic complex (Figure 11.5). In addition, lack of Pex5p substantially decreases the levels of the ATP/ADP carrier protein Pet9p and of the P_i carrier protein Mir1p in the mitochondrial membrane (Figure 11.5). These two proteins promote the synthesis of ATP by transporting the ADP and Pi substrates into the mitochondria from the cytosol and by coupling the import of ADP into mitochondria with the export of synthesized ATP into the cytosol (Figure 11.5). Furthermore, the *pex5Δ* mutation substantially lowers the amounts of the Hem14p protein involved in the mitochondrial heme biosynthesis pathway and of the Cyc3p protein that promotes the attachment of mitochondrially synthesized heme to the subforms 1 and 7 of cytochrome c, a mobile component of the mitochondrial ETC (Figure 11.5). The observed decrease of multiple protein components of the ETC and ATP synthesis in mitochondria of the *pex5Δ* mutant, in turn, shortens its life span (Figure 11.2). Of note, lack of either complex I protein Ndi1p or the complex II subunits Sdh1p or Sdh4p of the mitochondrial ETC extends the life span of *S. cerevisiae* cells grown under CR at 0.2% glucose (Figure 11.19).

Taken together, recent findings from Dr. Titorenko's laboratory on life span extension in *S. cerevisiae* mutants lacking either complex I or complex II components of the mitochondrial ETC, along with my proteomic data identifying crucial protein components of the mitochondrial ETC and ATP synthesis teams involved in longevity regulation, suggest the following scenario for the integration of the protein components that function in the mitochondrial electron transport and ATP formation into the global

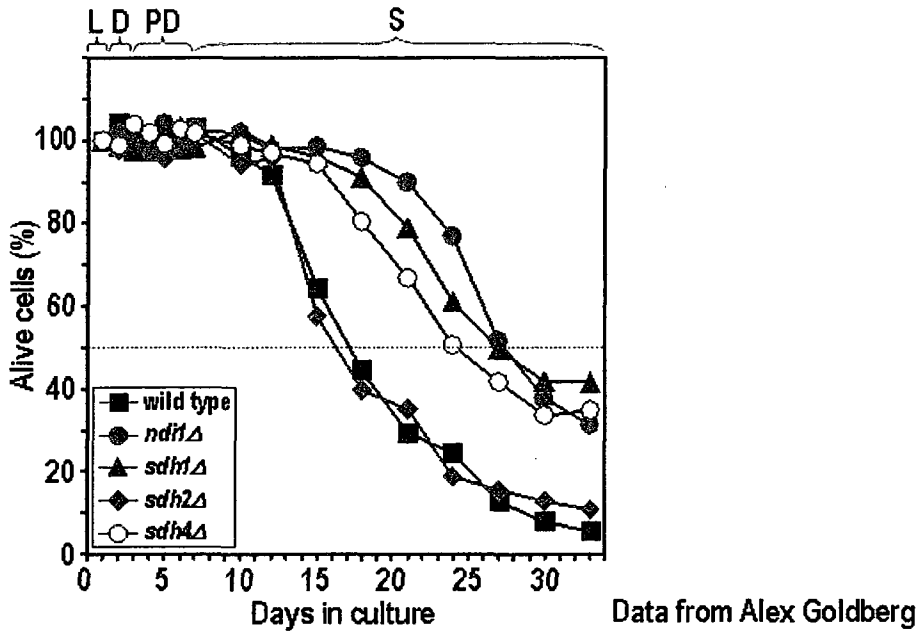

Figure 11.19. Lack of the Sdh1p, Sdh4p or Ndi1p components of the mitochondrial ETC extends the chronological life span of yeast grown under CR conditions.

cellular longevity network. Lack of either complex I or complex II components results in a reduced electron flow through the mitochondrial ETC but does not impair the mitochondrial ability to synthesize ATP. The reduced rate of the mitochondrial ETC in these mutants decreases the amount of mitochondrially produced ROS and therefore reduces the detrimental effect of ROS on mitochondrial macromolecules, ultimately resulting in life span extension.

11.4.3 The *pex5Δ* mutation remodels mitochondrial morphology

My quantitative proteomic analysis also revealed that the *pex5Δ* mutation remodels protein teams regulating mitochondrial morphology in the yeast *S. cerevisiae* (Figure 11.6). Mitochondrial morphology in a cell depends on a delicate balance between the processes of mitochondrial fusion and fission [262-264]. Furthermore, the relative rates

of mitochondrial fusion and fission have a strong impact on the intrinsic pathway of the apoptotic cell death [190, 191, 205-208]. The fusion process helps to maintain mitochondria in a network configuration to allow the efficient transfer of the mitochondrial membrane potential among cellular regions with varying degree of oxygenation. The mitochondrial network also facilitates mtDNA repair, thus substantially reducing signaling through mitochondrial pro-apoptotic pathways and preventing intrinsically-induced cell death [190, 191, 205-208]. The mitochondrial membrane proteins Fzo1p, Mgm1p, Ugo1p, Rbd1p, Mdm30p, Mdm37p and Mdm39 promote the formation of the mitochondrial tubular network by fusion of individual mitochondria [262]. At the same time, the proper inheritance of mitochondria during cell division requires a break-down of the mitochondrial network by the fission process. Mitochondrial fission can also cause respiratory defects, eventual loss of mtDNA due to accumulated mtDNA mutations, and increased rate of intrinsically-induced apoptotic cell death [190, 191, 205-208]. The mitochondria-associated proteins Dnm1p, Fis1p, Mdv1p and Mdm33p promote mitochondrial fragmentation by facilitating the fission of individual mitochondria into a mitochondrial tubular network [262]. In addition, several other proteins have been implicated in the regulation of mitochondrial morphology in *S. cerevisiae*, although their exact functions in mitochondrial fusion and fission remain to be elucidated [262].

According to my quantitative proteomic analysis, the *pex5Δ* mutation substantially increases the amounts of two proteins involved in mitochondrial fission, Dnm1p and Mdv1p (Figure 11.6). In non-stressed cells and in cells undergoing exogenously induced apoptosis, both these proteins stimulate fragmentation of the mitochondrial tubular

network [262]. Such fragmentation results from the coordinated action of the mitochondrial fission and fusion protein machineries, which control the release of cytochrome c and several other pro-apoptotic proteins from the mitochondrial intermembrane space [265]. In fact, mitochondrial fragmentation has been shown to promote the release of cytochrome c, Aif1p and Nuc1p (EndoG) from mitochondria to the cytosol in response to a short-term exposure of yeast to the pro-apoptotic stimuli hydrogen peroxide and acetic acid [266-268]. Furthermore, it has been also shown that once in the cytosol, cytochrome c activates yeast metacaspase 1, whereas both Aif1p and Nuc1p (EndoG) are transported into the nucleus where they promote DNA cleavage [269, 270]. My proteomic data provide evidence that the *pex5Δ* mutation decreases the levels of mitochondria-bound Fis1p and Mdm33p proteins, both of which are known to promote the fragmentation of the mitochondrial tubular network only in non-stressed cells (Figure 11.6) [262, 264]. However, lack of Fis1p does not impair mitochondrial fission in aging CR yeast but, in contrast to what was expected, accelerates the fragmentation of their mitochondrial network and shortens their life spans (Figure 11.20) [271]. Therefore, the observed in the *pex5Δ* mutant decrease in the mitochondria-bound pools of Fis1p and Mdm33p promotes the fragmentation of its mitochondrial tubular network and consequently shortens its life span (Figure 11.6).

My quantitative proteomic analysis also indicates that the premature aging of the *pex5Δ* mutant coincides with the dramatic decrease in the mitochondria-bound pools of

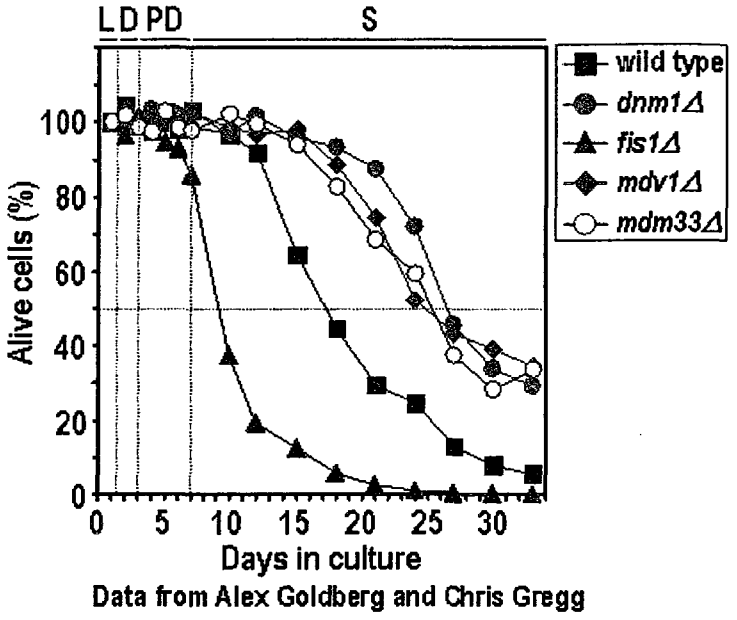

Figure 11.20. Lack of proteins that promote mitochondrial fission (except Fis1p) extends the lifespan of chronologically aging *S. cerevisiae* grown on CR diet.

numerous proteins that promote mitochondrial fusion into a tubular network, such as Fzo1p, Mgm1p, Rbd1p, Mdm37p, and Mdm39p (Figure 11.6). Therefore, my findings also suggest that the *pex5Δ* mutation promotes the fragmentation of the mitochondrial tubular network by down-regulating the synthesis and/or accelerating the degradation of several proteins promoting mitochondrial fusion. My hypothesis is supported by the recent data from Dr. Titorenko's laboratory showing that lack of several mitochondrial fusion-promoting proteins shortens the chronological life span of *S. cerevisiae* under CR conditions (Figure 11.21).

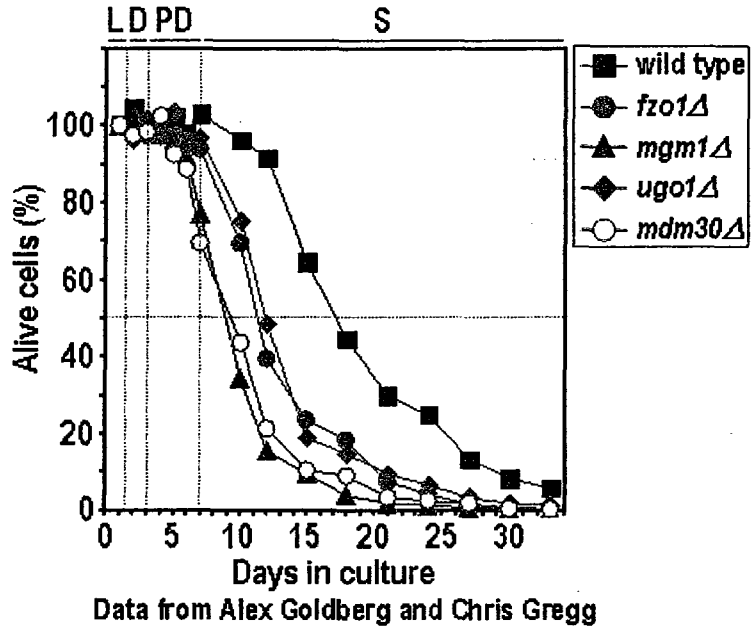

Figure 11.21. Lack of proteins that promote mitochondrial fusion shortens the chronological life span of *S. cerevisiae* grown under CR conditions at 0.2% glucose.

Altogether, my proteomic data and recent findings from Dr. Titorenko's laboratory strongly suggest that aging in yeast promotes mitochondrial fragmentation by stimulating the fission of the mitochondrial tubular network and inhibiting the fusion of individual mitochondria into the network. This, in turn, promotes the release of the pro-apoptotic proteins cytochrome c, Aif1p and Nuc1p (EndoG) from mitochondria to the cytosol, thereby culminating the aging process by activating the programmed cell death.

11.4.4 The *pex5Δ* mutation remodels protein teams that function in the response to stresses, stabilization of mitochondrial DNA (mtDNA) and biosynthesis of various amino acids

My quantitative proteomic analysis revealed that the *pex5Δ* mutation leads to a significant decrease in the levels of proteins that protect mitochondrial macromolecules from ROS-induced oxidative damage (Figure 11.7). In fact, the levels of two crucial

ROS-scavenging proteins Sod2p and Ccp1p are dramatically decreased in mitochondria of the *pex5Δ* mutant, as compared to those observed in wild-type strain (Figure 11.7). The decreased levels of these two proteins in the *pex5Δ* mutant result in the build-up of oxidatively-damaged mitochondrial macromolecules, thereby significantly reducing mitochondrial activity and function, stimulating mitochondrial fragmentation and the pro-apoptotic mitochondrial signaling, and shortening its life span [265-270].

According to my proteomic data, the *pex5Δ* mutation also alters the levels of proteins controlling the unfolding of proteins during their translocation into the mitochondrial matrix and/or their folding/refolding in the mitochondrial matrix (Figure 11.8). In fact, the levels of the molecular chaperones Ssc1p, Hsp60p and Cpr3p were considerably higher in mitochondria of the *pex5Δ* mutant than those observed in mitochondria of wild-type strain (Figure 11.8). In addition, the *pex5Δ* mutation elevates the levels of mitochondrial proteins regulating the synthesis of branched amino-acids and maintenance of mtDNA, such as Ilv5p, Ilv2p, Ilv3p, Bat1p, Idp1p and Shm1p (Figure 11.9). Of note, the levels of Abf2p, another protein involved in the stabilization of mtDNA, are significantly decreased by the *pex5Δ* mutation (Figure 11.9). These findings suggest that the *pex5Δ* mutation not only impairs the peroxisomal function in yeast, but also significantly diminishes mitochondrial functional activity and lowers the efficiency of mtDNA repair and maintenance. The insufficient synthesis of ATP in mitochondria resulting from the impaired peroxisomal production of acetyl-CoA and low glucose concentration under CR conditions may activate the biosynthesis of various amino acids in mitochondria of *pex5Δ* mutant and their subsequent catabolism allowing to use these amino acids as an alternative, albeit weak, energy source for the mutant. Thus, the

insufficient energy production and activated mitochondrial pro-apoptotic signaling could be the major causes of the dramatic decrease in the chronological life span of the *pex5Δ* mutant under CR conditions.

11.5 Conclusions

Altogether, my proteomic data and the recent data of metabolomic and functional studies conducted in Dr. Titorenko's laboratory demonstrate that the extension of the chronological life span in CR yeast can only be achieved if the fatty acid oxidation pathway in the peroxisome is fully functional. In fact, the cytosolic shuttling receptor Pex5p, which is required for peroxisomal import of two major enzyme components of fatty acid β-oxidation, plays a key role in longevity regulation of chronologically aging yeast under CR conditions by modulating the levels of proteins involved in such essential mitochondrial processes as the mitochondrial PDH complex, TCA cycle, ETC, heme biosynthesis and attachment, ATP synthesis, ATP/ADP exchange, as well as mitochondrial fusion and fission, mitochondrial pro-apoptotic signaling, maintenance of mtDNA, protein folding and unfolding, protein translocation into the mitochondrial matrix, and mitochondrial biosynthesis of various amino acids. In order to understand how defects in peroxisomal fatty acid oxidation process result in such profound effect on various mitochondrial functions, and to better define the contribution of lipid metabolism to longevity regulation in CR yeast, I explored the age-dependent dynamics of changes in the proteomes of the ER and lipid bodies taking place in wild-type and *pex5Δ* cells grown under CR conditions.

12 Quantitative proteomic analysis of the ER and lipid bodies purified from wild-type and *pex5Δ* strains of the yeast *S. cerevisiae* that were aged chronologically under CR conditions

12.1 Introduction

As glucose becomes limited in the growth medium, yeast cells undergo a diauxic shift in energy metabolism from glycolysis to mitochondrial respiration. Recent evidence from Dr. Titorenko's laboratory shows that in wild-type strain of *S. cerevisiae* this metabolic transition is accompanied by a substantial shortening of the length of ER membranes, almost complete disappearance of lipid bodies (LB) and massive proliferation of mitochondria (Figure 12.1).

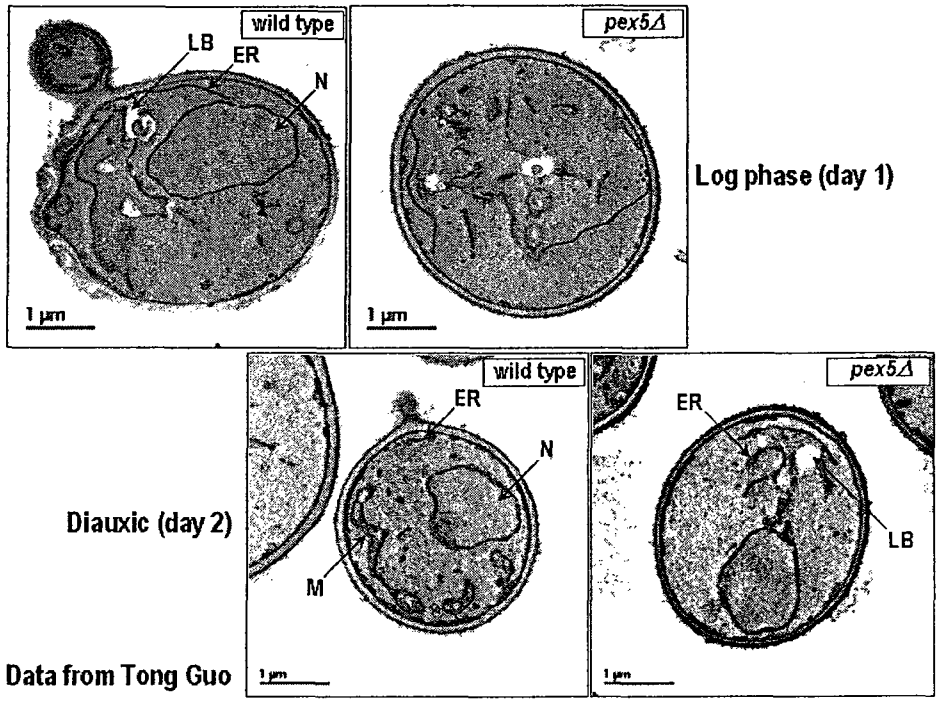

Figure 12.1. Electron micrographs illustrating a substantial shortening of the length of ER membranes and the disappearance of lipid bodies in the chronologically aging wild-type strain of *S. cerevisiae* grown under Cr conditions at 0.2% glucose. In contrast, the short-lived *pex5Δ* mutant displays ER expansion and lipid body accumulation under these conditions.

In contrast, cells of the short-lived *pex5Δ* mutant recovered from D phase displayed greatly extended ER membranes that were closely apposed to abundant LBs present in these cells; in addition *pex5Δ* cells showed no proliferation of mitochondria (Figure 12.1). As wild-type *S. cerevisiae* cells entered the PD growth phase, their mitochondria enlarged and increased in number, whereas PD-phase cells of the *pex5Δ* mutant showed no growth of the mitochondrial network and accumulate larger amounts of LBs as their ER membranes shorten (Figure 12.1).

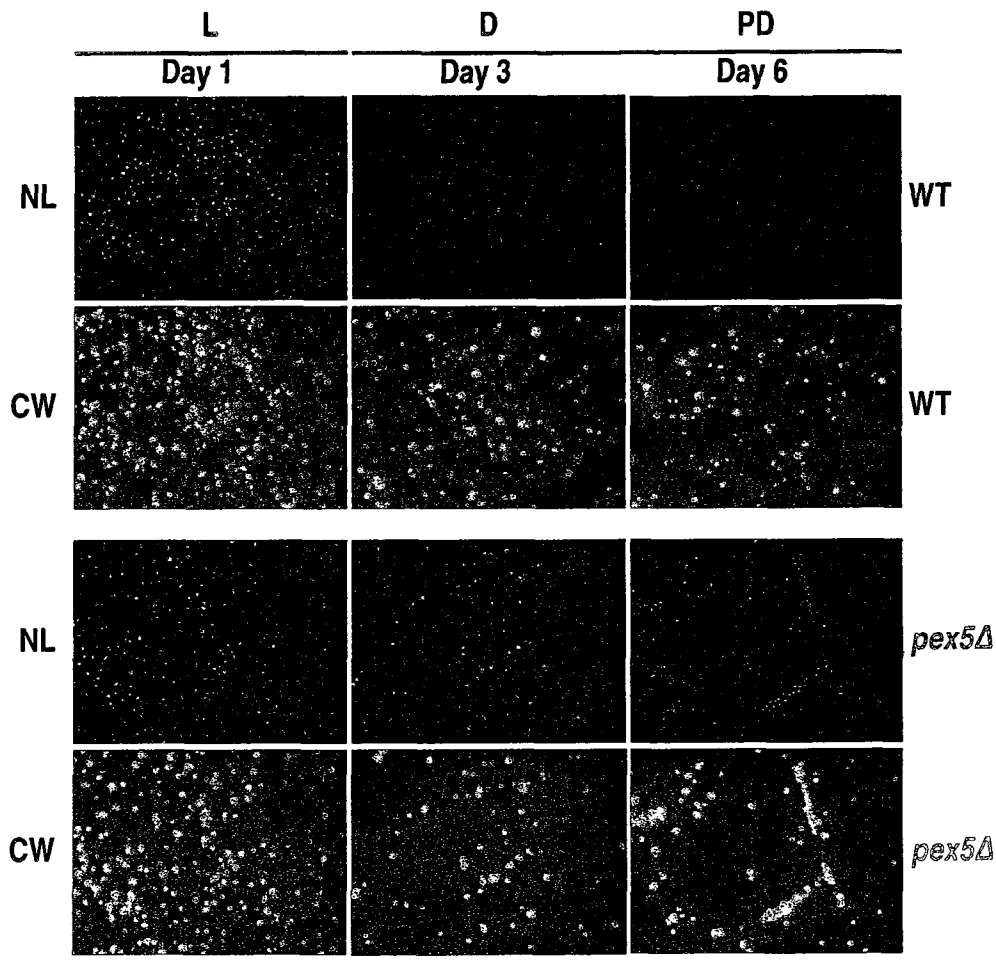

Figure 12.2. BODIPY staining showing the dynamics of lipid body consumption in chronologically aging wild-type and *pex5Δ* cells grown under CR conditions at 0.2% glucose.

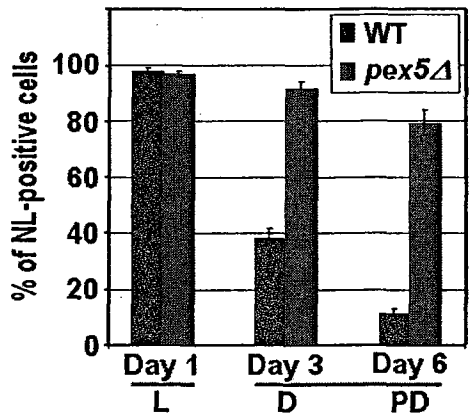

Figure 12.3. The age-dependent dynamics of neutral lipid consumption in chronologically aging wild-type and *pex5Δ* cells grown under CR conditions at 0.2% glucose.

In both wild-type and *pex5Δ* cells, LBs were found in close proximity to the ER (Figure 12.1), which is consistent with the ER origin of LBs. In fact, LB are formed between the two leaflets of the ER membrane after the droplets of newly formed NL are enveloped by a monolayer of ER-derived phospholipids containing proteins that lack transmembrane domains [272, 273]. Altogether, these findings suggest that during L phase both wild-type and *pex5Δ* cells under CR conditions generate energy by glycolysis and store the NL, FFA and phospholipids by forming LBs. Using electron and fluorescent microscopies, Dr. Titorenko's laboratory showed that wild-type and *pex5Δ* cells under CR conditions substantially differ in the age-dependent abundance and morphological appearance of their mitochondria, ER and LBs (Figures 12.1 and 12.2). In order to establish the roles of ER- and LBs-associated proteins in the aging process, I used mass spectrometry-based proteomics to analyze the proteomes of ER and LBs purified from wild-type and *pex5Δ* cells grown under CR conditions.

12.2 Materials and methods

Reagents and solutions

1. TSD reduction buffer: 0.1 M Tris/Sulfate (pH 9.4), 10 mM DTT
2. HEPES lysis buffer: 20 mM HEPES/KOH, pH 6.8, 50 mM KCl, 200 mM sorbitol, 2 mM EDTA, 1 mM DTT
3. Spheroplast medium A (pH 7.5): 0.67% yeast nitrogen base (w/o) amino acids, 2 % (w/v) glucose, 1 M sorbitol, 20 mM Tris/HCl (pH 7.5)
4. Spheroplast medium B: 0.67% yeast nitrogen base (w/o) amino acids, 2 % (w/v) glucose, 1 M sorbitol
5. 1.2 M sucrose/ HEPES, 36% (w/w): 7.2 g sucrose + 12.8 ml HEPES lysis buffer
6. 1.5 M sucrose/ HEPES, 43%(w/w): 8.6 g sucrose + 11.4 ml HEPES lysis buffer
7. MES buffer 1 (MES breaking buffer): 10 mM MES/Tris (pH 6.9), 12 % (w/w) Ficoll 400, 0.2 mM EDTA
8. MES buffer 2: 10 mM MES/Tris (pH 6.9), 8 % (w/w) Ficoll 400, 0.2 mM EDTA
9. MES buffer 3: 10 mM MES/Tris (pH 6.9), 0.6 M sorbitol, 8 % (w/w) Ficoll 400, 0.2 mM EDTA
10. MES buffer 4: 10 mM MES/Tris (pH 6.9), 0.25 M sorbitol, 0.2 mM EDTA
11. KPi buffer (pH 7.4): 20 mM KH_2PO_4/KOH (pH 7.4), 1.2 M sorbitol

Purification of ER

Wild-type and *pex5Δ* mutant cells were grown in YEPD (0.2% glucose) medium. Cultures were harvested at mid-exponential and diauxic phases, checked for contamination by bright-field microscopy and used to measure cell density at OD_{600}. The

non-contaminated wild-type and mutant cells were pelleted at 4,000 x g for 5 min at room temperature. Cells were then resuspended at 10 OD_{600} units/ml in TSD reduction buffer, incubated for 10 min at room temperature, and centrifuged for 5 min at 4,000 x g at room temperature. Pelleted cells were then resuspended at 20 OD_{600} units/ml in Spheroplast medium A and supplemented with Zymolyase 100T at a concentration of 7.5 μg per OD_{600} units of cells. 10 μl of each cell suspension was then removed, diluted in 990 μl of dH_2O and used to measure the OD_{600}. The remaining cell suspensions were incubated at 30°C for 30 min and the efficiency of cell wall removal was monitored by measuring the OD_{600}. Cell wall digestion was allowed to proceed until the OD_{600} measurement of the diluted cell suspension became 5% of the original value, with the total digestion time not exceeding 1 hour. Spheroplasts were then harvested by centrifugation at 1,500 x g for 5 min at room temperature, followed by resuspending at 1 to 5 OD_{600} units/ml in Spheroplast medium B by gentle swirling of the tube or gentle stirring with a glass rod. Spheroplasts were then harvested by centrifugation at 1,500 x g for 5 min at 4°C and then resuspended at a concentration of 1,000 OD_{600} units/ml of ice-cold HEPES lysis buffer with freshly-added DTT. Spheroplasts were then homogenized using 20 strokes and resulting lysates were centrifuged at 1, 000 x g for 10 min at 4°C. The supernatants (S_{1000}) were subjected to another round of centrifugation at 1, 000 x g for 10 min at 4°C, and resulting supernatants were further centrifuged at 27,000 x g for 10 min at 4°C. The pelleted membranes ($P_{27,000}$) were resuspended in 1.0 ml of HEPES lysis buffer (5,000 OD_{600} equivalents per ml) using a trimmed 1-ml pipette tip and carefully layered on top of a sucrose gradient prepared in advance (2.1 ml of 1.5 M sucrose/HEPES solution was deposited to the bottom of a Beckman Ultra-Clear centrifuge tube for the Beckman MLS-

50 rotor, and then overlaid with 2.1 ml of 1.2 M sucrose/HEPES solution). The gradient tubes were then placed in the pre-chilled swinging bucket Beckman MLS-50 rotor and centrifuged at 100,000 x g (36,000 rpm) for 1 hr at 4°C using the slow acceleration and deceleration setting to minimize disruption of gradients. 18 gradient fractions of 227 µl each were then collected starting from the top of the sucrose gradient and stored at -20°C for further analyses.

Purification of lipid bodies

Wild-type and *pex5Δ* mutant cells were grown in YEPD (0.2% glucose) medium. Cultures were harvested at mid-exponential and diauxic phases, checked for contamination by bright-field microscopy and used to measure cell density at OD_{600}. The non-contaminated wild-type and mutant cells were pelleted at 4,000 x g for 5 min at room temperature. The cells were then washed once with distilled water and resuspended in the TSD reduction buffer at 10 x OD_{600} units/ml. Following a 10-min incubation at room temperature, the cells were pelleted by centrifugation at 4,000 x g for 5min at room temperature and then washed once in Spheroplasts medium A. The cells were then resuspended in Spheroplasts medium A at 20 x OD_{600} units/ml, supplemented with Zymolyase 100T at a concentration of 2.5 µg per OD_{600} units of cells, and incubated at 30°C for 45 min on a shaker set at 75 rpm. Spheroplasts were then pelleted by 5min centrifugation at 1,500 x g at room temperature, resuspended in the ice-cold Spheroplasts medium B at 5 x OD_{600} units/ml using pipettes with cut tips, and centrifuged for 5 min at 1,500 x g at 4°C. Spheroplasts were then washed twice by resuspending the pellets in ice-cold KPi buffer at a concentration of 5 OD_{600} units/ml followed by centrifugation for 5

min at 1,500 x g at 4°C. After the second wash and centrifugation step, clean spheroplasts were resuspended in ice-cold MES Buffer 1 at a concentration of 1,000 OD_{600} units/ml using pipettes with non-cut tips. Spheroplasts were then lysed in a homogenizer using 20 strokes at 4°C. Lysates were centrifuged for 5 min at 5,000 x g at 4°C and the resulting supernatants ($S_{5,000}$) were transferred to pre-chilled centrifuge tubes kept on ice. Lipid bodies were then purified by subjecting the spheroplast lysates to a series of flotation gradient centrifugations using a MLS 50 swinging bucket rotor (Beckman). The first flotation gradient was prepared by placing 2.5 ml of the $S_{5,000}$ fraction to the bottom of a centrifuge tube (Ultra-Clear Beckman tubes for MLS 50 rotor) and overlaying it with 2.5 ml of ice-cold MES Buffer 1. Following 1 hour centrifugation at 100,000 x g (36,000 rpm) at 4°C, the floating layer from the top portions of the gradients was collected with a cut tip and transferred to the bottom of a new centrifuge tube, which was then supplemented with MES buffer 2 to a total volume of 2.5 ml and gently mixed by pipetting. Resulting suspension was overlaid with 2.5 ml of ice-cold MES buffer 2 and then centrifuged for 1 hr at 100,000 x g (36,000 rpm) at 4°C. The floating layer from the top portions of the gradients was again collected with a cut tip and transferred to the bottom of a new centrifuge tube, which was then supplemented with MES buffer 3 to a total volume of 2.5 ml and gently mixed by pipetting. Resulting suspension was overlaid with 2.5 ml of ice-cold MES buffer 4 and then centrifuged for 1 hr at 100,000 x g (36,000 rpm) at 4°C. The floating layer from the top portions of the gradients was collected with a cut tip and purified lipid bodies were stored -20°C for further analyses.

Protein precipitation, SDS-PAGE and silver staining of gels

Protein concentration was determined using the RC DC protein assay kit (Bio-Rad) according to the manufacturer's instructions. Proteins were then precipitated using TCA as described previously (section "Materials and methods" in chapter 5.2) and resuspended in the SDS-PAGE sample buffer to a final concentration of 1 mg/ml. Proteins were then resolved on 7.5%, 10%, 12.5% or 16% SDS-PAGE gels as described previously (section "Materials and methods" in chapter 5.2). The Bio-Rad unstained molecular marker and a 0.1 mg/ml solution of BSA in the SDS-PAGE sample buffer were also subjected to SDS-PAGE. The proteins were then visualized by silver staining as described previously (section "Materials and methods" in chapter 5.2).

Protein identification by mass spectrometry

Selected protein bands were excised from a silver-stained gel and prepared for the mass-spectrometric peptide mapping as described previously (section "Materials and methods" in chapter 5.2). My modifications to the standard procedure included supplementing the excised protein bands with a band containing 2 μg of bovine serum albumin (BSA) protein, which was resolved in a different well of the same SDS-PAGE gel. Therefore, the samples were supplemented with double volumes (as compared to the standard volumes) of all reagents, including the trypsin buffer (100 μl/tube). Mass accuracy was further improved by performing the internal calibration of peptide mass spectra for each sample using two intense peptide masses from BSA (1479.8 and 1639.9) and one intense peptide mass from trypsin (1045.5). The proteins were identified by the Mascot peptide

mass fingerprinting method as described previously (see section "Materials and methods" in chapter 5.2).

Calculating the relative level of a protein of interest using BSA

For calculating the relative level of a protein of interest, the intensity of the monoisotopic peak of each peptide recovered from the band containing this protein was divided by the intensity of the monoisotopic peak of a BSA peptide with the monoisotopic mass closest to the mass of the peptide of interest. For evaluating relative levels of the protein of interest found in the samples to be compared, a ratio "the intensity of the monoisotopic peak of a peptide originated from the protein of interest/the intensity of the monoisotopic peak of a BSA peptide with the monoisotopic mass closest to the mass of the peptide of interest" was calculated for each peptide originated from the protein of interest. Based on these data, the average value for relative levels of the protein of interest found in the two compared samples was calculated. The method for evaluating relative levels of the protein of interest recovered in different samples was validated by calculating relative levels of several standard proteins in the samples supplemented with different quantities of each of these proteins.

12.3 Results

12.3.1 The *pex5Δ* mutation alters the levels of numerous ER proteins early in yeast life span

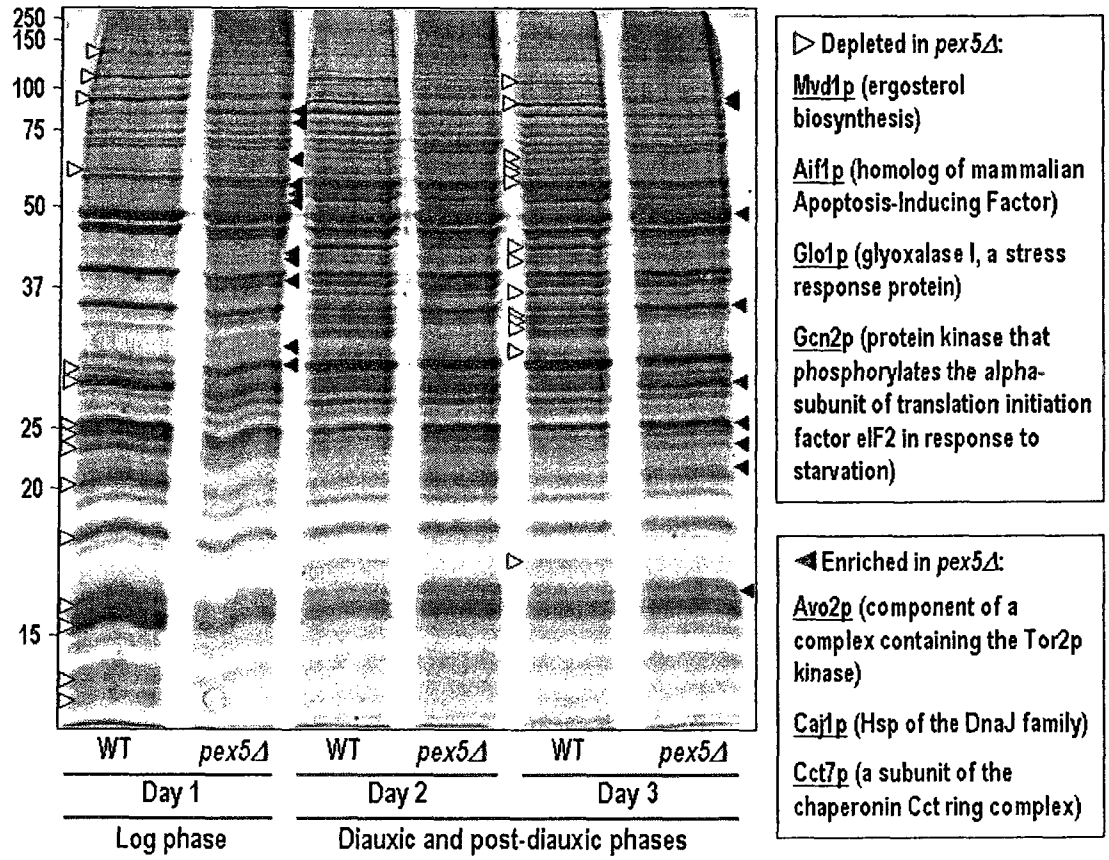

Figure 12.4. Silver-stained 12.5% SDS-PAGE gels of proteins recovered from the ER purified from wild-type and *pex5Δ* cells grown under CR conditions at 0.2% glucose.

12.3.2 The *pex5Δ* mutation alters the levels of numerous lipid body-associated proteins early in yeast life span

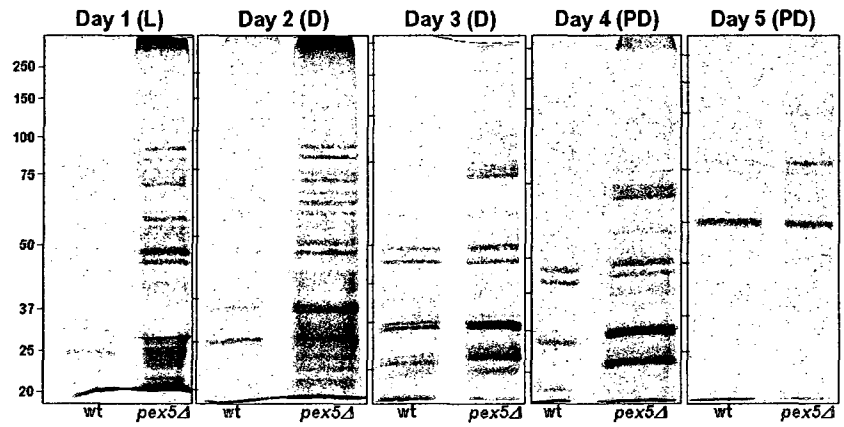

Figure 12.5. Silver-stained 12.5% SDS-PAGE gels of proteins recovered from lipid bodies purified from wild-type and *pex5Δ* cells grown under CR conditions at 0.2% glucose.

12.3.3 Early on in yeast life span, the *pex5Δ* mutation significantly elevates the levels of proteins involved in lipid biosynthesis and simultaneously decreases the levels of proteins that function in lipid degradation, ethanol metabolism and glycolysis

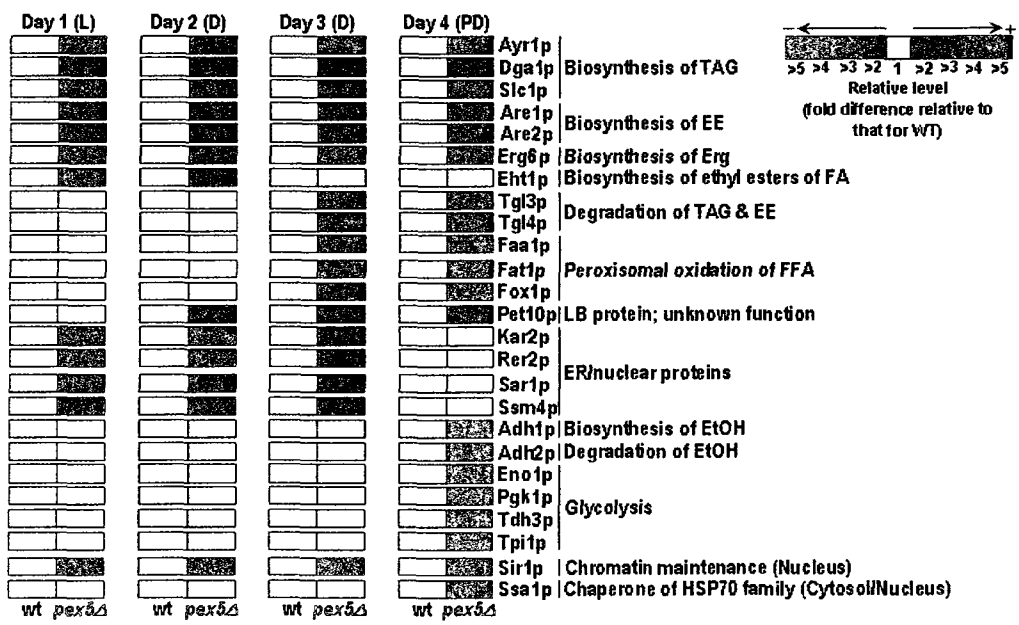

Figure 12.6. Relative levels of proteins identified in lipid bodies purified from wild-type and *pex5Δ* cells grown under CR conditions at 0.2% glucose.

12.4.4 Discussion

Using quantitative mass spectrometry, I compared the age-dependent dynamics of changes in the proteomes of ER and LBs purified from wild-type and prematurely aging *pex5Δ* cells. According to my proteomic data, the *pex5Δ* mutation altered the levels of numerous cytosolic, peroxisomal, ER and LB-associated proteins but only in aging cells that reached D and PD phases. In contrast, no significant differences were observed in the protein profiles of "young" wild-type and *pex5Δ* cells recovered from L phase (Figure 12.4). Proteomic analysis of the ER purified from chronologically aging wild-type and *pex5Δ* cells revealed that the *pex5Δ* mutation decreased the levels of a distinct group of proteins, including 1) Mvd1p, an enzyme involved in ergosterol biosynthesis; 2) Aif1p, a homolog of mammalian apoptosis-inducing factor; 3) Glo1p, a glyoxalase involved in stress response; and 4) Gcn2p protein kinase, which phosphorylates the α-subunit of eIF2 translation initiation factor in response to starvation (Figure 12.4). At the same time, the levels of some of the ER proteins were elevated in the short-lived *pex5Δ* mutant, including those of 1) Avo2p, a subunit of a complex containing Tor2p kinase; 2) Caj1p, a heat shock protein of the DnaJ family; and 3) Cct7p, a subunit of the chaperonin cct ring complex (Figure 12.4).

The data of my quantitative proteomic analysis suggest that the biogenesis of LBs in chronologically aging yeast progresses through several consecutive steps. Moreover, using this analysis, I was able to follow the age-related metabolic evolution of LBs during chronological aging. I found that throughout L, D and PD phases of life span, the *pex5Δ* mutation significantly elevated the levels of proteins involved in the biosynthesis of the neutral lipids TAG (Ayr1p, Dga1p, Slc1p) and EE (Are1p, Are2p), as well as the

levels of LB-associated proteins required for the biosynthesis of ergosterol (Erg6p) and ethyl esters of FFA (Eht1p). During L and D phases, the *pex5Δ* mutant also showed an increase in the levels of proteins composing the nuclear envelope and the ER, both of which are used as a template for LB formation. Some of these proteins are involved in the biosynthesis of ethyl esters of FA (Eht1p), while the others function in ER protein import and folding (Kar2p), ER protein sorting and dolichol synthesis (Rer2p), ER-to-Golgi protein transport (Sar1p) and ER protein catabolism (Ssm4p). During late D (day 3) and early PD (day 4) phases, the *pex5Δ* mutation also substantially decreased the levels of LB-bound proteins involved in the degradation of neutral lipids (Tgl3p and Tgl4p) and of peroxisomal proteins required for fatty acid oxidation (Faa1p, Fat1p and Fox1p). Faa1p, Fat1p and Fox1p have been shown to associate with distinct peroxisomal extensions known as pexopodia that penetrate LBs to promote the degradation of neutral lipids and to oxidize their FFA derivatives [274]. During early PD phase (day 4), the *pex5Δ* mutant strain showed a significant decrease in the levels of normally cytosolic proteins regulating glycolysis, especially those involved in the conversion of glyceraldehyde-3-phosphate to pyruvate (Eno1p, Pgk1p, Tdh3p and Tpi1p) as well as proteins involved in the metabolism of ethanol (Adh1p and Adh2p), a final product of glucose fermentation. Finally, during late D (day 3) and early PD (day 4) phases, the *pex5Δ* mutation considerably increased the levels of the LB-associated protein Pet10p of unknown function, the Sir1p protein required for chromatin maintenance in the nucleus, and the nuclear/cytosolic chaperone Ssa1p of the HSP70 protein family. In sum, my comparative proteomic analysis of LBs purified from wild-type and *pex5Δ* cells grown under CR conditions showed that several proteins were considerably elevated in LBs of *pex5Δ*

during L (day 1) and early PD (day 2) phases, whereas no significant differences in lipid body protein profiles were observed in wild-type and *pex5Δ* mutant during late D (day 3) and early PD (days 4 and 5) phases, although certain protein species were enriched or depleted in LBs purified from *pex5Δ*, as compared to those from wild-type cells (Figures 12.5 and 12.6).

Consistent with my proteomics data, studies in Dr. Titorenko's laboratory showed a similar dynamics of age-dependent consumption of TAG, EE, DAG and FFA in ER and LBs purified from wild-type and *pex5Δ* cells grown under CR conditions (Figure 12.7).

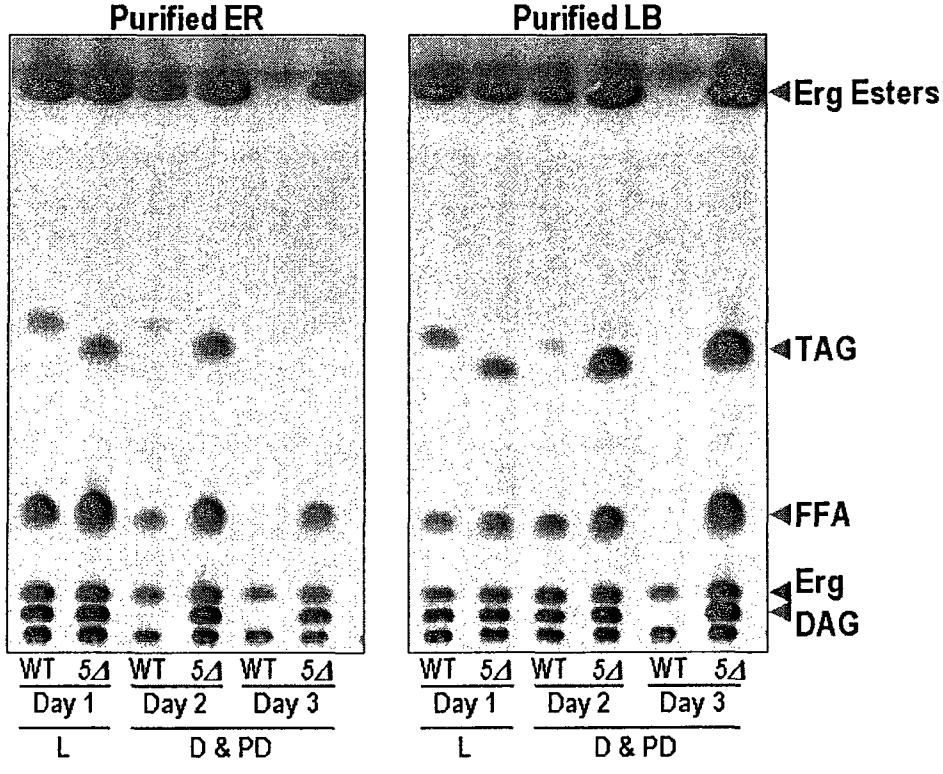

Figure 12.7. Lipid analysis by TLC revealed the age-dependent consumption of TAG, EE, DAG and FFA in the ER and lipid bodies purified from wild-type and *pex5Δ* cells grown under CR conditions.

12.5 Conclusions

My analysis of ER and LB proteomes, along with findings from Dr. Titorenko's laboratory on the effect of impaired degradation of storage lipids on longevity, provide evidence that peroxisomal compartmentalization of fatty acid oxidation is a crucial factor in regulating yeast longevity. Taken together, my proteomic analysis of the ER and LB purified from chronologically aging wild-type and *pex5Δ* cells and the data of functional and metabolomic analysis conducted in Dr. Titorenko's laboratory strongly suggest the following scenario for the biogenesis of LB during an early stage of the aging process. During e L phase, LB purified from both wild-type and *pex5Δ* cells are attached to their ER templates, which is consistent with my proteomics data showing that L-phase LBs contain several protein components of the nuclear envelope and ER (Figure 12.6). During early D phase (day 2), LBs of wild-type cells bud off from the ER, which would satisfactorily explain the association of these proteins with LBs (Figure 12.6). In contrast, LBs of the prematurely aging *pex5Δ* mutant strain remain associated with their ER template throughout the entire D phase (days 2 and 3), which is consistent with the proteomic data showing that substantial amounts of the ER and nuclear envelope proteins are still present in LBs purified from *pex5Δ* cells (Figure 12.6). It should be stressed that a significant deceleration of LB consumption observed in the *pex5Δ* mutant strain is supported by the results of my proteomic analysis, which revealed the elevated levels of proteins catalyzing neutral lipid biosynthesis and decreased levels of proteins catalyzing NL degradation in LBs of *pex5Δ* cells, as compared to those seen wild-type cells (Figures 12.6 and 12.7). As my proteomic analysis revealed, during late D phase (day 3) and early PD phase (day 4), LBs in wild-type cells contain considerable amounts of peroxisomal

enzymes catalyzing oxidation of fatty acids, whereas none of these peroxisomal enzymes was detected in LBs purified from *pex5Δ* cells (Figures 12.6). Of note, peroxisomal oxidation of NL-derived FFA in wild-type cells is known to coincide with the formation of distinct peroxisomal extensions known as pexopodia, which penetrate LBs in order to promote the lipolysis of neutral lipids and the oxidation of free fatty acids formed during this process [274]. However, no pexopodia formation was observed in the *pex5Δ* mutant strain [274]. Furthermore, my proteomic analysis revealed that LBs purified from wild-type cells recovered from early PD phase (day 4) contained enzymes involved in ethanol biosynthesis and degradation (Adh1p and Adh2p) along with a group of normally cytosolic proteins catalyzing several glycolytic reactions, especially those involved in the formation of pyruvate from glyceraldehyde-3-phosphate (Figure 12.6). Notably, these proteins normally function in the formation of acetyl-CoA, which is then transported into mitochondria to be used for ATP production. In contrast, no such proteins were detected in the LBs purified from *pex5Δ* mutant cells (Figure 12.6). These findings strongly suggest that the age-dependent association of all acetyl-CoA-generating enzymes with LBs of wild-type cells may considerably improve the efficiency of acetyl-CoA formation in LBs during FFA oxidation as well as facilitate the transport of acetyl-CoA from LBs to mitochondria.

Finally, my proteomic analysis of LBs purified from the short-lived *pex5Δ* mutant strain revealed a substantial increase in the levels of the following three proteins: 1) Pet10p, a protein of unknown function; 2) Sir1p, which is known to be involved in the maintenance of nuclear chromatin; and 3) the nuclear/cytosolic chaperone Ssa1p of the HSP70 protein family (Figure 12.6). It remains to be elucidated, what role, if any, the

association of these proteins with LBs plays in the longevity-related compartmentalization of lipid metabolism in the short-lived *pex5Δ* mutant strain.

13 A novel anti-aging molecule LA extends the chronological life span of the yeast *S. cerevisiae*

13.1 Introduction

Using a high-throughput assay for screening several combinatorial chemical libraries, Dr. Titorenko's laboratory in collaboration with Dr. David Thomas at McGill University has recently identified 22 compounds belonging to five chemically distinct groups that greatly extend the life span of the short-lived *pex5Δ* mutant strain under CR conditions (Figure 13.1).

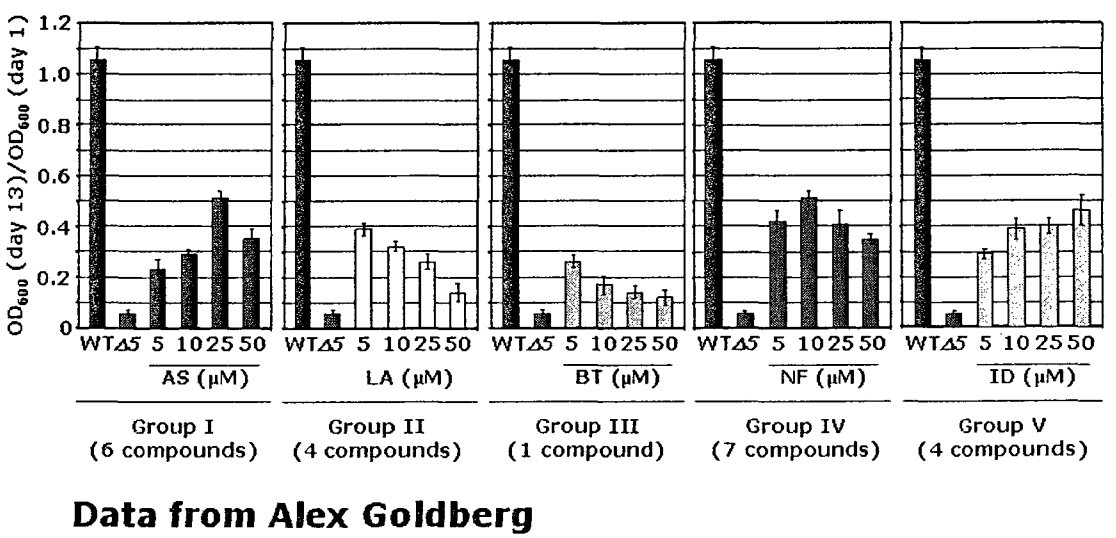

Figure 13.1. A high-throughput screening of several combinatorial chemical libraries for anti-aging small molecules revealed 22 novel compounds that cause a 6- to 10-fold extension of life span in the short-lived *pex5Δ* mutant of the yeast *S. cerevisiae* under CR conditions.

Of note, all of the anti-aging molecules identified by this assay are structurally different from another small anti-aging molecule, resveratrol, a constituent of red wine

that has been shown to extend the replicative life span of yeast and the chronological life spans of worms, flies and fishes through activation of the sirtuin family protein Sir2p [275-281]. Furthermore, the novel anti-aging compounds identified by Dr. Titorenko's laboratory are also structurally different from other molecules that, similar to resveratrol, delay aging and the onset of age-related diseases in rodent models by activating SIRT1 sirtuin protein [282-284]. It is conceivable therefore that the novel anti-aging compounds identified by Dr. Titorenko's laboratory extend the chronological life span of yeast by targeting the longevity-related cellular processes that are not modulated by resveratrol and/or other known sirtuin activators. To gain insight into these processes, Dr. Titorenko's laboratory focused on studying the molecular mechanisms underlying the anti-aging action of one of the compounds identified in the high-throughput screen. This compound, which is further referred to as 'LA', causes significant life span extension in both wild-type and *pex5Δ* mutant strains of the yeast *S. cerevisiae* grown under CR conditions at 0.2% glucose (Figure 13.2).

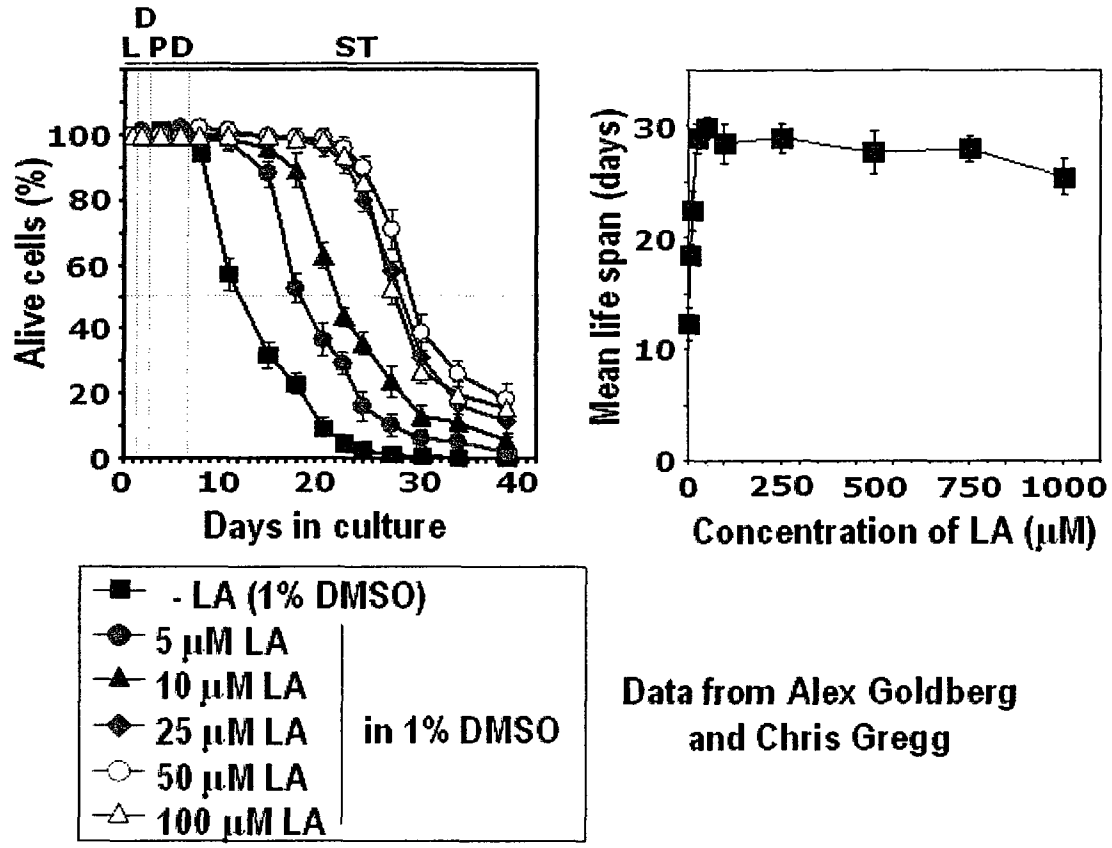

Figure 13.2. LA significantly extends the chronological life span of wild-type strain of the yeast *S. cerevisiae* grown under CR conditions.

In addition, a recent spot assay analysis conducted in Dr. Titorenko's laboratory using yeast cells exposed to exogenously added H_2O_2 demonstrated that LA increases the resistance of aging CR yeast to chronic oxidative stress (Figure 13.3).

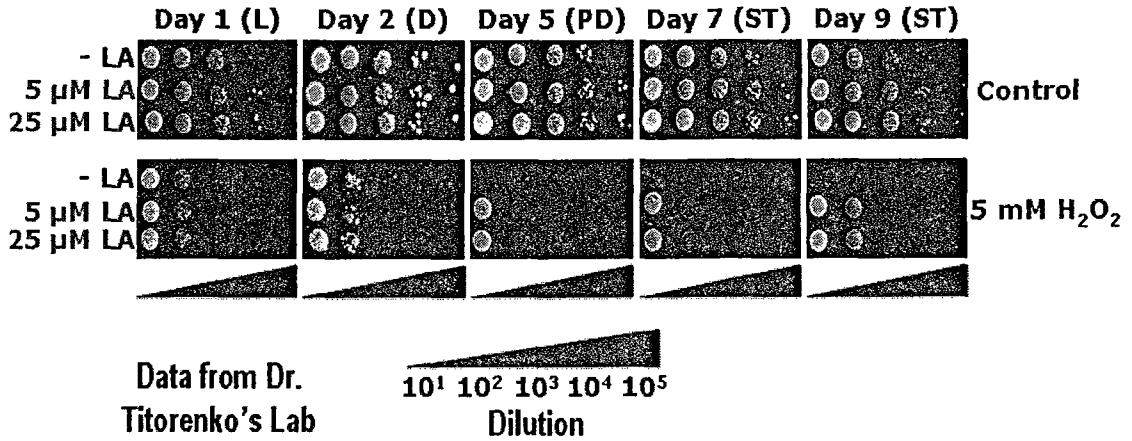

Figure 13.3. A spot assay analysis of yeast cells treated with H_2O_2 shows that LA increases the resistance of aging yeast to chronic oxidative stress.

To see if the beneficial effects of LA on yeast chronological life span results from a change in the steady-state levels of some key proteins involved in certain longevity regulation pathways, I used a mass spectrometry-based proteomic approach to identify proteins whose levels in yeast cells are altered in response to LA treatment and then to examine the age-dependent changes in their steady-state levels.

13.2 Materials and methods

Strains, media and growth conditions

The wild-type strain *Saccharomyces cerevisiae* BY4742 (*MATα his3Δ1 leu2Δ0 lys2Δ0 ura3Δ0*) was used in this experimental set-up. Contents of the YEPD (0.2% glucose) growth medium were as follows: 1% yeast extract, 2% peptone and 0.2% glucose. At the inoculation, yeast cultures were treated with either DMSO only, 25 μM 'LA' in DMSO or 50 μM 'LA' in DMSO.

Preparation of total cell lysates

Aliquots of yeast cells cultured in the presence or absence of LA were taken for proteomic analyses on days 1, 6, 10, 15 and 20. Total lysates of yeast cells were prepared as described in section 10.2 "Materials and methods".

Protein precipitation by TCA, SDS-PAGE and silver-staining

Proteins were precipitated from total cell lysates by the TCA method, resolved by SDS-PAGE and visualized by silver staining as described previously (section 5.2 "Materials and methods"). All modifications to the standard procedures of TCA precipitation and SDS-PAGE are described in section 10.2 "Materials and methods" of this thesis.

Protein identification and quantitation by mass spectrometry

Protein bands whose intensities differed from that in total lysates of CR yeast exposed to 25 or 50 μM LA, as compared to those of the untreated CR yeast, were excised from the gel and subjected to mass spectrometry-based protein identification and quantitation as described previously (see sections 5.2 and 10.2, "Materials and methods"). All modifications to the standard procedures of protein identification and quantitation by mass spectrometry are described in section 10.2 "Materials and methods" of this thesis.

13.3 Results

13.3.1 LA alters the levels of a limited group of proteins throughout yeast life span

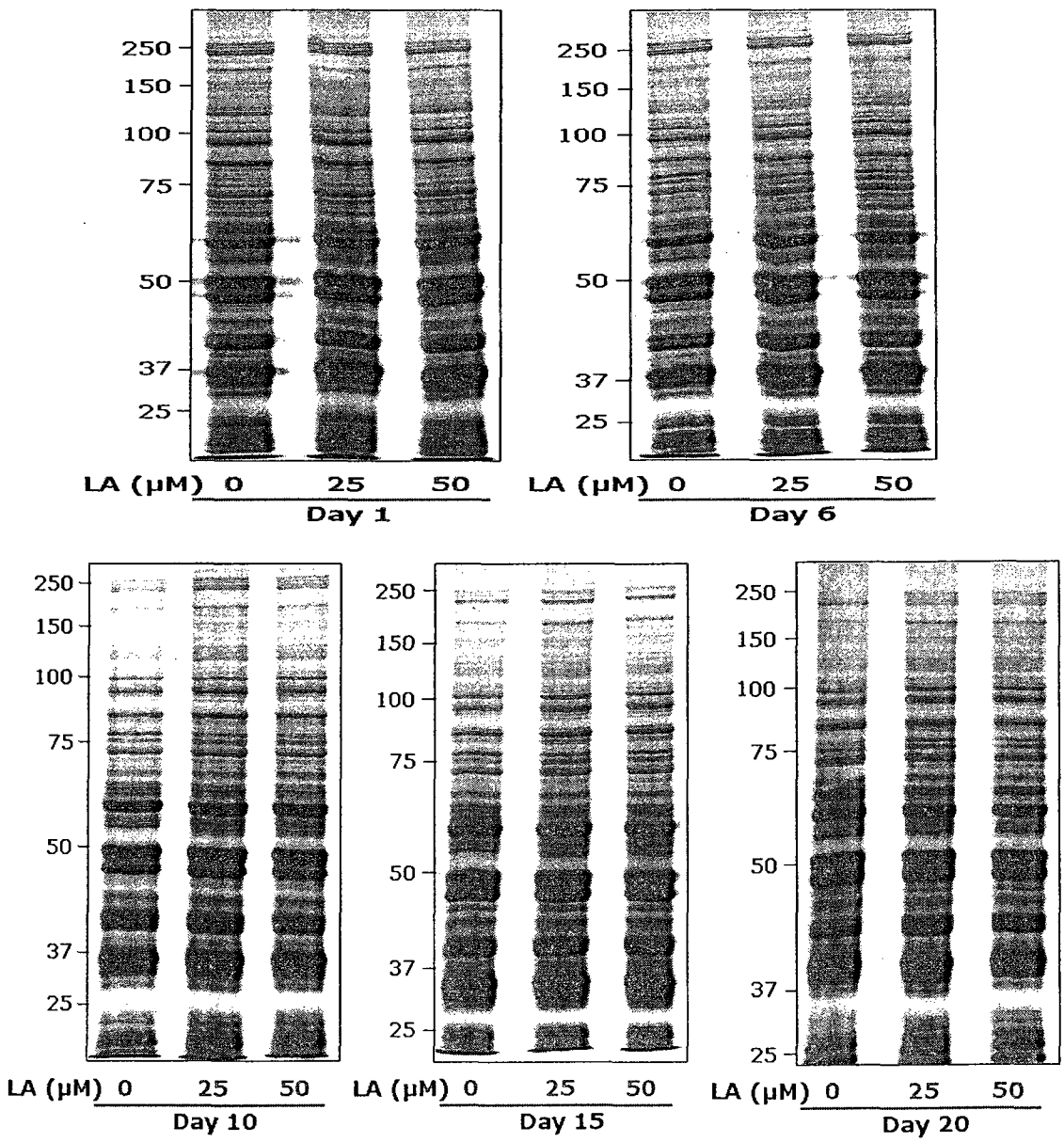

Figure 13.4. Silver-stained SDS-PAGE gels showing protein profiles of total lysates of yeast cells cultured in the presence or absence of LA taken at L (Day 1), PD (Day 6) or stationary (Days 10, 15 and 20) phase.

13.3.2 In aging CR yeast, LA increases the levels of proteins involved in stress response, detoxification of ROS, glycogen degradation, biosynthesis of neutral lipids, glycolysis, biosynthesis of acetyl-CoA, mitochondrial PDH complex, TCA cycle and mitochondrial synthesis of ATP; at the same time, LA decreases the levels of proteins operating in glyoxylate cycle, degradation of neutral lipids, mitochondrial division, and proteins with currently unknown functions

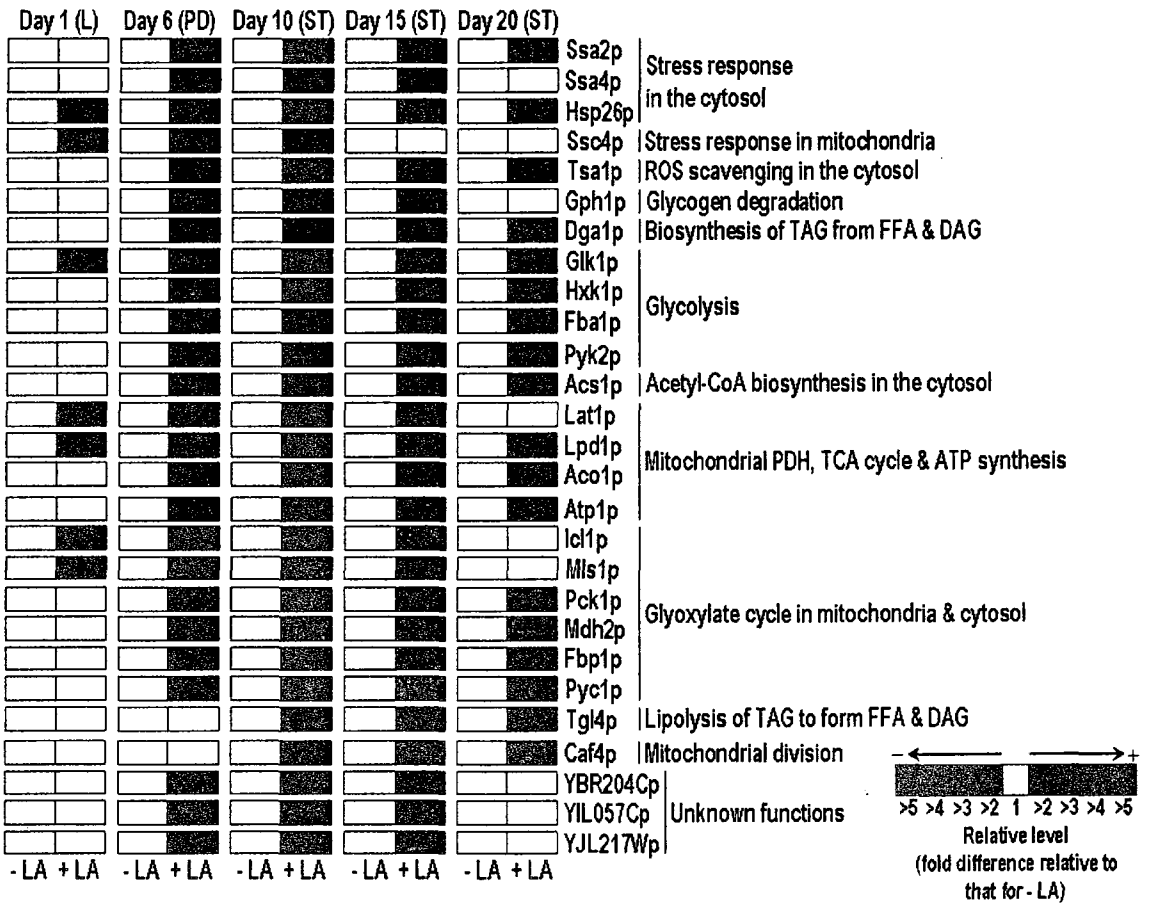

Figure 13.5. Dynamics of age-dependent changes in the levels of proteins recovered in total lysates of yeast cells cultured in the presence or absence of LA.

13.3.3 LA causes a significant increase in the levels of the chaperone protein Ssa2p, which mediates stress response in the cytosol

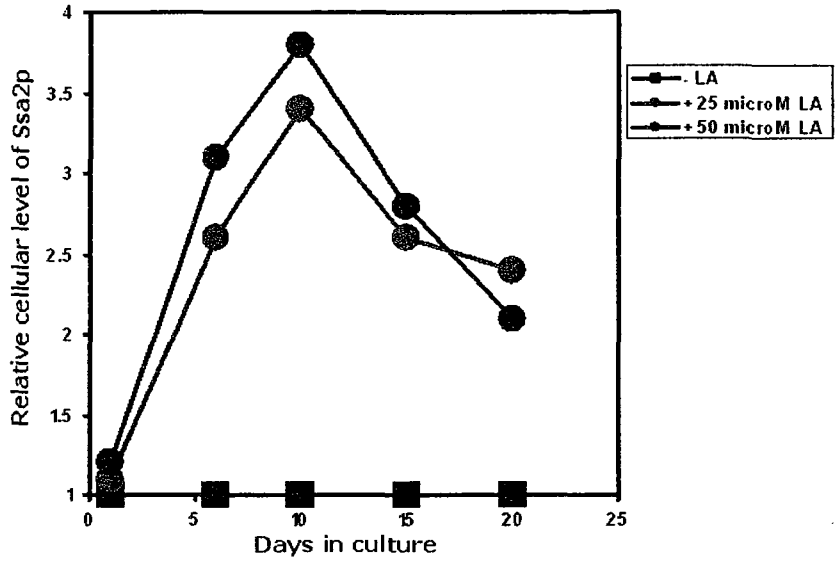

Figure 13.6. Dynamics of age-dependent changes in the steady-state levels of Ssa2p in LA-treated and untreated wild-type yeast cells grown under CR conditions.

13.3.4 LA causes a significant increase in the levels of the chaperone protein Ssa4p, which mediates stress response in the cytosol

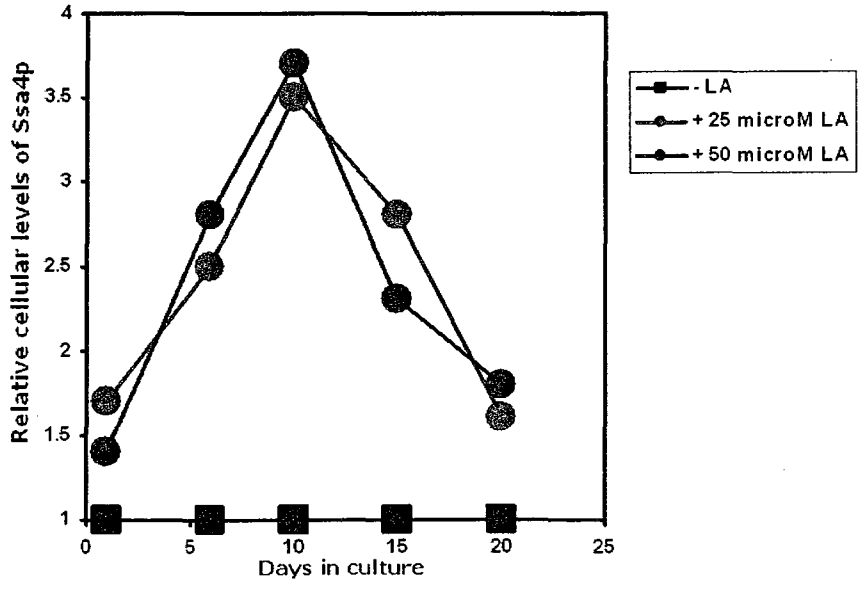

Figure 13.7. Dynamics of age-dependent changes in the steady-state levels of Ssa4p in LA-treated and untreated wild-type yeast cells grown under CR conditions.

13.3.5 LA causes a significant increase in the levels of the chaperone protein Hsp26p, which mediates stress response in the cytosol

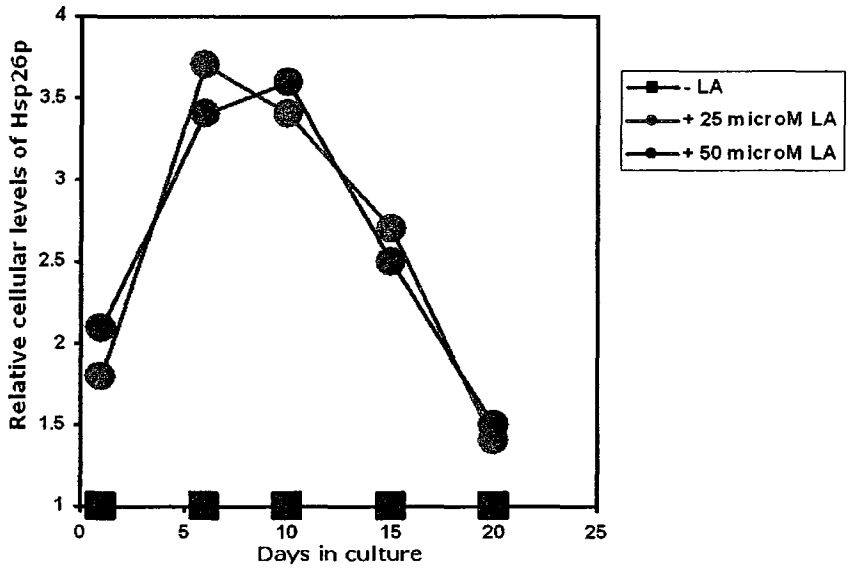

Figure 13.8. Dynamics of age-dependent changes in the steady-state levels of Hsp26p in LA-treated and untreated wild-type yeast cells grown under CR conditions.

13.3.6 LA causes a significant increase in the levels of the ROS scavenger protein Tsa1p, which detoxifies ROS in the cytosol

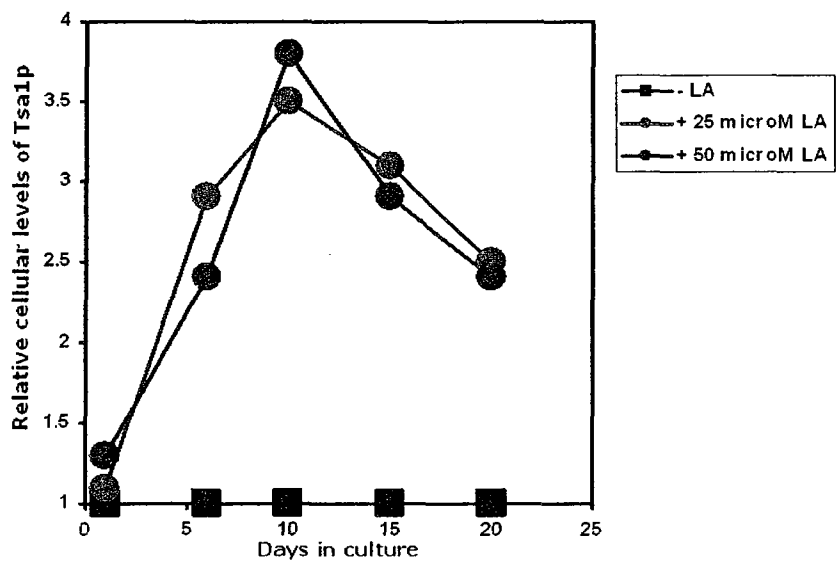

Figure 13.9. Dynamics of age-dependent changes in the steady-state levels of Tsa1p in LA-treated and untreated wild-type yeast cells grown under CR conditions.

13.3.7 LA causes a significant increase in the levels of the chaperone protein Ssc1p, which mediates stress response in mitochondria

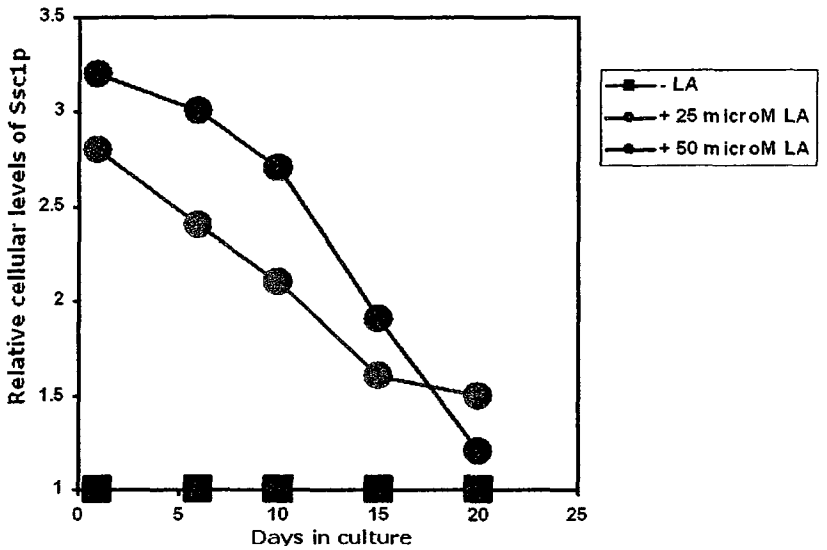

Figure 13.10. Dynamics of age-dependent changes in the steady-state levels of Ssc1p in LA-treated and untreated wild-type yeast cells grown under CR conditions.

13.4 Discussion

According to my proteomic data, the exposure of the yeast *S. cerevisiae* to La under CR conditions led to a significant increase in the steady-state levels of several molecular chaperone proteins, such as Ssa2p, Ssa4p, Ssc1p and Hsp26p, as well as proteins that protect cellular components from oxidative damage, such as Tsa1p (Figures 13.6, 13.7, 13.8, 13.9, and 13.10). The Ssa2p and Ssa4p proteins belong to the HSP70 subfamily of cytosolic chaperones that bind newly-translated proteins and assist in their proper folding, as well as prevent the aggregation of oxidatively or otherwise damaged proteins in the cytosol [285-288]. Of note, Ssa4p also protects yeast cells expressing human α-synuclein, a protein responsible for amyloid fiber formation in Parkinson's, from undergoing apoptosis [289]. Hsp26p is another cytosolic chaperone that belongs to the small heat shock protein family of molecular chaperones and, similar to Ssa2p and Ssa4p, also binds

damaged proteins and prevents their aggregation in the cytosol [290, 291]. According to my proteomic data, the steady-state level of Ssa2p substantially increased in LA-treated yeast cells by Day 6, which corresponds to the end of PD growth phase and an entry point into stationary phase, when the cell senescence process begins (Figures 13.5 and 13.6). The level of Ssa2p continued to elevate during stationary phase of in LA-treated yeast cells, reaching a maximum by day 10, at which point it began to decrease gradually, but yet remained high in comparison to that seen in untreated cells (Figures 13.5 and 13.6). The steady-state levels of Ssa4p and Hsp26p had undergone very similar age-dependent changes in LA-treated yeast cells (Figures 13.5, 13.7 and 13.8). Based on these findings and the fact that Ssa2p, Ssa4p and Hsp26p participate in the protein folding and stress response, it seems likely that the anti-aging effect of LA is partly due to its ability to increase the levels of these cytosolic chaperones, thus preventing the aggregation of damaged proteins, which accumulate in aging yeast due the progressive build-up of ROS. This hypothesis is indirectly supported by recent findings from Dr. Titorenko's laboratory, which showed that LA increased the resistance of yeast cells to chronic oxidative stress imposed by their long-term exposure to hydrogen peroxide (Figure 13.3). It should be stressed that my proteomic data support this hypothesis further by demonstrating that LA significantly elevates the steady-state level of Tsa1p in aging yeast (Figures 13.5 and 13.9). Tsa1p is a thioredoxin peroxidase that, under conditions of oxidative stress, can act as a potent ribosome-associated or cytosolic antioxidant by forming a high-molecular weight chaperone complex from association with its own proteins [292-294]. Similar to the levels of Ssa2p, Ssa4p and Hsp26p, the level of Tsa1p also significantly increased in LA-treated yeast cells by day 6, when yeast cells entered

stationary phase and became senescent (Figures 13.5 and 13.9). After Tsa1p levels peaked at day 10, they began to decline in LA-treated senescent yeast cells, while still remaining higher than those seen in untreated cells (Figures 13.5 and 13.9).

My proteomic data also demonstrate that LA significantly increases the steady-state levels of Ssc1p in aging yeast (Figures 13.5 and 13.10). Ssc1p is a mitochondrial chaperone protein of the HSP70 family that, in addition to being involved in proper protein folding and preventing aggregation of damaged proteins in the mitochondria, also facilitates the import of proteins into the mitochondrion and further assists in their folding process [286, 287, 294-296]. Of note, age-dependent dynamics of changes in the level of Ssc1p in LA-treated yeast cells differed from that observed for Ssa2p, Ssa4p, Hsp26p and Tsa1p. In fact, the level of Ssc1p in LA-treated yeast reached its maximum at the L and PD growth phases and then significantly decreased as yeast entered stationary phase and became senescent (Figures 13.5, 13.6, 13.7, 13.8 and 13.9). Taken together, the knowledge of the mitochondria-related functions of Ssc1p and the observed pattern of age-dependent changes in its steady state levels induced by LA (Figures 13.5 and 13.10), suggest that the longevity-promoting properties of LA are partially due to its ability to increase the levels of Ssc1p, which would have a beneficial effect on longevity as a result of: 1) Ssc1p acting to prevent the aggregation of damaged proteins that accumulate in the mitochondria due to a dramatic increase in the amount of mitochondrial production of ROS observed in aging CR yeast, and 2) Ssc1p assisting mitochondria in maintaining its oxidation-reduction processes that, according to recent experimental evidence from Dr. Titorenko's laboratory, are required for the anti-aging effect of LA.

My quantitative proteomic analysis also revealed that, in addition to significantly amplifying the response, LA remodeled carbohydrate metabolism in yeast by increasing the levels of proteins involved in glycogen degradation (Gph1p), glycolysis (Glk1p, Hxk1p, Fba1p and Pyk2p) and biosynthesis of Acetyl-CoA in the cytosol (Acs1p) (Figure 13.5), as well as by decreasing the levels of proteins involved in the glyoxylate cycle in the mitochondrion and cytosol (Icl1p, Mls1p, Pck1p, Mdh2p, Fbp1p and Pyc1p). Furthermore, LA remodeled lipid metabolism of chronologically aging yeast by elevating the level of Dga1p protein that catalyzes the biosynthesis of TAG and by decreasing the level of Tgl4p protein that catalyzes TAG breakdown (Figure 13.5). LA also significantly increased mitochondrial activity by elevating the levels of several mitochondrial proteins functioning in the PDH complex (Lat1p, Lpd1p), TCA cycle (Aco1p) and ATP synthesis (Atp1p). Moreover, LA altered mitochondrial morphology by decreasing the levels of Caf4p protein involved in mitochondrial division (Figure 13.5).

Of note, recent data from Dr. Titorenko's laboratory provided evidence that in "young", non-treated yeast cells grown under CR conditions, there is an intense spike in the level of mitochondrially produced ROS (Figure 13.11). The level of ROS then progressively declines throughout yeast life span (Figure 13.11). In fact, the levels of ROS observed in yeast cells that have not been exposed to LA and reached D phase are high enough to inflict a significant oxidative damage to their mitochondrial macromolecules. At the same time, considerably lowered levels of ROS during later

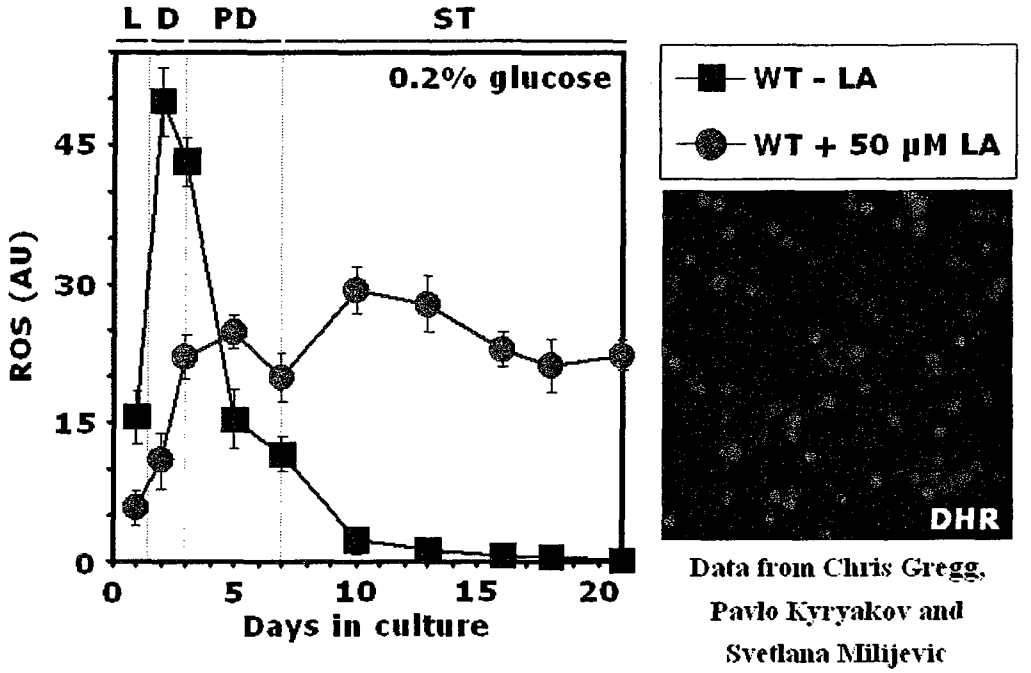

Figure 13.11. LA decreases the amplitude of the spike in ROS early (L and PD phases) and prevents the sharp decline in ROS levels during stationary phase, maintaining it at a steady-state level.

stages of the life span of these yeast are insufficient for the activation of the stress response, anti-aging pathways in chronologically aging CR yeast. In contrast, the treatment of yeast cells with LA significantly reduces the initial spike in ROS levels, thereby preventing the excessive oxidative damage to mitochondrial macromolecules (Figure 13.11). Moreover, LA appears to enable aging yeast cells to maintain their ROS production at an optimal level that prevents the excessive oxidative damage, while simultaneously activating their stress response. In fact, recent data from Dr. Titorenko's laboratory showed that LA-treated cells had similar patterns of age-dependent changes in their oxygen consumption and mitochondrial membrane potential (Figures 13.12 and 13.13).

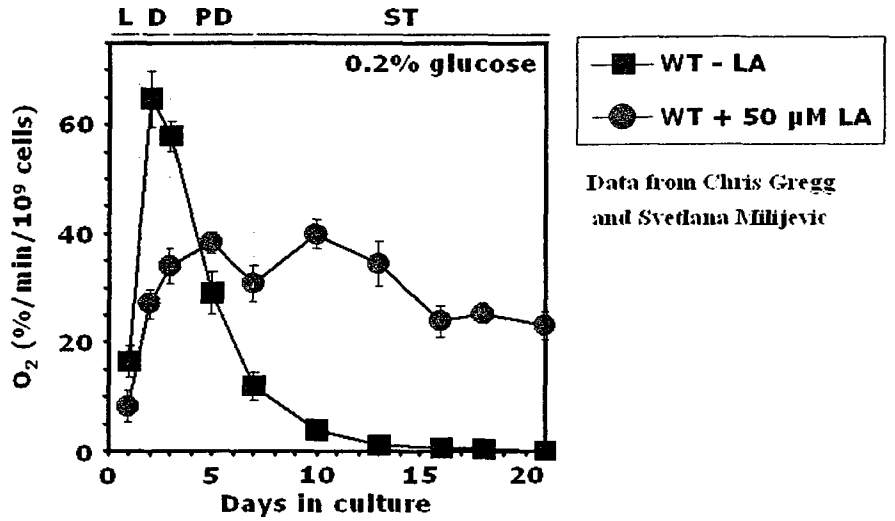

Figure 13.12. LA decreases the amplitude of the spike in O_2 consumption early (L and PD phases), and prevents the sharp decline in O_2 consumption later in stationary (ST) phase, maintaining it at a steady-state level.

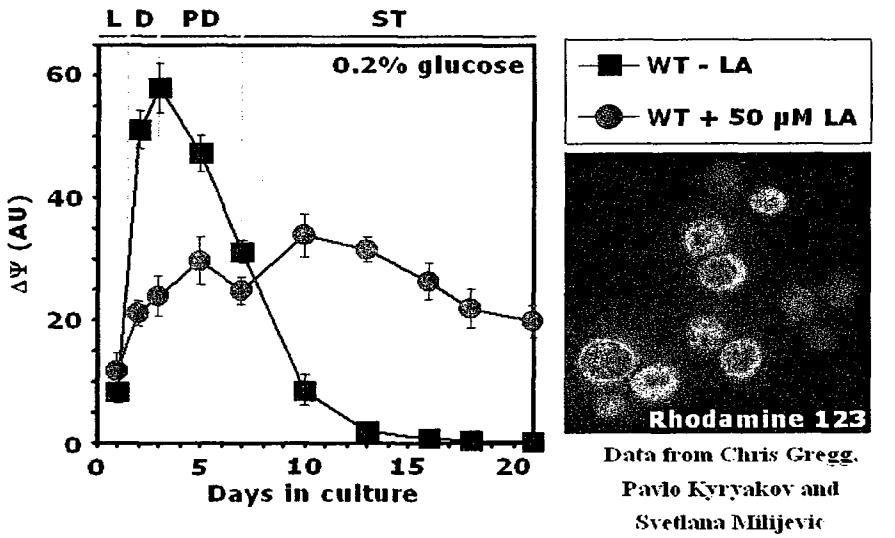

Figure 13.13. LA decreases the amplitude of the spike in the mitochondrial membrane potential (ΨΔ) early (L and PD phase), and prevents the sharp decline in ΨΔ later in stationary (ST) phase, maintaining it at a steady-state level.

Taken together, my proteomic analysis of the LA-induced, age-dependent changes in the steady-state levels of proteins and recent findings from Dr. Titorenko's laboratory strongly suggest the following model of lifespan extension by LA (Figure 13.14).

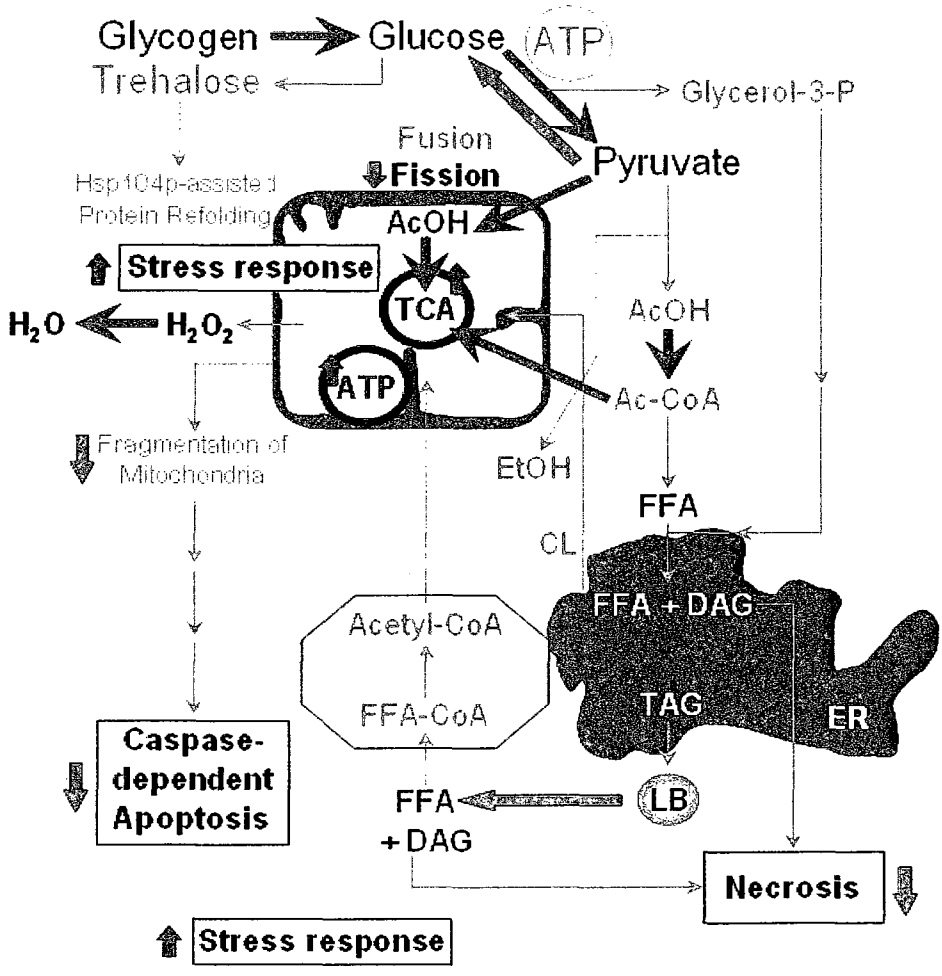

Figure 13.14. A model for life span extension due to a specific remodeling of various cellular processes by LA (red arrows represent processes accelerated by LA, while green arrows show processes that are decelerated by LA).

In this model, LA promotes the conversion of glycogen-derived glucose into pyruvate, which then enters mitochondria and is used by the PDH complex as a substrate to enter the TCA cycle, thereby boosting the synthesis of ATP in mitochondria. As a result, certain optimal levels of ROS are generated in mitochondria. These levels of ROS do not exceed the cytotoxic threshold but are sufficient to activate the stress response, anti-aging pathways without causing the excessive damage to mitochondrial macromolecules. At the same time, the sustained activity of mitochondria decreases

mitochondrial fragmentation, thereby delaying mitochondria-controlled apoptosis. Furthermore, by decreasing the lipolysis of neutral lipids deposited in LBs, LA lowers the levels of intracellular DAG, thereby down-regulating the DAG-dependent activation of necrotic cell death. These findings strongly suggest that the level of ROS generated in mitochondria appears is the major determinant of the rate of chronological aging in CR yeast. An optimal level of ROS that is sustained throughout the life span of yeast exposed to LA activates a variety of cellular repair and damage control pathways, which helps to maintain cellular fitness and, thus, to extend life span.

13.5 Conclusions

Altogether, my proteomic analysis of age-dependent changes in the steady-state levels of proteins in yeast treated with a novel anti-aging molecule LA strongly suggest that the beneficial effect of LA on longevity may be partly due to its ability to increase the levels of a distinct group of proteins (such as Ssa2p, Ssa4p, Ssc1p, Hsp26p and Tsa1p), which are involved in stress response and protection against oxidative damage. Therefore, by increasing the steady-state levels of these proteins in an age-dependent fashion, LA can extend yeast life span, in part, by helping to prevent the aggregation of oxidatively damaged proteins that accumulate in the cytosol and mitochondria of aging yeast due to the progressive build-up of ROS. In addition to attenuating the stress response, LA remodels carbohydrate metabolism in CR yeast by increasing glycogen degradation, glycolysis and biosynthesis of acetyl-CoA in the cytosol, while simultaneously decreasing the activity of the glyoxylate cycle in the mitochondrion and cytosol. Furthermore, LA remodels yeast lipid metabolism by promoting the biosynthesis of

neutral lipid TAG and preventing its breakdown to DAG and FFA, thereby significantly delaying DAG-activated necrotic cell death. The most profound effect of LA, however, is on the mitochondrial function and morphology. In fact, LA significantly increases activities of the mitochondrial PDH complex, TCA cycle and synthesis of ATP, while decreasing the rate of mitochondrial fission. As a result of increased ATP production in mitochondria, higher levels of ROS (which are maintained at a threshold, non-cytotoxic level) activate the stress response, anti-aging pathways. In fact, LA maintains the mitochondrial production of ROS at a level that is not sufficient to cause a significant oxidative damage to mitochondrial macromolecules but is sufficiently high to induce a potent stress response. Finally, sustained mitochondrial activity in yeast exposed to LA and the observed LA-induced decrease in mitochondrial division help to maintain the mitochondrial network, thereby delaying the mitochondria-controlled, age-dependent cell form of cell death. Taken together, these findings strongly suggest that the LA-induced life span extension in yeast is primarily a result of the effect of LA on mitochondrial ROS production, mitochondrial morphology and mitochondrially-induced apoptosis.

14 Aging mechanisms: summary and suggestions for future work

14.1 CR extends yeast life span by remodeling a distinct set of the key cellular processes

My quantitative proteomic analysis, along with the data of metabolomic and functional analyses from Dr. Titorenko's laboratory, implies that during L and D phases, "young" non-CR yeast meet their metabolic requirement by producing the bulk of ATP through glycolysis. In contrast, "young" CR yeast remodel their carbohydrate metabolism by shifting from glycolysis to gluconeogenesis, thereby producing the majority of their ATP

through mitochondrial oxidation of acetyl-CoA (Figure 14.1).

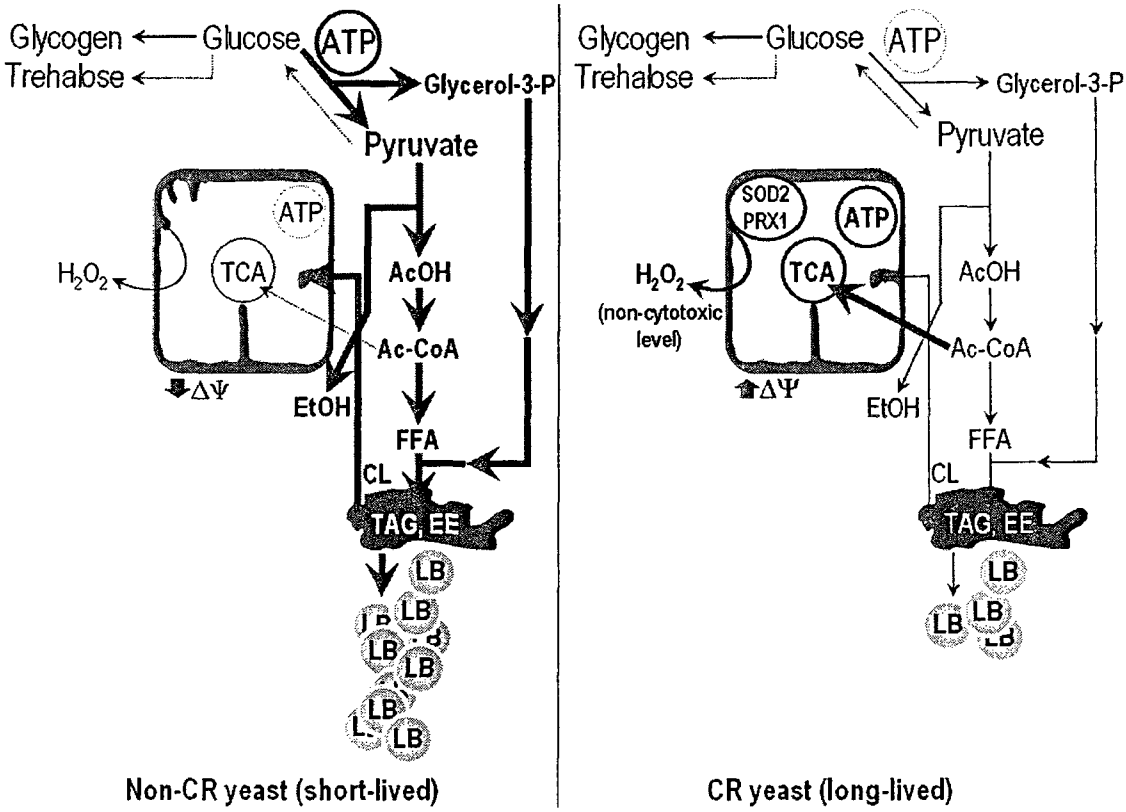

Figure 14.1. CR remodels carbohydrate and lipid metabolism early in the life span of chronologically aging yeast.

Considerable quantities of mitochondrial ROS generated during ATP production in CR yeast are then decomposed through the antioxidant reactions catalyzed by superoxide dismutase Sod2p and peroxiredoxin Prx1p, whose activities are promoted by the CR diet. In addition, the CR diet greatly accelerates the depletion of ethanol from yeast cells by altering the levels of enzymes involved in ethanol biosynthesis and degradation, thus greatly reducing the negative effect of ethanol on longevity. In contrast, no increase in the mitochondrial activity is observed in young non-CR yeast that synthesize ATP primarily via glycolysis, thereby generating substantial amounts of ethanol and actively

synthesizing neutral lipids that are deposited in LBs (Figure 14.1). The lowered mitochondrial activity in non-CR yeast decreases the mitochondrial membrane potential, eventually (*i.e.*, later in the aging process) causing the fragmentation of the mitochondrial network due to increased mitochondrial fission (Figure 14.2).

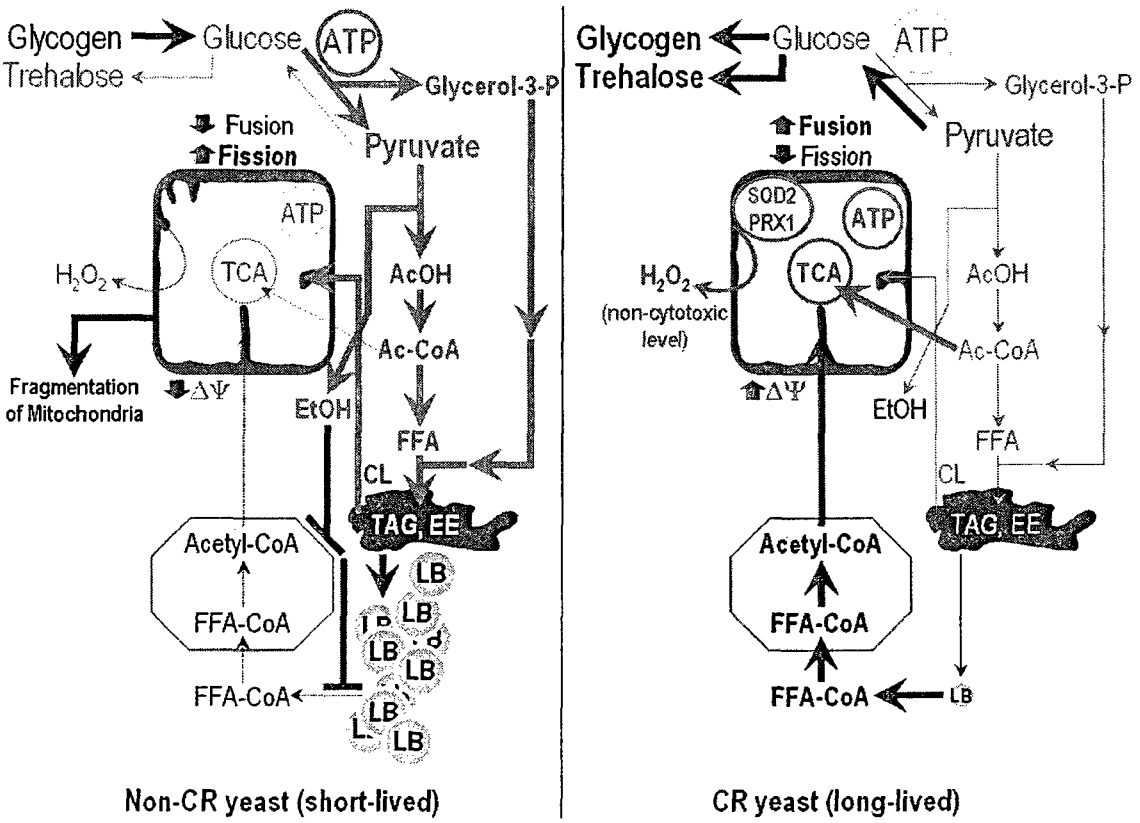

Figure 14.2. A CR-induced remodeling of cellular processes continues during PD growth phase in a diet-dependent fashion.

During PD phase, CR promotes the accumulation of glycogen and trehalose, two major glucose storage compounds, by activating the synthesis of enzymes catalyzing their biosynthesis and suppressing the synthesis of enzymes required for their degradation (Figure 14.2). In addition, CR remodels yeast lipid metabolism by accelerating the lipolytic consumption of LB-deposited neutral lipids TAG and EE (Figure 14.2). The

substantial amounts of FFA generated by such lipolytic degradation of neutral lipids are rapidly converted to FA-CoA. FA-CoA is first imported into peroxisomes and then converted to acetyl-CoA via the peroxisomal β-oxidation pathway (whose activity is also greatly accelerated by the CR diet) and then transported into mitochondria to be used for ATP synthesis (Figure 14.2). The elevated mitochondrial activity in chronologically aging CR yeast promotes mitochondrial fusion, thereby preventing the fragmentation of mitochondrial network observed in non-CR yeast (Figure 14.2). In contrast, chronologically aging yeast grown under non-CR conditions are unable to consume their neutral lipids deposited in LBs due to the inhibition of the peroxisomal β-oxidation pathway by ethanol, which results in the build-up of TAG in their LBs and also decelerate the exit of TAG from the ER (Figure 14.2). The accumulation of TAG in the ER of non-CR yeast, in turn, slows down its biosynthesis from FFA-CoA and DAG, leading to the build-up of DAG within the ER and thereby promoting necrotic cell death (Figure 14.3). As a result of being unable to delay the mitochondria-controlled apoptosis promoted by mitochondrial fragmentation and due to the accelerated cell death by necrosis resulting from the accumulation of DAG and FFA, chronologically aging non-CR yeast die faster then their CR counterparts (Figure 14.3).

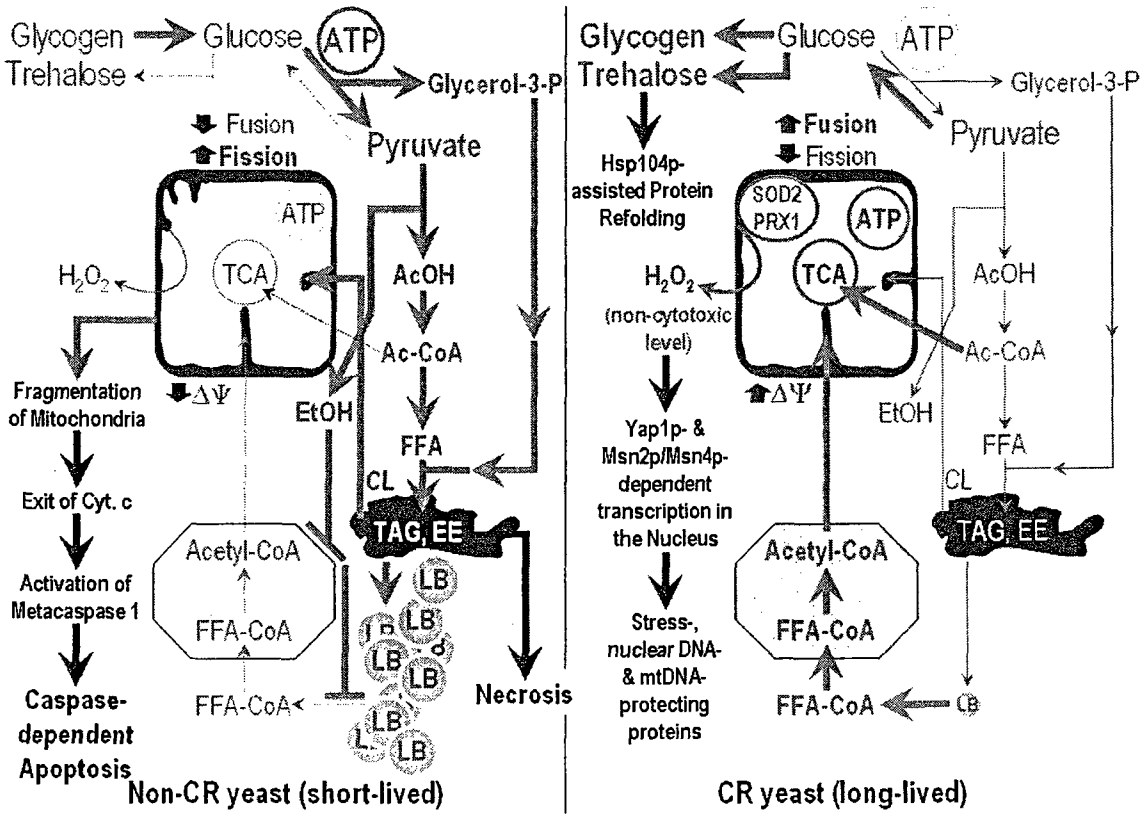

Figure 14.3. CR extends yeast life span by enhancing stress response and preventing the activation of both mitochondria-controlled apoptosis and necrotic cell death.

The early metabolic remodeling allows aging CR yeast to enjoy their "retirement" in the stationary phase by increasing their stress response, promoting the chaperone activity of trehalose in protein folding, and elevating the levels of ROS-scavenging enzymes as well as proteins helping to repair and protect mtDNA from oxidative damage (Figure 14.3).

14.2 Modular longevity network and its remodeling in CR yeast

My quantitative proteomic analysis, along with the data of metabolomic and functional analyses from Dr. Titorenko's laboratory, suggest that the rate of aging in yeast is controlled by what we call a "modular longevity network", which is established in a diet-

and genotype-specific fashion and undergoes remodeling throughout the aging process. Furthermore, the analysis of the spatiotemporal dynamics of the modular longevity network revealed that it integrates several processes and metabolic pathways, which we call "modules" and which regulate 1) trehalose and glycogen metabolism; 2) glycolysis, glucose fermentation to ethanol, and gluconeogenesis; 3) lipid metabolism in the ER, LBs and peroxisomes; 4) interorganellar metabolic flow; 5) oxidation-reduction reactions in mitochondria; 6) maintenance of ROS homeostasis; 7) protection of mtDNA from oxidative damage; 8) maintenance of a tubular mitochondrial network; and 9) mitochondria-controlled apoptosis (Figure 14.4). Based on my findings and on the extensive functional and metabolomic studies conducted in Dr. Titorenko's laboratory on how the individual modules of the network influence yeast life span, I propose a model for the integration of various key cellular processes into a modular longevity network and for the spatiotemporal dynamics of this network in chronologically aging yeast (Figure 14.5). In this model, before entering a non-proliferative state, yeast design a diet- and genotype-specific configuration of the network by establishing the rates of the processes taking place within each of its individual modules. Different configurations of the network established prior to entry into a non-proliferative state set different aging rates following such entry. Thus, by designing a specific configuration of the modular longevity network prior to reproductive maturation, yeast define their chronological life span. Taken together, my findings and data from Dr. Titorenko's laboratory provide evidence that yeast establish a diet- and genotype-specific configuration of the longevity network by setting up the rates of the processes within each of its modules prior to entry into non-proliferative stage. Furthermore, my model predicts that different configurations

of this network established early in yeast life result in different rates of chronological aging upon entry of yeast cells into a non-proliferative stage.

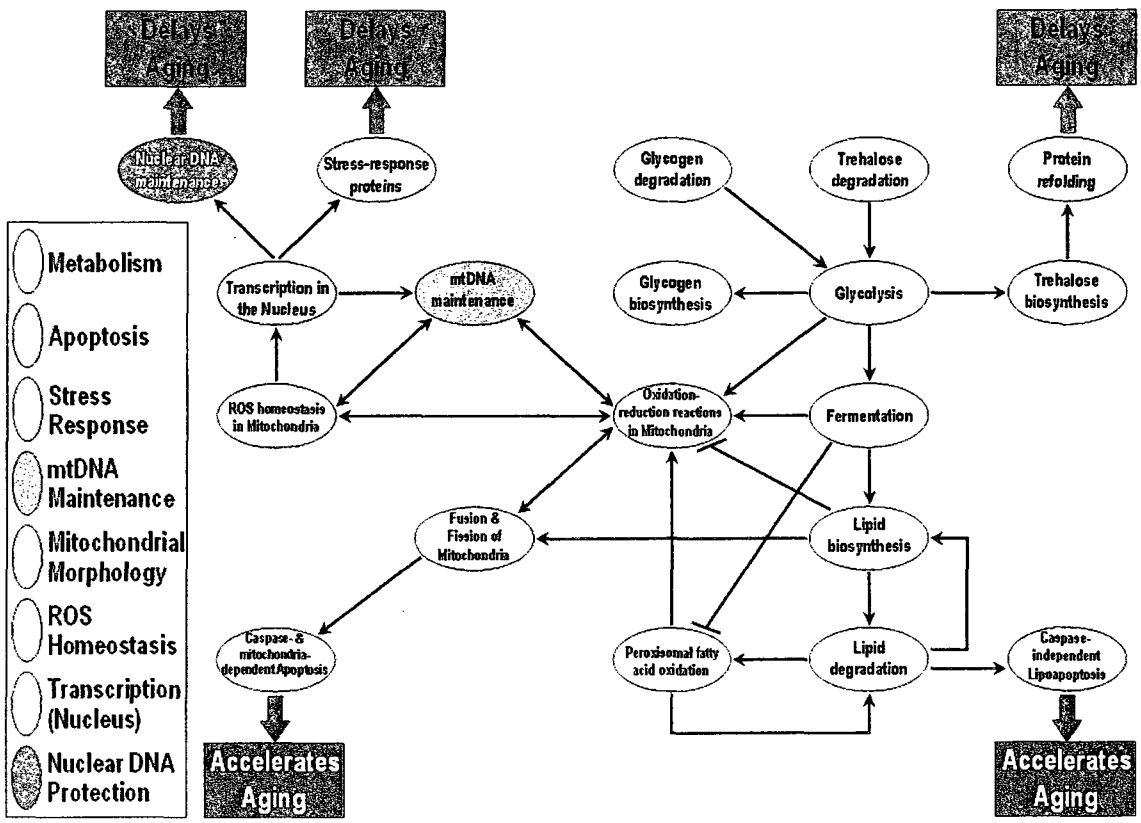

Figure 14.4. Numerous key cellular processes are merged as modules into a longevity network, which establishes the rate of chronological aging in yeast.

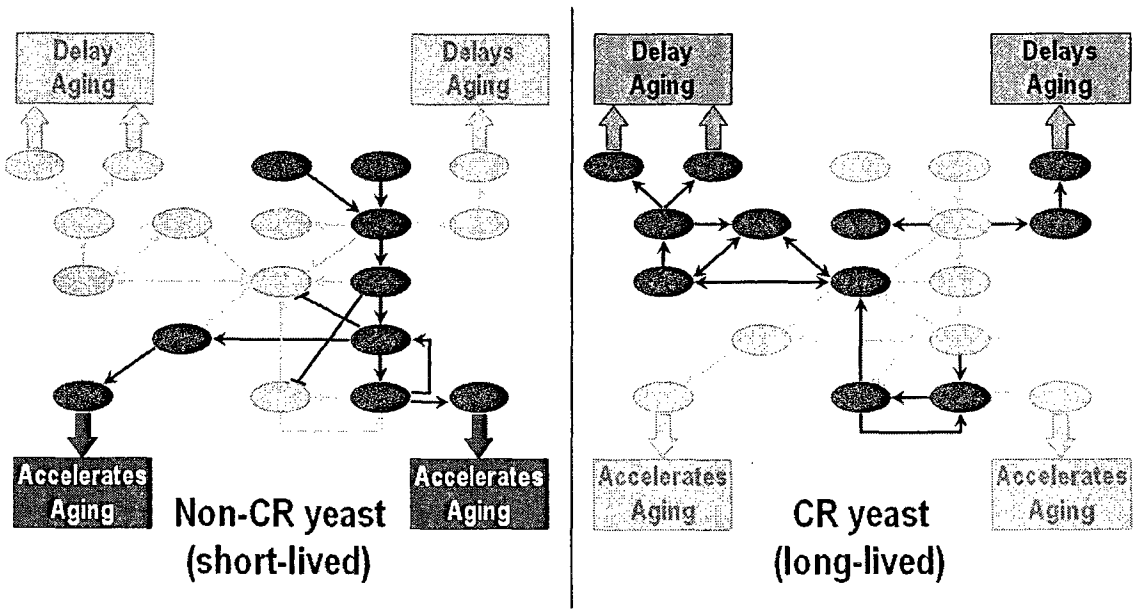

Figure 14.5. Different configurations of the modular longevity network are designed in a diet- and genotype-specific manner prior to entry of yeast cells into non-proliferative state (*i.e.*, stationary phase).

14.3 Longevity regulation by a novel anti-aging drug LA

It seems that the extension of yeast life span by a novel anti-aging molecule LA results to a significant extent from the effect that this compound has on mitochondrial morphology and function. According to my proteomic data and extensive metabolic and functional studies in Dr. Titorenko's laboratory, LA promotes mitochondrial fusion and help to maintain mitochondrial activity, thereby generating an "optimal" level of ROS that is sufficiently high to cause the activation of efficient stress response but is too low to lead to any significant oxidative damage of cellular macromolecules. These findings strongly suggest that the level of ROS generated in mitochondria is one of the major determinants of the rate of chronological aging in yeast (Figure 13.15). This "optimal" level of ROS, which is sustained throughout the entire life span, activates a variety of cellular repair and

damage control pathways, thereby helping to maintain cellular fitness and extend life span.

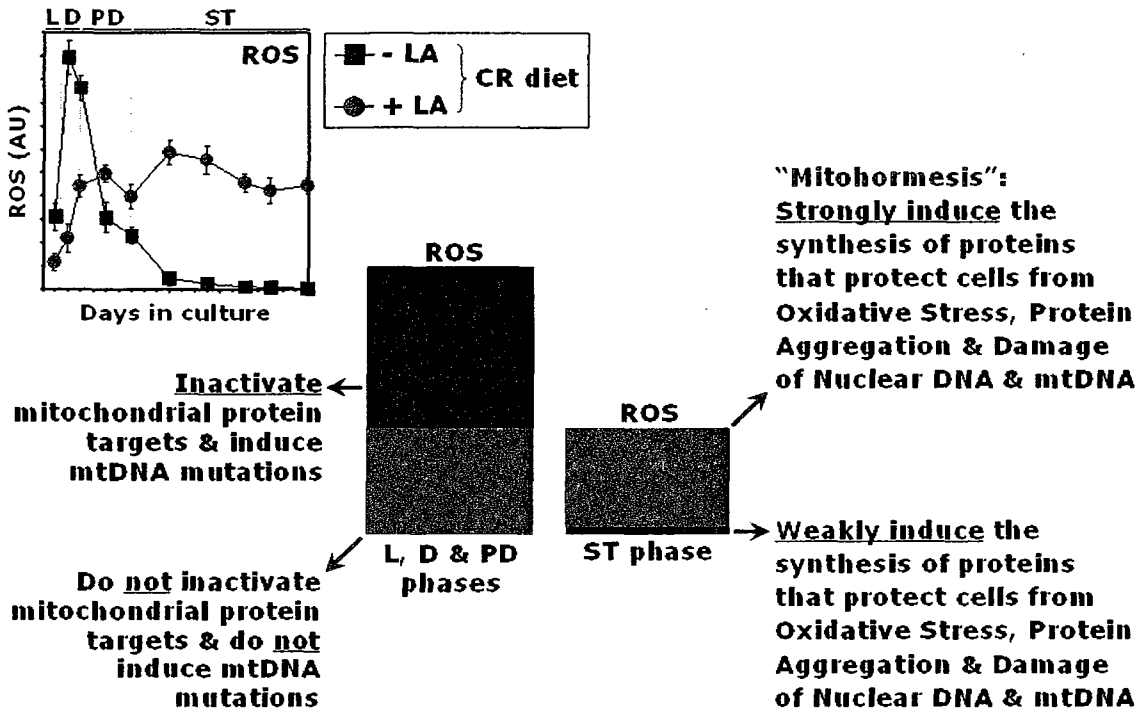

Figure 14.6. The extension of yeast lifespan by LA is due to a ROS-mediated "mitohormetic" signaling.

The novel anti-aging small molecules identified by Dr. Titorenko's laboratory can be used as pharmaceutical agents for aging and age-related disorders. In fact, recent evidence from Dr. Titorenko's laboratory demonstrated that, in addition to promoting mitochondrial fusion in yeast, LA also assists in the fusion of human mitochondria in vitro. Thus, one of the potential applications of LA may be as a drug to treat mitochondrial morphology disorders, all of which are neurological disorders. Furthermore, the LA-induced life span extension of CR yeast can be used as a model to study the molecular mechanisms by which age-dependent changes in mitochondrial ROS, mitochondrial morphology and mitochondrially induced apoptosis regulate longevity.

References

1. Lazarow, P.B., and Fujiki, Y. (1985). Biogenesis of peroxisomes. *Annu. Rev. Cell Biol.* 1:489-530.

2. Subramani, S. (1993). Protein import into peroxisomes and biogenesis of the organelle. *Annu. Rev. Cell Biol.* 9:445-478.

3. Purdue, P.E., and Lazarow, P.E. (2001). Peroxisome biogenesis. *Annu. Rev. Cell Dev. Biol.* 17:701-52.

4. Van den Bosch, H., Schutgens, R.B., Wanders, R.J., and Tager, J.M. (1992). Biochemistry of peroxisomes. *Annu. Rev. Biochem.* 61:157-197.

5. Wanders, R.J., and Tager, J.M. (1998). Lipid metabolism in peroxisomes in relation to human disease. *Mol. Aspects Med.* 19:69-154.

6. Wanders, R.J., Vreken, P., Ferdinandusse, S., Jansen, G.A., Waterham, H.R., van Roermund, C.W., and Van Grunsven, E.G. (2001). Peroxisomal fatty acid alpha- and beta-oxidation in humans: enzymology, peroxisomal metabolite transporters and peroxisomal diseases. *Biochem. Soc. Trans.* 29:250-267.

7. Singh, I. (1996). Mammalian peroxisomes: metabolism of oxygen and reactive oxygen species. *Ann. N.Y. Acad. Sci.* 804, 612-627.

8. Mannaerts G.P., Van Veldhoven P.P. (1996). Functions and organization of peroxisomal ß-oxidation. *Ann. N.Y. Acad. Sci.* 804, 99-115.

9. Krisans, S. (1996). Cell compartmentalization of cholesterol biosynthesis. *Ann. N.Y. Acad. Sci.* 804, 142-164.

10. Hajra, A.K., Das, A.K. (1996). Lipid biosynthesis in peroxisomes. *Ann. N.Y. Acad. Sci.* 804, 129-141.

11. Di-Poi, N., Tan, N.S., Michalik, L., Wahli, W., and Desvergne, B. (2002). Antiapoptotic role of PPARbeta in keratinocytes via transcriptional control of the Akt1 signaling pathway. *Mol. Cell* 10:721-733.

12. Footitt, S., Slocombe, S.P., Larner, V., Kurup, S., Wu, Y., Larson, T., Graham, I., Baker, A., and Holdsworth, M. (2002). Control of germination and lipid mobilization by COMATOSE, the Arabidopsis homologue of human ALDP. *EMBO J.* 21:2912-2922.

13. Gavva, N.R., Wen, S.C., Daftari, P., Moniwa, M., Yang, W.M., Yang-Feng, L.P., Seto, E., Davie, J.R., and Shen, C.K. (2002). NAPP2, a peroxisomal membrane protein, is also a transcriptional corepressor. *Genomics* 79:423-431.

14. Hu, J., Aguirre, M., Peto, C., Alonso, J., Ecker, J., and Chory, J. (2002). A role for peroxisomes in photomorphogenesis and development of Arabidopsis. *Science* 297:405-409.

15. Ma, L., Gao, Y., Qu, L., Chen, Z., Li, J., Zhao, H., and Deng, X.W. (2002). Genomic evidence for COP1 as a repressor of light-regulated gene expression and development in Arabidopsis. *Plant Cell* 14:2383-2398.

16. Michalik, L., Desvergne, B., Dreyer, C., Gavillet, M., Laurini, R.N., and Wahli, W. (2002). PPAR expression and function during vertebrate development. *Int. J. Dev. Biol.* 46:105-114.

17. Titorenko, V.I., and Rachubinski, R.A. (2004). The peroxisome: orchestrating important developmental decisions from inside the cell. *J. Cell Biol.* 164:641-645.

18. Titorenko, V.I., and Rachubinski, R.A. (2001). The life cycle of the peroxisome. *Nature Rev. Mol. Cell Biol.* 2:57-68.

19. Fagarasanu, A., Fagarasanu, M., and Rachubinski, R.A. (2007). Maintaining peroxisome populations: a story of division and inheritance. *Annu. Rev. Cell Dev. Biol.* 23: 321-344.

20. Saleem RA, Smith JJ, Aitchison JD (2006). Proteomics of the peroxisome. *Biochim. Biophys. Acta* 1763 (12): 1541–51.

21. Sacksteder, K.A., and Gould, S.J. (2000). The genetics of peroxisome biogenesis. *Annu. Rev. Genet.* 34:623-652.

22. Subramani, S. (1997). PEX genes on the rise. *Nature Genet.* 15:331-333.

23. Subramani, S., Koller, A., and Snyder, W.B. (2000). Import of peroxisomal matrix and membrane proteins. *Annu. Rev. Biochem.* 69:399-418.

24. Matsumoto, N., Tamura, S., and Fujiki, Y. (2003). The pathogenic peroxin Pex26p recruits the Pex1p-Pex6p AAA ATPase complexes to peroxisomes. *Nature Cell Biol.* 5:454-460.

25. Vizeacoumar, F.J., Torres-Guzman, J.C., Bouard, D., Aitchison, J.D., and Rachubinski, R.A. (2004). Pex30p, Pex31p, and Pex32p form a family of peroxisomal integral membrane proteins regulating peroxisome size and number in *Saccharomyces cerevisiae. Mol. Biol. Cell.* 15:665-677.

26. Hoepfner, D., Schildknegt, D., Braakman, I., Philippsen, P., and Tabak, H.F. (2005). Contribution of the endoplasmic reticulum to peroxisome formation. *Cell* 122 (1):85–95.

27. Schlüter A, Fourcade S, Ripp R, Mandel JL, Poch O, Pujol A (2006). The evolutionary origin of peroxisomes: an ER-peroxisome connection. *Mol. Biol. Evol.* 23: 838-45.

28. Titorenko, V.I., and Mullen, R.T. (2006). Peroxisome biogenesis: The peroxisome endomembrane system and the role of the ER. *J. Cell Biol.* 174:11–17

29. Fujiki, Y. (2000). Peroxisome biogenesis and peroxisome biogenesis disorders. *FEBS Lett.* 476:42-46.

30. Gould, S.J., and Valle, D. (2000). Peroxisome biogenesis disorders: genetics and cell biology. *Trends Genet.* 16:340-345.

31. Gould, S.G., Valle, D., and Raymond, G.V. (2001). The peroxisome biogenesis disorders. *In* The Metabolic and Molecular Bases of Inherited Disease. C.R. Scriver, A.L. Beaudet, W.S. Sly, and D. Valle, editors. McGraw-Hill, New York, pp. 3181-3217.

32. Wanders, R.J. (1999). Peroxisomal disorders: clinical, biochemical, and molecular aspects. *Neurochem. Res.* 24:565-580.

33. Powers, J.M., and Moser, H.W. (1998). Peroxisomal disorders: genotype, phenotype, major neuropathologic lesions, and pathogenesis. *Brain Pathol.* 8:101-120.

34. Moser, H.W. (1999). Genotype-phenotype correlations in disorders of peroxisome biogenesis. *Mol. Genet. Metab.* 68, 316-327.

35. Purdue, P.E., Skoneczny, M., Yang, X., Zhang, J.W., and Lazarow, P.B. (1999). Rhizomelic chondrodysplasia puncatata, a peroxisomal biogenesis disorder caused by defects in Pex7p, a peroxisomal protein import receptor: a minireview. *Neurochem. Res.* 24:581-586.

36. Titorenko, V.I., and Rachubinski, R.A. (2001). Dynamics of peroxisome assembly and function. *Trends Cell Biol.* 11:22-29.

37. Alberts, B., Bray, D., Johnson, A., Lewis, J., Raff, M., Roberts, K., and Walter, P. (1998). *Essential Cell Biology.* Garland Publishing, Inc., New York.

38. Lazarow, P.B. (2003). Peroxisome biogenesis: advances and conundrums. *Curr. Opin. Cell Biol.* 15:489-497.

39. Lodish, H., Berk, A., Zipursky, S.L., Matsudaira, P., Baltimore, D., and Darnell, J. (2000). *Molecular Cell Biology*, 4th edition. W.H. Freeman and Co., New York.

40. Titorenko, V.I., and Rachubinski, R.A. (1998). The endoplasmic reticulum plays an essential role in peroxisome biogenesis. *Trends Biochem. Sci.* 23:231-233.

41. Titorenko, V.I., Ogrydziak, D.M., and Rachubinski, R.A. (1997). Four distinct secretory pathways serve protein secretion, cell surface growth, and peroxisome biogenesis in the yeast *Yarrowia lipolytica*. *Mol. Cell. Biol.* 17:5210-5226.

42. Titorenko, V.I., and Rachubinski, R.A. (1998). Mutants of the yeast *Yarrowia lipolytica* defective in protein exit from the endoplasmic reticulum are also defective in peroxisome biogenesis. *Mol. Cell. Biol.* 18:2789-2803.

43. Mullen, R.T., Lisenbee, C.S., Miernyk, J.A., and Trelease, R.N. (1999). Peroxisomal membrane ascorbate peroxidase is sorted to a membranous network that resembles a subdomain of the endoplasmic reticulum. *Plant Cell.* 11:2167-2185.

44. Kragt, A., Voorn-Brouwer, T., van den Berg, M., and B. Distel, B. (2005). Endoplasmic reticulum-directed Pex3p routes to peroxisomes and restores peroxisome formation in a *Saccharomyces cerevisiae pex3*Δ strain. *J. Biol. Chem.* 280:34350-34357.

45. Tam, Y.Y.C., Fagarasanu, A., Fagarasanu, M., and Rachubinski, R.A. (2005). Pex3p initiates the formation of a preperoxisomal compartment from a subdomain of the endoplasmic reticulum in *Saccharomyces cerevisiae*. *J. Biol. Chem.* 280:34933-34939.

46. Haan, G.-J., Baerends, R.J.S., Krikken, A.M., Otzen, M., Veenhuis, M., and van der Klei, I.J. (2006). Reassembly of peroxisomes in *Hansenula polymorpha pex3* cells on reintroduction of Pex3p involves the nuclear envelope. *FEMS Yeast Res.* 6:186-194.

47. Kim, P.K., Mullen, R.T., Schumann, W., and Lippincott-Schwartz, J. (2006). The origin and maintenance of mammalian peroxisomes involves a *de novo* PEX16-dependent pathway from the ER. *J. Cell Biol.* 173:521-532.

48. Mullen, R.T., Flynn, C.R., and Trelease, R.N. (2001). How are peroxisomes formed? The role of the endoplasmic reticulum and peroxins. *Trends Plant Sci.* 6:256-261.

49. Tabak, H.F., Murk, J.L., Braakman, I., and Geuze, H.J. (2003). Peroxisomes start their life in the endoplasmic reticulum. *Traffic* 4:512-518.

50. Erdmann, R., Veenhuis, M., and W.-H. Kunau, Peroxisomes: organelles at the crossroads, *Trends Cell Biol.* 7:400–407.

51. Kunau, W.-H. (2005) Peroxisome biogenesis: end of the debate, *Curr. Biol* 15: R774–R776.

52. Schekman, R. (2005). Peroxisomes: another branch of the secretory pathway? *Cell* 122, pp. 1–2.

53. van der Zand, A., I. Braakman, H.J. Geuze and H.F. Tabak. (2006) The return of the peroxisome, *J. Cell Sci.* 119: 989–994.

54. Geuze, H.J., Murk, J.L., Stroobants, A.K., Griffith, J.M., Kleijmeer, M.J., Koster, A.J., Verkleij, A.J., Distel, B, and Tabak, H.F. (2003). Involvement of the endoplasmic reticulum in peroxisome formation. *Mol. Biol. Cell.* 14:2900-2907.

55. Eckert, J. H., and R. Erdmann. (2003) Peroxisome biogenesis. *Rev. Physiol. Biochem. Pharmacol.* 147:75–121

56. Yan, M., N. Rayapuram and S. Subramani, The control of peroxisome number and size during division and proliferation, *Curr. Opin. Cell Biol.* 17:376–383.

57. Beevers, H. (1979). Microbodies in higher plants. *Annu. Rev. Plant Physiol.* 30:159-193.

58. Baerends, R.J.S., Rasmussen, S.W., Hilbrands, R.E., van der Heide, M., K.N. Faber, K.N., Reuvekamp, P.T.W., Kiel, J.A.K.W., Cregg, J.M., van der Klei, I, J., and Veenhuis, M. (1996). The *Hansenula polymorpha PER9* gene encodes a peroxisomal membrane protein essential for peroxisome assembly and integrity. *J. Biol. Chem.* 271:8887-8894.

59. Elgersma, Y., Kwast, L., van den Berg, M., Snyder, W.B., Distel, B., Subramani, S., and Tabak, H.F. (1997). Overexpression of Pex15p, a phosphorylated peroxisomal integral membrane protein required for peroxisome assembly in *S. cerevisiae,* causes proliferation of the endoplasmic reticulum membrane. *EMBO J.* 16:7326-7341.

60. Mullen, R.T., and Trelease, R.N. (2000). The sorting signals for peroxisomal membrane-bound ascorbate peroxidase are within its C-terminal tail. *J. Biol. Chem.* 275:16337-16344.

61. Titorenko, V.I., Eitzen, G.A., and Rachubinski, R.A. (1996). Mutations in the *PAY5* gene of the yeast *Yarrowia lipolytica* cause the accumulation of multiple subpopulations of peroxisomes. *J. Biol. Chem.* 271:20307-20314.

62. Titorenko, V.I., and Rachubinski, R.A. (2000). Peroxisomal membrane fusion requires two AAA family ATPases, Pex1p and Pex6p. *J. Cell Biol.* 150:881-886.

63. Titorenko, V.I., Chan, H., Rachubinski, R.A. (2000). Fusion of small vesicles in vitro reconstitutes an early step in the *in vivo* multistep peroxisome assembly pathway of *Yarrowia lipolytica*. *J. Cell Biol.* 148, 29-43.

64. Subramani, S. (1996). Protein translocation into peroxisomes. *J. Biol. Chem.* 271, 32483-32486.

65. Snyder, W. B., Faber, K. N., Wenzel, T. J., Koller, A., Lüers, G. H., Rangell, L., Keller, G. A., Subramani, S. (1999). Pex19p Interacts with Pex3p and Pex10p and is essential for peroxisome biogenesis in *Pichia pastoris*. *Mol. Biol. Cell* 10, 1745-1761.

66. Faber, K.N., Heyman, J.A., Subramani, S. (1998). The AAA-family peroxins, PpPex1p and PpPex6p, interact with each other in an ATP-dependent manner and are associated with different subcellular membranous structures distinct from peroxisomes. *Mol. Cell. Biol.* 18, 936-943.

67. South, S.T., K.A. Sacksteder, K.A., Li, X., Liu, Y., and Gould, S.J. (2000). Inhibitors of COPI and COPII do not block PEX3-mediated peroxisome synthesis. *J. Cell Biol.* 149:1345-1360.

68. South, S. T., and S.J. Gould (1999). Peroxisome synthesis in the absence of preexisting peroxisomes. *J. Cell Biol.* 144:pp. 255–266.

69. Muñiz, M., Morsomme, P., and Riezman, H. (2001). Protein sorting upon exit from the endoplasmic reticulum. *Cell* 104:313-320.

70. Glick, B.S. (2001). ER export: More than one way out. *Current Biology* 11:R361-R363.

71. Watanabe, R., Funato, K., Venkataraman, K., Futerman, A.H., and Riezman, H. (2002). Sphingolipids are required for the stable membrane association of glycosylphosphatidylinositol-anchored proteins in yeast. *J. Biol. Chem.* 277:49538-49544.

72. Morsomme, P., Prescianotto-Baschong, C., and Riezman, H. (2003). The ER v-SNAREs are required for GPI-anchored protein sorting from other secretory proteins upon exit from the ER. *J. Cell Biol.* 162:403-412.

73. Mayor, S., and Riezman, H. (2004). Sorting GPI-anchored proteins. *Nature Rev. Mol. Cell Biol.* 5:110-120.

74. Veenhuis, M., and J.M. Goodman (1990). Peroxisomal assembly: membrane proliferation precedes the induction of the abundant matrix proteins in the methylotrophic yeast *Candida boidinii*, *J. Cell Sci.* 96:583–590.

75. Mañes, S., G. del Real, and C. Martínez-A. (2003). Pathogens: raft hijackers. *Nat. Rev. Immunol.* 3:557–568

76. Yan, M., Rayapuram, N., and Subramani, S. (2005). The control of peroxisome number and size during division and proliferation. *Curr. Opin. Cell Biol.* 17:376-383.

77. Hoepfner, D., van den Berg, M., Philippsen, P., Tabak, H.F., and Hettema, E.H.(2001). A role for Vps1p, actin, and the Myo2p motor in peroxisome abundance and inheritance in *Saccharomyces cerevisiae. J. Cell Biol.* 155:979–990.

78. Koch, A., Thiemann, M., Grabenbauer, M., Yoon, Y., McNiven, M.A., and Schrader, M. (2003). Dynamin-like protein 1 is involved in peroxisomal fission. *J. Biol. Chem.* 278:8597-8605.

79. Li, X., and Gould, S.J. (2003). The dynamin-like GTPase DLP1 is essential for peroxisome division and is recruited to peroxisomes in part by PEX11. *J. Biol. Chem.* 278:17012-17020.

80. Koch, A., Schneider, G., Luers, G.H., and Schrader, M. (2004). Peroxisome elongation and constriction but not fission can occur independently of dynamin-like protein 1. *J. Cell Sci.* 117:3995-4006.

81. Thoms, S., and R. Erdmann. (2005). Dynamin-related proteins and Pex11 proteins in peroxisome division and proliferation. *FEBS J.* 272:5169-5181.

82. Schrader, M. (2006). Shared components of mitochondrial and peroxisomal division. *Biochim. Biophys. Acta*, doi: 10.1016/j.bbamcr.2006.01.004.

83. Nebenfuhr, A., Frohlick, J.A., and Staehelin, L.A. (2000). Redistribution of Golgi stacks and other organelles during mitosis and cytokinesis in plant cells. *Plant Physiol.* 124:135-151.

84. Guo, T., Y.Y. Kit, J.-M. Nicaud, M.-T. Le Dall, S.K. Sears, H. Vali, H. Chan, R.A. Rachubinski and V.I. Titorenko (2003). Peroxisome division is regulated by a signal from inside the peroxisome, *J. Cell Biol.* 162 pp. 1255–1266.

85. Tan, X., H.R. Waterham, M. Veenhuis and J.M. Cregg (1995). The *Hansenula polymorpha PER8* gene encodes a novel peroxisomal integral membrane protein involved in proliferation. *J. Cell Biol.* 128:307–319.

86. Eitzen, G. A., R.K. Szilard and R.A. Rachubinski (1997). Enlarged peroxisomes are present in oleic acid-grown *Yarrowia lipolytica* overexpressing the *PEX16* gene encoding an intraperoxisomal peripheral membrane peroxin. *J. Cell Biol.* 137:1265–1278.

87. Mayor, S., and M. Rao. (2004) Rafts: scale-dependent, active lipid organization at the cell surface. *Traffic* 5:231–240

88. Corda, D., Hidalgo Carcedo, C., Bonazzi, M., Luini, A., and Spano, S. (2002). Molecular aspects of membrane fission in the secretory pathway. *Cell. Mol. Life Sci.* 59:1819-1832.

89. Hidalgo Carcedo, C., Bonazzi, M., Spanò, S., Turacchio, G., Colanzi, A., Luini, A., and Corda, D. (2004). Mitotic Golgi partitioning is driven by the membrane-fissioning protein CtBP3/BARS. *Science* 305:93-96.

90. Sprong, H., P. van der Sluijs and G. van Meer. (2001) How proteins move lipids and lipids move proteins. *Nat. Rev., Mol. Cell Biol.* 2:504–513.

91. Zimmerberg, J., and M.M. Kozlov. (2006). How proteins produce cellular membrane curvature. *Nat. Rev., Mol. Cell Biol.* 7:9–19.

92. Farsad, K., N. Ringstad, K. Takei, S.R. Floyd, K. Rose and P. De Camilli. (2001) Generation of high curvature membranes mediated by direct endophilin bilayer interactions. *J. Cell Biol.* 155:193–200.

93. Baron, C. L., and V. Malhotra. (2002) Role of diacylglycerol in PKD recruitment to the TGN and protein transport to the plasma membrane, *Science* 295:325-328.

94. Ford, M.G.J., I.G. Mills, B.J. Peter, Y. Vallis, G.J. Praefcke, P.R. Evans and H.T. McMahon. (2002). Curvature of clathrin-coated pits driven by epsin, *Nature* 419:361–366.

95. Bigay, J., P. Gounon, S. Robineau and B. Antonny. (2003) Lipid packing sensed by ArfGAP1 couples COPI coat disassembly to membrane bilayer curvature. *Nature* 426:563–566.

96. Bossy-Wetzel, E., M.J. Barsoum, A. Godzik, R. Schwarzenbacher and S.A. Lipton. (2003) Mitochondrial fission in apoptosis, neurodegeneration and aging, *Curr. Opin. Cell Biol.* 15:706–716

97. Freyberg, Z., A. Siddhanta and D. Shields. (2003) "Slip, sliding away": phospholipase D and the Golgi apparatus, *Trends Cell Biol.* 13:540–546.

98. Peter, B. J., H.M. Kent, I.G. Mills, Y. Vallis, P.J. Butler, P.R. Evans and H.T. McMahon. (2004) BAR domains as sensors of membrane curvature: the amphiphysin BAR structure. *Science* 303:495–499.

99. Yoshida, Y., M. Kinuta, T. Abe, S. Liang, K. Araki, O. Cremona, G. Di Paolo, Y. Moriyama, T. Yasuda, P. De Camilli and K. Takei. (2004) The stimulatory action

of amphiphysin on dynamin function is dependent on lipid bilayer curvature, *EMBO J.* 23:3483–3491.

100. Bonazzi, M., S. Spano, G. Turacchio, C. Cericola, C. Valente, A. Colanzi, H.S. Kweon, V.W. Hsu, E.V. Polishchuck, R.S. Polishchuck, M. Sallese, T. Pulvirenti, D. Corda and A. Luini. (2005) CtBP3/BARS drives membrane fission in dynamin-independent transport pathways, *Nat. Cell Biol.* 7:570–580.

101. McMahon, H. T., and J.L. Gallop. (2005) Membrane curvature and mechanisms of dynamic cell membrane remodeling, *Nature* 438:590–596

102. L.V. Chernomordik and M.M. Kozlov. (2003) Protein–lipid interplay in fusion and fission of biological membranes, *Annu. Rev. Biochem.* 72:175–207.

103. Kooijman, E. E., V. Chupin, B. de Kruijff and K.N.J. Burger. (2003) Modulation of membrane curvature by phosphatidic acid and lysophosphatidic acid. *Traffic* 4:162–174.

104. Cremona, O., and De Camilli, P. (2001) Phosphoinositides in membrane traffic at the synapse. *J. Cell Sci.* 114:1041–1052.

105. Bankaitis, V. A. (2002). Slick recruitment to the Golgi. *Science* 295:290-291.

106. Weigert, R., M.G. Silletta, S. Spano, G. Turacchio, C. Cericola, A. Colanzi, S. Senatore, R. Mancini, E.V. Polishchuk, M. Salmona, F. Facchiano, K.N. Burger, A. Mironov, A. Luini and D. Corda. (1999) CtBP/BARS induces fission of Golgi membranes by acylating lysophosphatidic acid, *Nature* 402:429–433.

107. Goni, F. M., and A. Alonso. (1999) Structure and functional properties of diacylglycerols in membranes, *Prog. Lipid Res.* 38:1–48.

108. Szule, J.A., N.L. Fuller and R.P. Rand. (2002) The effects of acyl chain length and saturation of diacylglycerols and phosphatidylcholines on membrane monolayer curvature, *Biophys. J.* 83:977–984.

109. Shemesh, T., A. Luini, V. Malhotra, K.N. Burger and M.M. Kozlov. (2003) Prefission constriction of Golgi tubular carriers driven by local lipid metabolism: a theoretical model. *Biophys. J.* 85:3813–3827.

110. Holthuis, J. C., and T.P. Levine, (2005). Lipid traffic: floppy drives and a superhighway, *Nat. Rev., Mol. Cell Biol.* 6:209–220.

111. van Roermund, C.W.T., Tabak, H.F., van den Berg, M., Wanders, R.J.A., and Hettema, E.H. (2000). Pex11p plays a primary role in medium-chain fatty acid oxidation, a process that affects peroxisome number and size in *Saccharomyces cerevisiae. J. Cell Biol.* 150:489-497.

112. Chang, C.C., South, S., Warren, D., Jones, J., Moser, A.B., Moser, H.W., and S.J. Gould, S.J. (1999). Metabolic control of peroxisome abundance. *J. Cell Sci.* 112:1579-1590.

113. Fan, C.Y., Pan, J., Usuda, N., Yeldandi, A.V., Rao, M.S., and Reddy, J.K. (1998). Steatohepatitis, spontaneous peroxisome proliferation and liver tumors in mice lacking peroxisomal fatty acyl-CoA oxidase. Implications for peroxisome proliferator-activated receptor αnatural ligand metabolism. *J. Biol. Chem.* 273:15639-15645.

114. Poll-Thé, B.T., Poll-Thé, B.T., Roels, F., Ogier, H., Scotto, J., Vamecq, J., Schutgens, R.B., Wanders, R.J., van Roermund, C.W., van Wijland, M.J., Schram, A.W., J.M. Tager, J.M., and Saudubray, J.-M. (1998). A new peroxisomal disorder with enlarged peroxisomes and a specific deficiency of acyl-CoA oxidase (pseudo-neonatal adrenoleukodystrophy). *Am. J. Hum. Genet.* 42:422-434.

115. Smith, J.J., Brown, T.W., Eitzen, G.A., and Rachubinski, R.A. (2000). Regulation of peroxisome size and number by fatty acid β-oxidation in the yeast *Yarrowia lipolytica*. *J. Biol. Chem.* 275:20168-20178.

116. Boukh-Viner, T., Guo, T., Alexandrian, A., Cerracchio, A., Gregg, C., Haile, S., Kyskan, R., Milijevic, S., Oren, D., Solomon, J., Wong, V., Nicaud, J.-M., Rachubinski, R.A., English, A.M., and Titorenko, V.I. (2005). Dynamic ergosterol- and ceramide-rich domains in the peroxisomal membrane serve as an organizing platform for peroxisome fusion. *J. Cell Biol.* 168 761-773.

117. Wang, H.J., Le Dall, M.T., Wach Y., Laroche C., Belin, J.M., Gaillardin C., and Nicaud, J.M. (1999). Evaluation of acyl coenzyme A oxidase (Aox) isozyme function in the *n*-alkane-assimilating yeast *Yarrowia lipolytica*. *J. Bacteriol.* 81:5140-5148.176

118. Titorenko, V.I., Smith, J.J., Szilard, R.K., and Rachubinski, R.A. (1998). Pex20p of the yeast *Yarrowia lipolytica* is required for the oligomerization of thiolase in the cytosol and for its targeting to the peroxisome. *J. Cell Biol.* 142: 403–420.

119. Szilard, R.K., Titorenko, V.I., Veenhuis, M., and Rachubinski, R.A. (1995). Pay32p of the yeast *Yarrowia lipolytica* is an intraperoxisomal component of the matrix protein translocation machinery. *J. Cell Biol.* 131:1453-1469.

120. Xu, X., R. Bittman, G. Duportail, D. Heissler, C. Vilcheze, and E. London. (2001) Effect of the structure of natural sterols and sphingolipids on the formation of ordered sphingolipid/sterol domains (rafts). Comparison of cholesterol to plant, fungal, and disease-associated sterols and comparison of sphingomyelin, cerebrosides, and ceramide. *J. Biol. Chem.* 276:33540–33546.

121. Xu, Z., Sato, K., and Wickner, W. (1998). LMA1 binds to vacuoles at Sec18p (NSF), transfers upon ATP hydrolysis to a t-SNARE (Vam3p) complex, and is released during fusion. *Cell* 93:1125-1134.

122. MacDonald, R.C., MacDonald, R.I., Menco, B.P.M., Takeshita, K., Subbarao, N.K., and Hu, L.-R. (1991). Small-volume extrusion apparatus for preparation of large, unilamellar vesicles. *Biochim. Biophys. Acta.* 1061:297–303.

123. Simons, K., and D. Toomre. (2000) Lipid rafts and signal transduction. *Nat. Rev. Mol. Cell Biol.* 1:31-39.

124. Foster, L.J., C.L. de Hoog, and M. Mann. (2003) Unbiased quantitative proteomics of lipid rafts reveals high specificity for signaling factors. *Proc. Natl. Acad. Sci. USA* 100:5813-5818.

125. Jahn, R., T. Lang, and T.C. Südhof. (2003). Membrane fusion. *Cell* 112:519–533.

126. Mayer, A. (2002) Membrane fusion in eukaryotic cells. *Annu. Rev. Cell Dev. Biol.* 18:289–314.

127. Mozdy, A.D., and J.M. Shaw. (2003) A fuzzy mitochondrial fusion apparatus comes into focus. *Nat. Rev. Mol. Cell Biol.* 4:468–478.

128. Teissier, E., and E.I. Pécheur, (2007). Lipids as modulators of membrane fusion mediated by viral fusion proteins, *Eur. Biophys. J.* 36:887–899.

129. Dimmer, K. S., S. Fritz, F. Fuchs, M. Messerschmitt, N. Weinbach and W. Neupert. (2006). Genetic basis of mitochondrial function and morphology in *Saccharomyces cerevisiae*, *Mol Biol Cell* 13:847–853.

130. Altmann, K., and B. Westermann, (2005). Role of essential genes in mitochondrial morphogenesis in *Saccharomyces cerevisiae*, *Mol. Biol. Cell* 16:5410–5417.

131. Catimel B., Schieber C, Condron M, Patsiouras H, Connolly L, Catimel J, Nice E.C, Burgess A.W., and Holmes A. B. (2008) The PI(3,5)P2 and PI(4,5)P2 interactomes. *J. Proteome Res.* 7:5295–5313.

132. Boman, A.L., M.R. Delannoy, and K.L. Wilson. (1992) GTP hydrolysis is required for vesicle fusion during nuclear envelope assembly in vitro. *J. Cell Biol* 116:281-294.

133. Berridge, M. J. and Irvine, R. F. (1984) Inositol trisphosphate, a novel second messenger in cellular signal transduction *Nature* 312:315-321.

134. Berridge, M. J. (1993) Inositol trisphosphate and calcium signalling *Nature* 361:315-325.

135. Vanhaesebroeck, B.; Leevers, S. J.; Ahmadi, K.; Timms, J.; Katso, R.; Driscoll, P. C.; Woscholski, R.; Parker, P. J.; Waterfield, M. D. (2001) Synthesis and function of 3-phosphorylated inositol lipids *Annu. Rev. Biochem.* 70:535-602.

136. Cantley, L. C. (2002) The phosphoinositide 3-kinase pathway. *Science* 296:1655-1657.

137. Martin, T. F. (1998) Phosphoinositide lipids as signaling molecules: common themes for signal transduction, cytoskeletal regulation, and membrane trafficking. *Annu. Rev. Cell Dev. Biol.* 14:231-264.

138. Toker, A. (2002) Phosphoinositides and signal transduction *Cell. Mol. Life Sci.* 59:761-779.

139. Lemmon, M. A. (2003) Phosphoinositide recognition domains *Traffic*, 44:201-213.

140. Hawkins, P., Terson, K.E., Davidson, K.; Stephens, L. R. (2006) Signalling through Class I PI3Ks in mammalian cells *Biochem. Soc. Trans.* 34:647-662.

141. Balla, T. (2005) Inositol-lipid binding motifs: signal integrators through protein-lipid and protein-protein interactions *J. Cell Sci.* 118:2093-2104.

142. Di Paolo, G.; De Camilli, P (2006) Phosphoinositides in cell regulation and membrane dynamics *Nature* 443:651-657.

143. Eitzen, G., Will, E., Gallwitz, D., Haas, A., and Wickner, W. (2000) Sequential action of two GTPases to promote vacuole docking and fusion. *EMBO J.* 19: 6713–6720.

144. Peters, C., and Mayer, A. (1998) Ca^{2+}/calmodulin signals the completion of docking and triggers a late step of vacuole fusion. *Nature* 396:575–580.

145. Peters, C., Andrews, P.D., Stark, M.J., Cesaro-Tadic, S., Glatz, A., Podtelejnikov, A., Mann, M., and Mayer, A. (1999) Control of the terminal step of intracellular membrane fusion by protein phosphatase 1. *Science* 285:1084–1087.

146. Brown, D.A., and J.K. Rose. (1992) Sorting of GPI-anchored proteins to glycolipid enriched membrane subdomains during transport to the apical cell surface. *Cell* 68:533–544.

147. Brown, D.A., and E. London. (2000) Structure and function of sphingolipid- and cholesterol-rich membrane rafts. *J. Biol. Chem.* 275:17221–17224.

149. Munro, S. 2003. Lipid rafts: elusive or illusive? *Cell* 115:377–388.

150. Bagnat, M., S. Keranen, A. Shevchenko, A. Shevchenko, and K. Simons. (2000) Lipid rafts function in biosynthetic delivery of proteins to the cell surface in yeast. *Proc. Natl. Acad. Sci. USA* 97:3254–3259.

151. Fried, B., and Sherma, J. (1999). Thin-Layer Chromatography. *Marcel Dekker, Inc., New York. pp 499.*

152. Röper, K., D. Corbeil, and W.B. Huttner. (2000) Retention of prominin in microvilli reveals distinct cholesterol-based lipid micro-domains in the apical plasma membrane. *Nat. Cell Biol.* 2:582–592.

153. Laloi,M., A.M. Perret, L. Chatre, S. Melser, C. Cantrel and M.N. Vaultier, (2007) Insights into the role of specific lipids in the formation and delivery of lipid microdomains to the plasma membrane of plant cells, *Plant Physiol* 143, pp.1-12.

154. Shevchenko, A., Jensen, O.N., Podtelejnikov, A.V., Sagliocco, F., Wilm, M., Vorm, O., Mortensen, P., Shevchenko, A., Boucherie, H., Mann, M. (1996) Linking genome and proteome by mass spectrometry: large-scale identification of yeast proteins from two dimensional gels. *Proc. Natl. Acad. Sci. USA* 93:14440–14445.

155. Jiménez, C.R., Huang, L., Qiu, Y., and Burlingame, A.L. (1998) Searching sequence databases over the Internet: protein identification using MS-Fit. In *Current Protocols in Protein Science.* J.E. Coligan, B.M. Dunn, H.L. Ploegh, D.W. Speicher, and P.T. Wigfield, editors. John Wiley and Sons, New York. 16.5.1–16.5.6.

156. Legros, F., Lombès, A., Frachon, P., and Rojo, M. (2002) Mitochondrial fusion in Human Cells is efficient, requires the inner membrane potential, and is mediated by mitofusins. *Mol. Biol. Cell* 12:4343-4354.

157. Sheahan, M. B., McCurdy, D. W., Rose, R. J. (2005) Mitochondria as a connected population: ensuring continuity of the mitochondrial genome during plant cell dedifferentiation through massive mitochondrial fusion. *Plant J.* 44:744-755.

158. Ishihara, N., Jofuku, A., Eura, Y., and Mihara K. (2003) Regulation of mitochondrial morphology by membrane potential, and DRP1-dependent division and FZO1-dependent fusion reaction in mammalian cells. *Biochem. Biophys. Res. Commun.* 301:891-898.

159. Ungermann, C., Wickner, W., and Xu, Z. (1999) Vacuole acidification is required for trans-SNARE pairing, LMA1 release, and homotypic fusion. *Proc. Natl. Acad. Sci.* 96: 11194-11199.

160. Seeley, E. S., Kato, M., Margolis, N., Wickner, W., and Eitzen, G. (2002) Genomic analysis of homotypic vacuole fusion. *Mol. Biol. Cell* 13:782-794.

161. Hidaka, H., and Tanaka, T. (1983) *Methods Enzymol.* 102:185-194.

162. Colombo, M., Beron, W., Stahl, P.L. (1997) Calmodulin regulates endosome fusion. *J. Biol. Chem.* 272:7707-7712.

163. Holroyd, C., Kistner, U., Annaert, W., and Jahn, R. (1999) *Mol. Biol. Cell* 10:3035-3044.

164. Stevens FC (1983). Calmodulin: an introduction. *Can. J. Biochem. Cell Biol.* 61:906–910.

165. Chin D, Means AR (2000). Calmodulin: a prototypical calcium sensor. *Trends Cell Biol.* 10:322–328.

166. Pomorski, T., J.C. Holthuis, A. Herrmann, and G. van Meer. (2004) Tracking down lipid flippases and their biological functions. *J. Cell Sci.* 117:805–813.

167. Pierini, L.M., and F.R. Maxfield. (2001). Flotillas of lipid rafts fore and aft. *Proc. Natl. Acad. Sci. USA.* 98:9471–9473.

168. Kenworthy, A.K., B.J. Nichols, C.L. Remmert, G.M. Hendrix, M. Kumar, J. Zimmerberg, and J. Lippincott-Schwartz. (2004) Dynamics of putative raft-associated proteins at the cell surface. *J. Cell Biol.* 165:735–746.

169. Slimane, T.A., G. Trugnan, S.C. van IJzendoorn, and D. Hoekstra. (2003) Raft-mediated trafficking of apical resident proteins occurs in both direct and transcytotic pathways in polarized hepatic cells: role of distinct lipid microdomains. *Mol. Biol. Cell* 14:611–624.

170. Helms, J.B., and C. Zurzolo. (2004) Lipids as targeting signals: lipid rafts and intracellular trafficking. *Traffic* 5:247–254.

171. Salaün, C., D.J. James, and L.H. Chamberlain. (2004) Lipid rafts and the regulation of exocytosis. *Traffic* 5:255–264.

172. Kirkwood, T.B.L. (2005). Understanding the odd science of aging. *Cell* 120:437-447.

173. Campisi, J. (2005). Senescent cells, tumor suppression, and organismal aging: good citizens, bad neighbors. *Cell* 120:513-522.

174. Chien, K.R. and Karsenty, G. (2005). Longevity and lineages: toward the integrative biology of degenerative diseases in heart, muscle, and bone. *Cell* 120:533-544.

175. Tanzi, R.E. and Bertram, L. (2005). Twenty years of the Alzheimer's disease amyloid hypothesis: a genetic perspective. *Cell* 120:545-555.

176. Antebi, A. (2005). Physiology. The tick-tock of aging? *Science* 310:1911-1913.

177. Longo, V.D., Mitteldorf, J., and Skulachev, V.P. (2005). Programmed and altruistic ageing. *Nat. Rev. Genet.* 6:866-872.

178. Skulachev, V.P., and Longo, V.D. (2005). Aging as a mitochondria-mediated atavistic program: can aging be switched off? *Ann. N. Y. Acad. Sci.* 1057:145-164.

179. Blagosklonny, M.V. (2007). Paradoxes of aging. *Cell Cycle* 6:2997-3003.

180. Lithgow, G.J. (2006). Why aging isn't regulated: a lamentation on the use of language in aging literature. *Exp. Gerontol.* 41:890-893.

181. Kirkwood, T.B.L. (2008). Understanding ageing from an evolutionary perspective. *J. Intern. Med.* 263:117-127.

182. Harman, D. (1988). Free radicals in aging. *Mol. Cell. Biochem.* 84, 155-161.

183. Fraga, C.G., Shigenaga, M.K., Park, J.W., Degan, P., and Ames, B.N. (1990). Oxidative damage to DNA during aging: 8-Hydroxy-2`-deoxyguanosine in rat organ DNA and urine. *Proc. Natl. Acad. Sci.* 87:4533-4537.

184. Stadtman, E.R. (1992). Protein oxidation and aging. *Science* 257:1220-1224.

185. Head, E., Liu, J., Hagen, T.M., Muggenburg, B.A., Milgram, N.W., Ames, B.N., and Cotman, C.W. 2002. Oxidative damage increases with age in a canine model of human brain aging. *J. Neurochem.* 82:375-381.

186. Liu, J., Head, E., Gharib, A.M., Yuan, W., Ingersoll, R.T., Hagen, T.M., Cotman, C.W., and Ames, B.N. (2002). Memory loss in old rats is associated with brain mitochondrial decay and RNA/DNA oxidation: Partial reversal by feeding acetyl-L-carnitine and/or R-α-lipoic acid. *Proc. Natl. Acad. Sci.* 99:2356-2361.

187. Parkes, T.L., Elia, A.J., Dickinson, D., Hilliker, A.J., Phillips, J.P., and Boulianne, G.L. (1998). Extension of *Drosophila* lifespan by overexpression of human SOD1 in motorneurons. *Nat. Genet.* 19, 171-174.

188. Longo, V.D. (1999). Mutations in signal transduction proteins increase stress resistance and longevity in yeast, nematodes, fruit flies, and mammalian neuronal cells. *Neurobiol. Aging* 20, 479-486.

189. Nicholls D. (2002) Mitochondrial bioenergetics, aging, and aging-related disease. *Sci. Aging Knowledge Environ.* 31:12.

190. Newmeyer DD, Ferguson-Miller S. (2003) Mitochondria: releasing power for life and unleashing the machineries of death. *Cell* 112:481-490.

191. Balaban, R.S., Nemoto, S., and Finkel, T. (2005). Mitochondria, oxidants, and aging. *Cell* 120:483-495.

192. Storz, P. (2007). Mitochondrial ROS - radical detoxification, mediated by protein kinase D. *Trends Cell Biol.* 17:13-18.

193. Muller, F. L., Lustgarten, M. S., Jang, Y., Richardson, A. and Van Remmen, H. (2007) Trends in oxidative aging theories. *Free Radic. Biol. Med.* 43: 477-503.

194. Alberts, B., Bray, B., Johnson, A., Lewis, J., Raff, M., Roberts, K., Walter, P. *Essential Cell Biology: An introduction to the Molecular Biology of the Cell.* Garland Publishing, Inc. New York, USA. 1998. p. 584-586.

195. Steller, H. (1995) Mechanisms and genes of cellular suicide. *Science.* 267:1445-1449.

196. Madeo, F., Herker, E., Wissing, S., Jungwirth, H., Eisenberg, T., and Frohlich, K.U. (2004). Apoptosis in yeast. *Curr. Opin. Microbiol.* 7:655-660.

197. Herker, E., Jungwirth, H., Lehmann, K.A., Maldener, C., Frohlich, K.U., Wissing, S., Buttner, B., Markus, F., Sigrist, S., and Madeo, F. (2004). Chronological aging leads to apoptosis in yeast. *J. Cell. Biol.* 164:501-507.

198. Büttner, S., Eisenberg, T., Herker, E., Carmona-Gutierrez, D., Kroemer, G., and Madeo, F. (2006). Why yeast cells can undergo apoptosis: death in times of peace, love, and war. *J. Cell Biol.* 175:521-525.

199. Büttner, S., Eisenberg, T., Carmona-Gutierrez, D., Ruli, D., Knauer, H., Ruckenstuhl, C., Sigrist, C., Wissing, S., Kollroser, M., Fröhlich, K.U., Sigrist, S., and Madeo, F. (2007). Endonuclease G regulates budding yeast life and death. *Mol. Cell* 25:233-246.

200. Madeo, F., Fröhlich, E., Ligr, M., Grey, M., Sigrist, S.J., Wolf, D.H. and Fröhlich, K.U. (1999). Oxygen stress: a regulator of apoptosis in yeast. *J. Cell Biol.* 145:757–767.

201. Madeo, F., Herker, E., Maldener, C., Wissing, S., Lachelt, S., Herlan, M., Fehr, M., Lauber, K., Sigrist, S.J., Wesselborg, S., and Frohlich, K.U. (2002) A caspase-related protease regulates apoptosis in yeast. *Mol. Cell* 9:911-917.

202. Fahrenkrog, B., Sauder, U., and Aebi, U. (2004). The S. cerevisiae HtrA-like protein Nma111p is a nuclear serine protease that mediates yeast apoptosis. *J. Cell Sci.*117:115-126.

203. Wissing, S., Ludovico, P., Herker, E., Büttner, S., Engelhardt, S.M., Decker, T., Link, A., Proksch, A., Rodrigues, F., Corte-Real, M., Fröhlich, K.U., Manns, J., Candé, C., Sigrist, S.J., Kroemer, G., and Madeo, F. (2004). An AIF orthologue regulates apoptosis in yeast. *J. Cell Biol.* 166:969-974.

204. Yamaki, M., Umehara, T., Chimura, T. and Horikoshi, M. (2001) Cell death with predominant apoptotic features in *Saccharomyces cerevisiae* mediated by deletion of the histone chaperone ASF1/CIA1. *Genes Cells* 6:1043–1054.

205. Adams, J.M. (2003) Ways of dying: multiple pathways to apoptosis. *Genes Dev.* 17:2481–2495.

206. Danial, N.N., and Korsmeyer, S.J. (2004) Cell Death: Critical Control Points. *Cell* 116:205-219.

207. Bredesen DE, Rao RV, Mehlen P. (2006) Cell death in the nervous system. *Nature* 443:796-802.

208. Lin, M.T., and Beal, M.F. (2006). Mitochondrial dysfunction and oxidative stress in neurodegenerative diseases. *Nature* 443:787-795.

209. Kenyon, C. (2001). A conserved regulatory system for aging. *Cell* 105:165-168.

210. Longo, V.D., and Finch, C.E. (2003). Evolutionary medicine: from dwarf model systems to healthy centenarians? *Science* 299:1342-1346.

211. Longo, V.D., and Kennedy, B.K. (2006). Sirtuins in aging and age-related disease. *Cell* 126:257-268.

212. Russell, S.J., and Kahn, C.R. (2007). Endocrine regulation of ageing. *Nat. Rev. Mol. Cell Biol.* 8:681-691.

213. Greer, E.L., and Brunet, A. (2008). Signaling networks in aging. *J. Cell Sci.* 121:407-412.

214. Kim, S.K. (2008). Genome-wide views of aging gene networks. In: Molecular Biology of Aging, eds. L.P. Guarente, L. Partridge, and D.C. Wallace, Cold Spring Harbor, New York: Cold Spring Harbor Laboratory Press, pp. 215-235.

215. Schwer, B., and Verdin, E. (2008). Conserved metabolic regulatory functions of sirtuins. *Cell Metab.* 7:104-112.

216. Lin, S.-J., and Sinclair, D. (2008). Molecular mechanisms of aging: insights from budding yeast. In: Molecular Biology of Aging, eds. L.P. Guarente, L. Partridge, and D.C. Wallace, Cold Spring Harbor, New York: Cold Spring Harbor Laboratory Press, pp. 483-516.

217. Kaeberlein M, Burtner CR, Kennedy BK (2007) Recent developments in yeast aging. *PLoS Genet.* 3: e84.

218. Bitterman, K.J., Medvedik, O., and Sinclair, D.A. (2003). Longevity regulation in *Saccharomyces cerevisiae*: linking metabolism, genome stability, and heterchromatin. *Microbiol. Mol. Biol. Rev.* 67:376-399.

219. Jiang, J., Wawryn, J., Shantha Kumara, H., and Jazwinski, S. (2002). Distinct roles of processes modulated by histone deacetylases Rpd3p, Hda1p, and Sir2p in life extension by caloric restriction in yeast. *Exp. Gerontol.* 37:1023-1030.

220. Bordone, L., and Guarente, L. (2005). Calorie restriction, SIRT1 and metabolism: understanding longevity. *Nat. Rev. Mol. Cell Biol. 6*, 298-305.

221. Sinclair, D.A. (2005). Toward a unified theory of caloric restriction and longevity regulation. *Mech. Ageing Dev.* 126:987-1002.

222. Weindruch, R., Walford, R.L., Fligiel, S., and Guthrie, D. (1986). The retardation of aging in mice by dietary restriction: Longevity, cancer, immunity and lifetime energy intake. *J. Nutr.* 116:641-654.

223. Sohal, R.S. and Weindruch, R. (1996). Oxidative stress, caloric restriction, and aging. *Science* 273:59-63.

224. Lane, M.A., Black, A., Handy, A., Tilmont, E.M., Ingram, D.K., and Roth, G.S. (2001). Caloric restriction in primates. *Ann. NY Acad. Sci.* 928:287-295.

225. Toda T., Cameron S., Sass P., and Wigler M. (1988) SCH9, a gene of *Saccharomyces cerevisiae* that encodes a protein distinct from, but functionally and structurally related to, cAMP-dependent protein kinase catalytic subunits. *Genes Dev.* 2:517-527.

226. Gallant, P., Shiio, Y., Cheng, P. F., Parkhurst, S. M., and Eisenman, R. N. (1996). Myc and Max homologs in Drosophila. *Science* 274:1523-1527.

227. Coschigano K.T., Clemmons D., Bellush L.L., and Kopchick J.J. (2000) Assessment of growth parameters and life span of GHR/BP gene-disrupted mice. *Endocrinology* 141:2608-2613.

228. Jazwinski, S.M. (2002). Biological aging research today: potential, peeves, and problems. *Exp. Gerontol.* 37:1141-1146.

229. Zhu, H., Guo, Q., and Mattson, M.P. (1999). Dietary restriction protects hippocampal neurons against the death-promoting action of presenilin-1 mutation. *Brain Res.* 842, 224-229.

230. Duan, W. and Mattson, M.P. (1999). Dietary restriction and 2-deoxyglucose administration improve behavioral outcome and reduce degeneration of dopaminergic neurons in models of Parkinson's disease. *J. Neurosci. Res.* 57:195-206.

231. Ingram, D.K., Weindruch, R., Spangler, E.L., Freeman, J.R., and Walford, R.L. (1987). Dietary restriction benefits learning and motor performance of aged mice. *J. Gerontol.* 42, 78-81.

232. Moroi-Fetters, S.E., Mervis, R.F., London, E.D., and Ingram, D.K. (1989). Dietary restriction suppresses age-related changes in dendritic spines. *Neurobiol. Aging* 10:317-322.

233. Mattson, M.P. (2000). Neuroprotective signaling and the aging brain: Take away my food and let me run. *Brain Res.* 886:47-53.

234. Guarente, L. and Picard, F. (2005). Calorie restriction - the SIR2 connection. *Cell* 120:473-482.

235. Bonawitz, N.D., Chatenay-Lapointe, M., Pan, Y., and Shadel, G.S. (2007). Reduced TOR signaling extends chronological life span via increased respiration and upregulation of mitochondrial gene expression. *Cell Metab.* 5:265-277.

236. Lin, S.J., Defossez, P.A., and Guarente, L. (2000). Requirement of NAD and SIR2 for life-span extension by calorie restriction in *Saccharomyces cerevisiae. Science* 289:2126-2128.

237. Masoro, E.J. (2006). Caloric restriction and aging: controversial issues. *J. Gerontol. Biol.* Sci. 61A:14-19.

238. Kenyon, C. (2005). The plasticity of aging: insights from long-lived mutants. *Cell* 120:449-460.

239. Guarente L (2006) Sirtuins as potential targets for metabolic syndrome. *Nature* 444: 868-874.

240. Haigis MC, Guarente LP (2006) Mammalian sirtuins - emerging roles in physiology, aging, and calorie restriction. *Genes Dev.* 20:2913-2921

241. Longo VD (2003) The Ras and Sch9 pathways regulate stress resistance and longevity. *Exp. Gerontol.* 38:807-811.

242. Wolff S, Dillin A (2006) The trifecta of aging in *Caenorhabditis elegans*. *Exp. Gerontol.* 41: 894-903.

243. Russell, S.J., and Kahn, C.R. (2007). Endocrine regulation of ageing. *Nat. Rev. Mol. Cell Biol.* 8:681-691.

244. Jazwinski, S.M. (2005). Yeast longevity and aging - the mitochondrial connection. *Mech. Ageing Dev.* 126:243-248.

245. Panowski SH, Wolff S, Aguilaniu H, Durieux J, Dillin A (2007) PHA-4/Foxa mediates diet-restriction-induced longevity of *C. elegans*. *Nature* 447:550-555.

246. Giannakou ME, Partridge L (2004) The interaction between FOXO and SIRT1: tipping the balance towards survival. *Trends Cell Biol.* 14:408-412.

247. François J, Parrou JL (2001) Reserve carbohydrates metabolism in the yeast *Saccharomyces cerevisiae*. *FEMS Microbiol. Rev.* 25:125-145.

248. Singer MA, Lindquist S (1998) Multiple effects of trehalose on protein folding in vitro and in vivo. *Mol. Cell* 1:639-648.

249. Simola M, Hänninen AL, Stranius SM, Makarow M (2000) Trehalose is required for conformational repair of heat-denatured proteins in the yeast endoplasmic reticulum but not for maintenance of membrane traffic functions after severe heat stress. *Mol. Microbiol.* 37:42-53.

250. Benaroudj N, Lee DH, Goldberg AL (2001) Trehalose accumulation during cellular stress protects cells and cellular proteins from damage by oxygen radicals. *J. Biol. Chem.* 276: 24261-24267.

251. Singer MA, Lindquist S (1998) Thermotolerance in *Saccharomyces cerevisiae*: the Yin and Yang of trehalose. *Trends Biotechnol.* 16:460-468.

252. Bordone L, Guarente L (2005) Calorie restriction, SIRT1 and metabolism: understanding longevity. *Nat. Rev. Mol. Cell Biol.* 6:298-305.

253. Picard F, Kurtev M, Chung N, Topark-Ngarm A, Senawong T, Machado De Oliveira R, Leid M, McBurney MW, Guarente L (2004) Sirt1 promotes fat mobilization in white adipocytes by repressing PPAR-γ. *Nature* 429:771-776.

254. Gerhart-Hines Z, Rodgers JT, Bare O, Lerin C, Kim SH, Mostoslavsky R, Alt FW, Wu Z, Puigserver P (2007) Metabolic control of muscle mitochondrial

function and fatty acid oxidation through SIRT1/PGC-1α. *EMBO J.* 26:1913-1923.

255. Haemmerle G, Lass A, Zimmermann R, Gorkiewicz G, Meyer C, Rozman J, Heldmaier G, Maier R, Theussl C, Eder S, Kratky D, Wagner EF, Klingenspor M, Hoefler G, Zechner R (2006) Defective lipolysis and altered energy metabolism in mice lacking adipose triglyceride lipase. *Science* 312:734-737.

256. Czabany T, Athenstaedt K, Daum G (2007) Synthesis, storage and degradation of neutral lipids in yeast. *Biochim. Biophys. Acta* 1771:299-309.

257. Low CP, Liew LP, Pervaiz S, Yang H (2005) Apoptosis and lipoapoptosis in the fission yeast *Schizosaccharomyces pombe*. *FEMS Yeast Res.* 5:1199-1206.

258. Merry BJ (2002) Molecular mechanisms linking calorie restriction and longevity. *Int. J. Biochem. Cell Biol.* 34:1340-1354.

259. Feng H, Ren M, Chen L, Rubin CS (2007) Properties, regulation and *in vivo* functions of a novel protein kinase D: *C. elegans* DKF-2 links diacylglycerol second messenger to the regulation of stress responses and lifespan. *J. Biol. Chem.* 282:31273-88.

260. Spitaler M, Cantrell DA (2004) Protein kinase C and beyond. *Nat. Immunol.* 5:785-790.

261. Fabrizio P, Gattazzo C, Battistella L, Wei M, Cheng C, McGrew K, Longo VD (2005) Sir2 blocks extreme life-span extension. *Cell* 123: 655-667.

262. Okamoto, K., and Shaw, J.M. (2005). Mitochondrial morphology and dynamics in yeast and multicellular eukaryotes. *Annu. Rev. Genet.* 39:503-536.

263. Cerveny, K.L., Tamura, Y., Zhang, Z., Jensen, R.E., and Sesaki, H. (2007). Regulation of mitochondrial fusion and division. *Trends Cell Biol.* 17:563-569.

264. Hoppins, S., Lackner, L., and Nunnari, J. (2007). The machines that divide and fuse mitochondria. *Annu. Rev. Biochem.* 76:751-780.

265. Suen, D.F., Norris, K.L., and Youle, R.J. (2008). Mitochondrial dynamics and apoptosis. *Genes Dev.* 22:1577-1590.

266. Pereira, C., Camougrand, N., Manon, S., Sousa, M.J., and Côrte-Real, M. (2007). ADP/ATP carrier is required for mitochondrial outer membrane permeabilization and cytochrome c release in yeast apoptosis. *Mol. Microbiol.* 66:571-582.

267. Pozniakovsky, A.I., Knorre, D.A., Markova, O.V., Hyman, A.A., Skulachev, V.P., and Severin, F.F. (2005). Role of mitochondria in the pheromone- and amiodarone-induced programmed death of yeast. *J. Cell Biol.* 168:257-269.

268. Ludovico, P., Rodrigues, F., Almeida, A., Silva, M.T., Barrientos, A., and Côrte-Real, M. (2004). Cytochrome c release and mitochondria involvement in programmed cell death induced by acetic acid in *Saccharomyces cerevisiae. Mol. Biol. Cell* 13:2598-2606.

269. Samejima, K., and Earnshaw, W.C. (2005). Trashing the genome: the role of nucleases during apoptosis. *Nat. Rev. Mol. Cell Biol.* 6:677-688.

270. Taylor, R.C., Cullen, S.P., and Martin, S.J. (2008). Apoptosis: controlled demolition at the cellular level. *Nat. Rev. Mol. Cell Biol.* 9:231-241.

271. Fannjiang, Y., Cheng, W.C., Lee, S.J., Qi, B., Pevsner, J., McCaffery, J.M., Hill, R.B., Basañez, G. and Hardwick, J.M. (2004). Mitochondrial fission proteins regulate programmed cell death in yeast. *Genes Dev.* 18, 2785–2797.

272. Brown, D.A. 2001. Lipid droplets: Proteins floating on a pool of fat. *Curr. Biol.* 11:R446-R449.

273. Zweytick, D., Athenstaedt, K. and Daum, G. 2000. Intracellular lipid particles of eukaryotic cells. *Biochim. Biophys. Acta* 1469:101-120.

274. Binns D, Januszewski T, Chen Y, Hill J, Markin VS, Zhao Y, Gilpin C, Chapman KD, Anderson RG, Goodman JM. 2006. An intimate collaboration between peroxisomes and lipid bodies. *J. Cell Biol.* 173: 719-731.

275. Howitz, K.T., Bitterman, K.J., Cohen, H.Y., Lamming, D.W., Lavu, S., Wood, J.G., Zipkin, R.E., Chung, P., Kisielewski, A., Zhang, L.L., Scherer, B., and Sinclair, D.A. (2003). Small molecule activators of sirtuins extend *Saccharomyces cerevisiae* lifespan. *Nature* 425:191-196.

276. Bauer, J.H., Goupil, S., Garber, G.B., and Helfand, S.L. (2004). An accelerated assay for the identification of lifespan-extending interventions in *Drosophila melanogaster. Proc. Natl. Acad. Sci. USA* 101:12980-12985.

277. Wood, J.G., Rogina, B., Lavu, S., Howitz, K., Helfand, S.L., Tatar, M., and Sinclair, D. (2004). Sirtuin activators mimic caloric restriction and delay ageing in metazoans. *Nature* 430:686-689.

278. Viswanathan, M., Kim, S.K., Berdichevsky, A., and Guarente, L. (2005). A role for SIR-2.1 regulation of ER stress response genes in determining *C. elegans* life span. *Dev. Cell* 9:605-615.

279. Baur, J.A., Pearson, K.J., Price, N.L., Jamieson, H.A., Lerin, C., Kalra, A., Prabhu, V.V., Allard, J.S., Lopez-Lluch, G., Lewis, K., Pistell, P.J., Poosala, S., Becker, K.G., Boss, O., Gwinn, D., Wang, M., Ramaswamy, S., Fishbein, K.W., Spencer, R.G., Lakatta, E.G., Le Couteur, D., Shaw, R.J., Navas, P., Puigserver, P., Ingram, D.K., de Cabo, R., and Sinclair, D.A. (2006). Resveratrol improves health and survival of mice on a high-calorie diet. *Nature* 444:337-342.

280. Valenzano, D.R., Terzibasi, E., Genade, T., Cattaneo, A., Domenici, L., and Cellerino, A. (2006). Resveratrol prolongs lifespan and retards the onset of age-related markers in a short-lived vertebrate. *Curr. Biol.* 16:296-300.

281. Chen, D., and Guarente, L. (2007). SIR2: a potential target for calorie restriction mimetics. *Trends Mol. Med.* 13:64-71.

282. Curtis, R., Geesaman, B.J., and DiStefano, P.S. (2005). Ageing and metabolism: drug discovery opportunities. *Nat. Rev. Drug Discov.* 4:569-580.

283. Milne, J.C., Lambert, P.D., Schenk, S., Carney, D.P., Smith, J.J., Gagne, D.J., Jin, L., Boss, O., Perni, R.B., Vu, C.B., Bemis, J.E., Xie, R., Disch, J.S., Ng, P.Y., Nunes, J.J., Lynch, A.V., Yang, H., Galonek, H., Israelian, K., Choy, W., Iffland, A., Lavu, S., Medvedik, O., Sinclair, D.A., Olefsky, J.M., Jirousek, M.R., Elliott, P.J., and Westphal, C.H. (2007). Small molecule activators of SIRT1 as therapeutics for the treatment of type 2 diabetes. *Nature* 450:712-716.

284. Yang, H., Ren, Q., and Zhang, Z. (2008). Cleavage of Mcd1 by caspase-like protease Esp1 promotes apoptosis in budding yeast. *Mol. Biol. Cell* 19:2127-2134.

285. Becker, J. and Craig, E.A. (1994) Heat-shock proteins as molecular chaperones. *Eur. J. Biochem* 219:11-23.

286. Hartl, F.-U. (1996) Molecular chaperones in cellular protein folding. *Nature* 381:571-579.

287. Bukau, B. and Horwich, A.L. (1998) The Hsp70 and Hsp60 chaperone machines. *Cell* 92:351-366.

288. Glover, J.R. and Lindquist, S. (1998) Hsp104, Hsp70, and Hsp40: a novel chaperone system that rescues previously aggregated proteins. *Cell* 94:73-82.

289. Flower, T.R., Chesnokova, L.S., Fröhlich, C.A., Dixon, C. and Witt, S.N. (2005) Heat shock prevents alpha-synuclein-induced apoptosis in a yeast model of Parkinson's disease. *J. Mol. Biol.* 351:1081-1100.

290. Petko, L. and Lindquist, S. (1986) Hsp26 is not required for growth at high temperatures, nor for thermotolerance, spore development, or germination. *Cell* 45:885-894

291. Burnie, J.P., Carter, T.L., Hodgetts, S.J., and Matthews, R.C. (2006) Fungal heat-shock proteins in human disease. *FEMS Microbiol. Rev.* 30:53-88.

292. Wong, C.M., Zhou, Y., Ng, R.W., Kung, H.F., and Jin, D.Y. (2002) Cooperation of yeast peroxiredoxins Tsa1p and Tsa2p in the cellular defense against oxidative and nitrosative stress. *J. Biol. Chem.* 277:5385-5394.

293. Wong, C.M., Siu, K.L., and Jin, D.Y. (2004) Peroxiredoxin-null yeast cells are hypersensitive to oxidative stress and are genomically unstable. *J. Biol. Chem.* 279:23207-23213.

294. Trotter, E.W., Rand, J.D., Vickerstaff, J., and Grant, C.M. (2008) The yeast Tsa1 peroxiredoxin is a ribosome-associated antioxidant. *Biochem. J.* 412:73-80.

294. Toos, W. and Rottgers, K. (2002) Molecular chaperones as essential mediators of mitochondrial biogenesis. *Biochim. Biophys. Acta* 1592:51-62.

295. D'Silva, P.D., Schilke, B., Walter, W., Andrew, A., and Craig, E.A. (2003) J protein cochaperone of the mitochondrial inner membrane required for protein import into the mitochondrial matrix. *Proc. Natl. Acad. Sci. USA* 100:13839-13844.

296. Kozany, C., Mokranjac, D., Sichting, M., Neupert, W., and Hell, K. (2004) The J domain-related cochaperone Tim16 is a constituent of the mitochondrial TIM23 preprotein translocase. *Nat. Struct. Mol. Biol.* 11:234-241.